Multibody dynamics modelling of the masticatory system of the house mouse (*Mus musculus*)

Anna Chabokdast (MSc, BSc)

being a Dissertation submitted in partial fulfilment of

the requirement for the Degree of

PhD

in the University of Hull and the University of York

Hull York Medical School

May 2015

Abstract

Understanding the function of masticatory system of the mouse, the model of choice for craniofacial studies is invaluable, yet has been investigated poorly. Multibody dynamic analysis (MDA), which is a 3D computer modelling technique used in this study, is ideally suited to replicate and investigate this complex system. To mechanically solve this intricate system, system indeterminacy should be tackled using optimisation algorithms. The mouse has two types of teeth, hence two very different types of biting: incisal and the molar biting. To understand the masticatory function, modelling these two types of biting is invaluable. This study aims to investigate the differences in muscle function between incisors and molar biting. It was hypothesized that the generated bite force in the first molar would be higher than the incisor, due to the mechanical advantage of the latter. Moreover, the model sensitivity to the optimisation algorithms and the constraint types as well as muscle attributes such as intrinsic stress value and cross sectional area were studied. Functional development of the masticatory system of the mouse was an additional interest in this study.

The first MDA model of the adult mouse masticatory system was developed and two optimisation algorithms, Dynamic geometric optimisation (DGO) and minimisation of overall muscle energy (MOME), were used to overcome the system indeterminacy. Furthermore, individual-specific adult model were developed and maximal and sub-maximal incisor and first molar biting were simulated. In addition, a simplistic model of the juvenile incisal biting was developed in which maximal incisal bite force and muscle activation pattern was studied.

Some divergences were predicted from DGO and MOME, which were resulted from different basis of the activation factors in the two algorithms. Nevertheless, DGO was chosen as the optimisation algorithm mainly because it allowed for the simulation of a full biting cycle and for inclusion of some key developments in the future. The maximum predicted bite force in incisal biting was lower than the *in vivo* measurement, which was possibly due to averaging PCSA across specimens. A

correction factor of 25% was added to muscle intrinsic stress value to compensate for this underestimation. Moreover as expected, the maximum predicted bite force at the first molar position was larger than that of the incisor. It was also found that the ratio of muscle forces between incisal and molar biting did not remain constant, however, was more consistent for simulation of low bite forces. In addition, incisal bite force in juvenile model was in agreement with *in vivo* bite force measurement from the same individual.

MDA presented here provides a model which may be used to study many functional tasks and to investigate functional development and intertwined relationship between function and development in the mouse and similar rodents.

Contents

List of Figures

List of Tables

Acknowledgement

First and foremost, I would like to express my gratitude to my supervisors Dr. Samuel Cobb and Prof. Michael Fagan, whom consistently provided excellent support and encouragement. I would also like to thank University of Hull for funding my PhD.

I would also like to thank Dr Anthony Herrel for collection of experimental data for this thesis and Dr Stuart Humphries for his support and encouragement in the teaching advisory panel meetings.

Furthermore, I would like to thank all people whom I worked with in Biological and Medical Engineering Research group and Centre for Anatomical and Human Sciences (HYMS), in particular Dr. Neil Curtis and Dr. Peter Watson for their continuous help and support in MDA techniques. Moreover, I would like to thank Dr Michael Berthaume whom read my work and gave me valuable feedback. I would also like to thank Dr. Hester Baverstock for advice and assistance regarding muscle morphology and segmentation techniques.

Many thanks to Sue Taft for CT-scanning the specimens, as well as making the working environment more pleasant.

Finally, my special gratitude goes to my family and friends whose continuous encouragement has always been motivating, especially to my father who has always been my inspiration, my mother whom taught me to believe in myself; and to whom I will always remain grateful, Saeed: “without your support and presence I would have never enjoyed this experience as much, Thank you”.

Author's declaration

I confirm that this work is original and that if any passage(s) or diagram(s) have been copied from academic papers, books, the internet or any other sources these are clearly identified by the use of quotation marks and the reference(s) is fully cited. I certify that, other than where indicated, this is my own work and does not breach the regulations of HYMS, the University of Hull or the University of York regarding plagiarism or academic conduct in examinations. I have read the HYMS Code of Practice on Academic Misconduct, and state that this piece of work is my own and does not contain any unacknowledged work from any other sources.

Chapter 1. Introduction and literature review

1.1. Introduction

Functional analysis of the masticatory system has applications in biomechanical, developmental and evolutionary studies. Understanding the function of masticatory system of different species sheds light onto the relationship between form and function; helping researchers understand the changes that species undergo during different stages of their development. It can also shed light on the evolutionary processes that have acted on that species. Furthermore, masticatory studies have clinical application not only in disorders and dysfunctions of masticatory joints and muscles, but also with some studies linking the reduction in mastication to the development of brain disease (Bjertness, 1991, Jones et al., 1993, Onozuka et al., 1999). For these reasons, the masticatory system of different animals has been studied at various levels for many years.

Mechanical forces play a large role in skeletal development (Bertram and Swartz, 1991, Pearson and Lieberman, 2004, Ruff et al., 2006), but interestingly this role is understudied in craniofacial development. Bone loading is a particularly important factor in the modelling and remodelling of bone morphology. In the masticatory system, loads are applied through three key mechanisms: contraction of masticatory muscles, biting on a food item, and reaction of those forces at the temporomandibular joints. The magnitude and direction of these forces during development will vary and are likely to influence the morphology of the mandible and cranium. In addition, the evolution of the masticatory system of different species can potentially be explained by incorporating diet into our functional analyses. Therefore to understand the development of cranium and mandible, understanding the function of the masticatory system is crucial.

The most common mammal model for genetic and medical studies is the house mouse (*Mus musculus*). In addition to a similar genetic basis to human, they are widely available, convenient to experiment upon and are generally low-cost. Surprisingly, function and morphology of the masticatory system has not been well

studied in this species. Investigation of the function of the masticatory system from the biomechanical perspective including the function of each and every muscle during normal mastication within this system and during development are among the areas that have been overlooked.

The dental arcade of rodents consists of two types of teeth, the incisors and molars, separated by a large diastema. This results in two very different types of biting: molar and incisal. Despite the small, manageable size of the mouse, there is little published bite force data, in particular for molar biting – due to the large diastema which makes it difficult to measure voluntarily bite force *in vivo*. As experimentation is very difficult, biomechanical modelling provides an alternative means to estimate this bite force.

Furthermore, the mandibular diastema is smaller than that of the maxillary, to occlude the molars or incisors an antereoposterior translation of the mandible is required. This translation changes the muscle orientations and consequently the activation patterns of the muscles, increasing the complexity of the system. Moreover the kinematics of the mandible during incisal chewing are different from the kinematics during molar chewing. Thus obtaining muscle activation patterns during incisal and molar chewing will also help us understand masticatory system.

Although extensive work has been carried out on the morphology of mammalian masticatory muscles, it was long after the invention of electromyography (EMG) that muscle activations could expressively be measured. EMG is a method in which the electrical impulse generated by muscles are detected, amplified and recorded. There are two approaches: invasive and non-invasive, where invasive methods require the insertion of thin needles into the muscle, and non-invasive methods involve the placement of electrodes on the skin. In the case of the mouse its miniscule muscles requires needles and electrodes to be produced in a miniature scale. Even when needles and electrodes are produced at the correct scale, invasive methods can cause muscle damage after inserting the needles, interfering with normal function introducing error to the measurement. On the other hand, non-invasive method can have a high level of interference due to cross talk between the

muscles and measurements can be easily affected, especially when the skull is small and the electrodes are attached close together. As a result, although EMG experimentation has been carried out on the mouse (Kobayashi et al,. 2002a, Yamada et al., 2006, Utsumi et al., 2010), the results are associated with limitations, namely, solely superficial muscles, i.e. masseter, temporalis and digastric muscles were studied, different functional groups of these muscles were not separately studied and data was reported for each muscle as the whole. Moreover, due to the cross talk between the muscles the reported activation is likely to be unreliable.

An alternative way to understand muscle activation patterns is biomechanical modelling, but due to the multifaceted, integrated anatomical structure of the masticatory system, which serves a variety of functions, complex modelling is essential if realistic and reliable values are to be produced. For example, during jaw opening, muscle forces, elongations and orientations change, altering the active and passive forces exerted in the masticatory system. Multibody dynamic analysis (MDA) is ideally suited for modelling this complexity. MDA is a 3D computer modelling technique that can be used to simulate varying muscle forces to predict bite and joint reaction forces or to simulate mandibular kinematics to predict bite forces, muscle activations, joint forces during static and dynamic motions.

In MDA modelling of the mammalian masticatory system, the mastication cycle can be modelled as several intervals each of which can be solved using only six independent equations: three for the sum of the forces in three directions and three for the sum of moments about these axes. The number of unknowns (individual muscle forces, joint reaction forces and bite force), however, will inevitably be much greater than six. Thus, an unlimited combination of muscle activation patterns could result in the same bite force or joint reaction force, leading to an unlimited number of solutions. This phenomenon is known as indeterminacy, and, in this application, muscle redundancy. There are a number of optimisation methods that have previously been proposed to overcome muscle redundancy and provide an optimised solution. One approach is minimisation of muscle energy (Shi et al., 2012) another which has recently been developed specifically for masticatory system analysis, is dynamic geometric optimisation

(DGO) which works based on this assumption that the orientation of each muscle is optimised for its function (Curtis et al., 2010a). This means that when a vertical force is required, for example to crush a food item, the muscles that are orientated more vertically at that gape are optimal to generate force, hence they are expected to have a higher activation level.

Both optimisation methods are credible, and the muscle activation patterns predicted by both methods have been shown to be in general agreement with available EMG data. When the two methods are in disagreement and EMG data is available, the accuracy of the models can be tested and model validation can be used to choose or optimise the method. For the mouse, model accuracy cannot be tested via EMG, as sufficiently sophisticated EMG data is not available. However comparison of the results gained from the two optimisation methods can be used to test the precision of the models.

Morphology and function have a reciprocal relation during ontogeny. While masticatory function depends on its structure, it also has profound influence on further musculoskeletal growth (Herring, 1985). Development of the masticatory system is not a simple scaling of the components, but different parts of the mandible and the skull as well as adjoining muscles develop with different rates and undergo changes during different stages of development, and function is an additional factor which modulates and forms the craniofacial development (Dechow and Carlson, 1990). In particular, dramatic change in the masticatory function, which is transition from sucking behaviour to mastication after weaning, results in significant developmental changes during ontogeny. There are a number of simultaneous changes associated with craniofacial growth which all can influence its function, namely modelling and remodelling of the cranium and mandible (Hall, 1982, Atchley et al., 1985a, Byron et al., 2004, Willmore et al., 2006, Odman et al., 2008, Tanner et al., 2010, Anderson et al., 2014), enlargement of masticatory muscles (Rayne and Crawford, 1972, Houston, 1974, Nakata, 1981, Langenbach and Weijs, 1990), change of occlusal bite force (Dechow and Carlson, 1990), change of diet and finally change of contact surfaces of the teeth.

Therefore, masticatory function is a factor that affects the development. In reverse, the non-linear development of the masticatory system may result in non-linear adaptations in leverage of masticatory system as well as in muscle volumes in different stage of the ontogeny. Thus, masticatory development affects its function too. Hence, understanding the function of the masticatory system during development is crucial to understand complex relationship between its function and development.

The aim of this thesis is to study the masticatory system of the house mouse using multibody dynamic modelling techniques. Individual-specific MDA model of the mouse masticatory system is developed, in which optimisation criteria is required to conclude a unique muscle activation pattern from an MDA model. Two commonly used optimisation criteria, minimisation of overall muscles energy and dynamic geometric optimisation, are used in this thesis and the resulted muscle activation patterns are compared. After understanding each method and its requirements, the more suitable of the two methods is selected to model the masticatory muscles function during incisor and molar biting. Maximum bite force at incisor and molar region are predicted and the former is compared against *in vivo* data to validate the model. In addition, the muscle activation patterns during sub-maximal and maximal bite force is studied and compared in both biting positions. And last but not the least, function of the masticatory system in the juvenile mouse is modelled for incisal biting and compared to the adult one.

1.2. Anatomy of the masticatory system in the mouse

Rodents have played, and continue to play, an important role in masticatory studies. However, while comparative and comprehensive studies of masticatory system of many rodents (Hiiemae, 1967, Hiiemae, 1971a, Popwics and Herring, 2006, Williams et al., 2009, Druzinsky, 2010a, Druzinsky, 2010b, Cox and Jeffery, 2011) have been thoroughly investigated, one rodent has been overlooked. The mouse has been widely used as a model in craniofacial studies, but except for two studies (Patel, 1978, Baverstock et al., 2013), has not had its masticatory system well investigated.

The masticatory system consists of many different tissue types including bone, muscle, teeth and ligaments. Hiiemae (1967) describes the masticatory apparatus as an integrated unit, which consists of four distinct parts:

- the teeth,
- the cranium and mandible,
- the mandibular joints, which include the mandibular symphysis and the temporomandibular joint (TMJ), and
- the masticatory muscles which control mandibular kinematics.

In addition, there are accessory structures that act to facilitate the masticatory process. These include the tongue and oral tissues, the hyoid bone, pharyngeal muscles and the salivary glands, which are beyond the scope of this study.

1.2.1 Teeth

There are four classes of teeth in mammals: incisors, canines, premolars and molars. The incisors and canines are located in the anterior portion of the oral cavity and are used for grasping food items and breaking them into smaller pieces, whereas the molars and premolars, also called as cheek teeth, are located in the posterior portion of the oral cavity and are used for chewing (see Figure 1.1).

Figure 1.1 Mouse dentition composed of only three molars and incisors which are separated by diastema.

One of the factors that differentiate rodents from other mammals is their teeth. Unlike most other mammals, rodents do not have canines or premolars. In particular, the mouse has one incisor and three molars in each quadrant (Figure 1.2). Incisors are located at the anterior most portion of the mandible, and a large diastema separates them from the molars. The incisors grow continuously throughout the life of the mouse, with wear, caused by food items and counterpart teeth, keeping them short and sharp.

In molars, the role of crown shape is to concentrate stress while chewing. Some crowns such as the ones with cusps act like mortar and pestle and crush the food. Some other molar crowns function like shearing blades and cut the food (Popwics and Herring, 2006). The number of and morphology of cusps varies between three and eight in each molar (see Figure 1.3).

Teeth in different mammals have, more or less, the same composition. The outer surface is covered by enamel, which is the most mineralized tissue in the body and consists of 97% minerals. This high mineralization results in very high compressive, but low tensile strength as well as high resistance to wear (Popwics and Herring, 2006). In the case of the mouse, mandibular teeth have thicker enamel than their maxillary counterparts (Moinichen et al., 1996, Lyngstadaas et al., 1998).

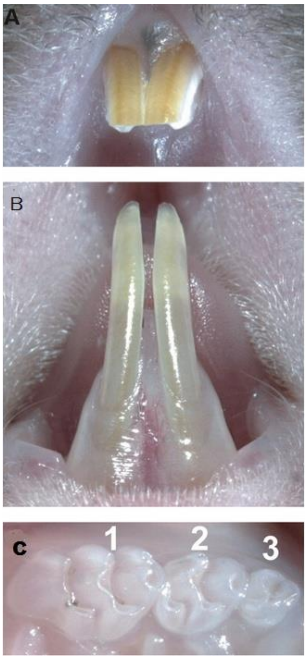

Figure 1.2 A) Upper incisors, B) Lower incisor and C) The first, second and third upper molars of the mouse (Kist et al., 2005)

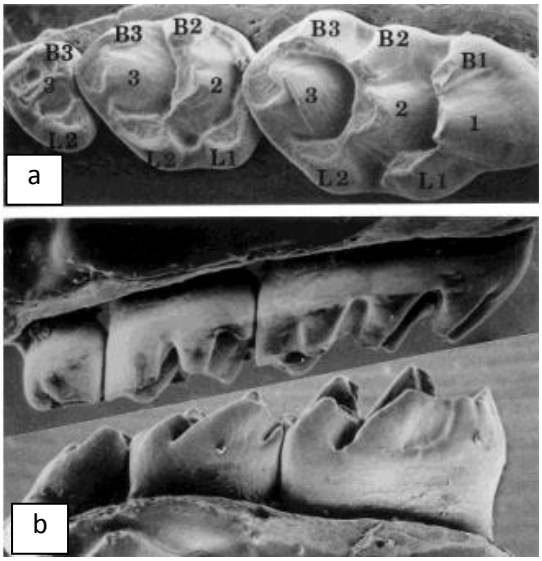

Figure 1.3 Morphology of molar cusps in a 5 week old mouse: a) Occlusal view of right maxillary molars, Buccal cusps (B1, B2, B3), lingual cusps (L1, L2), and central cusps (1, 2, 3); b) Buccal view of the upper and lower right molars (M1,M2 and M3- right to left) (Lyngstadaas et al. (1998))

Beneath the enamel, there is a layer of living tissue called dentin. Unlike enamel, which is found strictly in the crown of the tooth, dentin can be found in the crown and root of the tooth. Dentin is less mineralized than enamel (around 70%) and contains more water and organic material. Therefore, it is softer and when exposed, it wears faster. Dentin can be regenerated throughout an individual's lifetime with the help of odontoblasts. While the dentine in the tooth crown is surrounded by enamel, the dentin in the tooth root is surrounded by cementum. Cementum is also highly mineralized tissue which serves to connect the dentin to the periodontal ligaments. Inside the dentine is pulp, which is unmineralized tissue containing typically 70% water. The outer layer of pulp, adjacent to the dentine, is covered by odontoblasts which secrete dentine. A schematic figure of tooth structure is presented in Figure 1.4.

Teeth are joined to bone by the periodontium, which consists of periodontal ligaments and alveolar bone, and provides viscoelastic support for the teeth (Popwics and Herring, 2006). Thus, during mastication, the resultant forces are transferred through the periodontium to the maxilla and mandible.

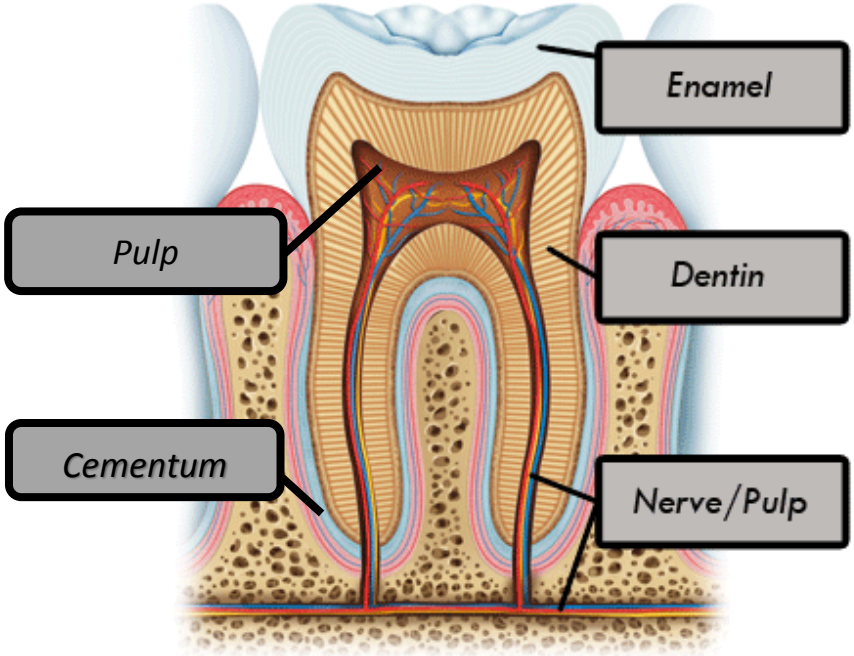

Figure 1.4 Structure of a tooth (adapted from www.auburnfamilydental.com). Note that periodontium is not shown in the figure.

1.2.2 Cranium

The cranium is a bony structure that houses many important organs including the brain, nose, ears and eyes. It composed of a number of bony components including maxilla, premaxilla and zygomatic that articulate via sutures (see Figure 1.5). Sutures are growth sites of the cranium (Opperman, 2000), which allow for changes in cranial shape and size during development. In addition, unfused sutures transfer and absorb mechanical stresses that are experienced through the application of physical loads, such as those that occur during mastication (Alaqeel et al., 2006). In normal development, when the cranium is mature, sutures fusion occurs however, in some cases, sutures fuse prematurely leading to abnormal shape of cranium. Sutural growth and fusion is largely modulated by mechanical stimuli (Mao, 2002), the extent of which also plays a role in final cranial shape.

There are several factors involved in the form and development of the mandible and cranium, including genetics, hormones, vascularisation, diet and biomechanical loading (Atchley et al., 1985b). The latest factor includes the loading resulted from the development and the activation of the muscles adjacent to each anatomical part. The key muscle attachment sites on the cranium are introduced in Figure 1.6 and are discussed in details in Section 1.3. As shown in Figure 1.7, there is a large variation in skull size and shape in different strains of the mouse, of which there are about 450 types in total (Barton and Keightley, 2002). The C57BL strain, which is the most common wild type strain and was already being used in parallel ongoing research, was used in this study. Although this strain is not particularly known as being a great biter, it was still well suited to develop a general working computer model of the mouse masticatory system.

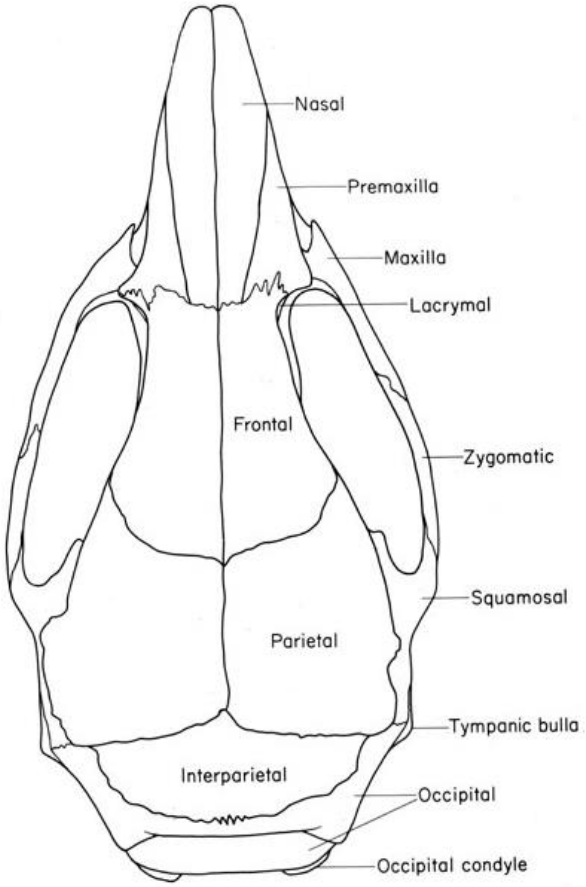

Figure 1.5 Dorsal view of the skull and its components parts, taken from informatics.jax.org

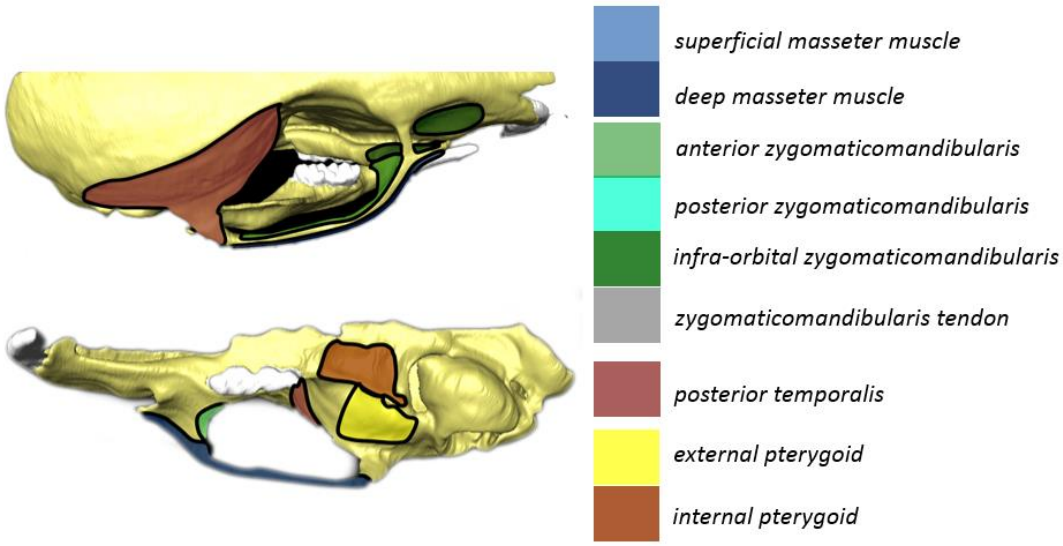

Figure 1.6 Key muscle attachment areas in the cranium; upper: dorsal view, lower: ventral view (Baverstock et al., 2013).

Figure 1.7 The skull of seven strains of mice, the C57 was the subject of this study. Adapted from Kawakami and Yamamura (2008).

1.2.3 Mandible

The mandible is a bony structure to which all masticatory muscles insert. Different parts of the mandible can be identified according to their function and development, namely: the basal unit, the condylar process (articular surface of temporomandibular joint and attachment area of lateral pterygoid muscle), the coronoid process (attachment area of temporalis muscle), the angular process (attachment area of masseter and medial pterygoid muscles), the alveolar bone (bone surrounding the mandibular dentition) and the symphysis (unfused attachment point of two hemi-mandibles) (see Figure 1.8).

During development several genetic, biomechanical and dietary components affect the shape of the mandible, resulting in a very complicated process. While most of the postnatal growth in the mandible occurs in the condylar process, there are other parts of mandible involved in its development too. For example the length of the condylar process increases in early stages of ontogeny together with coronoid and angular process size (Hall, 1982, Atchley et al., 1985a), whereas the body of the condylar process starts to increase as a response to mechanical stimuli associated with mastication in later stages of ontogeny. In addition, lateral growth occurs in the symphysis (De Beer, 1937, Lieberman and Crompton, 2000). There are several other remodelling changes that occur in various other parts. For example in the posterior border of the ramus, bone deposition occurs in the coronoid, angular and condylar process, whereas in the anterior region, bone deposition occurs in the

symphysis. In addition, weaning and the subsequent weight gain is correlated with increased width of the condyle and height of the incisors (the latter area is shown with the red vertical dotted line in Figure 1.8) (Atchley et al., 1985a).

Development of different anatomical parts of the mandible are independent and partly influenced by activation and development of their adjacent muscles (Atchley et al., 1985a). For example, removal of the medial pterygoid or masseter muscles is reported to result in resorption of the angular process, whereas removal of the temporalis muscle results in shrinkage of the coronoid process (Hall, 1982). The key muscle attachment areas are shown in Figure 1.9.

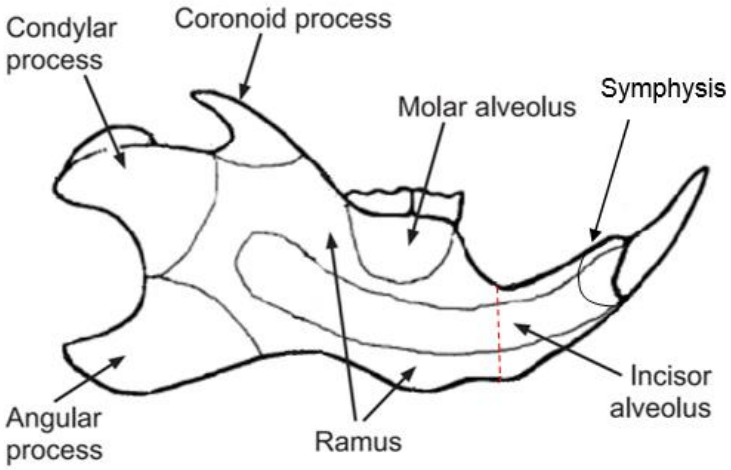

Figure 1.8 Anatomy of the mouse mandible. The different anatomical parts are presented. The dotted line is presenting the height of the incisors which increases after weaning (adapted from Klingenberg et al. (2003)).

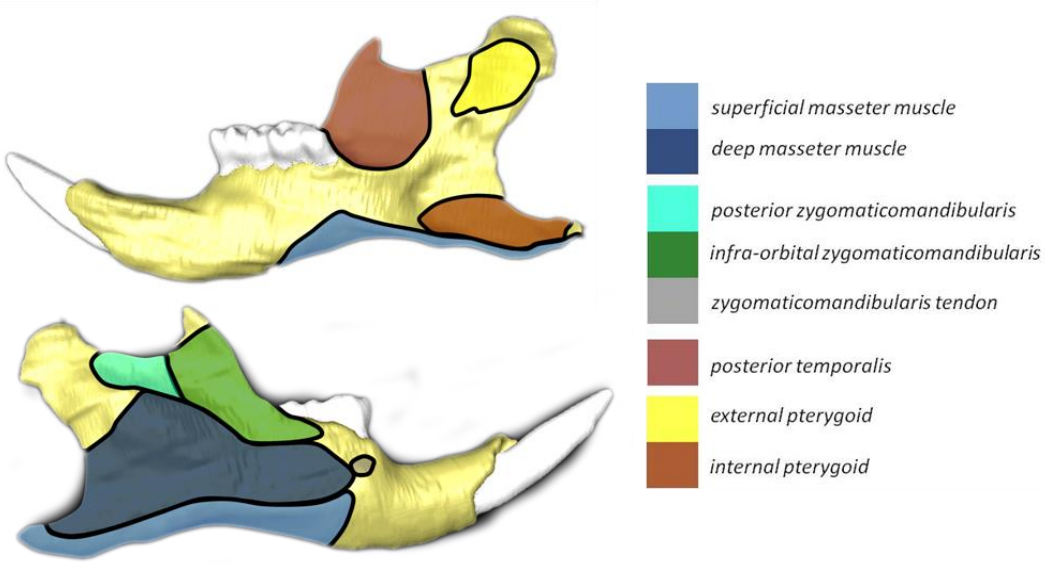

Figure 1.9 Muscle attachment area in the mandible of the mouse; upper: medial side of the mandible, lower: lateral side of the mandible (Baverstock et al. (2013))

1.2.4 Temporomandibular joints

The jaw joints, also known as the temporomandibular joint (TMJ), is a synovial joint which is composed of two articulating surfaces; the condyle in the mandible and the glenoid fossa of the temporal bone in the cranium. The articulating track of the condyle and the glenoid fossa in the mouse is rather flat and, unlike carnivorous, there is no bony process limiting the translational movement of the mandible (Popwics and Herring, 2006).

The condyle is a secondary tissue which forms during the later stages of ontogeny. As it is the dominant growth site of the mandible, any injury to the TMJ area, can cause malformation and malocclusion of the mandible (Popwics and Herring, 2006). The head of the condyle is half of the length and two thirds of the width of the glenoid fossa (Weijs, 1975). The difference in the size of the condyle and glenoid fossa is essential, as TMJs in rodents, including the mouse, have an antero-posterior (translational) movement as well as rotational movement. The head of the condyle, which is larger than the ramus beneath it, starts to broaden and ossify after weaning (Kawata et al., 1997).

During incision, the condyle moves anteriorly to allow the incisors to occlude, and posteriorly for the molars to occlude in mastication. The condyle head has two articulating parts; anterior and posterior. The anterior part of the condyle articulates with posterior part of the glenoid fossa for molar occlusion in mastication, whereas the posterior part of the condyle and anterior part of glenoid fossa articulate mutually to facilitate incisor occlusion during incision. The morphology of the fossa is such that the anterior part is located ventral to the posterior part, thus when the condyle articulates with the anterior part of the glenoid fossa, the mandible naturally drops down (Hiiemae, 1967).

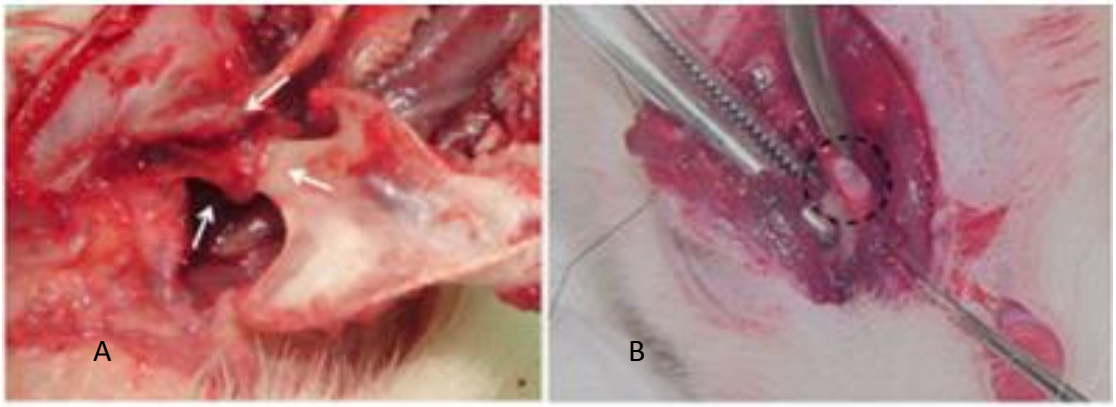

Figure 1.10 Macroscopical evaluation of the soft tissue. A) TMJ capsule covering condyle and glenoid fossa shown with white arrows; B) articular disc (Porto et al., 2010).

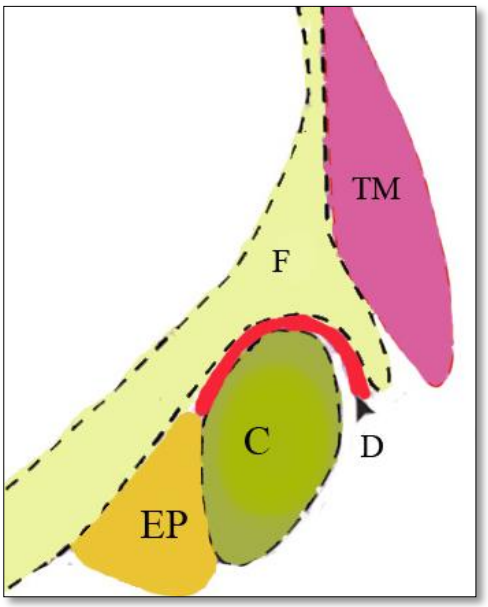

Figure 1.11 Schematic figure of the TMJ in the mouse; C, condyle; D, articular disc; F, glenoid fossa; EP, external pterygoid muscle; TM, temporalis muscle (Redrawn from Purcell et al. (2012)).

The TMJ disc is an intra-articular fibrous structure which separates the condyle from the glenoid fossa. The disc acts as a cushion for the articulating surfaces and allows complex movement in the jaw joint of the mouse (see Figure 1.10B and Figure 1.11). It consists of collagenous fibres that are oriented longitudinally with variable thickness along the condyle; thinnest at the midpoint and thickest at the anterior and posterior ends. The TMJ is enclosed by a hyaline capsule, consisting of fibrous tissue and a synovial lining (Figure 1.10A), that protects the articulating surfaces as well as the disc (Weijs, 1975, Porto et al., 2010, Wang et al., 2011).

Ligaments also surround the TMJ which, together with the masticatory muscles play a role in the stabilization and control of the position of the condyle against the glenoid fossa. Their contribution however is minor, because they consist of collagen, fibroblasts and elastic fibres (Hiiemae, 1967), which provide flexibility over a reasonable range, but can be damaged if stretched excessively (Cuccia et al., 2011). To avoid this, the muscles play the major role in controlling the movement. In addition, a relatively high reaction force can be created at the TMJ during biting (Satoh, 1998), but since the glenoid fossa does not have a bony process to hold the condyle in place, counterbalancing muscle action is essential to prevent any potential damage to the joint. Satoh (1998) proposed that the posterior temporalis plays an important role in the stabilization of the mandibular condyle against the glenoid fossa in incisal biting. Hiiemae (1967), however, suggested that it was the external pterygoid which acted as the principal controller of the mandibular condyle.

1.2.5 Symphysis

The mandibular symphysis is a moveable joint that is located at the anterior part of the mandible, high on the medial side of the incisors' alveolar bone (see Figure 1.12). Symphysis consists of fibrocartilage and connects the two hemi-mandibles, allowing each to rotate about its long axis. It is also the site of anterior development of the mandible, especially in antero-posterior direction (Lieberman and Crompton, 2000, Bernick and Patek, 1969). At the anterior region of the symphysis, bone deposition occurs (Atchley et al. 1985a). The bone deposition not only results in an increase in the length of the anterior part of the mandible , but

also its directional growth determines the shape and form of the anterior part of the mandible (Bernick and Patek, 1969). Just anterior to the symphysis one strong horizontal ligament connects the rami, and a little posterior to it, a further row of inter-crossing ligaments connects the two hemi-mandibles. Although these ligaments limit the transverse angular movement between the rami, there is still a considerable rotation in all directions (Weijs, 1975). In some species, the symphysis is less movable or fused completely (Popwics and Herring, 2006), but in most of the rodents including the mouse, it is free and flexible (Satoh, 1998).

The transverse components of the masticatory muscles result in rotation of the hemi-mandibles, which ultimately generates compression or tension in the symphyseal ligaments. The flexible unfused symphysis has low tensile strength, hence to prevent damage to it, muscle activations in the transverse plane must counteract one another. For example, the deep masseter has a considerable medial component as well as high mechanical advantage which could lead to tension in the symphysis. However, this can be counterbalanced by the external pterygoid which inserts on condylar process of the mandible, and pulls the condyle medially (Hiiemae, 1967). Internal pterygoid appears to have a primary function of counterbalancing the high tensile force on ligaments and protecting the symphysis from tear (Hiiemae, 1971a, Satoh, 1998).

Figure 1.12 Medial view of mouse mandible, adapted from (Bab et al., 2007).

1.3. Masticatory muscles and their functions

Skeletal muscles, including masticatory muscles, are essentially biological motors that exert force and produce mechanical work, besides their other functions such as acting as force transmitters, shock absorbers etc. In this thesis, however, solely function of the muscle in force production is studied.

1.3.1 Muscle structure

Structure of skeletal muscle plays the key role in its function. The comprising units of the muscle are fascicles, fibres, myofibrils, and sarcomeres respectively. The outmost layer of the muscle is fascia and a further connective tissue known as epimysium which wraps around fascicles that are running alongside each other. Fascicles compose of several fibres which are wrapped in a connective tissue that is called perimysium. Muscle fibre is the next comprising unit of muscle which consists of individual muscle myofibrils surrounded by a connective tissue called endomysium. Fibres consist of parallel myofibrils (Figure 1.13).

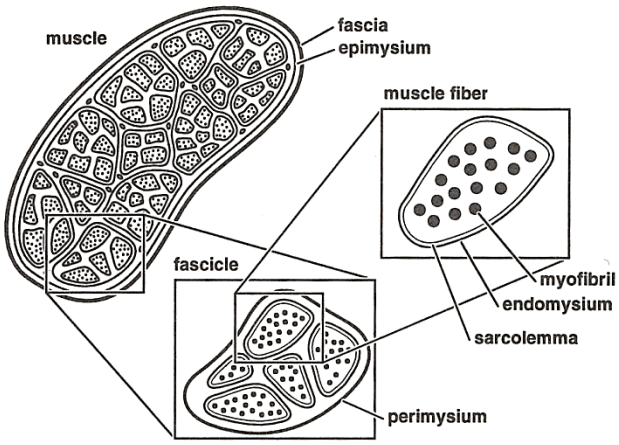

Figure 1.13 Schematic illustration of comprising structures and sub-structures of a muscle (Herzog, 1994)

The repetitive contractile unit of the muscle which forms myofibril is sarcomere. There can be thousands of sarcomeres within only one muscle cell (Figure 1.14). Sarcomeres are composed of actin (thin) and myosin (thick) filaments which are protein molecules, and their interaction results in shortening of the sarcomere and

ultimately muscle contraction. Thick filaments are made of multiple myosin molecules which are large proteins, each with a long tail portion and a globular head that extends outward. The myosin molecules are arranged in a way that their tail is placed toward the centre of the filament. Thus globular heads are oriented in opposite directions in two halves of the thick filament. This region of the muscle fibre, in which the myosin is situated, is called “A band” (A=anisotropic). A-band also includes the region in which myosin and actin overlap. M-line is the region where proteins attach the thick filaments together and stabilize their positions in the centre of the sarcomere. Z-lines are perpendicular protein plates which form the lateral boundary of sarcomeres. . The region of the myofibril, in both sides of Z-line, in which only thin filaments are situated and there is no overlapping between the thin and the thick filaments is called “I-band”(I=isotropic) (Herzog, 1994). The globular head of myosin contains a binding site for actin which pulls upon actin and pulls it towards the centre of the sarcomere, hence shortens it, and an enzymatic site that acts as catalyser for chemical reaction which leads to energy release required within the muscle. The process of binding the head of myosin to actin is called cross-bridging which requires energy release of the muscle and transforms chemical energy to produce movement (see Figure 1.15). Cross-bridge repeats in the sarcomere, with formation of every cross-bridge the myosin offsets 14.3nm and a constant force is generated.

When the sarcomere contracts, the length of “A band”, which contain myosin, remains constant, whereas the length of “I band”, which is rich in actin, changes. This suggests that length of the myosin remains the same, whereas actin slides past myosin. At the lateral ends of each sarcomere “z bands” are located to which actin is tethered, hence the shortening of actin leads to shortening of sarcomeres and consequently contraction of the muscle. There are some other proteins such as titin in the structure of sarcomere too, which control the passive force of the muscle rather than the contractile force and troponin and tropomyosin which have a crucial role in muscle contraction. However, this thesis provides an overview of the muscle contraction and detailed study of muscle function in molecular level is out of the scope of this thesis.

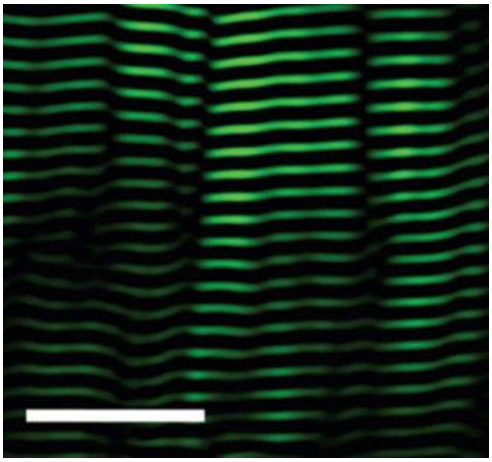

Figure 1.14 Gastrocnemius muscle of the mouse with striped pattern of sarcomeres, band-pass-filtered SHG (second harmony generation) images acquired using a 350-mm-diameter microendoscope and a laser-scanning microscope. The myosin rods are artificially coloured green, and appear as stacked horizontal stripes of similar lengths. The black gaps in between the greed myosin rods are Z-disks mitochondria (White scale bar = 25 µm.)(see Llewellyn et al., 2008 for more details).

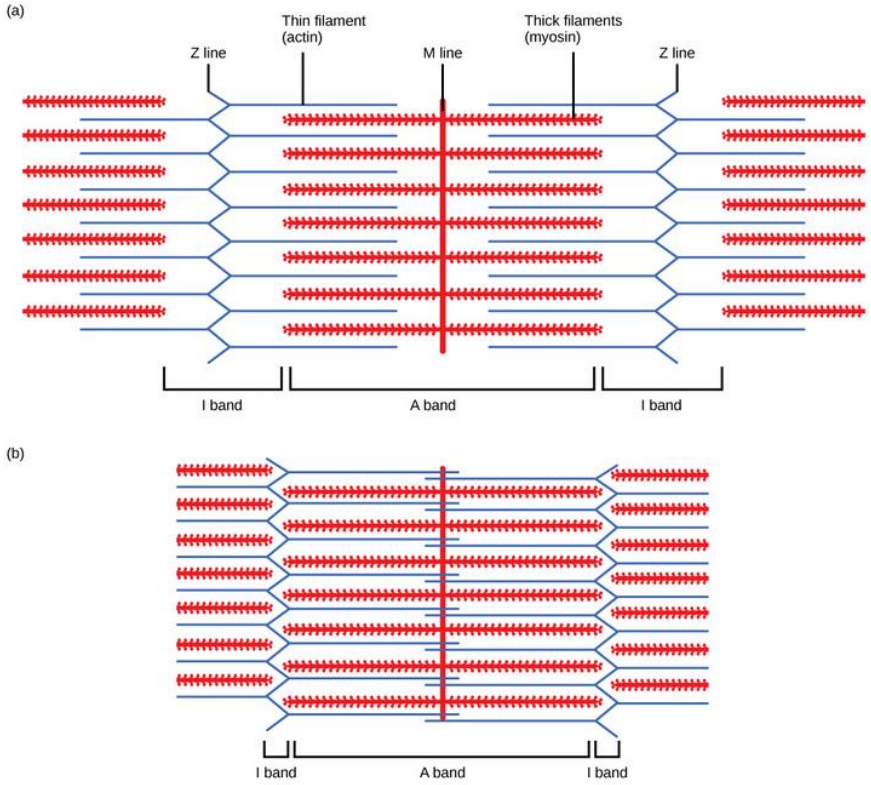

Figure 1.15 Basic organization of a sarcomere sub-region, showing the centralized location of myosin (A band). When (a) a sarcomere (b) contracts, the Z-lines (band) move closer together and the I-band shortens. The width of A-band remains the same and, at full contraction, the thin filaments overlap. (cnx.org accessed on 09/09/2014)

Intrinsic physical properties of muscles, in particular force-length and force-velocity properties, have commonly been used in biomechanical modelling. Force-length relationship describes the maximal force of muscle depending on its length, and is related to the force that is released through cross-bridge. Each cross-bridge is assumed to generate the same amount of force. In addition, the movement of the myosin over actin is constant (14.3 nm, Herzog, 1994). Although length of the thick filament appears to be consistent among vertebrates (about 1.6 μm), the length of thin filaments, however, varies among different species and even among different muscles. Hence the generated force in sarcomeres varies among species, which affects force-length properties between the muscles (Herzog, 1994) (Figure 1.16). Moreover, relations of maximum muscle force and its instantaneous rate of change in length is described in the force-velocity relationship. This simply is the fact that energy consumption increases with increasing speed of muscular contraction (Figure 1.16). The maximum rate of produced work which is the peak power is developed at around one third of max contraction velocity and the peak efficiency of the mechanical work is at slightly lower velocity (Herzog, 1994).

Skeletal muscles are organized in motor units which are a group of muscle fibres and a motor neuron. The contractile force in a motor unit, among other parameters, depends on the number of fibres activated. Thus a small motor unit in a small muscle might consist of only few fibres and provides great control of movement, whereas a motor unit in a large muscle can contain thousands of muscle fibres and generate great force. Hence another factor in force generation of a muscle is number of fibres activated. Assuming all the sarcomeres have the same stress-strain curves, force will be a function of number of parallel fibres which can be approximated as the cross-section of the muscle. Although the anatomical cross sectional area is a good approximation for the parallel fibred muscles, it underestimates the number of fibres in pinnate muscles. Pinnate muscles are muscles in which the muscle fibres are positioned at an angle relative to the muscle tendon. A more accurate approximation of the number of muscle fibres is known as physiological cross sectional area (PCSA) of the muscle and is calculated as ratio of the muscle volume to the length of the muscle fibre (Alexander and Vernon, 1975).

In a parallel fibered muscle, PCSA is approximately equal to the anatomical cross sectional area. However PCSA is larger than the anatomical cross sectional area in pinnate muscle.

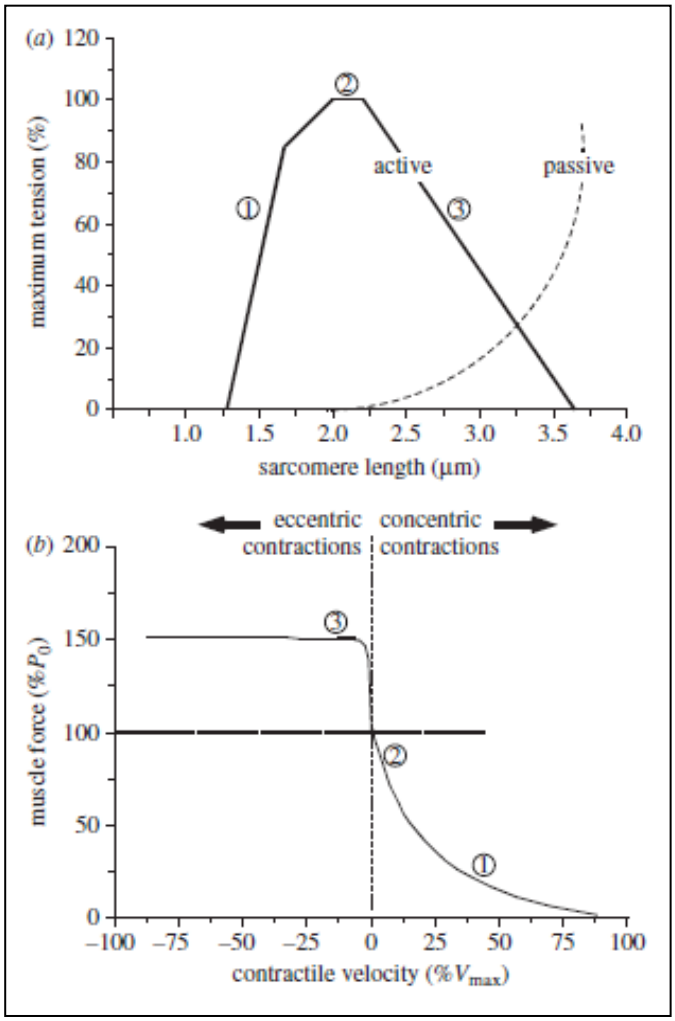

Figure 1.16 Basic biomechanical properties of skeletal muscle, higher: force-length relation; lower: velocity-length relations (Lieber and Ward, 2011).

The length change of a muscle is directly related to number of sarcomeres in series which means fibre length. So comparing two muscles with the same volume, but different fibre length, both will have the same strain; but the muscle with longer fibres has the higher capacity for length change. If we assume sarcomeres in both have the same force-velocity properties, peak strain rate will be the same for both of them. In addition, because both muscles have the same volume, they have equal number of cross bridges, and consequently equal peak power. But the muscle with longer fibres will provide this peak force in higher velocity because it has longer

fascicles. On the other hand muscle with shorter fibres provides higher force. Thus the muscle with longer fibres can contract more rapidly and it proves that it is more suitable for rapid movements (Wilson and Lichtwark, 2011).

1.3.2 Muscle architecture

When considering muscle function it is also necessary to study muscle architecture, which is the number and orientation of the muscle fibres within the muscle. Although the fibres in one fascicle are parallel, arrangement of fascicles in the entire muscle can vary. Thus, muscles are classified as parallel-fibre, fusiform, pinnate, convergent, or circular muscles. Parallel-fibred and fusiform muscles are both formed with fascicles that are arranged along the line of muscle force action, with parallel-fibered muscles shaped as a strap and fusiform muscles shaped as a spindle. In pinnate muscles which look like a feather, fascicles are attached to the tendon at an angle and can be further grouped into uni-pinnate, bi-pinnate and multi-pinnate muscles. Pinnate-fibered muscles have shorter fibres than parallel-fibered and fusiform muscles that extend at an angle along the length of the muscle. Convergent muscles are fan-shaped and broad at origin and converge to a small attachment area at the insertion. Circular muscles are formed from fibres that are arranged around an opening and their contraction results in decrease of opening, e.g. orbicularis oris muscle of the mouth. Except for circular muscles, the classification of muscles is not very exact, as muscle architecture in each muscle is unique and many muscles do not fit only in one class and have a combined structure with a tendency towards one of these architectures (Zatsiorsky and Prilutsky, 2012).

As it was mentioned earlier, maximal force generation in each muscle, which is estimated using PCSA value, is a factor of volume and muscle fibre length. In muscles that the fibres are orientated at an angle to the muscle tendon, an additional factor becomes important in estimation of force generation: pinnation angle. Pinnation angle is the angle that forms between the muscle fibres and the muscle tendon. On one hand, shorter fibres of pinnate-fibred muscles results in higher PCSA value and force generation. Pinnate muscles enable higher number of cross bridges which leads to higher force generation (Anapol and Barry, 1996). On

the other hand, contraction of pinnate fibres, which are attached to the tendon, generates a force at an angle to line of action of the muscle. Hence, effective force of each fibre is a component of generated force that is parallel to the line of action. This results in reduction of the force generation in the muscle.

Moreover force/length and velocity/length relationships of the muscle is not only dependent on the fibres, but also on pinnation angle and properties of the central tendon to which muscle fibres are attached.

1.3.3 Morphology of masticatory muscles

Masticatory muscles are classified into two functional groups: jaw closing and jaw opening muscles. Jaw closing muscles, also known as jaw adductors, are complex, sub-divided and inter-connected and are considerably larger than jaw opening muscles, also known as depressors. Masticatory muscles can activate either synergistically or antagonistically to produce forces to move the mandible, control its movement and provide occlusal or bite force. Moreover masticatory muscles counterbalance other forces that are applied to the mandible, as discussed previously.

In rodents, protractive muscles are well-developed due to the need for substantial anterior translation of the mandible to occlude incisors in incision and molars in chewing. Also the arrangement and functional division of the muscles are such that they control and stabilize the movement of the mandible, to manage the lack of a strong joint capsule or ligament (Hiiemae, 1967).

Six muscle groups are identified in the masticatory system of the mouse: five jaw closing muscles and one jaw opening muscle. The two largest adductor muscles are the masseter and the temporalis which compose of at least three and two sub-divisions respectively (for jaw closing muscles see Table 1.1). The external and internal pterygoid muscles are the other two adductor muscles identified in the mouse. The only jaw opening muscle is the digastric.

Table 1.1 Muscle volumes and percentage of overall volume in the mouse, (Baverstock et al., 2013).

Muscles		Muscles volumes (mm^3)	Percentage of overall muscle volume of adductors
Masseter	Superficial	64	19.13
	Deep	100	33.32
Zygomaticomandibularis	Infra-orbital		8.08
	Anterior	25	
	Posterior		
Temporalis	Anterior	60	22.44
	Posterior		
External pterygoid		10	4.74
Internal pterygoid		32	11.56

In the masticatory system of omnivores with antereoposterior movement, including the mouse, the masseter and internal pterygoid are more emphasized compared to carnivores in which the temporalis muscle is more dominant (Herring, 2007).

Jaw closing muscles

Masseter

The masseter in rodents is enlarged and has high mechanical advantage which makes it the most important adductor muscle in producing a bite force (Hiiemae, 1971a, Satoh, 1998). The masseter is made of at least three sub-divisions; superficial masseter, deep masseter and zygomaticomandibularis.

The superficial masseter is a uni-pinnate muscle which is made of two parts; the tendon sheet and the bulk of the muscle. The origin of the tendon sheet is below the infraorbital foramen which ends to the muscle bulk that runs diagonally to the angular process (Figure 1.6 and Figure 1.9). The superficial masseter is triangular in shape which joins the anterior part of the cranium to the posterior part of the

mandible, covering almost half of the underling deep masseter. The muscle fibres insert on both lateral and medial sides of the angular process covering slender medioventral and lateroventral ridge of the mandible all the way up to a point ventral to the first molar (see Figure 1.17).

The superficial masseter is the prime transitional mover of the mandible. It also functions to elevate the mandible in the protracted position, and acts as the regulator of the mandibular position during the incisor power stroke and chewing (Hiiemae, 1971a). In rodents the superficial masseter muscle is enlarged due to adaption to the considerable anterior translation of the mandible that is required to engage the incisors. Moreover, the large anterior component of the power stroke during chewing may contribute to its enlargement. Thus to power these translational movements most efficiently, a large and horizontal masseter is needed (Hiiemae, 1967).

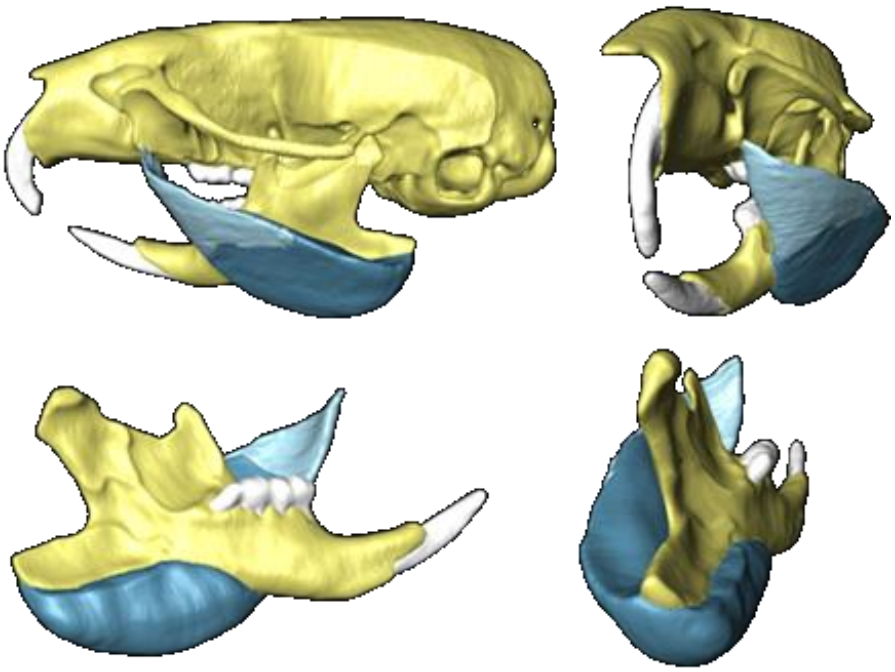

Figure 1.17 Superficial masseter in *Mus musculus*. The pale blue represents the tendon sheet of the superficial masseter and the dark blue represents the deep masseter muscle (adapted from Baverstock et al., 2012)

The deep masseter, which is the largest muscle in the mouse, originates from the vento-lateral surface of the zygomatic arch and inserts into the lateral surface of

the mandible (Figure 1.6 and Figure 1.9). Its shape is like a parallelogram and unlike other rodents, it is reported as one single muscle with no distinct sub-divisions (Baverstock et al., 2013). The muscle fibres run posterioventrally and insert on a considerable proportion of the lateral side of the mandible, just above the attachment area of the superficial masseter (see Figure 1.18).

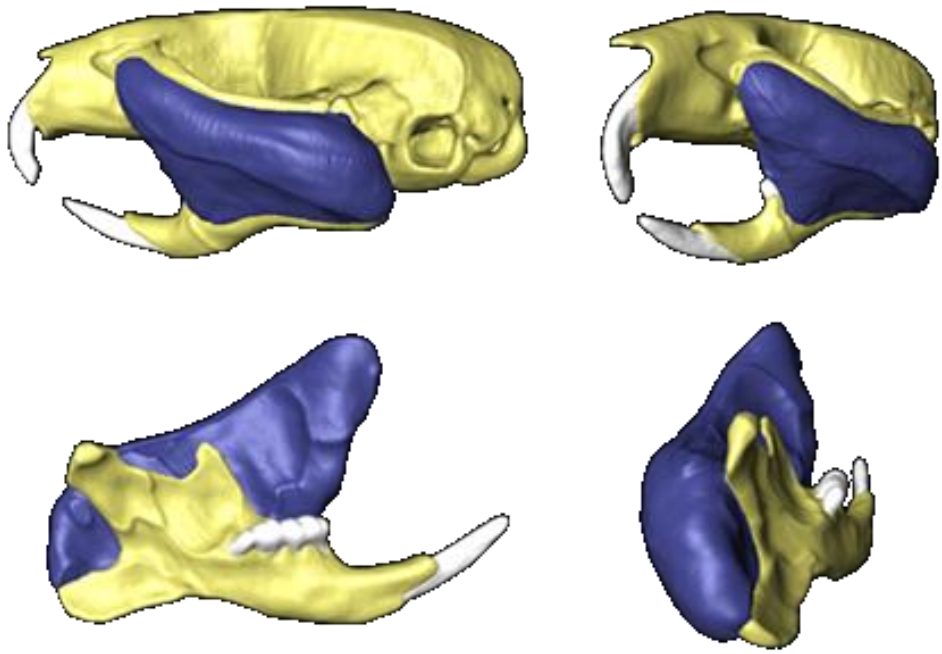

Figure 1.18 Deep masseter in *Mus musculus* (adapted from Baverstock et al., 2013)

The deep masseter has the largest dorsoventral component of the masticatory muscles (Satoh, 1997). This suggests that the deep masseter has a significant role in elevation of the mandible during free movement, as well as in producing the bite force, particularly during the power stroke of chewing (Hiiemae, 1971a). It also has a considerable anterior component, which suggests it is involved in protraction of the mandible in the power stroke of incision together with the superficial masseter. As discussed previously, the lateral component of the deep masseter also places the hemi-mandibles in tension, which can be counterbalanced in part by the medial component of the internal pterygoid (Hiiemae, 1971a, Satoh, 1998).

Zygomaticomandibularis

The zygomaticmandibularis is a slim, short muscle which lies medial to the deep masseter. In a number of rodent studies, the zygomaticomandibularis is classified as a subsection of the masseter (Hiiemae, 1971b, Byrd, 1981, Satoh, 1997, Satoh, 1998, Satoh, 1999) and is addressed as medial masseter (Wood, 1965, Woods, 1972, Hautier and Saksiri, 2009). However, other studies have proposed that it should be classified as a separate muscle because a distinct division is observed between it and the deep masseter in some rodents, including the mouse (Turnbull, 1970a, Weijs, 1973, Cox and Jeffery, 2011, Baverstock et al., 2013). In order to be consistent with previous studies, particularly with the most recent studies regarding the morphology of the mouse masticatory system, the nomenclature zygomaticmandibularis is used in this research.

The zygomaticmandibularis consists of three different sections: anterior, posterior and infraorbital parts. The muscle takes its origin from the dorso-medial surface of the zygomatic arch, and inserts into the lateral surface of the mandible, dorsal to the attachement of the deep masseter (Figure 1.19).

The anterior zygomaticomandibularis, which is the largest part of the three, takes its origin from the mediodorsal edge of the zygomatic arch, anteriorly from the medial surface of the squamosal plate to the suture of the zygomatic arch posteriorly (Figure 1.6). It runs ventrally and inserts on the lateral surface of the mandible just dorsal to the attachement area of the deep masseter, anteriorly from the mid-point of the first molar to coronoid process, sparing the tip of the coronoid process (Figure 1.9).

The infraorbital zygomaticomanibularis accounts for one third of the muscle's mass. It originates from a concavity in the maxilla, ventral to the nasal bone and runs postreioventrally to attach on the lateral side of the mandible (and Figure 1.19). It attaches ventral to M1, via a thick tendon, onto the mandible, anterior to the attachemet of the deep masseter and dorsal to the attachement of the superficial masseter (Figure 1.9).

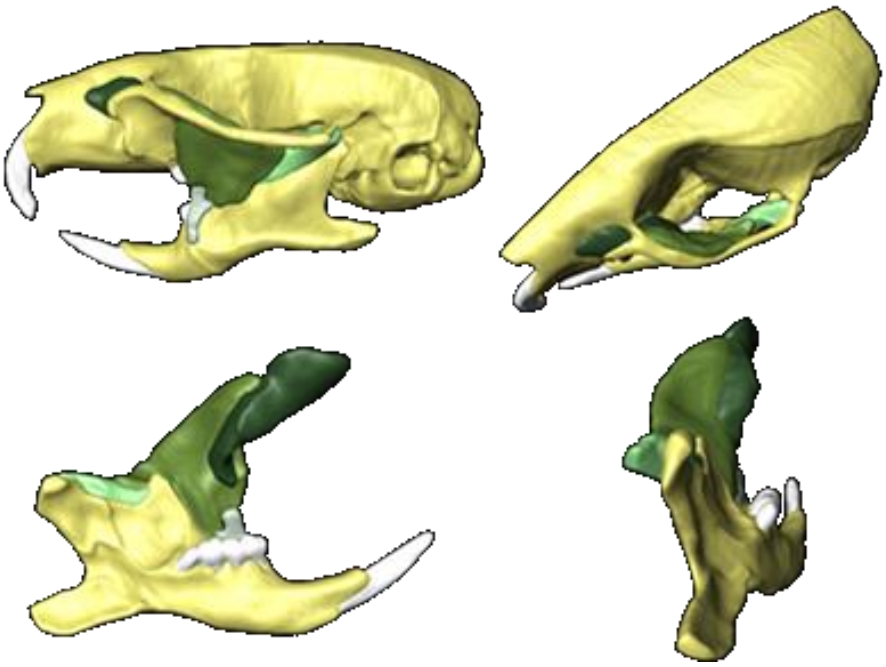

Figure 1.19 Zygomaticmandibularis in *Mus musculus* (adapted from Baverstock et al., 2013)

The posterior zygomaticomandibularis, which is the smallest of the three parts, originates from the posterior border of the zygomatic arch (Figure 1.6), and runs anteroventrally to insert on the point with the greatest curvature between the condylar and coronoid process (Figure 1.9).

Temporalis

The temporalis is the second largest masticatory muscle in the mouse. In carnivores with hinge-like TMJs, this muscle is the most prominent masticatory muscle (Hiiemae, 1971a). In the mouse, it has a large dorsoventral component, indicating that it is involved in jaw elevation. It also has considerable posterior component, making it the major retractor of the mandible.

The temporalis muscle is divided into at least two parts which again have been referred to with different terminology: medial and lateral parts (Baverstock et al., 2013), and more commonly as anterior and posterior parts (Turnbull, 1970b, Hiiemae and Houston, 1971, Gorniak, 1977, Woods and Howland, 1979, Druzinsky, 2010a, Druzinsky et al., 2011). To be consistent with the most commonly used form in the literature, anterior and posterior terms are used here. Moreover, they do

reflect the anatomical positions of the muscles more accurately. In addition, some other studies have identified a third part of the temporalis, called the suprazygomatic temporalis (De Gueldre and De Vree, 1988, Druzinsky, 2010a, Druzinsky et al., 2011).

The posterior temporalis originates from a large area on the lateral side of the temporal bone, and extends from the posterior border of the temporal fossa in the cranium to the posterior border of M1. It passes medial to the zygomatic arch and inserts on the medial part of the mandible. The anterior temporalis takes its origin from the temporal fossa, anterior to the origin of the medial temporalis. Baverstock et al. (2013) have only identified these two parts in their observations.

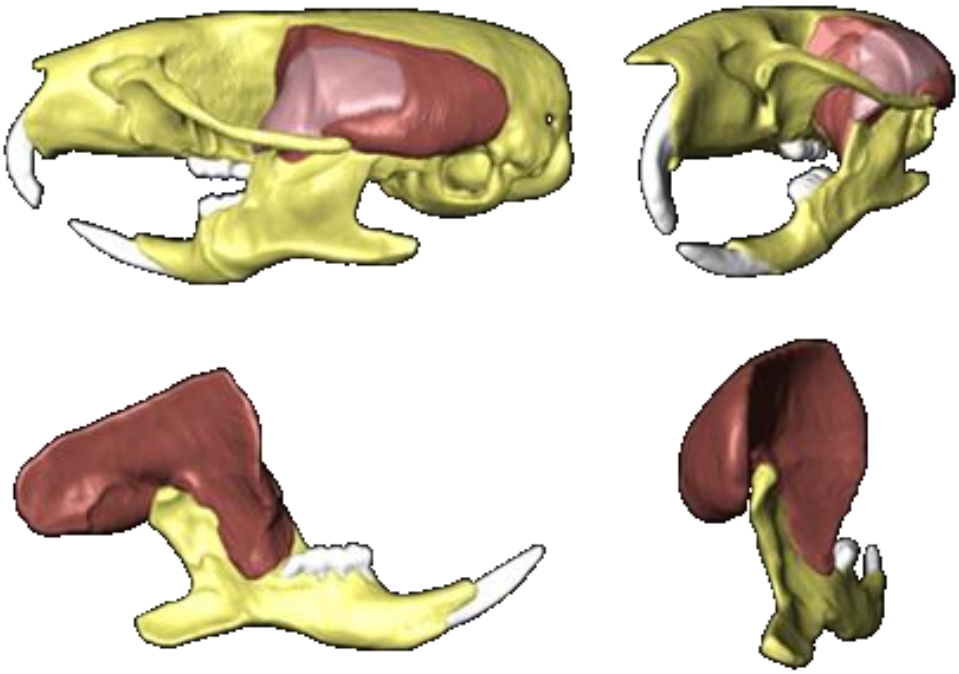

Figure 1.20 Posterior (red) and anterior (pink) temporalis muscles in *Mus musculus* (adapted from Baverstock et al., 2013)

The anterior and posterior parts of the temporalis muscle are reported to function independently, with their muscle fibres aligned anteroventrally, suggesting that they both have important roles in elevation and retraction of the mandible. Indeed, the anterior and posterior temporalis are the only two retractive muscles present in the masticatory system of rodents, including the rat and the mouse (Hiiemae

(1971a); who, similar to Baverstock et al. (2013), did not recognize the suprazygomatic temporalis as a separate part). The anterior temporalis has a larger vertical component than horizontal, indicating it is involved primarily in mandible elevation. Thus it can stabilize the mandible horizontally and vertically, and elevate it during free movement and the power stroke of chewing (Hiiemae, 1971a). In contrast, the posterior part has larger horizontal component than vertical, suggesting its prime role is in retraction of the mandible, both to facilitate molar occlusion and food grinding (Hiiemae, 1967). Also, the posterior temporalis plays an important role in stabilizing the condyle in the glenoid fossa during the incision phase (Satoh, 1998).

The suprazygomatic temporalis, which wraps around zygomatic plate, only has very small vertical component and moment arm. Hence it is not efficient in the elevation of the mandible, and is mainly involved in retraction of the condyle.

The Pterygoids

The pterygoid muscles are the only two muscles with significant mediolateral components. The internal pterygoid, which is considerably larger than its external counterpart, originates from the pterygoid fossa, medial to the attachment area of the external pterygoid (Figure 1.21). However, even though it is larger, its cranial attachment area is half the size of the latter (Baverstock et al., 2013). The muscle fibres are aligned posteroventrally and medially and insert onto the angular process of the mandible, just dorsal to the attachment area of the superficial masseter. The internal pterygoid controls the position of the angular process and limits the hemi-mandibles from rotating laterally around their long axis due to the lateral component of the masseter (Hiiemae, 1967).

The external pterygoid, which is the smaller of the two, originates from the cranial base and runs to the medial surface of the condylar process (). Its fibres are orientated ventrolaterally and its insertion is very close to the TMJs, which results in a very small lever arm. Hence the external pterygoid is not well suited for moving the mandible; instead it is effective at controlling the position of condyle against the glenoid fossa (Hiiemae, 1967).

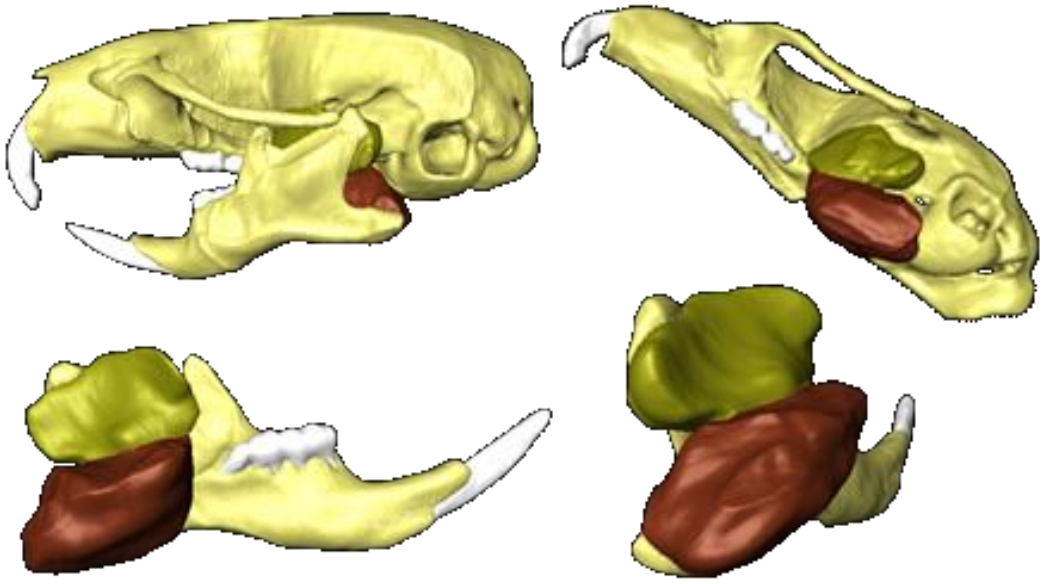

Figure 1.21 External (yellow) and internal (red) pterygoid muscles in *Mus musculus* (adapted from Baverstock et al., 2013)

Jaw opening muscle

Digastric

The digastric muscle, which consists of anterior and posterior bellies, is the only jaw opening muscle. The head of the anterior belly is attached to the anterior point of the mandible, just inferior to the symphysis. The posterior part composes of two separate parts, which attach to the posterior part of the cranium, just ventral to the paraoccipital process, anterior to the occipital condyle.

Digastric activates twice during one cycle of biting. It activates first during jaw opening, and then again, in a minor role, during the latter half of masseter activation in the middle of the jaw-closing phase of chewing (Kobayashi et al., 2002b), and grinding of food (Cobos et al., 2001). It is thought that this secondary activation is to antagonise elevation produced by posterior temporalis and superficial masseter (Hiiemae, 1967).

1.4. Phases of mastication

From a biomechanical point of view, mastication is divided into two phases; incision and chewing. Although there is a third phase involved in a complete masticatory cycle, known as deglutition or swallowing, in this study only incision and chewing are considered.

Incision is the process when ingestion of the food takes place, the incisors are in contact with the food item, resulting in separation of a piece of the food. Chewing is when the separated food is transferred to the molar region for further size reduction. Ingestion typically consists of 1 to 3 cycles, whereas chewing might consist of 3 to 40 cycles in rats (Weijs, 1975). As stated by both Hiiemae (1967) and Kobayashi et al. (2002b), there is an obvious change in both amplitude and rhythm of the cycles from incision to chewing. Thus the jaw kinematics change from fast and small movements during incision, to slow and large-amplitude movements during chewing (Hiiemae and Ardran, 1968, Kobayashi et al., 2002b).

Both incision and chewing cycles initiate from the rest position, which is a reproducible, symmetrical position of the mandible in which neither molars, nor incisors are in contact. At the rest position, the tips of the lower incisors are located posteriorly and slightly superiorly to the upper ones, whereas the lower molars are located separate from and anterior to the upper molars. In the rest position, the condyle is in contact with the intermediate part of the glenoid fossa (Hiiemae, 1967).

There are three steps involved in both incision and chewing (Popwics and Herring, 2006):

1) Preparatory stroke consisting of opening of the mouth and simultaneous transportation of the food.
2) Relatively rapid closing movement of the jaw, which terminates as the teeth contact the food item (fast close, FC).
3) Closing of the jaw against the food resistance, called the power stroke.

The preparatory stroke during incision consists of depression and protraction of the mandible, whereas for chewing, it involves depression and retraction of the mandible. During the power stroke of both incision and chewing, elevation and protraction of the mandible occurs (Hiiemae and Ardran, 1968).

Incision in rodents involves symmetrical movements in the sagittal plane, resulting from symmetrical muscle activations. In muscles with a transverse component, such as the internal and external pterygoid, the transverse component of the force of one side is counteracted by its counterpart on the opposite side. Hence the resultant force lies on sagittal plane (Satoh, 1998).

In most mammals, chewing occurs on one side of the jaw at a time (the working side). However, because the molars in some rodents, including the mouse and the rat, are located in such a way that simultaneous occlusion of both sides is possible, bilateral chewing is feasible. Hiiemae and Ardran (1968) pointed out that in the rat, either chewing is bilateral or switching between working and balancing sides is so fast that it is difficult to detect. They concluded that although bilateral chewing occurred occasionally, the rat often chewed on one side only and switched to the alternate side. On the other hand, Weijs (1975) stated that chewing in the rat was often bilateral, and the rami of the mandible remained symmetrical in the sagittal plane. When bilateral chewing does occur, both halves of the mandible move medially and anteriorly during the power stroke, resulting in small reduction of the angle of the rami.

1.5. Kinematics of incision and chewing

If the dynamic movement of the mandible is divided into a sequence of many static intervals, the orientation and mechanical advantage of the muscles will vary in each interval due to its different position and orientation. Hence an understanding of mandibular kinematics is essential to study the biomechanics of the masticatory system.

Mandibular movement involves movement along three principal planes: a horizontal or antero-posterior movement (normally referred to as translation), a

vertical or open-close movement (referred to as rotation), and a transverse movement. There is great diversity in the relative importance of these types of movements in different species. In herbivorous animals, translation of the mandible is important because of grinding. In contrast, in carnivores, rotation is more important and the TMJ works like a hinge joint, with the bony process of the glenoid fossa preventing the translational movement of the mandible (Popwics and Herring, 2006). In rodents, the mandible has both translational and rotational capabilities. The translation of the mandible is important for two main reasons: firstly, the mandible must move anteriorly in order to put the incisors into occlusion; secondly, food grinding requires anterior sliding of the mandibular molars against the cranial molars (Utsumi et al., 2010).

Masticatory kinematics of many rodents, including the mountain beaver, woodchuck, large field mouse, red back vole, golden hamster and rat, have been studied previously (Druzinsky, 1995, Satoh, 1998, Gorniak, 1977, Hiiemae and Ardran, 1968, Weijs, 1975). Although Kobayashi et al. (2002a) reported on the kinematics of the mouse during incision, they reported little information about the movements of the mandible. In contrast, precise movements of the mandible of the mouse have been reported by Utsumi et al. (2010) during chewing. No studies have been undertaken to compare the kinematic behaviour of the mouse to other rodents, and because of the size differences, application of their kinematics to the mouse needs to be undertaken with caution. Nevertheless, notwithstanding that reservation, the incisal kinematics of the rat, the most similar species to the mouse, is considered in this current study, while Utsumi's published kinematics are used for chewing.

1.5.1 Kinematics of incision

Incisal biting of mountain beaver and woodchuck has been investigated by Druzinsky (1995), while Satoh (1998) studied incision in the large field mouse (*Apodemus speciosus*) and red back vole (*Clethrionomys*), but focussed on muscle force and mechanical advantage rather than quantitative kinematics. Similarly, the kinematics of the mouse during incision was studied briefly by (Kobayashi et al.,

2002a), but the reported primarily on the rate and frequency of the biting cycles rather than mandibular movements. The closest species to the mouse, whose kinematics have been studied, is the rat (*Rattus norvegicus)*. Hiiemae and Ardran (1968) studied chewing and incision of the rat (*Rattus norvegicus*), but presented more qualitative than quantitative kinematics. Weijs (1975) also studied the kinematics of an albino rat (*Rattus norvegicus)* and did present detailed quantitative data. Although the morphology of masticatory system of the rat shows considerable similarity to the mouse (Kobayashi et al., 2002a), the scale of their kinematics is obviously different, and hence only a qualitative description of the kinematics of the rat incision is presented here.

For incisal biting in the rat, there is a simultaneous depression and anterior movement of the mandible in a preparatory stroke. This movement can be as large as 40° of rotation for bulky food items. During opening, the angular velocity of the mandible builds up quickly, then remains constant in the first half, while it decelerates in the latter half of the opening phase until it reaches zero (when the mandible stops to change direction). The opening phase is associated with anterior movement of the condyle, while the angle between two hemi-mandibles remains constant. This is followed by elevation and protraction of the mandible during the incisive stroke, and finally a recovery stroke which comprised of simultaneous retraction and elevation of the mandible to locate the lower incisors posterior to the upper ones.

1.5.2 Kinematic of chewing

Kinematics of chewing has been investigated in a few rodents. Gorniak (1977) studied simultaneous mastication kinematic and muscle activation of the golden hamster, while chewing kinematics of *Rattus norvegicus* have been investigated by Weijs (1975) and Hiiemae and Ardran (1968). However, until recently there was not possible to track the jaw movement and obtain kinematics data for the mouse. A group of researchers developed a novel three dimensional tracking system that was attached to the head of the mouse to track the relative movements of the cranium and the mandible (Koga et al., 2001). The system consisted of four magnetic sensors

positioned above the head and a magnet that was attached to the mandible (Figure 1.22).

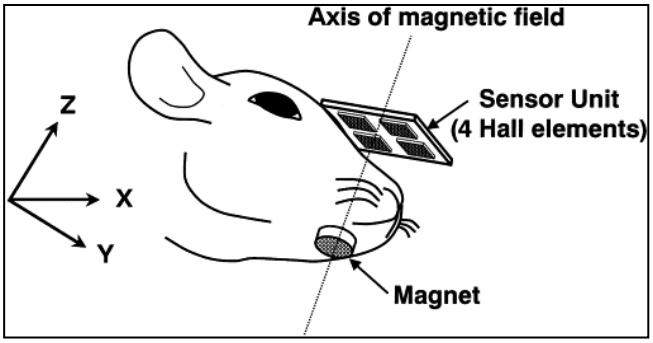

Figure 1.22 Arrangement of sensor unit and magnet. X–Y plane: parallel to occlusal plane. X–Z plane: parallel to mid-sagittal plane. Z-axis: parallel to axis of magnetic field (Koga et al., 2001)

The magnet was attached to the midline of the anterior part of mandible, inferior to symphysis, with the whole system being small enough to be implanted on the mouse head and sensitive enough to detect very small displacements. The advantage of the system was that the mouse could move freely and thus the feeding behaviour and movement of the mouse was unaffected while obtaining the kinematic data. Kinematic data for mastication of soft and hard food was collected from 21 male C3H/HeJJc1 mice.

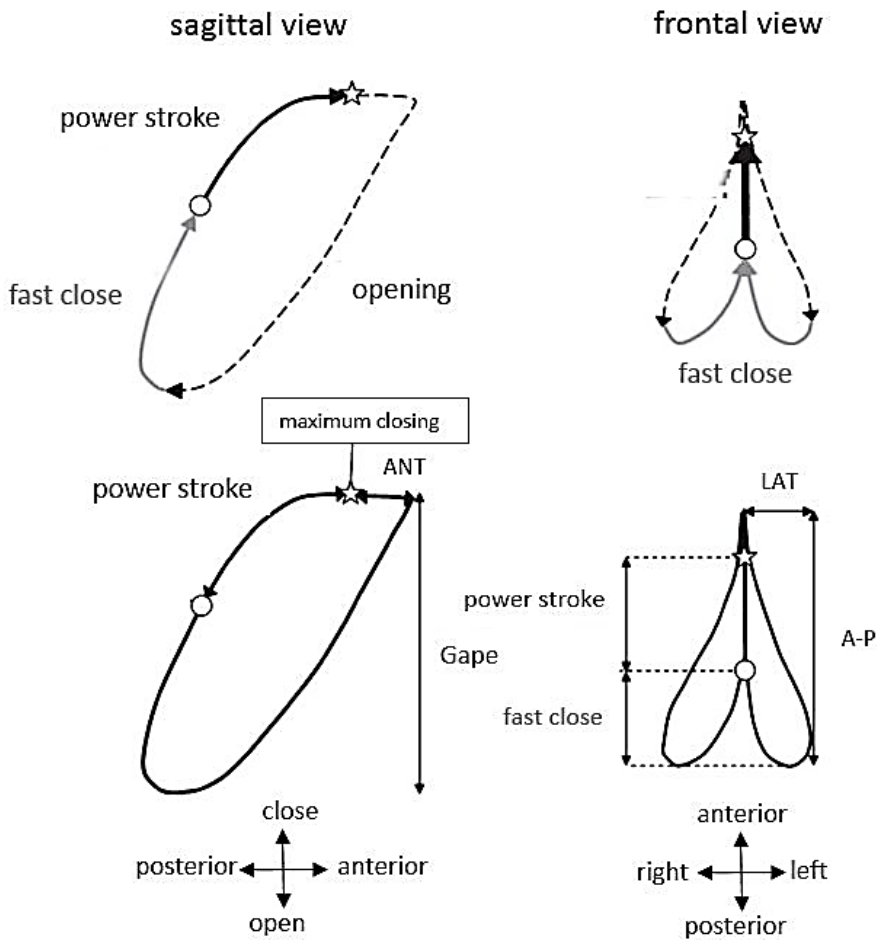

Figure 1.23 Upper tracings: phase analysis of jaw movement. Dotted line, grey solid line and black solid line indicate: opening phase, fast closing phase and power stroke phase, respectively. Each arrow indicates the direction of jaw movement. The open circle represents the point on which power stroke initiates and the open star represents maximum closing; lower tracings: lines with arrows show the distances measured. Gape: gape size; LAT: lateral excursion; ANT: anterior excursion in opening phase; A-P: antero-posterior excursion, adapted from Utsumi et al. (2010). The position of the tracker was the midline of the anterior of the mandible (see Figure 1.22)

The opening phase starts with an initial protraction of the mandible (mean value of 346 and 292µm for hard and soft food respectively, see Table 1.2), followed by retraction and depression (see Figure 1.23). Also there is a lateral movement of the mandible during the opening phase. The bite gape, *i.e the* vertical displacement of the mandible, is reported with a mean values of 1187 and 1303µm for hard and soft food respectively.

Table 1.2 Comparison of jaw movements between hard and soft food chewing. Values are presented as S.E.M. of each group. See the legend of Figure 1.23 for further details. Redrawn from Utsumi et al. (2010).

	Gape (µm)	LAT (µm)	Power stroke excursion (µm)	ANT (µm)	A-P (µm)	Fast close /A-P (µm)	Power stroke /A-P (µm)
Hard food	1187±43	356±101	710±32	346±20	1366±46	422±54	598±24
Soft food	1303±52	347±112	476±46	292±19	1246±44	610±42	344±26

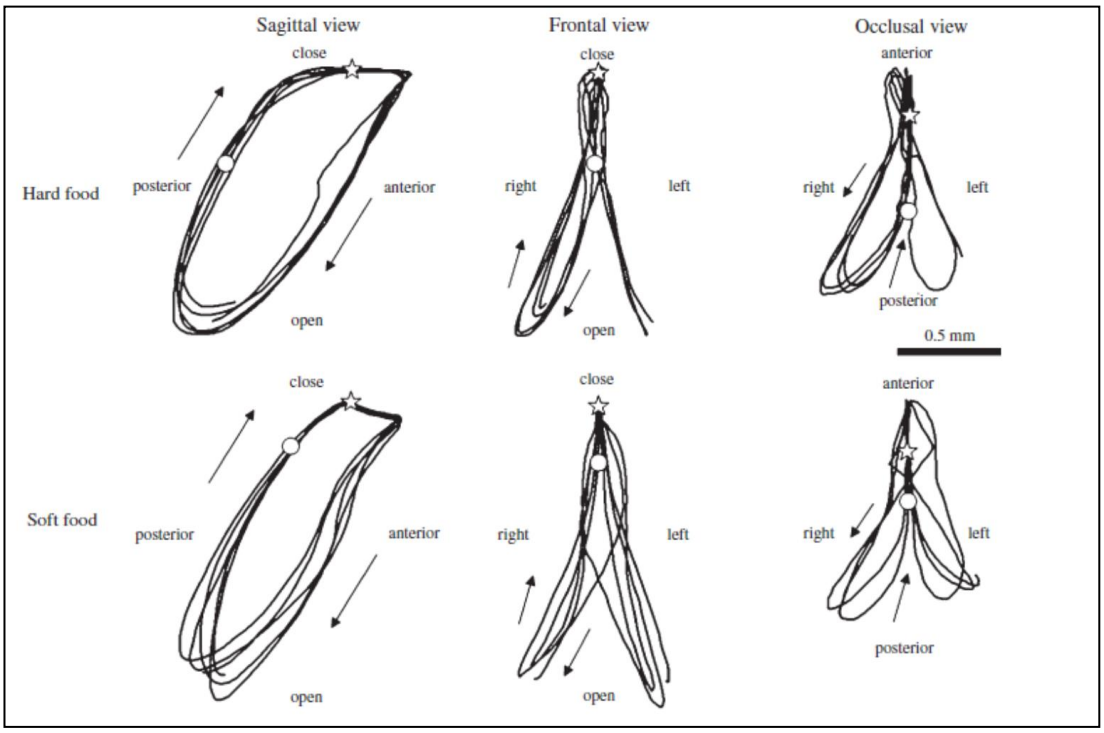

Figure 1.24 Jaw movement trajectories in the sagittal, frontal and occlusal plane. Upper tracings: chewing of hard food; lower tracings: chewing of soft food. Tracings show five consecutive chewing cycles superimposed. The open circle represents the point on which power stroke initiates and the open star represents maximum closing (Utsumi et al., 2010).

Jaw closure starts with a fast closing phase, consisting of an arched anterior movement in the sagittal plane, and a medial movement in the occlusal plane. As expected and shown in Figure 1.24, the main difference between chewing hard and

soft food is observed during the closing phase. In hard food chewing, initiation of the power stroke occurs earlier, so the jaw contacts the food item earlier. Consequently, anterior movement during the power stroke is larger than with soft foods. In rodents grinding occurs with anterior sliding of the mandibular molar against the cranial molars. Therefore larger anterior movement of the mandible while chewing hard food provides a higher level of grinding (see occlusal view of Figure 1.24).

The transverse component of the jaw movement included a lateral movement during opening and a medial movement during closing of the jaw. This transverse movement was switched alternatingly between left and the right side of the jaw. However, note that the power stroke phase of chewing in the mouse does not involve any transverse component, and consists only of protraction and elevation of the mandible (occlusal and frontal views in Figure 1.23).

1.6. Biomechanical modelling of masticatory system

Masticatory system is a complex biomechanical system which composes of the cranium, the mandible, muscles and joints with multiple degrees of freedom between the two former parts. Masticatory muscles originate from the cranium and insert to the mandible and their interaction results in force production in contact areas i.e. TMJ and biting points. Relative movements of the cranium and the mandible results in varying muscle orientations, and as a consequence muscle forces, bite force and joint reaction forces change too. Hence, in order to fully understand the function of the masticatory system, many variables ought to be simultaneously studied at every stage of the jaw movement, for example muscle forces, joint reaction forces etc. Obtaining large number of experimental variables simultaneously is difficult, if not impossible.

Biomechanical modelling can be used as an alternative way to understand different aspects of masticatory function. Initial biomechanical models were mainly 2D over-simplified static mathematical models, majority of which overlooked not only mediolateral component of the system but also kinematics, which are both

important in understanding of masticatory muscles' function. Multibody dynamics analysis (MDA) is a relatively new approach which is suited to study such complex dynamic biological systems and their function. MDA is a 3D computer modelling technique that provides the means to analyse relative movements of the mandible and the cranium and clarify the relationships between muscle structure and function. Once only available through complex manual mathematical calculations, multibody dynamic modelling techniques are nowadays more accessible for biologists and biomechanists through specialised computer software (e.g. ADAMS LIFEMOD (LifeModeler, Inc.), ANYBODY (AnyBody Technology, Aalborg, Denmark), SIMM (MusculoGraphics, Inc.)), therefore are more commonly used to analyse complex biological systems.

MDA is the mechanical analysis of rigid body movements in which multiple bodies undergo very little deformation and are constrained at joints and/or contacts. There are internal and external forces acting on the system, e.g. in the case of masticatory system muscle forces and bite forces respectively. Mechanical analyses of different bodies i.e. the cranium and the mandible, muscles, tendons, ligaments and temporomandibular joints can be performed in MDA. The position of these anatomical features is defined by landmark data. In addition, mechanical behaviour of anatomical features can be incorporated in the model through defining appropriate material properties. The equations that are used in MDA are based on classical mechanic and Newton's law with some re-formulations such as Newton-Euler and Euler-Lagrange approaches. For more details about multibody dynamic equations and solutions see Shabana (2005) and Otten (2003).

The masticatory system of different vertebrate species, including a number of mammals, has previously been modelled using MDA (Koolstra and van Eijden, 1992, de Zee et al., 2007, Iwasaki et al., 2003a, Curtis et al., 2008, Moazen et al., 2008b, Curtis et al., 2010a, Shi et al., 2012, Gröning et al., 2013b, Watson et al., 2014). MDA models can be developed for several motivations, for example, to understand muscles function trough prediction of muscle activation pattern, to study the effect of muscle factors on the function of the masticatory system, to explore the kinematics of the mandible, and to predict loading in joints and bite points.

Like any other dynamic problem, there are two approaches to solve multibody dynamic problem; forward and inverse approaches. In the forward approach the internal forces acting on the system are known, from which rigid body motions and/or external forces are derived. This approach is not as effective in musculoskeletal systems and in particular masticatory systems in most cases, considering the muscle forces are internal forces, because: 1) measuring multiple muscle forces which are formed in different layers is not easily achieved experimentally, and 2) estimating the effect of change of one of these forces on the forces and kinematics of the rest of the system is very difficult. Hence the inverse approach is used to model masticatory systems in general, in which kinematics and external forces are used to derive internal forces, i.e. in this case muscles activation pattern. Moreover, a combination of inverse and forward dynamic approaches is also feasible and useful (Otten, 2003), which is the case in one part of this study, using kinematics and internal forces to predict maximum bite force in one part of the study. In other parts of this thesis, the inverse approach was employed in which bite force and kinematics were used to predict muscle activation pattern.

In dynamic solutions of such a complex system as the masticatory system, at least with the inverse approach, one inherent disadvantage exists, which is existence of larger number of unknown variables than the equations. To solve the dynamic simulation (in the Newton-Euler method) six equations for each solid-body are used: three for the forces in principal axes and three for the moments about these axes, leading to $6n$ equations for n bodies. So for the masticatory system, composed of the cranium and the mandible, 12 equations exist. However, a larger number of unknowns actually exist in the system (e.g. individual muscle forces, joint reaction forces *etc*). This leads to an issue known as indeterminacy, specifically in biomechanical modelling known as muscle redundancy, which is the existence of unlimited number of muscle activation combinations that satisfy particular condition of the problem (Glitsch and Baumann, 1997, Koolstra and van Eijden, 2001, Rasmussen et al., 2001, de Zee et al., 2007, Curtis, 2011). To conclude a unique muscle activation pattern, optimisation criteria have been introduced to the system which acts as constraint equations and are normally formed based on some

biological or neural condition. There are a number of optimisation criteria which have previously been proposed in the masticatory system, for example minimisation of muscle force, joint load, muscle effort, muscle stress and maximisation of the bite force.

In this section, some literatures that analysed MDA models of masticatory systems are presented and some optimisation criteria that have been used are discussed.

1.6.1 Two-dimensional (2D) mathematical modelling of masticatory system

Early biomechanical studies of the masticatory system involved two-dimensional static analysis of the mandible, cranium and masticatory muscles. There are several such mathematical models of the masticatory system in various human and non-human species. For example, Greaves (1978) modelled the jaw in ungulates as a lever system and investigated the mechanical advantage of grinding teeth. The aim was to explain the efficiency of grinding action of teeth in correlation to their location. Throckmorton and Throckmorton (1985) used gradual increase of muscle forces, bite force and their moment arms in their model to investigate the effect of each factor on TMJ reaction force in human. They suggested the calculation of TMJ reaction force was most sensitive to relative length of moment arms of bite force and muscle force. Sinclair and Alexander (1987) developed mathematical models of three reptiles and studied the magnitude and direction of the bite force and TMJ reaction forces. Cleuren et al. (1995) developed a relatively sophisticated model of the crocodilian reptile and instead of using the peak muscle force, they measured the level of individual muscle activity from surface EMG. They modelled the static jaw with different biting positions and food orientations and investigated the magnitude of the bite force and direction and magnitude of the joint reaction force. Herrel et al. (1998) modelled the static biting of four lizards to investigate the stabilising role of the temporal ligament. Spencer (1998) developed a model of human masticatory system and investigated whether the standard lever model was valid. He measured the activity of the superficial masseter and anterior temporalis during production of a large bite force at different points of dental arcade in human and observed substantial difference in muscle activity. He found the highest muscle

activity was affiliated with biting at M1 and at any position posterior or anterior to that, the muscles activated to a lesser degree, and concluded that the standard lever model was incomplete to model the masticatory system accurately.

As it was concluded by Spencer (1998), despite the fact that two-dimensional analysis provided useful data on comparative bite force and TMJ reaction force, a number of simplistic assumptions were made that affected the prediction of the model fundamentally. For example, the third component of the muscle force was neglected; the line of action of all muscles was assumed to remain constant; the dynamic behaviour of the system was neglected; and the majority of analyses used peak muscle forces and muscles were assumed to activate fully. Hence, the output data was not accurate and there was limitation in the data that this type of modelling could provide. Therefore, 3D modelling techniques were better suited for analysis of the masticatory system.

1.6.2 Three-dimensional (3D) mathematical and computational modelling of masticatory system

One of the first 3D mathematical models of the masticatory system was developed by Osborn and Baragar (1985) for bilateral biting of the human. In this model muscles were modelled as more than one unit, resulting in 12 muscle units in each side, which could activate independently. The maximum force of each muscle was calculated using PCSA values that existed in the literature. The model was developed by including directions and magnitude of maximal muscle forces, bite force and joint reaction forces to derive muscle recruitment of the system. A linear computer program was used to solve the model numerically and predict muscle activation patterns both at different bite positions and different positions of the mandible (as the mandible moved in a cycle of biting). As acceleration of the mandible required considerably less force than producing the bite force, the mandible was assumed to be in equilibrium and its acceleration was rightfully disregarded. Hence, to solve the model six equilibrium equations were used (for equilibrium of forces and moments). However, by including more independent muscle units the complexity of the system and the number of unknowns increased too, which led to static indeterminacy. The authors envisaged that there was a

mechanism in the muscles or joint force that acted as a tension/pressure sensor and fired at a rate proportional to the tension in the muscle or the force on the joint. Based on this assumption, the authors proposed minimisation of the sum of muscle forces and minimisation of the joint reaction forces as optimisation criteria. Muscle recruitment resulting from minimisation of the sum of muscle forces was found to be in better agreement with previous observations in human subjects. In contrast, optimisation based on minimisation of the joint load did not result in comparable muscle activation pattern to EMG data.

Koolstra et al. (1988) developed an individual-specific 3D model of the human masticatory system by using *in vivo* PCSA data from the same individual. The aim was to predict the maximum bite force magnitude and its direction. They incorporated the muscle wrapping to some extent in their model too. Unilateral and bilateral biting of human was simulated and the maximum bite force magnitude and its direction in various biting locations and mandibular position were predicted by using computer program and optimisation based on minimisation of the relative activity of the most active muscle. Validity of this optimisation criterion was later assessed by developing seven individual-specific models of human masticatory system to minimise errors caused by average data set. With the purpose of prediction of muscle activation pattern, they used magnetic resonance image (MRI), *in vivo* bite force and EMG to develop and validate the model (Koolstra and van Eijden, 1992). While the trend of results derived from minimisation of relative activity of the most active muscle demonstrated relatively good correspondence to EMG data, the standard deviation between individuals was high.

Likewise, Iwasaki et al. (2003a) developed seven individual-specific models of human masticatory system using radiographs and EMG data, from which muscle recruitment was predicted. But he used two different optimisation criteria: minimisation of joint loads and minimisation of muscle effort. Although both optimisation criteria showed variable comparability to EMG data at times, the minimisation of muscle effort showed better agreement to EMG data (for 6 out of 7 individuals). The validity of minimisation of muscle effort as an optimisation

criterion was further studied by de Zee et al. (2007) in human masticatory system. They used ANYBODY modelling software (AnyBody Technology, Aalborg, Denmark) which had built-in min/max objective function that acted as an optimisation algorithm and was effectively equivalent to minimisation of muscle effort. The model was validated against *in vivo* EMG data, to which muscle groups overall showed poor agreement, with some muscles were predicted more comparable than the others.

Moreover, Schindler et al. (2007) studied three different optimisation criteria in masticatory system of human: minimisation of the joint reaction force, minimisation of the overall muscle force and minimisation of the total muscle elastic energy. They compared muscle and joint forces resulted from optimisation with calculations based on *in vivo* data and reported that the results from minimisation of the total muscle elastic energy agreed *in vivo* data the best, followed by minimisation of the overall muscle forces. Similarly, findings of Rues et al. (2008) coincided well with Schinldler and they too reported on the minimisation of the muscle elastic energy as the optimal criterion, between the same three criteria, based on their comparison to *in vivo* data.

Moreover, several other studies have implemented analysis to assess the accuracy of minimisation of sum of squared or cubed muscle forces in other joints e.g. (Li et al., 2006, Wang et al., 2004, Heintz and Gutierrez-Farewik, 2007) and reported on the comparable results between predicted muscle activation and the *in vivo* data for both approaches.

Based on studies discussed above, optimisation criteria based on minimisation of muscle force, stress, energy or effort seems to agree *in vivo* data the best. Regarding the minimisation of the muscle force, the numerical difficulty arising from the direction of the force is a potential cause of error, which seems to be the case in sum of cubed muscle forces too; Rasmussen et al. (2001) compared muscle activation patterns resulted from minimisation of sum of squared muscle forces (muscle energy/effort) to minimisation of sum of cubed muscle forces and claimed the numerical calculations of the minimisation of sum of cubed muscle force is

much more complicated. Hence, in this thesis, minimisation of muscle energy was used as one of the optimisation criteria to predict muscle activation pattern of the mouse masticatory system.

Using minimisation of muscle energy as an optimisation criterion of MDA model of the mouse masticatory system in this thesis was achieved by following modelling techniques of a similar study to some extent (Shi et al., 2012). This study was an MDA modelling of a macaque skull, which modelled one instance of the biting cycle using ADAM (MSC Software Corp, USA). In this model, force generation of the muscles was predicted based on minimisation of muscle stress from which they predicted working and balancing side muscle force ratios, peak bite force and joint reaction forces during unilateral biting. Force generation within each muscle was defined by simplified version of Hill-type muscle models (Equation 1.1), in which F_{max} was the maximum muscle force that was estimated from PCSA, F_Q was activation factor of the muscle which was varied randomly (Shi et al., 2012).

$$F = F_{max} \times F_Q \tag{1.1}$$

Multiple subsections of muscles and wrapping in temporalis muscle were incorporated into the model, as they had found previously that muscle presentation (number, orientation and wrapping of muscle strands) has profound effect on the MDA predictions (Curtis et al., 2008, Figure 1.25). The food was modelled as a stiff, incompressible spring element that was positioned unilaterally from which the bite force was predicted. The bite force was equal to the force that was generated in the food spring and was a result of relative activities of masticatory muscles. In this model the motion of condyle against cranial articular surface was controlled in the model.

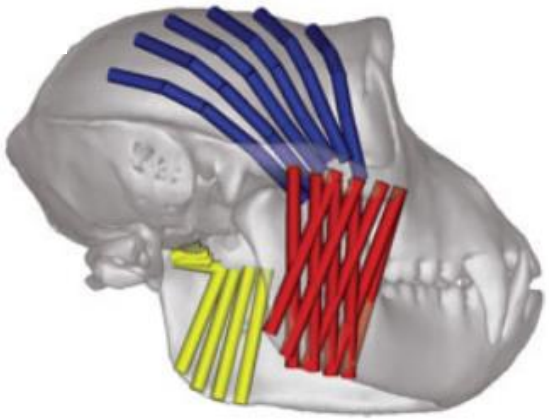

Figure 1.25 Macaque skull modelled with accurate representations of muscles (Curtis et al., 2008)

The authors simulated numerous combinations of muscle forces (3000, 5000 and 8000 simulations) in which the activation factor of muscles (F_Q) was randomly changed to predict the bite force, TMJ reaction force and muscle activation pattern. The optimal combination of muscle forces which resulted in a particular bite force (equal to *in vivo* bite force) with minimum sum of muscle stresses was selected, and the maximum bite forces were predicted which were comparable to published *in vivo* bite force. Moreover, the authors predicted independent activation of muscle subsections would enable muscles to activate optimally.

Another optimisation criterion which was developed more recently, specifically for the masticatory system, is dynamic geometric optimisation (DGO). DGO works based on the key assumption that muscle anatomy, in terms of orientation and line of action, is optimized for its function, the function in this case following the kinematics. In other words muscle activation pattern is determined by muscles orientation and the movement of the jaw. For example, a muscle with larger vertical component is more efficient for producing vertical force, hence when vertical movement of the jaw is required, that muscle activates to a higher degree (Curtis et al., 2010a). MDA model of reptile *sphenodon* was developed with ADAMS, using detailed muscle input and anatomical features. Sagittal components of each muscle (horizontal and vertical components) were determined from their anatomy,

and were incorporated into the model. The movement of the mandible, which were derived from literature, were decomposed into vertical and horizontal displacements of the movement and were incorporated into the model as moving path. The activation of masticatory muscles was a factor of required movement and muscle orientation. The activation factor of the muscle force in each muscle was determined using the formulation presented in Figure 1.26 and Equation 1.2. This activation factor was then used to calculate the muscle forces using Equation 1.1.

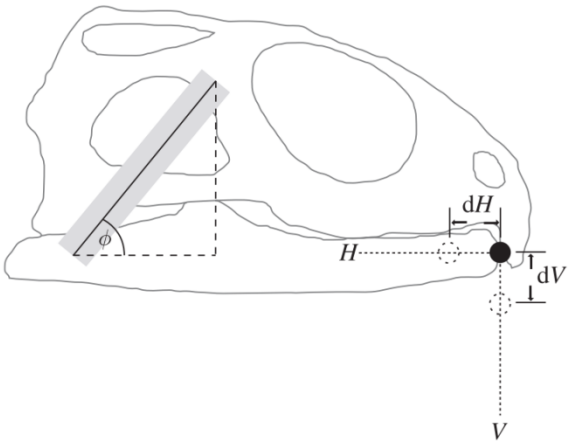

$$F_Q = (V_a \times dV) + (H_a \times dH)$$

$$\text{where } Va = \frac{Ø}{90} \text{ and } Ha = 1 - \frac{Ø}{90}$$

(1.2)

Figure 1.26 and Equation 1.2 Muscle force calculation in Sphenodon, F_Q, muscle activation factor; V_a vertical activation factor; H_a, horizontal activation factor; dV, gap between tip of lower jaw and vertical motion reference point; dH, gap between tip of lower jaw and horizontal motion reference point. H and V represent the full vertical and horizontal trajectories of the kinematic data. Ø represents the angle of the muscle strand with horizontal axis. 90 is in degree which has been used to normalize the factor and return a number between zero and one. (Curtis et al., 2010a).

Another novelty of the model was the unconstrained joints which were defined according to accurate anatomical features of contact surfaces. Instead of defining an over-simplified joint, which in the majority of cases over-constrains the relative movement of condyle, Curtis et al. (2010a) used geometry of the contact surfaces to limit the natural movement of the quadrate-articular joints. The results of this method was compared against published EMG and the trend of muscle activity was generally found to agree well with experimental data, despite some differences that was attributed to difference in bite point and food properties.

This optimisation method was put into test in biomechanical modelling of a lizard skull (Gröning et al., 2013b). An Individually specific MDA model of the masticatory system of a lizard was developed using ADAMS in which maximum bite force was predicted and compared against *in vivo* bite force measurement of the same specimen. Gröning et al. (2013b) used all anatomical data, i.e. muscle PCSA and orientation, joints geometries and kinematics that were obtained from the same specimen. Two different representations of the muscles in separate models were studied, one of which included only straight-lined muscles and the other included muscle wrapping too, with the final model containing 116 strands. The sensitivity of the maximum bite force predicted from the model to muscle attributes such as fibre length, intrinsic muscle stress and muscle representation was studied. The predicted bite force was consistent with *in vivo* bite force measurement, however, it was demonstrated that the model was very sensitive to mentioned muscle attributes and accurate muscle definition was essential to obtain realistic prediction from the model.

DGO was exploited by another study in which biomechanics of rabbit skull was studied by MDA techniques (Watson et al., 2014). Watson et al. (2014) again developed individual-specific model of the rabbit masticatory system in which anatomical data were obtained from both manual dissections and 3D imaging techniques, i.e. MRI and μCT, hence were claimed to be even more accurate. This model simulated the shearing of the food in molar region, which occurred through mediolateral movement of the mandible, as well as crushing of the food in molar and biting in incisal regions. The predicted incisal biting was then used to validate the model through comparison with *in vivo* incisor bite force measurements, which were in agreement.

1.7. Aims and objectives of the project

Based on what has been presented in this chapter, the aim of this thesis is to develop an accurate multibody dynamic model of the masticatory system of the adult house mouse, a species which is commonly used in laboratories in craniofacial studies, but its masticatory function has been poorly understood. MDA modelling of

masticatory system has been proven as an invaluable means to study and incorporate complexity of the system, and investigate different aspect of its function.

In this thesis, the main focus is on the muscle activation pattern of the mouse masticatory system. However, as system indeterminacy is an issue in solving the problem and concluding a unique muscle activation pattern, two different optimisation criteria are used: minimisation of the overall muscles energy and dynamic geometric optimisation. Both optimisation criteria have been used before and their validity were tested; hence, it is of interest to investigate whether they both would result in similar muscle activation patterns. Application of the two optimisation criteria is achievable through different methods of modelling. Therefore, in this thesis, two different individually specific models of the adult mouse masticatory system are developed. In this process, the required experimental data and the modelling methods associated with each optimisation criterion are investigated and finally the comparability of predicted muscle activation patterns resulted from these two criteria are compared. Choosing the optimisation criterion for the subsequent chapters of this thesis is not only based on the validity of optimisation criteria alone, but experimental data which are available for this study are critical point in decision making too.

Moreover, the peculiar dental arch of the mouse with large diastema is suggesting the molar and incisal biting would have different characteristics. Therefore, the comparison of muscle activation patterns, between incisal and molar biting, would be of value to understand the general function of the mouse masticatory system. Hence, in subsequent chapters models of individual-specific incisal and molar biting are developed in adult mouse in which the chosen optimisation criterion is used to predict maximum bite force in each biting position. Models are not only different in bite position, but the mandible position and corresponding kinematics are different too. Subsequently, the maximum predicted incisal bite force is compared against *in vivo* incisal bite measurement. In addition, the same two adult models are then used to predict differences in muscle activation patterns and joint reaction forces between molar and incisal biting for the same bite forces.

The final part of this thesis presents the development of a MDA model of a juvenile mouse to investigate the difference in masticatory function between adult and juvenile. Development of the masticatory system involves nonlinear adaptations in bones and muscles (detailed introduction of these adaptation are presented in Chapter 5).Hence it is of interest to assess whether biomechanics of the system changes in a linear manner. An Individually specific MDA model of the juvenile mouse is developed to simulate incisal biting from which muscle activation patterns and TMJ reaction force were predicted and compared against adult mouse.

All results chapters, i.e. chapter 3, 4 and 5, are written in the format of a paper, in request of the principal supervisor, Dr Sam Cobb. Hence each result chapter has individual introduction, methods, results, discussion and conclusion sections. Therefore, some repetition in materials, especially in methods sections was inevitable.

Chapter 2. Experimental and modelling methods

2.1. Introduction

Multibody dynamic analysis (MDA) is an engineering modelling technique, which has already been used successfully to model the masticatory system of a small range of vertebrate taxa (e.g. Watson et al. (2014), Gröning et al. (2013b), Curtis et al. (2010a), Curtis et al. (2010c), Moazen et al. (2008a), Curtis et al. (2008), Hannam et al. (2008), Langenbach et al. (2002)). This technique, however, has never been used in any rodent before. To develop such an MDA model of the masticatory system, requires information on cranium and mandible geometry and joints, the masticatory muscles, and kinematic data for the mandible. This chapter presents data collected for both adult and juvenile mice, and the development of two MDA models. Furthermore, *in vivo* maximum bite force measurements were collected from both juvenile and adult specimens to validate the models' predictions.

The importance of individual-specific data in accurate MDA modelling had been demonstrated previously (Gröning et al., 2013b, Curtis et al., 2010c, Iwasaki et al., 2003a, Koolstra and van Eijden, 1992). Hence, individual-specific data were used wherever possible to construct the models in ADAMS/view 2013 (MSC Software Corp, USA). MDA studies of the masticatory system use inverse dynamics in the majority of cases, in which indeterminacy of the system is an inherent issue. Various optimization methods are possible to solve for the system unknowns. In this particular research, two methods were used: dynamic geometric optimisation (DGO) and minimisation of muscle energy, which have been studied, separately, by our research group previously. These two optimization methods, however, have never been compared and their convergence and/or differences have never been studied before. As it was discussed earlier, the comparison of the two methods is one part of this thesis.

Subsequent sections of this chapter give a detailed description of the methods and protocols that were used to collect the experimental data to construct the MDA model of the mouse, as well as steps involved in model development. Moreover,

optimisation methods, required input data and modelling adaptations in each method are discussed.

2.2. Experimental methods and protocols

Collection of experimental data in this study was carried out by our collaborator, Dr Anthony Herrel at the Muséum National d'Histoire Naturelle (MNHN), Paris. For the adult mouse, ten C57 wild-type 12-week old house mice were used, obtained from Charles River Laboratories (Chatillon-sur-Chalaronne, France). This series was used to collect *in vivo* maximum bite force, PCSA data and muscle insertion and origin points. For the juvenile mouse, one single C57 wild-type three-week old house mouse was used to obtain cineradiography, maximum *in vivo* bite force, PCSA data and muscle insertion and origin points. Therefore, experimental data for the adult mouse was averaged across all specimens, whereas for the juvenile mouse the specific data from the same specimen was used. Moreover, for measuring the age-dependant maximum bite force, five C57 wild-type mice at ages 3,6,9 and 12 weeks (20 in total) were utilized which were obtained from Charles River Laboratories (Chatillon-sur-Chalaronne, France). The single juvenile specimen, which was mentioned previously, was one of these specimens.

All experiments were approved by the Animal Care and Use Committee at the MNHN.

2.2.1 Maximum *in vivo* bite force

Incisor bite force measurements were collected using a piezoelectric isometric force transducer (Kistler type 9203, +/-500 N, Winterthur, Switzerland) connected to a bite plate and a Kistler charge amplifier (type 5995A, Kistler Inc., Winterthur, Switzerland). Force measurements were taken with an incisal gape angle of 25±5° during voluntary biting, with five trials for each mouse (Table 2.1). The average of the maximum bite forces from ten adult mice was used for the MDA model, and is referred to as the *in vivo* maximum bite force. For the juvenile mouse, however, the maximum bite force recorded out of five trials for the same specimen was used as

in vivo maximum bite force. And finally for the age-dependant bite force measurements, the maximum bite force of each individual was picked.

The bite gape of 25±5° was chosen, which was well below the maximum gape size of the same specimen (C57) which was reported by Vinyard and Payseur (2008). They have reported on the bite gape in this specific strain of the mouse in 10-week-old to be between 13.5 and 14.5mm. They also reported on significant phenotypic variation in gape based on the body size and they referenced the phenotypic formula (gape/body weight$^{0.33}$) to calculate the maximum bite gape. Considering the average body mass of our 10 adult specimens was 23.69 gr (consult Table 2.2), the bite gape of our average adult 12-week specimen can be calculated as 14.21 mm, which is within the measured range of the same study. Measuring the distance between the TMJ and higher and lower incisor, we can calculate the bite gape in degrees. This value will be equal to 40^{o} in our individual (consult Table 5.3 for the out-lever distances of incisors). Thus bite force of 25±5° is in natural working range of the adult specimens.

Table 2.1 *In vivo* bite force measurements in adult specimens at bite gape of 25±5°

Individual	bite 1(N)	bite 2(N)	bite 3(N)	bite 4(N)	bite 5(N)	max(N)
1	8.71	8.18	9.23	8.16	8.27	9.23
2	7.96	8.00	7.83	8.17	7.24	8.17
3	8.68	9.15	8.64	8.30	9.14	9.15
4	6.44	7.49	7.64	6.22	6.24	7.64
5	8.94	8.98	8.01	7.04	8.40	8.98
6	7.97	8.46	8.61	9.15	7.50	9.15
7	9.29	8.34	8.80	8.94	9.17	9.29
8	8.84	8.03	7.97	7.52	7.60	8.84
9	8.34	8.97	9.64	9.00	7.29	9.64
10	9.22	9.37	9.64	9.45	8.88	9.64

Table 2.2 Details of adult specimens, the aspects of the study that each specimen was used in and head length, body mass and maximum bite force in each specimen. The last row represents mean value of these measured entities along with standard deviation.

Individual	Age	µCT	Dissected	Max Bite force (N)	Head length (mm)	Body Mass (gr)
1	90 days	✓	✓	8.71	23.98	24.4
2	90 days	✓	✓	7.96	23.44	21.3
3	90 days	-	-	8.68	24.24	24.4
4	90 days	-	-	6.44	24.03	23.7
5	90 days	-	-	8.94	23.9	22.4
6	90 days	✓	✓	7.97	23.83	23.7
7	90 days	✓	✓	9.29	24.08	25.1
8	90 days	-	-	8.84	24.15	24
9	90 days	-	-	8.34	23.5	23.8
10	90 days	✓	✓	9.22	23.83	24.1
Mean± STD				**8.97±0.60**	**23.90±0.25**	**23.69±1.03**

As it can be seen in Table 2.2, there is not a considerable difference in head-length and body mass of the ten individuals (1% and 4% standard deviation respectively). Also from our observations after µCT scans, it was observed that all five scanned specimens were more or less similar in morphology too. Therefore, choosing any of the five scanned specimens was a reasonable choice. The specimen, which was chosen in this thesis, was specimens number six. It has a reasonably close body mass, bite force and head length to the average house mouse (see Figure 2.1, Figure 2.2 & Figure 2.3). It should be noted that only the cranium and mandible morphologies were taken from this specific individual and the rest of the data, i.e. muscle mass, muscle fibre length and PCSA data were averaged across all five individuals.

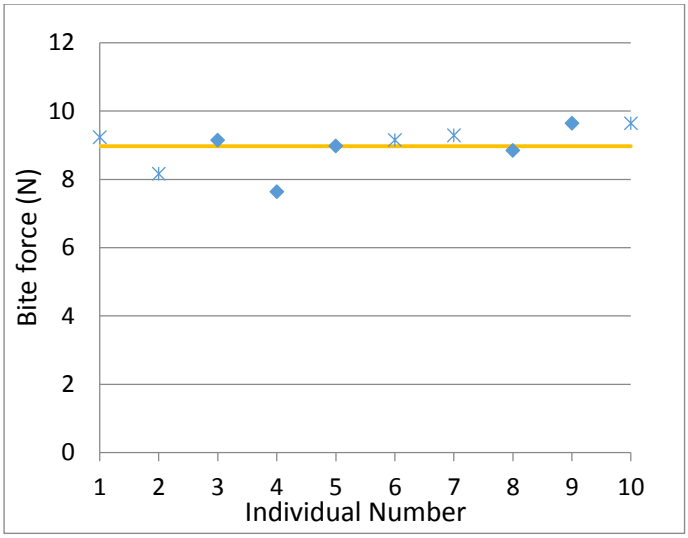

Figure 2.1 Bite force measurement in 10 adult specimens. The average bite force (averaged across 10 specimens) is shown in yellow line.

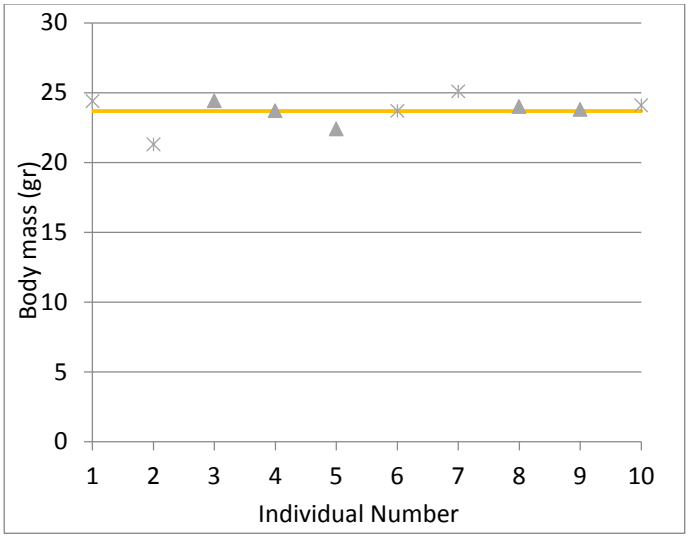

Figure 2.2 Body mass measurement in 10 adult specimens. The specimens which have been µCT scanned, are shown with cross sign. The average body mass (averaged across 10 specimens) is shown in yellow line.

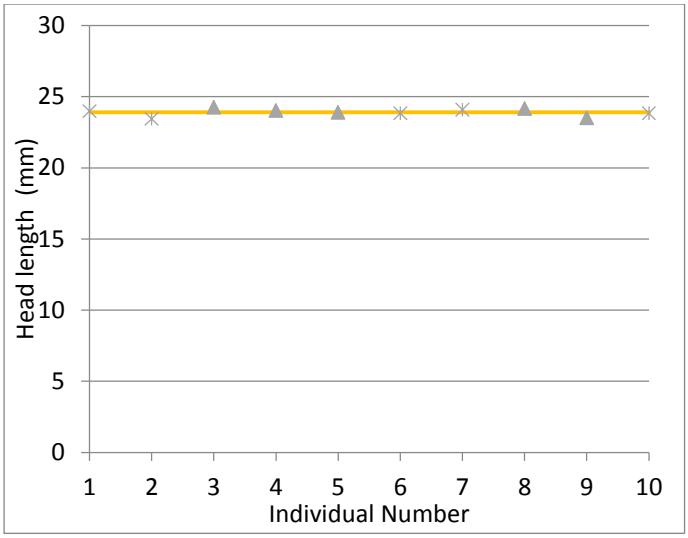

Figure 2.3 Head length measurement in 10 adult specimens. The specimens which have been µCT scanned, are shown with cross sign. The average head length (averaged across 10 specimens) is shown in yellow line

2.2.2 Muscle insertion and origin points

After the collection of maximum bite force, all specimens were sacrificed by injecting pentobarbital, fixed overnight in a 15% formaldehyde solution, rinsed and transferred to a 70% ethanol solution. Two methods were used to obtain accurate attachment area and orientation of muscles: dissection and virtual segmentation. The masticatory muscles (superficial and deep masseter, infra-orbital, anterior and posterior zygomaticomandibularis, anterior, posterior and suprazygomatic temporalis, internal and external pterygoid) were identified and dissected from one side of the head in five of the adult and from one side of the head of the single juvenile mice, each muscle was removed complete and transferred to labelled vials containing 70% ethanol aqueous solution. The attachment area of each muscle was observed carefully and photographs were taken using a Canon EOS 40D.

Muscle dissections

The dissection of the masticatory muscles started from the ventral side of the skull, which dissection of the digastric muscle. The digastric muscle was removed from the jaw as a whole (Figure 2.4).

Figure 2.4 Dorsal and lateral views of the digastric muscle in the mouse

The superficial and the deep masseter were next dissected respectively. Our observation about insertion and origin points of these muscle was in agreement with Baverstock et al. (2013). The suerficial masseter, however, was not divided to the tendon sheet and the muscle belly and was considered as a whole body (Figure 2.5).

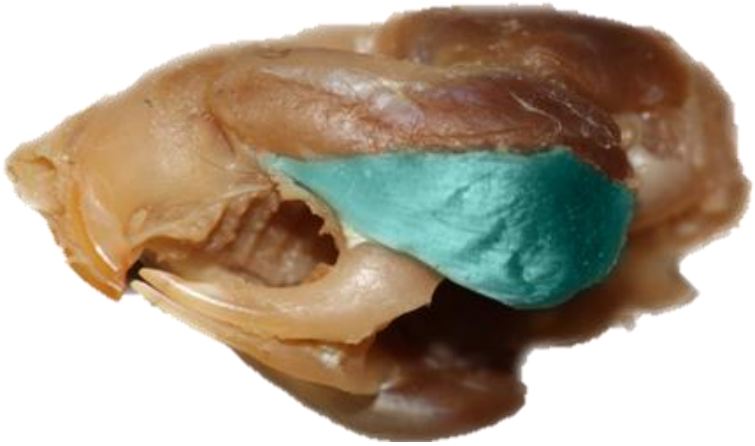

Figure 2.5 Superficial masseter muscle in the mouse

Figure 2.6 Masticatory system with superficial masseter reflected (pale blue) and the deep masseter (dark blue) laying underneath.

Figure 2.7 The three parts of the emporalis muscle of the mouse. Anterior (fuchsia), posterior (red) and suprazygomatic temporalis (orange).

Unlike observations of Baverstock et al. (2013) who reported only two visible divisions of the temporalis, anterior and posterior sections, in the current study the suprazygomatic temporalis was also distinctly observed. Moreover, Baverstock et al. (2013) states that the lateral part of the temporalis is similar to fascia, hence it is difficult to be distinguished as a separate part. However, in the dissections of the current study, all three distinct sub-sections of the temporalis were clearly visible. The suprazygomatic temporalis originates from superior and posterior areas of the zygomatic arch and inserts onto the coronoid process of the mandible. All three sub-sections of the temporalis are shown in Figure 2.7.

Figure 2.8 Lateral view of the mouse masticatory system. The superficial and deep masseter are removed and the three parts of the zygomaticomandibularis are highlighted (the most anterior part, shown in forest green is the infra-orbital zygomaticomandibularis; the middle part which is shown in dark green is the anterior zygomaticomandibularis and the bright green represents the posterior zygomaticomandibularis).

The zygomaticomandibularis muscle, composing of three sub-sections, was dissected next. Although observations of the current study were in general in

agreement with Baverstock et al. (2013), one interesting difference was found. The posterior zygomaticomandibularis was reported to origin from the posterior border of the zygomatic arch and run anteroventrally on the curvature between condylar and coronoid process. In curernt study, however, it was observed that postreior zygomaticomandibularis runs posteroventrally and inserts between angular and condylar process (Figure 2.8). This observation, however, was noticed later in the stage of the modelling when the model was already constructed. To be consistent in all models this orientation, which was reported by Baverstock et al. (2013) was used.

Figure 2.9 Ventral view of mouse masticatory system. Internal pterygoid muscle is shown in the picture.

The pterygoids were the last two muscles that were dissected. The internal pterygoid was dissected first (Figure 2.9), which was separated from the external pterygoid with intervention of a nerve (Figure 2.10).

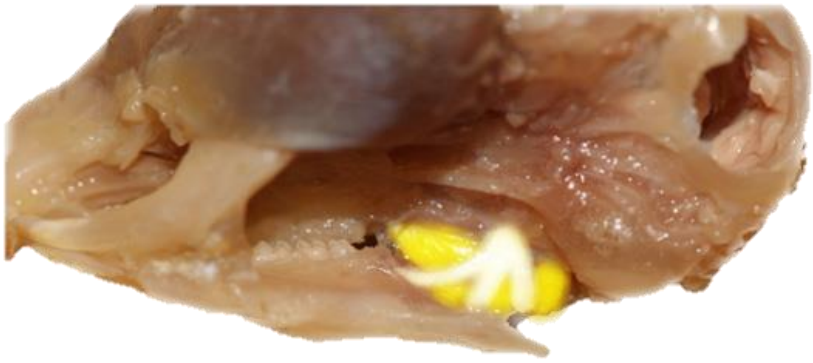

Figure 2.10 External pterygoid is shown in the picture. It attaches just posterior to the third molar on pterygoid bone (the nerves which separate the external and internal pterygoid is presented in white).

Subsequently, the partially dissected heads of the same six mice (five adults and one juvenile) with muscles intact only on one side were stained in 5% phosphomolybdic acid, diluted in 70% ethanol, for four days and then scanned using high resolution micro-computed-tomography (µCT). Four of five adult mice were scanned in one batch in MNHN (AST-RX platform) with voxel size of 0.046 mm in all three directions (v|tome|x L 240, GE Sensing & Inspection Technologies Phoenix). The juvenile mouse was scanned separately in the School of Engineering, University of Hull (X-Tek HMX160; X-Tek Systems Ltd, Tring, UK) with a voxel size of 0.014 mm in all three directions. The four adult and one juvenile mouse scans were then segmented using AVIZO 6.3 image processing software (Visualization Science Group (VSG)), and the masticatory muscles were identified and labelled individually. Muscle attachment areas were inspected and compared against dissection images and observations.

Attachment areas of the muscles on the cranium and the mandible were landmarked in AVIZO 6.3 using pairs of markers, spread uniformly over the attachment areas, where each pair of landmarks represented one sub-section of the muscle. Thus if five pairs of landmarks were used, the muscle was defined with five sub-sections, termed as “muscle strands” in the remainder of this thesis. For example, in the case of superficial masseter (Figure 2.11), the attachment area on the mandible, was visualised using four landmarks equally spaced on the central axis of the attachment area. The number of pairs of landmarks was dependant on the size of the muscle attachment areas and complexity of the muscle orientation. In addition, where a muscle wrapped around the bone, it was further divided into sections with a fixed joint at the via point. For example, anterior temporalis wraps around the cranium (see Figure 2.12), hence each muscle strand was subdivided into two parts to allow the muscle strands to wrap around the curved cranium.

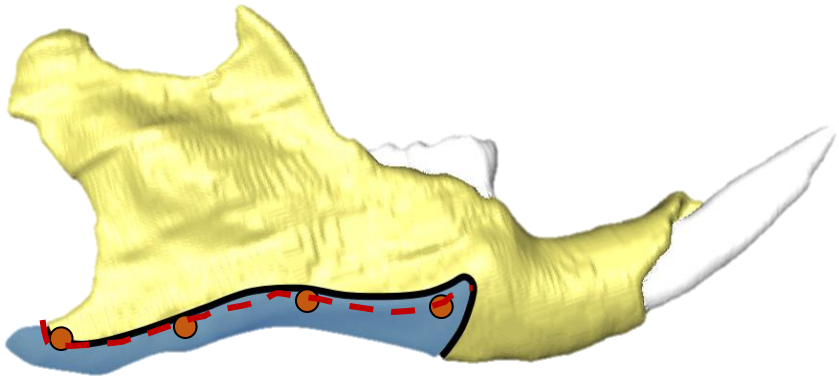

Figure 2.11 Lateral view of the mandible with muscle attachment areas. The red dash line represents the centre line of the attachment area of the superficial masseter (in blue) and the red markers show the attachment locations of the four muscle strands used to represent the muscle. Adapted from Baverstock et al. (2013).

The landmarks were defined on the right side of the head and then reflected to the left side, then, since the cranium and the mandible were not perfectly symmetrical, small adjustments were carried out to ensure they lay on the bones. 3D landmark coordinates from AVIZO were subsequently imported into ADAMS/view.

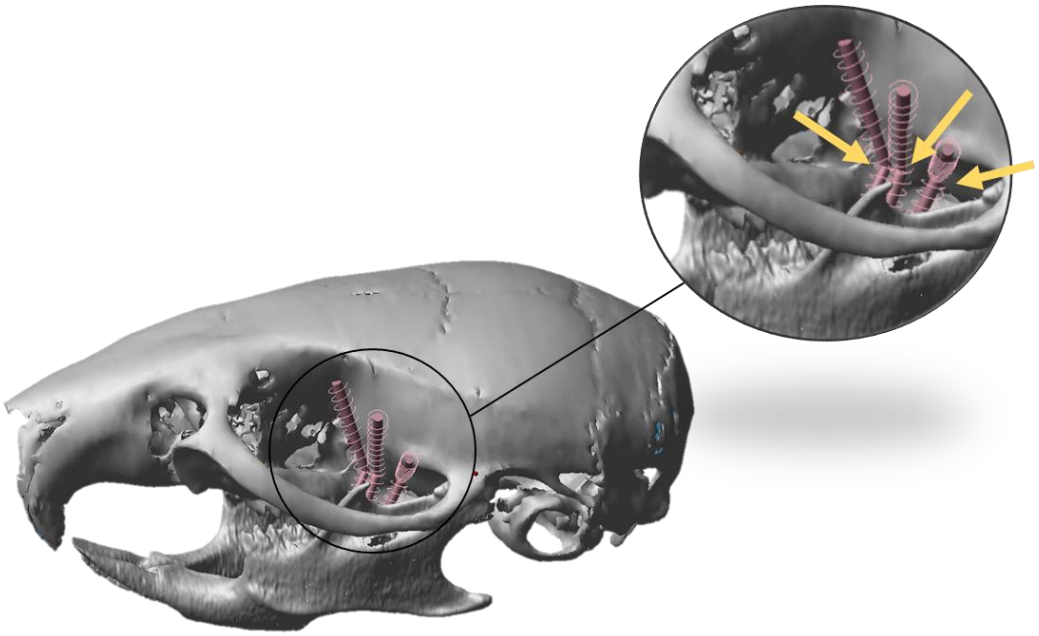

Figure 2.12 Anterior temporalis muscle strands defined in two parts. Arrows are indicating the via points.

2.2.3 Physiological cross sectional area (PCSA)

The magnitude of the force generated by a muscle depends on a number of factors, including the arrangement of the fibres within the muscle. However, precise determination of the number and arrangement of fibres *in vitro* is not always feasible, especially for complex multi-pinnate muscles with varying fibre arrangements. Physiological cross sectional area (PCSA) is a mathematical measure, which theoretically predicts maximal muscle contraction force generation by using muscle mass, density and mean fibre length (Anapol and Barry, 1996). This commonly used method was used in this study to estimate the maximum muscle contraction force for each muscle.

The previously dissected muscles were removed from the vial, blotted and masses were recorded to the nearest 0.01 mg using a microbalance (Mettler AE100).

Table 2.3 Mass of the dissected masticatory muscles measured to four decimal points

INDIVIDUAL NUMBER	SM (G)	DM (G)	AT (G)	PT (G)	SZT (G)	AZM (G)	IOZM (G)	PZM (G)	IP (G)	EP (G)	DG (G)
1	0.0203	0.0356	0.0122	0.0071	0.002	0.0053	0.0027	0.002	0.0118	0.0044	0.0132
2	0.0181	0.0311	0.0085	0.0069	0.0023	0.0048	0.0019	0.0022	0.0082	0.0031	0.0109
6	0.0207	0.0329	0.0099	0.0109	0.0015	0.0039	0.0027	0.003	0.012	0.0034	0.0137
7	0.0242	0.0361	0.0123	0.0112	0.0025	0.0064	0.0032	0.0031	0.0117	0.0062	0.0135
10	0.0172	0.0283	0.0112	0.0049	0.002	0.0018	0.0052	0.0019	0.0076	0.0039	----
MEAN (G)	0.0201	0.0328	0.0108	0.0082	0.0021	0.0044	0.0031	0.0024	0.0103	0.0042	0.0128
SD	0.0024	0.0029	0.0014	0.0025	0.0003	0.0015	0.0011	0.0005	0.0019	0.0011	0.0011
RELATIVE SD %	**12.11**	**8.82**	**13.37**	**29.91**	**16.42**	**34.85**	**35.38**	**20.83**	**18.90**	**26.04**	**8.78**

Subsequently, each muscle was transferred to an individual vial of 30% aqueous nitric acid solution and left for 20–24 hours after which the solution was replaced by a 50% aqueous glycerin solution. Individual fibres were teased apart using blunt tipped glass needles, 10 fibres were randomly selected from each muscle and traced using a binocular microscope with an attached camera lucida (MT5 Wild). Drawings were scanned and fibre lengths determined using ImageJ V1.31 software.

Fibre length was measured for all six individuals (see Appendix I) and was averaged for each muscle in each individual. Muscle mass and average muscle fibre length measurements obtained for each of six mice were used (Equation 2.1) to calculate physiological cross sectional area (PCSA) of each muscle. The standard tissue density of 1.0564 g/cm^3 was used for the PCSA calculation of the muscles (Murphy and Beardsley, 1974). The muscle architecture and pinnation angle, however, were not included in this study and all muscles were assumed to be parallel fibred; therefore the effect of pinnation angle on muscle force production was not included.

$$PCSA = \frac{muscle\ mass}{muscle\ denisty\ \times muscle\ fibre\ length} \quad (2.1)$$

$$Force = PCSA\ \times intrinsic\ stress\ of\ skeletal\ muscle \quad (2.2)$$

The average of the PCSA across all five adults was used to estimate masticatory muscle forces in adult mouse, whereas PCSA data of the same individual was used for the juvenile mouse.

The average PCSA, which is presented in Chapter3, was found to be relatively close to the PCSA of the chosen number six specimen (Table 2.4). It seems, however, that PCSA values of the specimen number 6 are consistently higher than the average data. The highest difference belonged to the external pterygoid muscle with standard deviation of 43%, whereas all other muscles had standard deviation of 25% and less. The largest and most effective masticatory muscles in mouse though, i.e. the masseter and the temporalis, showed maximum difference of 22.9% (for the posterior part of the temporalis).

Table 2.4 Comparison of the average PCSA data with the PCSA data of the chosen specimen in modelling of the adult mouse. STD: standard deviation, which was calculated as the subtraction of the PCSA value of the average data number divided by the average data.

PCSA	SM	DM	AT	PT	SZT	AZM	IOZM	PZM	IP	EP	DG
Average	0.0759	0.1017	0.0386	0.0226	0.0078	0.0165	0.0105	0.0093	0.0389	0.0139	0.0354
Mouse6	0.0872	0.1092	0.0423	0.0278	0.0095	0.0217	0.0120	0.0117	0.0458	0.0200	0.0376
STD	0.1489	0.0740	0.0957	0.2293	0.2170	0.3160	0.1398	0.2546	0.1775	0.4376	0.0614
STD %	**14.9**	**7.4**	**9.6**	**22.9**	**21.7**	**31.6**	**14.0**	**25.5**	**17.7**	**43.8**	**6.1**

Muscle force was calculated from the PCSA value and intrinsic stress of skeletal muscle (Equation 2.2). It was not possible to measure the masticatory muscle intrinsic stress value in this study, but published intrinsic stress values of skeletal muscle vary between 25 N/cm^2 and 87.1 N/cm^2 for different species, ages and muscle types (fast versus slow twitching muscles) (Hatze, 1981, Vanspronsen et al., 1989, Weijs and Hillen, 1985, Gonzalez et al., 2000), with predicted bite force in an MDA model linearly related to intrinsic muscle stress (Gröning et al., 2013b). The value of 39.7 N/cm^2 is reported for the young adult mouse *soleus* muscle (Gonzalez et al., 2000), and it was the initial value that was used for the calculation of muscle forces. However, considering that there are a couple of assumptions in the model that may result in underestimation of the bite force, namely usage of the average PCSA data rather than the individual data and excluding pinnation angle from PCSA calculations, underestimation of the bite force was likely. In our provisional studies, we indeed found that the maximal bite force values from models with averaged PCSA data could not match *in vivo* bite force data. To compensate for this underestimation arose from our assumptions, the initial value was increased by 25% and the value of 50 N/cm^2 was used in all models which was still in the range of previously reported values.

In an effort to confirm the PCSA values and test the accuracy of virtual segmentation techniques, a combination of dissection and virtual segmentation of muscles was used in this work. In doing so, several muscles were segmented as well as individual muscle fascicles in the most superficial muscles i.e. superficial and deep master and temporalis. Unfortunately the volumes from the segmentation did not match the (correct) dissected values and, despite a significant effort, the error in the method could not be determined. Hence, the virtual results are not presented, and all subsequent modelling was carried out by using PCSA value from dissections.

Segmented muscles were used to study the shape of their cross sectional area for sensitivity studies (Chapter 4). The line of action of each muscle was defined, then muscle's cross sectional area which was perpendicular to, and in the mid-point of, the line of action was observed. The shape of the cross sectional area was

determinant of the muscle distribution in the model. If the shape was close to rectangle, uniform distribution of the muscle strands was used in the model. In contrast, if the shape of the cross sectional area was close to triangle, then additional muscle strands were added to the thicker part of the cross sectional area (Figure 2.13 to Figure 2.16).

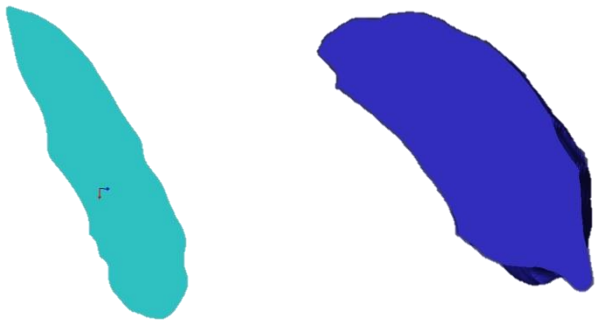

Figure 2.13 Cross-sectional area of superficial (left) and deep masseter (right)

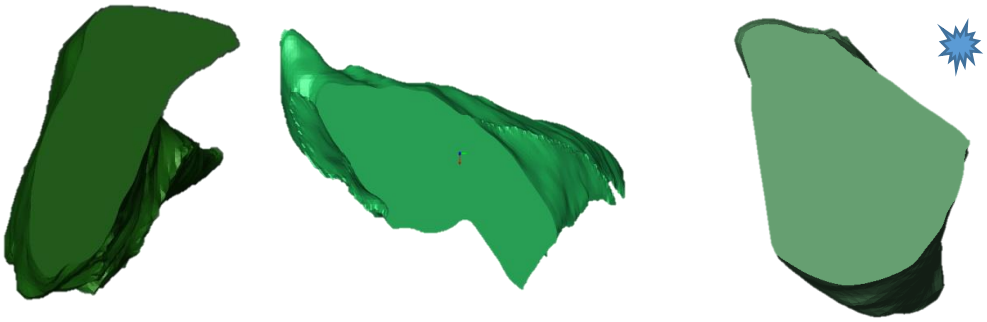

Figure 2.14 Cross-sectional area of infra-orbital (left), anterior (middle) and posterior (right) zygomaticomandibularis. Posterior zygomaticomandibularis had triangular cross sectional area.

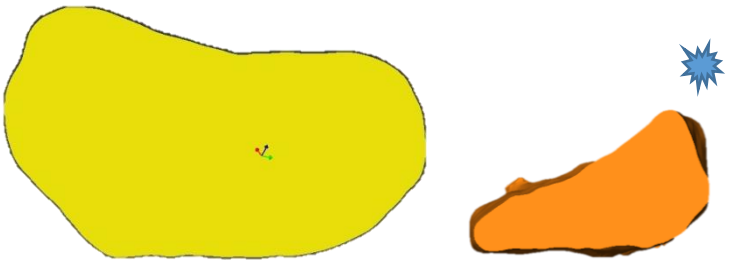

Figure 2.15 Cross-sectional area of internal pterygoid (left) and external pterygoid (right). External pterygoid had triangular cross sectional area.

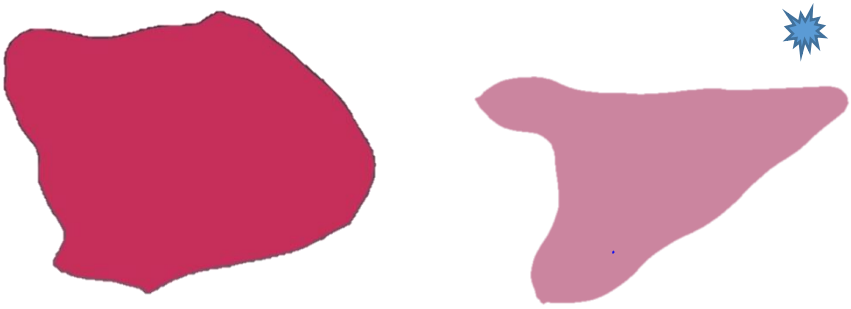

Figure 2.16 Cross-sectional area of posterior (left) and anterior (right) temporalis. Anterior temporalis had triangular cross-sectional area.

2.2.4 Kinematics of the mouse masticatory system

The kinematics of incisor and molar biting are different, incision composes of short and fast movements of the mandible whereas mastication consists of longer and higher amplitude movement of mandible (Figure 2.17, Utsumi et al., 2010).

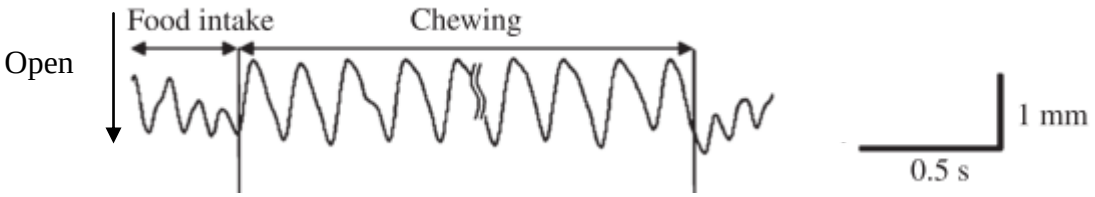

Figure 2.17 Vertical movement in incision and chewing cycles in the mouse. Incision consists of short and low magnitude movements whereas chewing consists of longer and higher magnitude movements of the mandible (Utsumi et al., 2010)

Kinematic data of chewing in the adult mouse was obtained from the literature (Utsumi et al., 2010). The significance of lateral movement in chewing, however, was inconsistent between different studies; Okayasu et al. (2003) reported a great deal of the lateral movement, whereas Utsumi et al. (2010) reported on minor lateral movement. Hence, transverse movement was disregarded in this thesis. Moreover, Published kinematics of the incisor biting of the mouse is variable both in gape and movement trajectories and hugely affected by food consistency (Kobayashi et al., 2002a). As incorporating published quantified food characteristics, i.e. soft and hard or pellet and paste food, was difficult, incision was assumed to be only simple close rotary movement in the TMJ (open-close). Furthermore, there was no data specifically published for kinematics of juvenile mouse, hence, cineradiography of the same individual was used to obtain kinematics trajectories. Similar to the adult mouse, only 2D movements were considered in the juvenile specimen and transverse movements were disregarded.

To emulate movement of the mandible in the adult mouse, sagittal trajectories of the chewing cycles reported by Utsumi et al. (2010) were used. Nine landmarks were placed on the cycles, starting from point 1 in Figure 2.18, which were then digitised using tpsDig 2.17 (by F. James Rohlf) a plug-in for ImageJ, and vertical and horizontal coordinates of the landmarks were calculated (Figure 2.19). This coordinates represented the position of the mandible, just beneath the symphysis, in each point of time. In this thesis, the same trajectories were used for the tip of the incisors, which is presented in Figure 2.19. When the food item is uncompressible, the tip of the mandible cannot follow the normal movement trajectories and the vertical position of the mandible remains the same after touching the food (orange line in Figure 2.19).

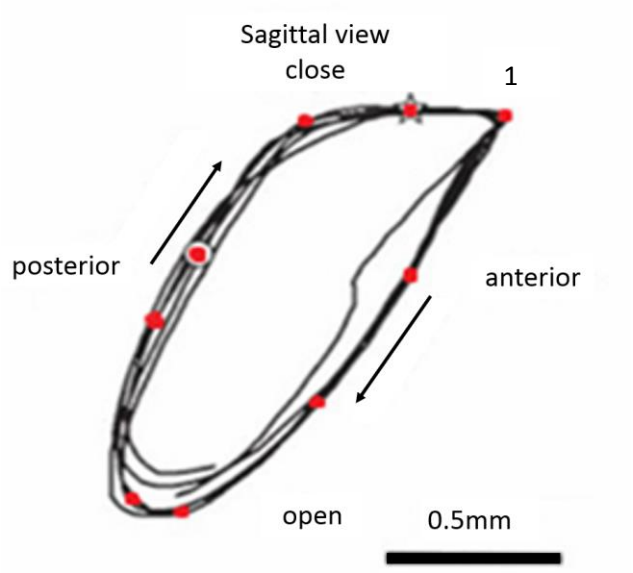

Figure 2.18 Sagittal trajectories of the mouse mandible. Nine landmarks were used to replicate the movement. The point marked as 1 is the first landmark and the starting point of the cycle and the star represents position when the jaws are fully closed.

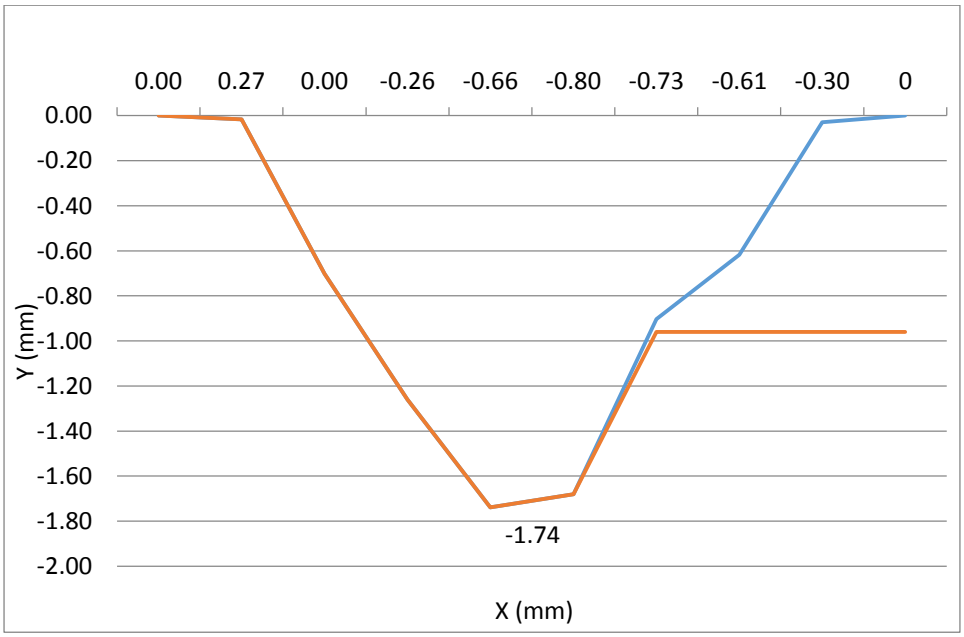

Figure 2.19 Sagittal trajectories of the mandible during molar chewing obtained from digitisation of the Figure 2.18 (X: movement in antero-posterior direction; Y: movement in dorsoventral direction). The blue line represents the X and Y coordinates of the tip of the mandible for a successful cycle of biting, while the orange line represents its position in biting of a hard, uncompressible food.

The kinematics of the juvenile mouse was obtained through landmarking of cineradiography data. Three incision cycles were used to obtain the average maximum gape angle from which the maximum bite gape dimension was calculated, calibrated to the cranial length, where the length of the cranium was measured from a 3D reconstruction in AVIZO. Only incisal biting of the juvenile mouse was modelled, so to maintain comparability of the model to the adult incisal biting, only rotary movement of the mandible was included in the MDA model. Hence, as it was found that the movement used in the adult model was in functional range of the movement of the juvenile mouse, i.e. juvenile's maximal vertical movement was larger than what was used in the adult MDA, the same vertical trajectory as the adult mouse was used for the juvenile too.

2.3. Model construction

The general steps of model construction were the same for all analyses, including the models for investigation of the optimisation criteria, the adult incisor and molar biting models, and the juvenile model. These steps include: extraction of accurate geometries of the mandible and cranium, and definition of the muscle morphologies, joints and constraints. Once the model is developed, optimisation criteria was used to simulate the model and predict muscle force, bite force and joint reaction forces. These steps are now described in details.

2.3.1 Geometries of the skull and mandible

The sample adult mouse and juvenile mouse used in the MDA models were scanned in the School of Engineering, University of Hull (X-Tek HMX160 (X-Tek Systems Ltd, Tring, UK)). The same juvenile specimen that was used for staining was scanned after being stained in phosphomolybdic acid (section 2.2.2). The adult, however, was one of the five remaining undissected specimens and was scanned with voxel sizes of 0.018 mm in all three directions. The μCT scans were segmented using AVIZO and 3D shell surfaces of the cranium and the two hemi-mandibles were exported to MSC ADAMS/view 2013 multibody dynamics software. Since the speed of the biting simulations was slow in the analysis, inertial loadings were not

considered in the analyses, and thus the mass properties of the geometries were not specified in the models. The surfaces therefore were used only as a guide for accurate placement of the muscle attachments and any muscle wrapping.

In addition, the articulating surfaces of the TMJ, i.e. condylar process and glenoid fossa were reconstructed separately with special care to assure the smoothness of surfaces. These articulating surfaces were defined as solid volumes in the contact-constrained models.

2.3.2 Muscle definition

Accurate muscle definition is essential in the creation of MDA models, so careful attention was paid to their specification. As previously discussed in section 2.2.2 each muscle was divided into a number of strands, with the number of strands dependant on the complexity of the muscle and size of its attachment areas. The number of strands used for each muscle are presented in Table 2.5. The insertion and origin of each strand was defined by a pair of landmarks connecting the insertion and origin areas. These landmarks were then imported to ADAMS/view, where they were modelled as a spring-damper which was defined using a series of user-defined macros. These macros also renamed each landmark to a unique name incorporating the name of the muscle and side of the head (left or right), with the respective spring-dampers defined between each pair of landmarks. There was very little difference caused by asymmetry of the cranium and mandible.

Anterior temporalis, which wraps around the temporal bone of the cranium, was modelled as three strands (Figure 2.22), the length of each was defined as two parts, to allow wrapping of each strand; the higher part laid over the cranium while the lower part extended between the upper strand and the mandible. So in reality the active part of each muscle strand was the lower part. A similar arrangement was adopted for infra-orbital zygomaticomandibularis (modelled with two muscle strands each composing of two parts and active part presented in Figure 2.26) and suprazygomatic temporalis (modelled as one strand composed of two parts (Figure 2.24)). In both cases the active part of the muscle strand was the lower part,

defined between the cranium and mandible, in contrast to the higher part which was constrained to the cranium.

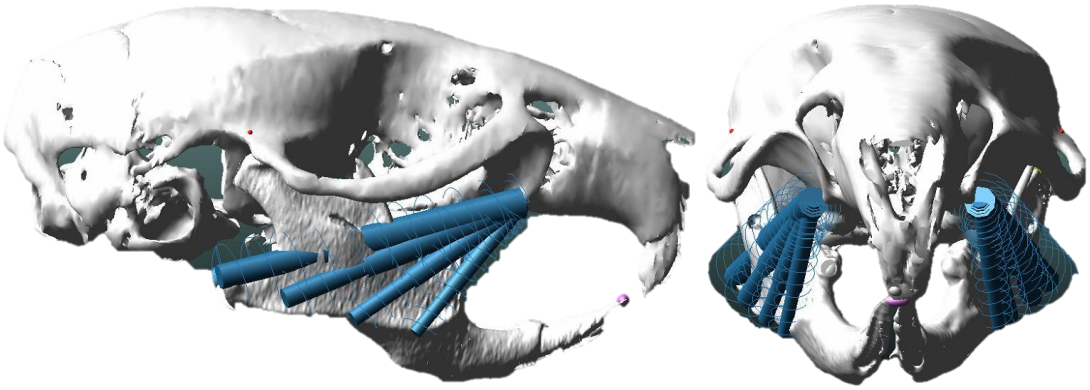

Figure 2.20 Sagittal and frontal view of superficial masseter muscle strands

The superficial and deep masseter muscles (Figure 2.20 & Figure 2.21), posterior temporalis (Figure 2.23), anterior and posterior zygomaticomandibularis (Figure 2.25 & Figure 2.27) and the pterygoids (Figure 2.28 & Figure 2.29) were all defined as muscle strands composed of only one part and no wrapping was included. As it was mentioned in section 2.2.2, the orientation of the posterior zygomaticomandibularis was defined according to the observation of Baverstock et al. (2013), hence it runs postereoventrally.

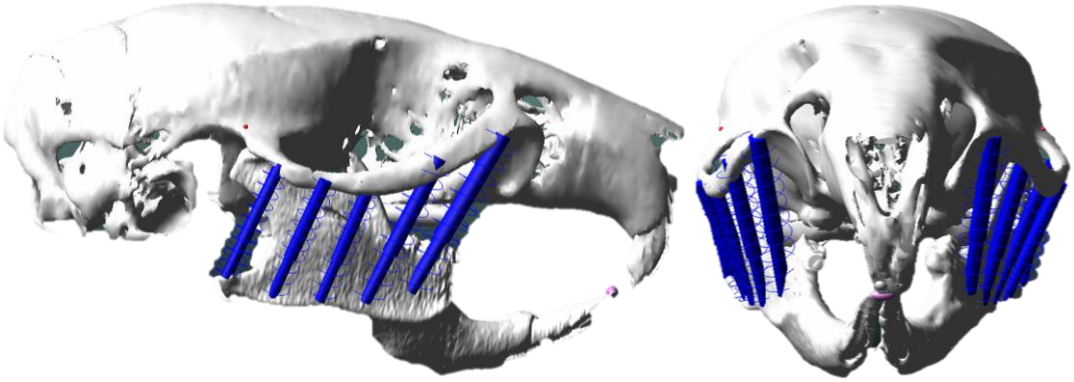

Figure 2.21 Sagittal and frontal view of deep masseter muscle strands

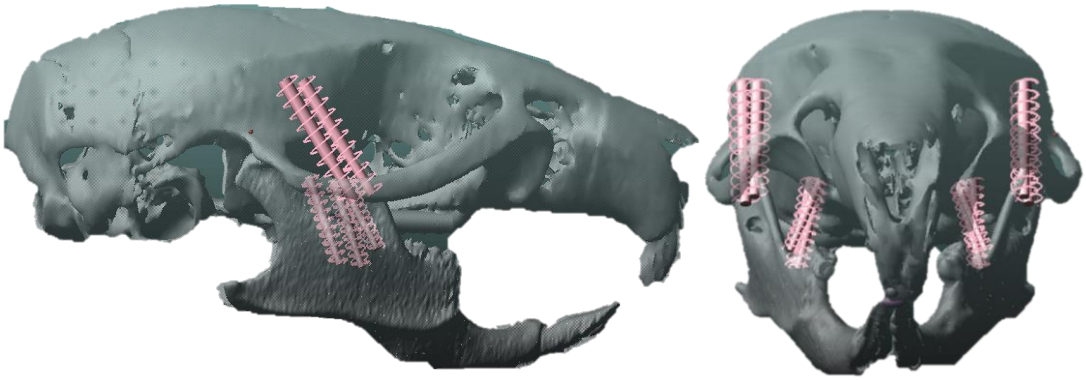

Figure 2.22 Sagittal and frontal view of anterior temporalis muscle strands

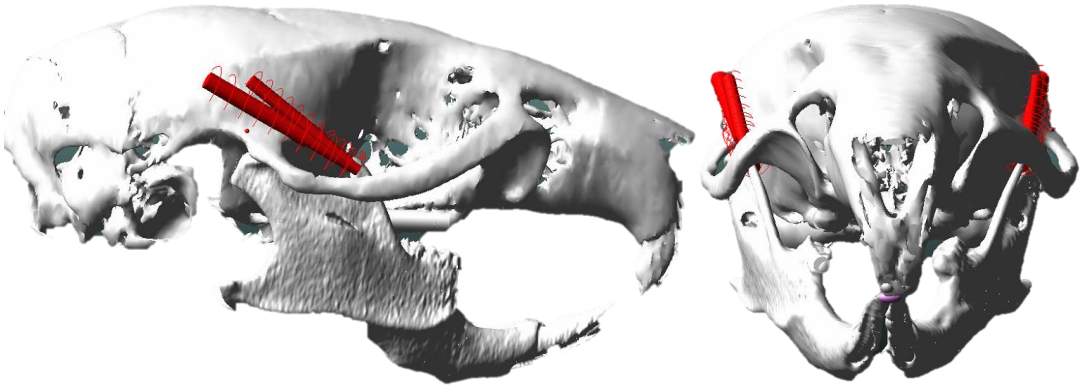

Figure 2.23 Sagittal and frontal view of posterior temporalis muscle strands

Figure 2.24 Sagittal and frontal view of supra zygomatic temporalis muscle strands

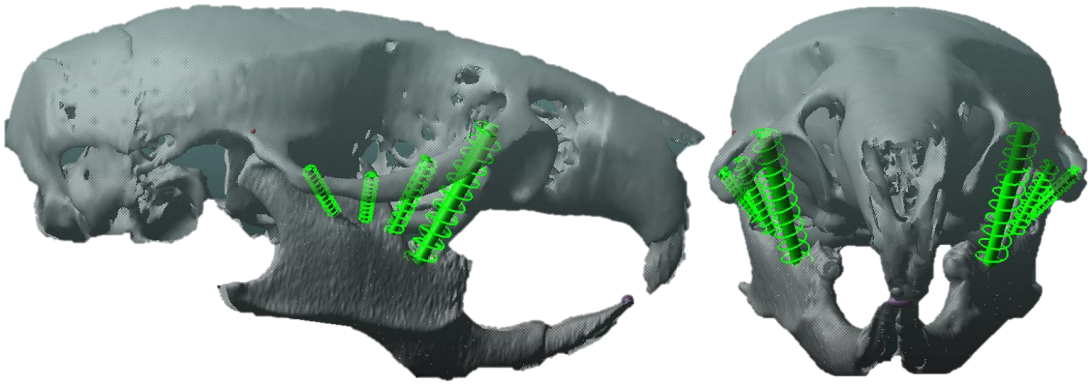

Figure 2.25 Sagittal and frontal view of anterior zygomaticomandibularis muscle strands

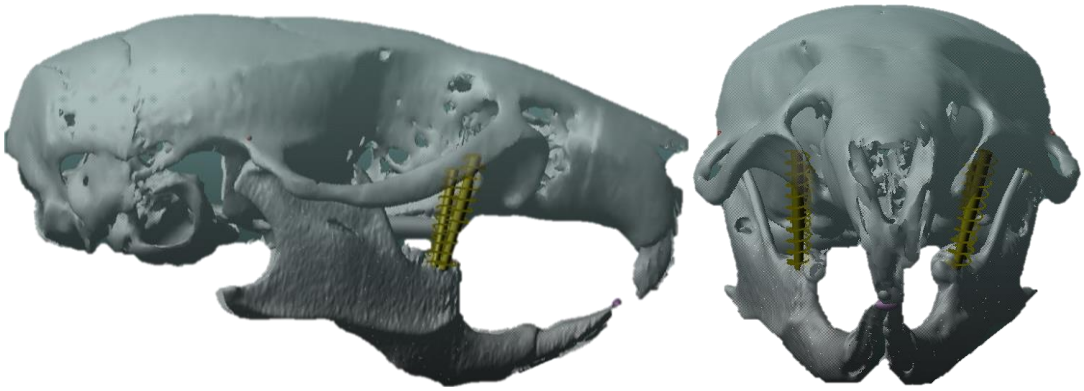

Figure 2.26 Sagittal and frontal view of infra-orbital zygomaticomandibularis muscle strands

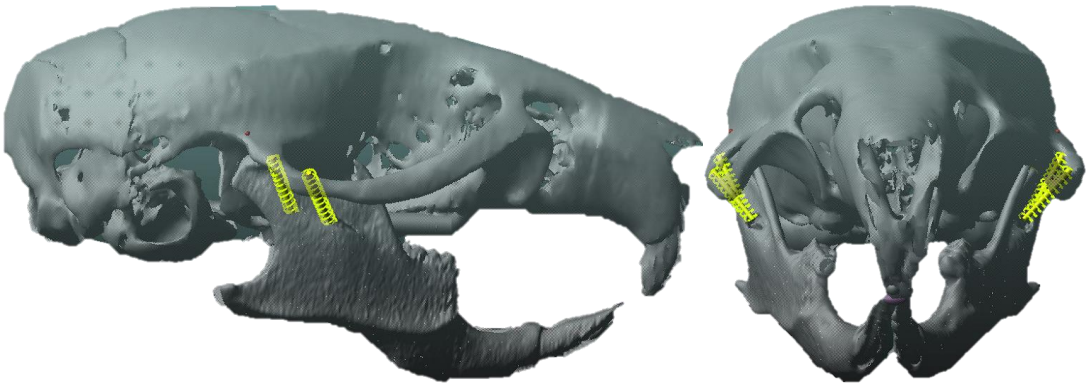

Figure 2.27 Sagittal and frontal view of posterior zygomaticomandibularis muscle strands

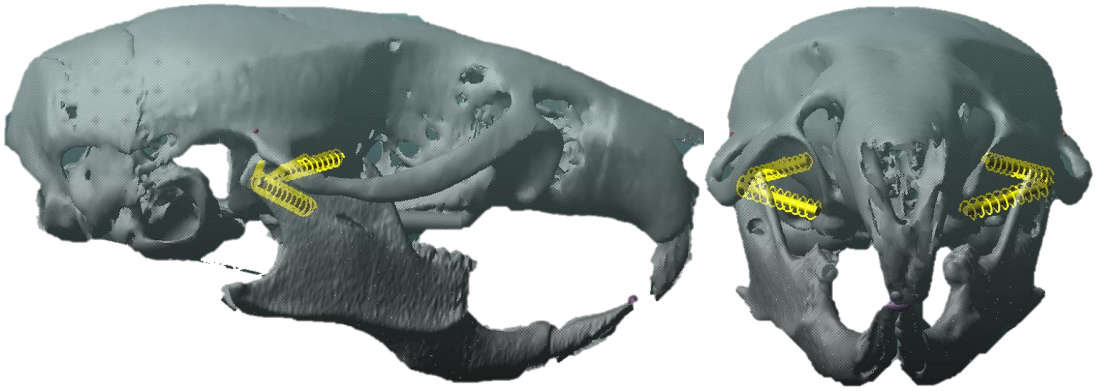

Figure 2.28 Sagittal and frontal view of external pterygoid muscle strands

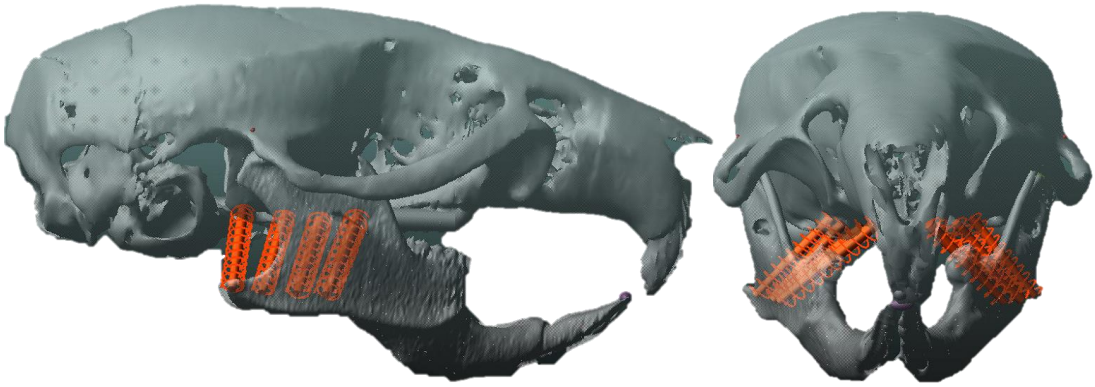

Figure 2.29 Sagittal and frontal view of internal pterygoid muscle strands

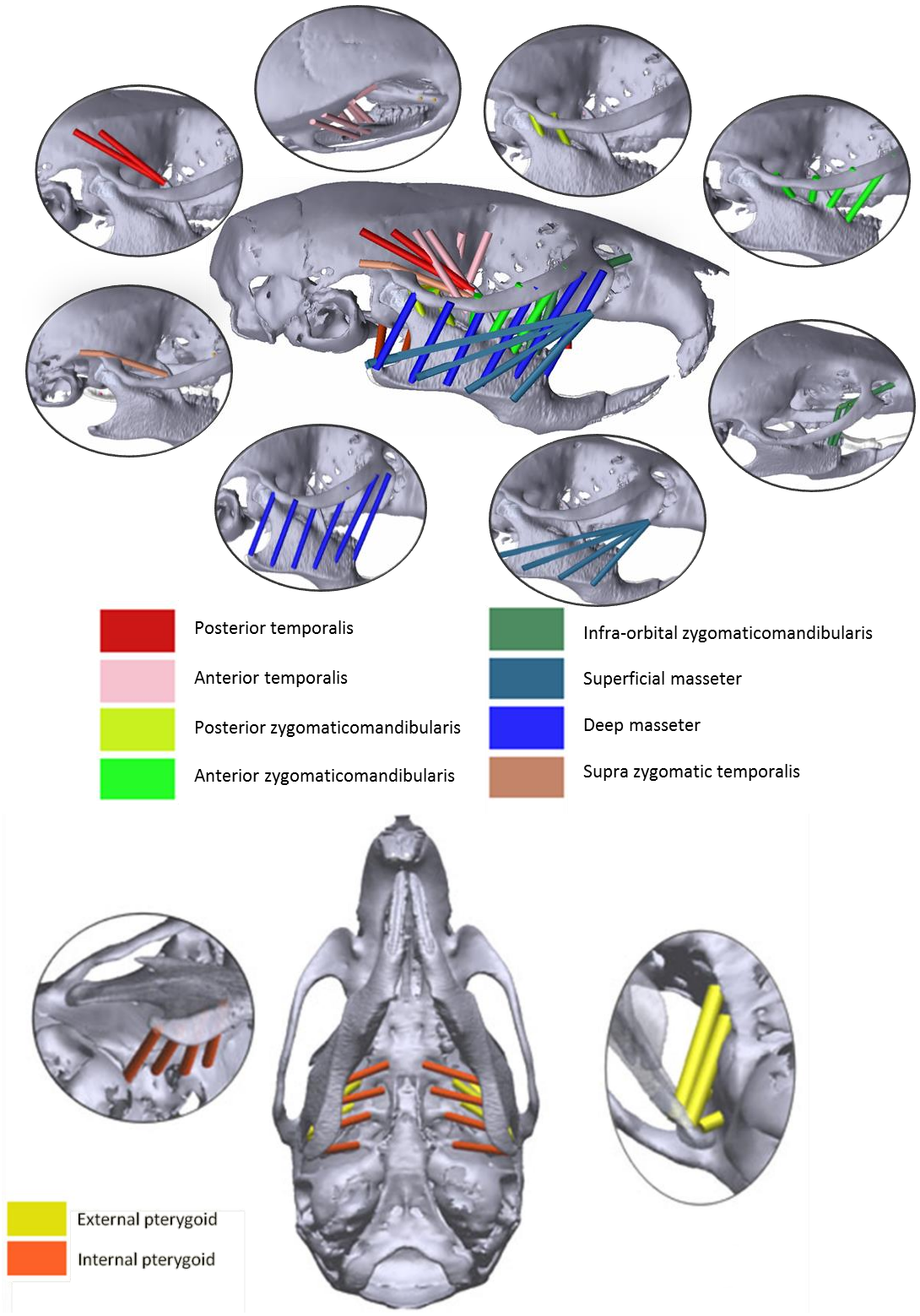

Figure 2.30 Masticatory muscles definition in the model of adult mouse. Ten groups and sub-groups of jaw closer muscles are defined in the model, each of which compose of different number of strands based on their origin and insertion area.

Table 2.5 Number of muscle strands in the model

Muscles	Superficial masseter	Deep masseter	Anterior temporalis	Posterior temporalis	Supra zygomatic temporalis	Anterior zygomaticomandibularis	Infra orbital zygomaticomandibularis	Posterior zygomaticomandibularis	Internal pterygoid	External pterygoid	Digastric
Number of strands	4	6	5	2	1	4	2	2	4	4	2

The force generation within a muscle is defined by van Ruijven and Weijs (1990) (equation 2.3):

$$F = F_{max} \times F_Q \times F_A + F_p \quad (2.3)$$

where:

F_{max} is the maximum force that the muscle can generate. This is estimated from PCSA

F_Q is an activation factor of the muscle which varies between zero and one

F_A is the muscle force/length relationship

F_p is the muscle passive force.

The activation factor of the muscle is generated by the modelling algorithm (see section 2.3.5 for more details). The force/length relationships for the muscles were incorporated in the model with inclusion of F_A which can change between 0 and 1. These relationships, however, were not known in this study; hence it was assumed that all muscles were at their optimum length. Thus F_A was assumed to be equal to one. This assumption, obviously, leads to consistent overestimation of muscle activations. However, the relative position of the cranium and mandible, in large, define how the length of the muscle and subsequently the force/length relationships changes. Since the position of the cranium and mandible are the same in both adult models (DGO vs MOME), it can be assumed that each muscle is at

same point in its force/length curves. Therefore, assuming all muscles are at their optimum length, overestimates the muscle activations consistently, however, this overestimation is consistent between the two adult models and can be disregarded. Passive force values are explained separately for each optimisation criterion in section 2.3.5.

2.3.3 Joints and Constraints

The masticatory system of the mouse includes two types of joints: the temporomandibular joints (TMJs) and the mandibular symphysis. The symphysis, located between the anterior tips of the two hemi-mandibles, is a flexible joint that permits relative rotations of each hemi-mandible along its long axis. The symphysis was modelled as a spherical joint, with three degrees of freedom. However, in the minimally-constrained models in which the TMJs were modelled using contact constraints, the movement of the symphysis had to be restrained to some extent to stabilise the system. Two methods were used to limit the symphyseal freedom of movement. For all models, except for sub-maximal biting, the tip of incisors were locked to each other, making the mandible as one whole part. In models considering sub-maximal biting, however, a bushing element was added at the symphysis. Bushing elements have 6 degrees of freedom (3 translations, 3 rotations) with independent stiffness properties and can measure and/or limit the forces and torsions acting between two points.

The mouse TMJ is a relatively open joint, with little presence of bony processes in the glenoid region to constrain movements. Ligaments, and muscles surrounding the TMJ are therefore very important in constraining the movements of the mandible against the cranium. In MDA modelling, there are a number of joints of varying complexity that can be used to simulate this behaviour.

For the initial steps of the model development, a simple hinge joint was used (with one rotational degree of freedom). The mandible was orientated in the rest position relative to cranium, in this position upper and lower teeth are separated by a small gap and the mandible is constrained to the cranium in region of glenoid fossa. The initial position of the mandible is different between molar and incisor

biting because the mandible and its diastema are smaller than the cranium. Therefore during incisor biting the mandible is positioned more anteriorly than during molar biting, to allow for incisor occlusion; this also means that the condyle and TMJ hinged-joints are more anteriorly positioned for an incisor bite.

Hinge joints of course do not allow for antereoposterior movement of the mandible, which is reported to be substantial in molar biting (Utsumi et al, 2010). Hence TMJs were constrained using contact. Contact is an open constraint with six degrees of freedom which controls the movements of articulating surfaces based on their geometries. The articulating surfaces were imported into ADAMS/view as solids and merged into the cranium and the mandible. The rest of the cranium and mandible were still left as shell surfaces to minimise the solution times. This was particularly important for optimization by minimisation of overall muscles energy which requires thousands of simulation trials.

Contact constraint allows translational and rotational movements of the condyle against glenoid fossa in all three directions, however, to avoid excessive movement of the condyle, bushing elements were used as described previously. In this case the bushing force stiffness were defined with minimum values that allowed the required movement in the vertical and horizontal directions, while providing the necessary stability of the system.

2.3.4 Food item

The food item was modelled as a spring, between the teeth, where the force generated within the spring as a result of muscle activation was equivalent to the bite force. As unilateral biting was modelled, the food item was placed on one side (right) of the face. In the models used to test the optimisation criteria, the food was modelled as one spring simply positioned between the right first molars (M1) (Figure 2.31, A). In the models used to investigate incisor and molar biting, the food item was modelled as a spring attached to two plates which and was positioned between the incisors and in the right molar region (Figure 2.31, B). Although the former was attached to the teeth during the whole cycle, it had no stiffness during opening of the mandible, only becoming stiff during closure. The latter, however,

was not attached to teeth surfaces and was just moved between the teeth after closing of the mandible.

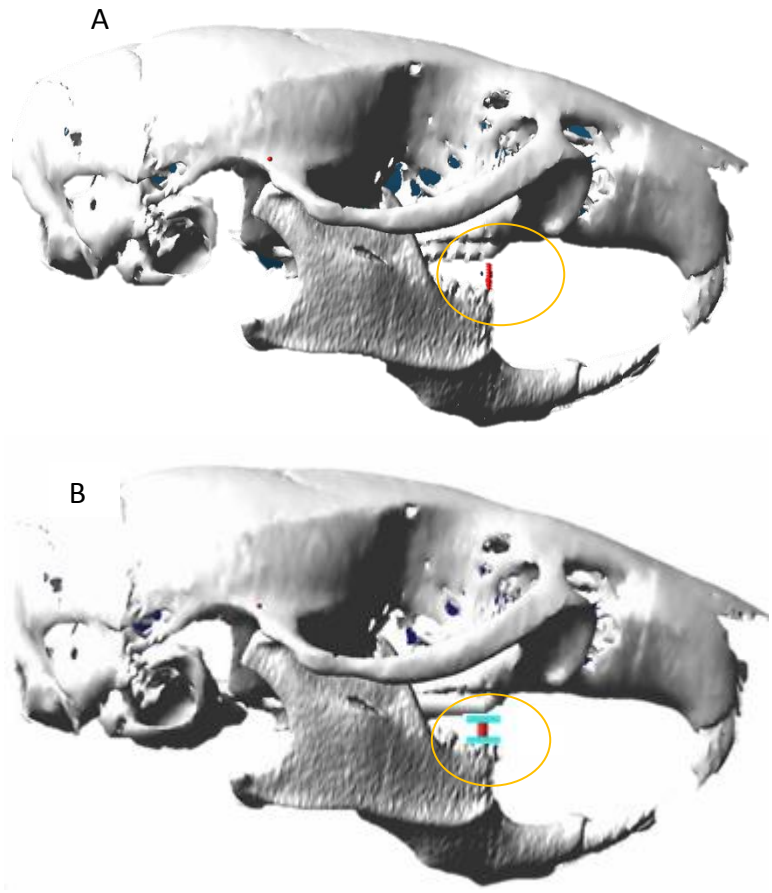

Figure 2.31 Representation of the food item, A: simple spring attached to teeth; B: spring attached to two plates.

2.3.5 Optimisation criteria

Indeterminacy is a problem in systems which include a high number of unknowns, including the masticatory system considered here. To overcome this issue and determine a unique answer from MDA models, additional constraints in the form of optimisation criteria were applied to the system. Two optimisation criteria were considered, both of which have previously been used for masticatory studies: (1) minimisation of muscle energy/effort and stress, which have previously used for MDA of masticatory system of a number of primates and humans (Shi et al., 2012, Rues et al., 2008, Schindler et al., 2007, Iwasaki et al., 2003a); and (2) dynamic

geometry optimisation (DGO) (Watson et al., 2014, Gröning et al., 2013b, Curtis et al., 2010a).

These two optimisation criteria require different modelling techniques. In particular, the optimisation criterion based on minimisation of overall muscle energy requires the solution several hundred or thousand simulations at each position of the biting cycle. Hence modelling the whole cycle would result in enormous data sets, most of which would be redundant. Therefore, in the case of minimisation of overall muscle energy, only one position was modelled, whereas a complete biting cycle was modelled using the DGO method.

Dynamic geometric optimisation (DGO)

DGO is an optimisation criteria which has been developed specifically for MDA modelling of the masticatory system (Curtis et al., 2010a). The method is based on this assumption that masticatory muscles are orientated optimally for their function, in other words, a muscle functions optimally along its line of action. Hence, DGO calculates muscle activation as a factor of its orientation and required function. For example, a more horizontally positioned muscle relative to the occlusal plane (e.g. superficial masseter in the mouse) is more efficient in moving the jaw either posteriorly or anteriorly compared to a vertically aligned muscle (e.g. deep masseter in the mouse), and therefore during antereoposterior motions would be activated to a greater extent.

DGO calculates muscle activation based on the required movement and its vertical and horizontal muscle components. It therefore decomposes each muscle strand, as well as the required kinematics vector to their vertical and horizontal components (V_a and H_a are vertical and horizontal components of the muscle strand in Figure 2.32). The kinematic vector is the difference between the current position of the tip of the mandible (landmark 1 in Figure 2.32) and the position of the mandible in next instant (landmark 2) and dV and dH are vertical and horizontal component of the kinematics vector in Figure 2.32. Subsequently, it calculates the activation of each muscle using equation 2.5.

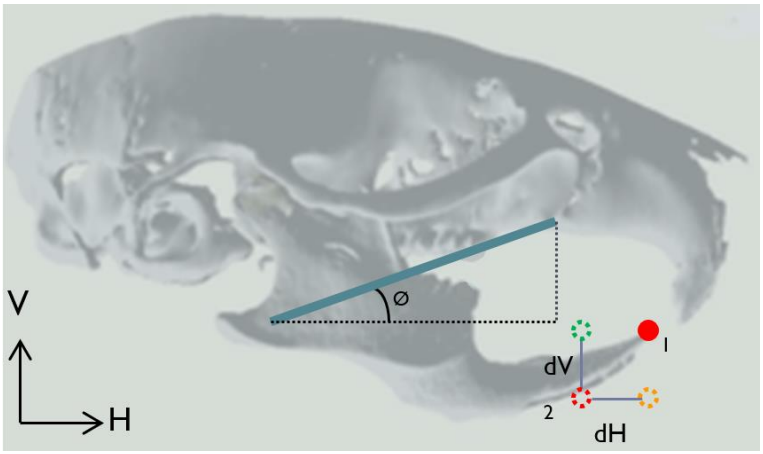

Figure 2.32 One strand of superficial masseter presented as an example to describe the DGO algorithm. The solid red landmark (no. 1) is the current position of tip of the mandible, the hollow red landmark (no. 2) is the required position of the tip of mandible. dV and dH are the vertical and horizontal components of the kinematic vector.

$$F_Q = (Va \times dV) + (Ha \times dH) \tag{2.5}$$

where $Va = \frac{Ø}{90}$ and $Ha = 1 - \frac{Ø}{90}$

Thus, the algorithm results in a higher level of activation during vertical movement of the mandible, for vertically orientated muscles, while muscles that have large horizontal components activate to a higher extent when horizontal movement of the mandible is required.

Moreover, passive force was included in DGO and was defined as 0.1% of the muscle strand force. This force was present when the muscle strand was beyond its optimal length, when it was involuntarily elongated. Hence muscle force generation in DGO is simplified to equation 2.6.

$$F = F_{max} \times F_Q + \frac{F_{max}}{100} \tag{2.6}$$

Minimisation of sum of muscles energy

Minimisation of the sum of muscles energy, effort and stress are analogous constraint equations that have previously been used as optimisation criteria in biomechanical studies of masticatory system (Shi et al., 2012, Rues et al., 2008, Schindler et al., 2007, Iwasaki et al., 2003a). Using this method requires the solution of numerous trials (possibly thousands) at every bite position to allow identification of the optimum muscle activation pattern (Shi et al., 2012), and is very computer intensive. As a result only one bite position was modelled.

Moreover, passive force only exists when the muscle is beyond its optimal length, thus F_P was assumed to be zero. Hence the equation to determine muscle force was simplified significantly to equation (2.7).

$$F = F_{max} \times F_Q \qquad (2.7)$$

For each muscle strand F_{max} was defined as the muscle maximum force divided by the number of strand, while F_Q was a variable that varied between zero and one. As a result, since 68 jaw closing muscle strands were defined in the head (34 in each side), 68 muscle variables were defined in the system which could vary independently. These variables were exported to ADAMs/insight where different combinations were created, each combination termed as one “trial”. Moreover, two objective functions were defined in ADAMS/insight: the sum of the muscles’ energy (sum of muscle forces squared), and the bite force (in the food spring). These objective functions were predicted from the simulation of each trial.

Within ADAMS/Insight many combinations of muscle activations were then created, known as trials (generated using a Latin Hypercube sampling technique), which were individually applied to the multibody model in ADAMS and the equations of motion solved (solver in ADAMS uses an Euler–Lagrangian solution method (Rana and Joag, 1991)). A curve fitting routine in ADAMS/insight then identified the optimum combination of muscle forces that minimised the muscle energy while producing the required bite force (Shi et al., 2012).

Selected optimisation criteria

Both optimisation criteria are tested in this thesis (Chapter 3), each of which involved different modelling techniques. Despite both optimisation criteria being validated formerly (Watson et al., 2014, Gröning et al., 2013b, Shi et al., 2012), the comparability of the two methods has not been previously investigated. In this thesis, results of modelling of the adult mouse showed some comparability in activity of only some muscles between the two methods, and some other muscles showed different activity patterns. As EMG data were unavailable to compare against the results of these two different approaches, the selection of a suitable optimisation criterion was based on the fact that DGO is capable of simulation of one full cycle of the mastication, in contrast to MOME in which only one instant of the power stroke can be simulated (Figure 2.33). This is because MOME involves numerous trials from which the optimal trial can be chosen and simulation of a full biting cycle is a huge computational task and is not feasible. DGO, however, allows for dynamic simulation of the full cycle, involves one single trial and results in time-dependant bite force, muscle activations and joint reaction forces. The key requirement of DGO is kinematic data, which is available (Utsumi et al., 2010). While selecting the biologically accurate method confidently requires EMG data, the mentioned advantages of the DGO are the basis of selecting this technique as the optimisation criterion for the rest of this thesis.

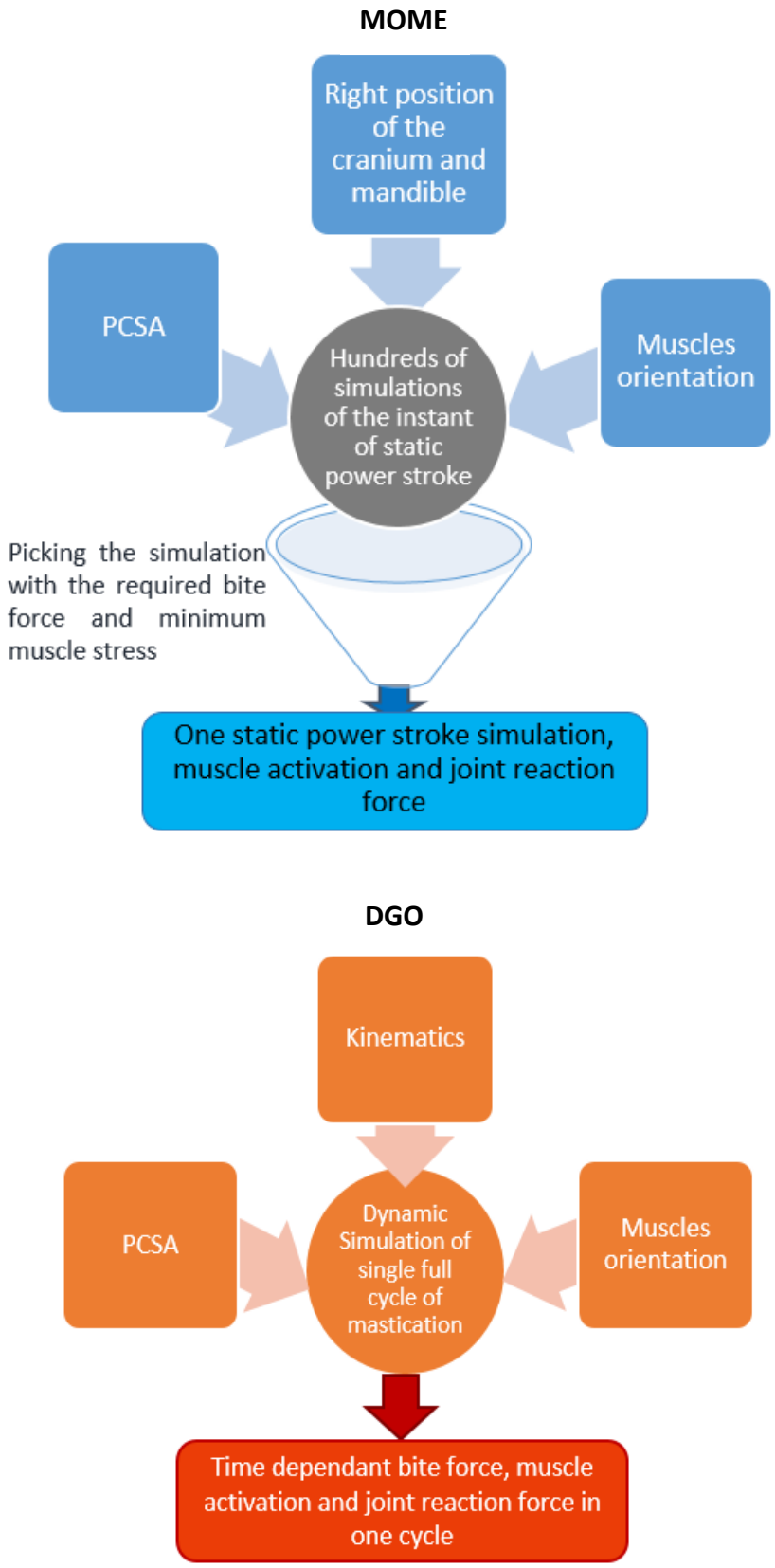

Figure 2.33 schematic of the two optimisation methods; the MOME method simulates only one instant of the power stroke through hundreds of computer simulations, whereas DGO simulates single but full masticatory cycle

Chapter 3. Investigation of optimisation criteria

3.1. Introduction

Multibody dynamic modelling is an engineering technique which has been utilised to study complex engineering structures for many years. In recent years with advances in computational performance, multibody dynamic modelling techniques have become even more advanced in the form of multibody dynamic analysis (MDA) which is available not only for engineering applications, but also for biomechanical proposes through specialised software such as ADAMS/view (MSC Software Corp, USA). MDA is suited to investigate complex biological structures in which convenient experimental and theoretical methods are not adequate. A prominent area of biomechanical studies, in which MDA has been exploited widely, is masticatory system analysis. MDA has been used for both extant and extinct species (Watson et al., 2014, Gröning et al., 2013b, Bates and Falkingham, 2012, Shi et al., 2012, Jones et al., 2011, Curtis et al., 2011b, Curtis et al., 2010a, Moazen et al., 2008b, Curtis et al., 2008, de Zee et al., 2007, Iwasaki et al., 2003a, Langenbach et al., 2002, Koolstra and van Eijden, 1992, Osborn and Baragar, 1985).

MDA of the masticatory system, like any other mechanical system, can be developed through two general approaches: a direct way in which activation of the muscles, in form of electromyography (EMG) data, are available and models are defined to predict bite force, joint reaction forces and/or kinematics; and the inverse approach in which bite force and/or the kinematics are available and muscle activation pattern is predicted. The inverse approach, which is mainly undertaken in this study, is more commonly used in masticatory analysis and is particularly suitable for extinct animals or species that obtaining EMG data is not feasible or easily achieved, such as animals with small size.

The general aim of this thesis is to investigate muscles activation pattern and joints reaction forces in masticatory system of the mouse, using MDA modelling techniques. As detailed EMG data for the mouse masticatory system is unavailable, the inverse approach is used to predict muscle activation pattern. Nevertheless, the

inverse approach of MDA modelling is associated with some disadvantages, the main one being indeterminacy in the system, which in this particular application is termed as “redundancy in the musculoskeletal system”. This can be explained as existence of indefinite number of solutions for the system; the masticatory cycle can be modelled as several intervals each of which can be solved using only six independent equations: three for the sum of the forces in three principal axes and three for the sum of moments about these axes. The number of unknowns (e.g. individual muscle forces, joint reaction forces and bite force in some models), however, will inevitably be much greater than six. Hence there is indefinite number of answers fulfilling the conditions. In the case of masticatory system, muscle redundancy means that there is not only one unique combination of muscle activations that provides the specific movement and/or bite force, but several combinations of muscle activation can satisfy the equations.

In reality, however, only few of these combinations are possible. Central nervous system coordinates muscle recruitment in masticatory system, however, the strategy that central nervous system uses to recruit muscles is a long-standing question. Therefore some optimisation criteria in multibody dynamic modelling are required to evaluate the possible combinations and to assist with selecting the optimal unique answer. Various optimisation algorithms have been commonly formed based on physiologically reasonable neuromuscular strategies in masticatory system of human and other species. One of the most commonly validated neuromuscular strategy, in many dynamic biological systems including masticatory system, is optimisation based on minimisation of muscle energy (or effort). Schindler et al. (2007) and Rues et al. (2008) both studied three different optimisation criteria to calculate muscle activation pattern in human bilateral biting: minimisation of the joint reaction force, minimisation of the overall muscle force and minimisation of the total muscle energy. They both compared resultant muscle activation pattern against *in vivo* EMG data from the same subjects and uniformly reported that the results from minimisation of the total muscle energy agreed their calculations the best. Iwasaki et al. (2003a) compared minimisation of total muscle effort (equivalent to muscle energy in previous studies) and

minimisation of joint reaction force to predict muscle activations and they too revealed that minimisation of total muscle effort resulted in more comparable muscle activation to *in vivo* EMG data.

Several other studies have implemented analysis to assess the accuracy of minimisation of sum of squared or cubed muscle forces in other joints (Li et al., 2006, Wang et al., 2004, Heintz and Gutierrez-Farewik, 2007) and reported on the comparable results between predicted muscle activation and the *in vivo* data for both approaches. However, as it was pointed out by Rasmussen et al. (2001), the optimisation using minimisation of sum of cubed muscle forces would impose some numerical difficulties, whereas minimisation of squared muscle forces (equivalent to muscle energy and muscle effort) would not be problematic in numerical calculations, yet provides robustness and efficiency. Hence the latter, in current study termed as "minimisation of overall muscle energy (MOME)", is favoured, between the two, by this thesis and is used as one of the two algorithms of optimisation to predict muscle activation pattern in the mouse masticatory system.

Shi et al. (2012) used minimisation of muscle stress as optimisation criteria to predict muscle activation pattern from MDA model of masticatory system of macaque. They modelled only one instant of the biting cycle using ADAMS/view from which the working and the balancing side muscle force ratios, peak bite force and joint reaction forces during unilateral biting were predicted. Using minimisation of muscle stress as optimisation criteria in MDA, similar to minimisation of overall muscle energy, involved numerous (hundreds to thousands) simulations to study various random combinations of muscles activation in order to allow selection of global minimum of overall muscle stress, which was a time and computer intensive operation. Modelling the full cycle of biting would greatly increase simulation's time and required memory, hence, one instant of biting was modelled instead. In current study similar modelling technique was used and static instantaneous biting of the mouse masticatory system was simulated using individual-specific MDA model, in which the mandible was in gape angle equal to the bite gape of *in vivo* bite force measurements (25^{o}).

In order to investigate whether the results derived from MOME algorithm agreed well to *in vivo* muscles activation in the mouse, EMG data is required to compare against the predicted data. However detailed EMG data is unavailable for this diminutive species. Considering that the prediction of muscles activation pattern in the mouse masticatory system is the primary goal of this study, it is invaluable to compare resulted muscle activation pattern against predictions of another optimisation algorithm to investigate their affinity and divergence.

The second algorithm that is investigated here is dynamic geometric optimisation (DGO). DGO algorithm operates based on this assumption that the muscle orientation is optimal for its function. In other words for a specific movement of the mandible, muscles that are orientated optimally to produce that movement activate to a higher extent. DGO does not include numerous trials, but only one, hence is not as time-intensive and requires lower amount of computational capacity. Moreover DGO provides the possibility of modelling one full cycle of biting, as opposed to instantaneous biting that could be modelled by MOME.

DGO was developed to predict muscles activation pattern in the masticatory system of *sphenodon* reptile (Curtis et al., 2010a) and was used and validated in *Tupinambis merianae* lizard and rabbit (Gröning et al., 2013b, Watson et al., 2014). Although muscle activation patterns that were predicted from MDA modelling of *sphenodon* were consistent to the muscle activation of the living animals, the predicted bite force was underestimated in this model (Curtis et al., 2010a). Considering that the mentioned model was not a subject-specific one, Gröning et al. (2013b) suggested that subject-specific data are to be used to construct an accurate model. They claimed that MDA model was very sensitive to the muscle attributes, such as fibre length and orientation and muscle intrinsic stress value, hence accurate measurement of such properties was essential to construct a realistic MDA model. Thus, they developed subject-specific MDA model of lizard and validated their data against *in vivo* bite force. Likewise, Watson et al. (2014) further proved the validity of DGO algorithm in subject-specific MDA model of the rabbit masticatory system, which again predicted comparable bite force to *in vivo* measurements.

Based on what has been discussed, both optimisation criteria are credible, and the muscle activation patterns predicted by both criteria have been shown to be in general agreement with available EMG data. However as it was reported by Schindler et al. (2007) and Rues et al. (2008) the muscle activation pattern is sensitive to optimisation criteria. When results from two optimisation criteria are in disagreement and EMG data is available, the accuracy of the models can be tested and model validation can be used to choose how to optimise the model. For the mouse the model accuracy cannot be tested via EMG, as sufficiently sophisticated EMG data is not available. However comparison of the results gained from the two optimisation methods can be used to test the precision of the models.

Hence in this study subject-specific model of the mouse masticatory system was developed, using an accurate muscle attachment and PCSA data. Initially the hinge-constrained temporomandibular joints (TMJs) were modelled which were gross over-simplifications, but useful in the initial stages of model development. Subsequently, more sophisticated model with contact-constraint TMJs was built. Both models were simulated to produce molar bite force of 8.97 N, using MOME and DGO optimisation algorithms, each of which that was associated with different modelling techniques. Resultant muscle activation patterns and joint reaction forces from MOME was compared against results of one instant of DGO simulation, which had the same bite gape and mandible position as the model in MOME. Moreover, muscle energy in both models was investigated.

Subsequent sections of this chapter gives brief description of the general experimental procedures to collect *in vivo* bite force measurement, accurate muscle attributes as well as of modelling techniques. In addition, brief account of modelling techniques required for development of MDA of the mouse as well as each of the two optimisation criteria, are given. Furthermore, PCSA calculations are presented, which have been used to develop multibody dynamic model of the mouse as well as muscle activation patterns and joint reaction forces which are derived from DGO and MOME, in both models with over-simplified hinge-constrained and realistic contact-constrained TMJs.

3.2. Methods

Development of MDA model required 3D geometries of the cranium and the mandible and accurate origin and insertion points, orientations and PCSA values of the masticatory muscles. Additionally, kinematics were required for DGO in order to simulate the whole cycle of biting and predict corresponding muscle forces. Moreover *in vivo* bite force data were crucial to validate the model.

3.2.1 Collection of the experimental data

All experimental data were collected at the Muséum National d'Histoire Naturelle (MNHN), Paris. All subsequent experiments were approved by the Animal Care and Use Committee at the MNHN.

Maximum *in vivo* bite force measurements were undertaken for 10 adult mice using a piezoelectric isometric force transducer (Kistler type 9203, +/-500 N). Measurements were taken with an incisal gape angle of 25±5° during voluntary biting, with 10 repeats for each mouse. The average of the maximum bite forces from the 10 mice was used for the MDA, and is referred to as the *in vivo* maximum bite force.

After sacrificing the specimens, masticatory muscles of one side of the head in five of the mice were dissected, while their attachment areas were carefully observed. Then their mass was measured to the nearest 0.01 mg using a microbalance (Mettler AE100) and averaged across all five specimens. Moreover, length of 10 random muscle fibres were measured and averaged for each muscle in each specimen after muscle digestion. Physiological cross sectional (PCSA) was calculated as outlined in chapter 2 with average muscle mass and fibre length obtained from each specimen and then was averaged across all five specimens. The average PCSA value was used in MDA modelling. Furthermore, due to unavailability of the measurement of the intrinsic stress for masticatory muscles two values were explored: 39.7 N/cm^2 and 50 N/cm^2.

3.2.2 Model construction

The generic multibody dynamic model of the masticatory system of the adult mouse is described in details in chapter 2. Geometries of the cranium and mandible were reconstructed as 3D shells from high resolution micro-computed-tomography (μCT) scans of the full head of one adult mouse which were performed on X-Tek HMX160 (X-Tek Systems Ltd, Tring, UK) in the School of Engineering, University of Hull with voxel size of 0.0183 mm in all three directions. The geometries of articulating surfaces (i.e. head of condyle and glenoid fossa) were carefully reconstructed and exported to ADMAS as solid parts to serve as contact surfaces at temporomandibular joints (TMJs). Muscle strands were defined between the cranium and the mandible, number of which was dependant on the attachment areas and complexity of the model Figure 3.1.

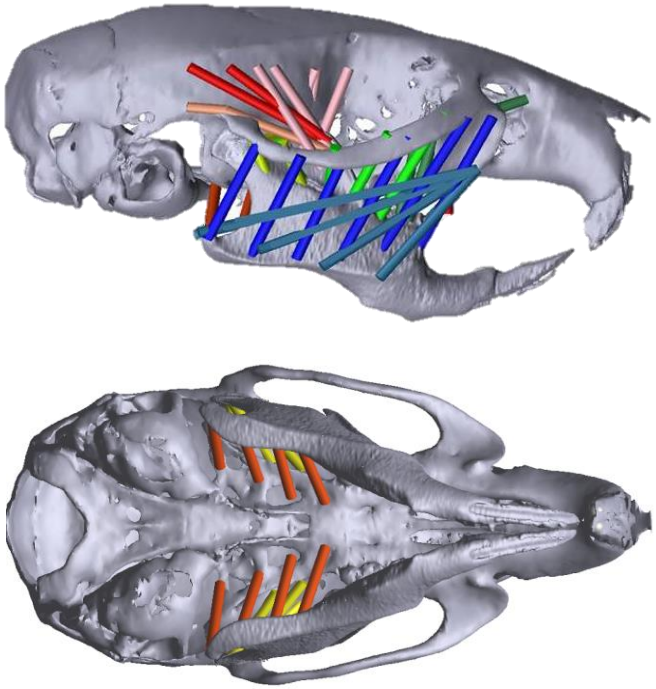

Figure 3.1 Muscle definition in the model of adult mouse.

The cranium was fixed in space while the hemi-mandibles could move independently and were connected together at the symphysis and to the cranium at the temporomandibular joints (TMJs). In reality, the symphysis of the mouse is

unfused and the hemi-mandibles are able to rotate about their long axes. In this part of the study, however, the symphysis was modelled as a fixed joint, making the mandible as one whole solid part to facilitate stability of the system.

The TMJs are also relatively unconstrained, but regulated by both ligaments and surrounding muscles. In this thesis, two different types of constraints were considered in the MDA models: hinge joints with one degree of freedom (rotational) and contact-constrained joints with six degrees of freedom. The contact constraint eliminated any extra constraints on joint and controlled the position of the joint based on the geometry of the contact surfaces. A similar arrangement to temporomandibular ligaments between the mandible and the cranium is used in the contact-constraint MDA model where the condyles contact the glenoid fossa via a bushing with stiffness of 80 N/mm in antereoposterior translational direction, 8 N/mm in translational and 20 N/mm rotational in mediolateral directions. In the remaining directions, the movement is unconstrained and controlled merely by articulating geometries. The bushing stiffness was defined with the minimum values that allowed the required movement in the vertical and horizontal directions. The high stiffness in the antero-posterior direction is defined in order to counteract the large horizontal component of the deep and superficial masseter, as well as the internal pterygoid. The activation of these muscles was associated with a relatively large anterior component which pulls the mandible forward and counterbalancing them required a high stiffness. The mediolateral rotational stiffness is relatively high to imitate the function of temporomandibular ligaments in stabilizing the mandible and preventing the condyle from excessive mediolateral movement. The stiffness in mediolateral translation is defined to counterbalance any asymmetry in muscles of the right and left side of the mandible. Generally, the mediolateral component of the muscles are equal and in opposite direction, hence the overall muscle force vector should lie in sagittal plane, however, a minor asymmetry in muscle definition would result in the unstable mandible in the absence of the rotational and translational mediolateral bushing. The food was simulated using an incompressible spring (stiffness of 200 N/mm) which was positioned at the first molar (M1) of the right side of the jaw.

In this study dynamic geometric optimization (DGO) and optimisation based on minimisation of overall muscles energy (sum of muscle force squared which is denominated as MOME in this study) were used to estimate muscles activation pattern (Shi et al., 2012, Curtis et al., 2010a). In the former approach, kinematic data is used to define the movement of the mandible and those muscles more aligned to the direction of required motion are activated preferentially to those that are more inclined to that motion direction. In contrast, the latter solves hundreds or thousands of random combinations of muscle recruitments to obtain the optimal combination which results in minimum overall muscle energy while producing required bite force.

In DGO, published data of cyclical jaw movement were used to define the instantaneous position of the mandible during the simulation (Utsumi et al., 2010). Force generation in each muscle was defined as Activation factor of each muscle was predicted Details about DGO is presented in chapter 2. Although DGO was readily exploitable to model 3D movements of the mandible, in this study only vertical and antereoposterior trajectories of mandible movement were used to define the position of mandible and the mediolateral movement was disregarded. The mandible was opened to a maximum gape of 1.2mm (reported as gape of hard food by Utsumi et al. (2010)) and then jaw closer muscles activate to close the mandible. At the gape of 0.96mm (equivalent to 25^{o} gape angle which is the angle that *in vivo* bite force measurement were obtained) the first molars contact the food item which is modelled an incompressible spring. The food springs has no stiffness during opening phase, effectively it does not exist, but at gape of 0.96mm it becomes stiff and incompressible. At this point, bite force, muscle forces and joint reaction forces were extracted from the MDA model.

In MOME, a fixed biting gape of 25^{o} was used to minimise the time of simulation. The position of the jaw was estimated from the kinematic data at the required bite gape, and orientation of the muscles was estimated accordingly. The food item was again modelled as an incompressible spring with constant stiffness of 200N/mm as one instantaneous biting was modelled.

For each muscle strand a variable called muscle activation factor (f_Q) was defined, that could vary randomly between zero and one. Force generation in each muscle strand was calculated was a factor of activation factor (f_Q) and maximum muscle force (F_{max}) ($F=F_{max}\times F_Q$). Maximum muscle force was predicted by PCSA value and then was divided equally between sub-sections of each muscle (strand) to find the proportion of each muscle strand (F_{max}). As the force in each muscle strand was a factor of its variable activation factor (f_Q) and constant maximum muscle force (F_{max}), generated muscle strand force would vary between zero and F_{max}.

There were nine functional group of muscles defined in the model, and each one of them was defined as multiple muscle strands, resulting in 68 strands in total which could activate independently. ADAMS/insight was used to make random combinations of 68 muscle forces (generated using a Latin Hypercube sampling technique) and then each combination, termed as one "trial", was run using Adams/view. Moreover, two objective functions were defined in ADAMS/insight: the overall muscles' energy (sum of muscle forces squared), and the bite force (food generated in the food spring). These objective functions were predicted from the simulation of each trial. 3200 trials were simulated in ADAMS/view with the equations of motion solved (solver in ADAMS uses an Euler–Lagrangian solution method (Rana and Joag, 1991)). Afterwards, the results of individual trials were imported to ADAMS/insight and optimisation was performed to select the optimum answer. A curve fitting routine in ADAMS/insight then identified the optimum combination of muscle forces that minimised the muscle energy while producing the required bite force (equal to *in vivo* bite force of 8.97N). Results from optimal muscle activation pattern were compared to results from DGO in the same gape.

3.3. Results

3.3.1 *In vivo* bite force measurements

The maximum recorded bite force for each of ten adult mice is presented in Table 3.1, where their average and standard deviation is also presented. The *in vivo* maximum bite force in the adult mouse, which is used to validate the model, was

considered as the average of these 10 values to assure the bite force value was representative of a typical mouse in this age group.

Table 3.1 *In vivo* bite force measurements from adult mice, measured from incisors.

Individual number	Maximum bite force (N)
1	9.23
2	8.17
3	9.15
4	7.64
5	8.98
6	9.15
7	9.29
8	8.84
9	9.64
10	9.64
Average	**8.97**

The standard deviation was not very high (normalised value of 6.35%), showing that although there were discrepancy within the group, it was negligible. Moreover, the majority of this discrepancy corresponded to individual number 4, who was not a great biter.

3.3.2 PCSA calculations

Muscle mass measurements

Average mass and standard deviation of each muscle and its sub-sections are presented in Table 3.2 (for individual muscle mass values see Table 2.3). Muscle mass across all five dissected adult mice are averaged and standard deviation and normalised standard deviation is calculated. The standard deviation was in range of 8% to 35%, the lowest of which belonged to the digastric and the deep masseter and the highest was correspondent to Infra-orbital zygomaticomandibularis. This differences arises not only from normal variance of muscle size within the group, but also, considering the small size of muscles, from inaccuracy in dissection. Using the average muscle mass values instead of mass of one specimen, reduces the effect of errors resulted from dissections inaccuracy.

Table 3.2 Average mass of muscles' functional sub-sections (in gram) across all five adult specimens and standard deviation (in percentage relative to the average mass). SM: superficial masseter; DM: deep masseter; AT: anterior temporalis; PT: posterior temporalis; SZT: suprazygomatic temporalis; AZM: anterior zygomaticomandibularis; IOZM: infra-orbital zygomaticomandibularis; PZM: posterior zygomaticomandibularis; MP: Internal pterygoid; EP: external pterygoid; DG: digastric.

Individual number	SM (G)	DM (G)	AT (G)	PT (G)	SZT (G)	AZM (G)	IOZM (G)	PZM (G)	IP (G)	EP (G)	DG (G)
Average (g)	0.020	0.033	0.011	0.008	0.002	0.004	0.003	0.002	0.010	0.004	0.013
SD (%)	12.11	8.82	13.37	29.91	16.42	34.85	35.38	20.83	18.9	26.04	8.78

Muscle mass is one of the factors indicating the force production of each muscle. The ratio of muscle mass to the overall jaw closing muscles mass is invaluable in studying the importance of each muscle in force generation, which is presented in Figure 3.2. The masseter, which composed of deep and superficial parts, comprised 54% of jaw closers mass. Temporalis was the second largest muscle, which comprises of 21%, followed by zygomaticomandibularis and internal pterygoid. The smallest muscle was external pterygoid (Table 3.3). Moreover, standard deviation expressed in percentage with respect to the average mass of each jaw closer muscle is presented and the highest value belongs to pterygoid muscles. Considering the difficult position of the pterygoid muscles, dissection of these muscles are the most inconvenient. Hence, the inaccuracy in dissected muscles is likely. On the other hand, the standard deviation of zygomaticomandibularis as the whole muscle is considerably less than individual sub-sections. The latter is suggesting that although the zygomaticomandibularis as the whole muscle was distinct, division between sub-sections was not clear. Likewise, temporalis muscle ensemble was distinct, but separation between sub-sections was not clearly visible.

Table 3.3 Relative mass of jaw closer muscles; T: temporalis (composing of SZT, AT and PT); ZM: zygomaticomandibularis (composing of IOZM, AZM, and PZM);

JAW CLOSER	SM (%)	DM (%)	T (%)	ZM (%)	IP (%)	EP (%)
RELATIVE MASS (%)	20.42	33.46	21.36	10.17	10.36	4.23
SD	0.41	1.64	0.78	0.52	1.11	0.71
SD (%)	2.01	4.90	3.64	5.11	10.73	16.72

Proportion of each functional part (sub-sections) of jaw closer muscles is presented in Figure 3.2. The deep and superficial masseter, anterior temporalis and internal pterygoid are the four largest sub-sections of jaw closers respectively. The five smallest functional muscle sub-sections are suprazygomatic temporalis and all three parts of zygomaticomandibularis and external pterygoid.

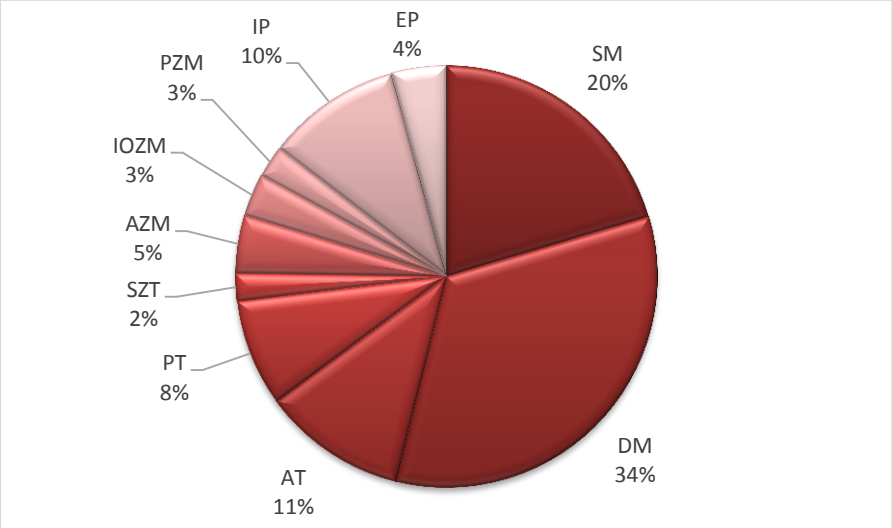

Figure 3.2 Relative mass of jaw closer muscles averaged across five dissected adult specimens. This value is calculated as the ratio of average mass of each jaw closer to the overall average mass of jaw closer muscles. For abbreviations see caption of Table 3.2.

Muscle fibre measurements

Average fibre length, standard deviation and relative standard deviation across all five specimens in both jaw closer muscles and jaw opener muscle (digastric) are presented in Table 3.4 (for full range of measurements see appendix I). The posterior temporalis and digastric muscles had the longest fibres, followed by the deep masseter. Relative standard deviation of muscle fibres (percentage of SD divided by the mean value) across all samples was in range of 10% to 30%. The

existence of some variation in muscle fibre length was indeed expected due to the subtle differences of the muscle fibre length within the muscle structure and between the groups of specimens. The high relative standard deviation of the muscle fibre measurement in this study can arise for several reasons, for example, complex multi pinnation architecture of the muscle, variability within the group of specimens and errors in drawing and measuring of the muscles. The relative standard deviation is the highest in all three parts of the zygomaticomandibularis and of the temporalis, as well as the external pterygoid. The high relative standard deviation might indicate the complexity of muscle architecture, as it coincides with muscles such as temporalis and zygomaticomandibularis with non-direct wrapping orientation. The averaging of the muscle fibre measurements results in a maximum of ±30% in the PCSA calculations.

Table 3.4 Average muscle fibre measurements across all five dissected adult specimens along with standard deviation and relative standard deviation (percentage of SD/average)

MUSCLES	AVERAGE FIBRE LENGTH (CM)	SD	RELATIVE SD (%)
SM	0.2508	0.0243	10.58
DM	0.3052	0.0559	16.15
AT	0.2650	0.0427	20.48
PT	0.3430	0.0372	28.43
SZT	0.2495	0.0619	19.35
AZM	0.2524	0.0442	29.71
IOZM	0.2794	0.0368	32.20
PZM	0.2456	0.0268	22.06
IP	0.2508	0.0267	18.72
EP	0.2871	0.0517	25.47
DG	0.3425	0.0322	11.11

Using average muscle mass and fibre lengths, PCSA values of the muscle were calculated which are presented in Table 3.5. Moreover, two sets of muscle forces were calculated, force $_1$ which was calculated using muscle intrinsic stress value of 39.7 N/cm^2 (Gonzalez et al., 2000) and force $_2$ which was calculated with muscle

intrinsic stress value of 50 N/cm^2 (see section 2.2.3 for further details). In this chapter, force $_2$ was used in models.

Table 3.5 Calculation of PCSA and maximum force for each muscle in the model, estimated from and averaged across all five adult dissected specimens; Force $_1$ is calculated with muscle intrinsic stress value of 39.7 N/cm^2 and Force $_2$ is calculated with muscle intrinsic value of 50 N/cm^2.

MUSCLES	MASS (G)	MUSCLE FIBRE LENGTH (CM)	VOLUME (CM^3)	PCSA (CM^2)	FORCE $_1$ (N)	FORCE$_2$ (N)
SM	0.0201	0.2508	0.0190	0.0759	3.01	3.79
DM	0.0328	0.3052	0.0310	0.1017	4.04	5.21
AT	0.0108	0.2650	0.0102	0.0386	1.53	1.96
PT	0.0082	0.3430	0.0078	0.0226	0.90	1.12
SZT	0.0021	0.2495	0.0020	0.0078	0.31	0.40
AZM	0.0044	0.2524	0.0042	0.0165	0.66	0.81
IOZM	0.0031	0.2794	0.0029	0.0105	0.42	0.52
PZM	0.0024	0.2456	0.0023	0.0093	0.37	0.47
IP	0.0103	0.2508	0.0098	0.0389	1.54	1.93
EP	0.0042	0.2871	0.0040	0.0139	0.55	0.69
DG	0.0128	0.3425	0.0121	0.0354	1.40	1.77

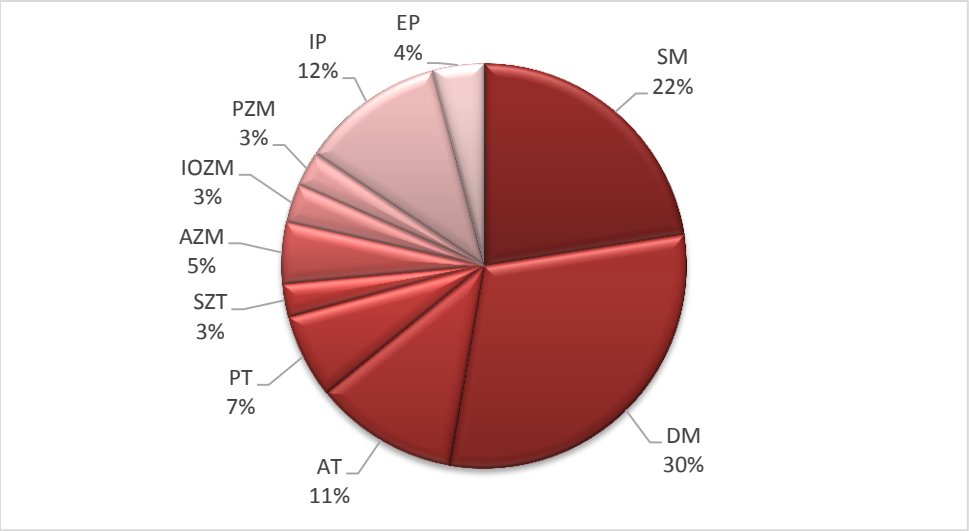

Figure 3.3 Relative force in jaw closer muscles averaged across five dissected adult specimens. For abbreviations see caption of Table 3.2.

The pie chart in Figure 3.3 presents relative maximum force of each jaw closer muscle calculated from PCSA values. The two largest relative force belongs to deep and superficial masseter respectively, which together comprise more than 52% of the overall jaw closing force. The next most important muscle is temporalis comprising of 21% of overall jaw closers force. Internal pterygoid followed by zygomaticomandibularis, which composes of three parts, generate the next two largest forces. The smallest force is generated by external pterygoid.

3.3.3 Modelling results

The relative muscles activation in both hinge and contact-constrained models during first molar biting at a bite gape of 25^{o} was predicted by DGO and MOME and is presented in Table 3.6. The muscle activations were predicted for a molar bite force of 8.97N.

Table 3.6 Predicted relative muscle activation percentage in both hinge and contact-constrained models, optimised by MOME and DGO. Abbreviations: F_{pred}: predicted force from modelling; F_{max} : maximum muscle force estimated from PCSA; WS: working side; BS: balancing side.

Muscles	F_{pred}/F_{max} % hinge-constrained, MOME		F_{pred}/F_{max} % hinge-constrained, DGO		F_{pred}/F_{max} % contact-constrained, MOME		F_{pred}/F_{max} % contact-constrained, DGO	
	Left (B S)	Right (WS)	Left (B S)	Right (WS)	Left (B S)	Right (WS)	Left (B S)	Right (WS)
SM	47.1	47.5	26.3	26.3	43.3	46.0	24.8	25.3
DM	29.1	40.6	61.8	62.1	26.3	42.4	61.3	61.3
AT	51.5	49.8	40.0	40.0	30.0	42.2	35.4	35.4
PT	26.3	27.2	45.7	45.7	17.3	23.2	45.3	45.3
SZT	25.9	25.2	0	0	35.8	17.7	0.00	0.00
AZM	77.0	75.2	100	100	86.1	75.6	100	100
IOZM	100	100	100	100	100	100	100	100
PZM	48.7	47.2	100	100	8.0	50.0	100	100
IP	15.7	15.7	100	100	22.1	11.7	100	100
EP	66.9	59.8	100	100	39.7	16.7	100	100

Muscles activation for hinge and contact-constrained models resulting from DGO were more or less similar; only a minor difference was predicted in the activity of the masseter and temporalis which were predicted to be slightly more active in the hinge-constrained model than the contact-constrained model. The same general

pattern was observed for predictions from MOME in hinge and contact-constrained models; considering the muscles ensemble, they were predicted to be more active in hinge-constrained model with exception of internal pterygoid of the balancing side and masseter and zygomaticomandibularis of working side (Figure 3.5).

However, the activation of functional divisions of muscles in hinge and contact-constrained joints were more varied in MOME; the suprazygomatic temporalis and anterior zygomaticomandibularis of the balancing side and deep masseter and posterior zygomaticomandibularis of working side were activated to a higher extent in the contact-constrained model. The highest difference in magnitude of muscle activation between hinge and contact-constrained model predicted from MOME, was for external pterygoid and temporalis muscle in both working and balancing side and masseter of the balancing side; which were all over-estimated in hinge-constrained model.

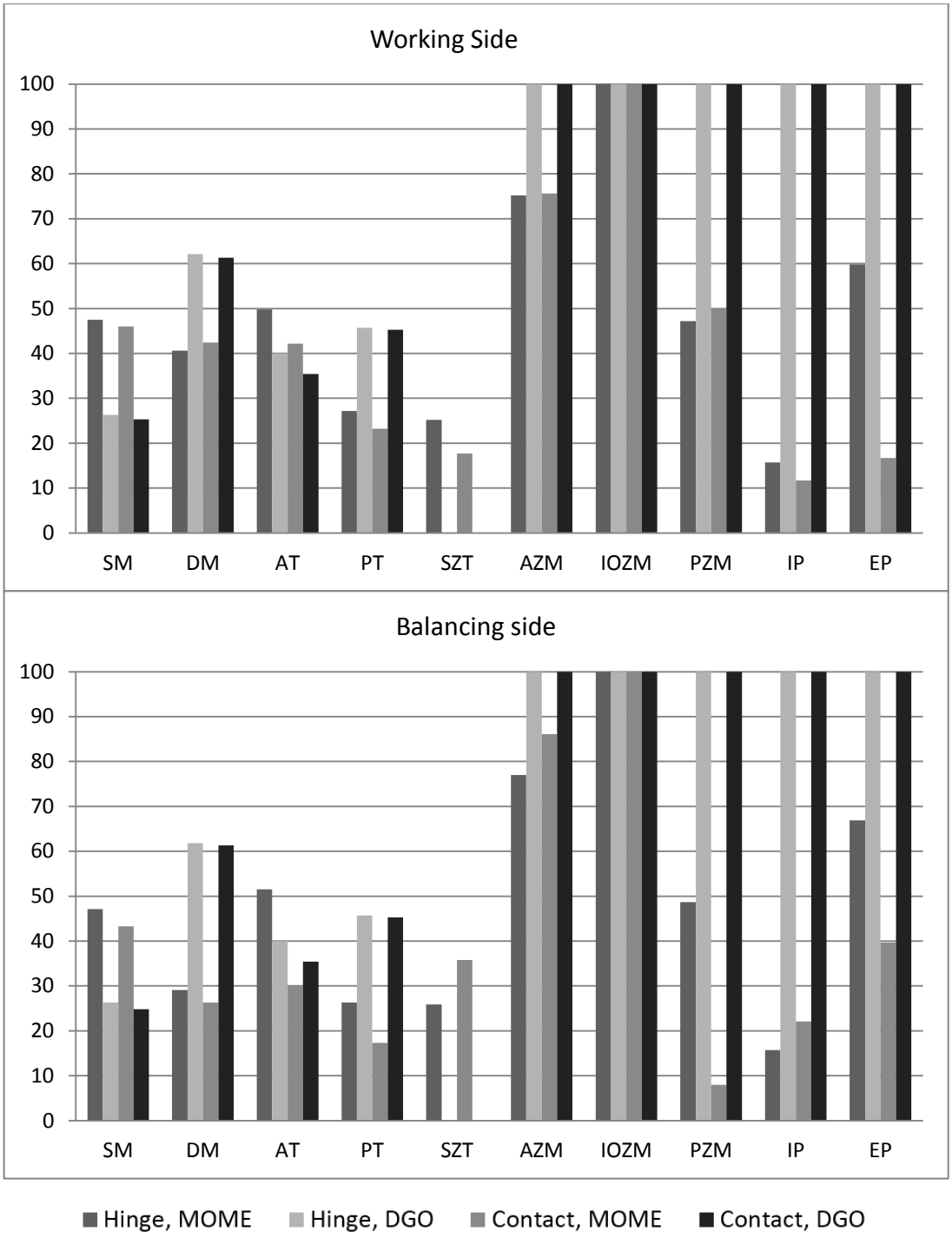

Figure 3.4 Relative functional muscle sub-sections activity in working and balancing side predicted from the modelling. For Abbreviations see Table 3.2.

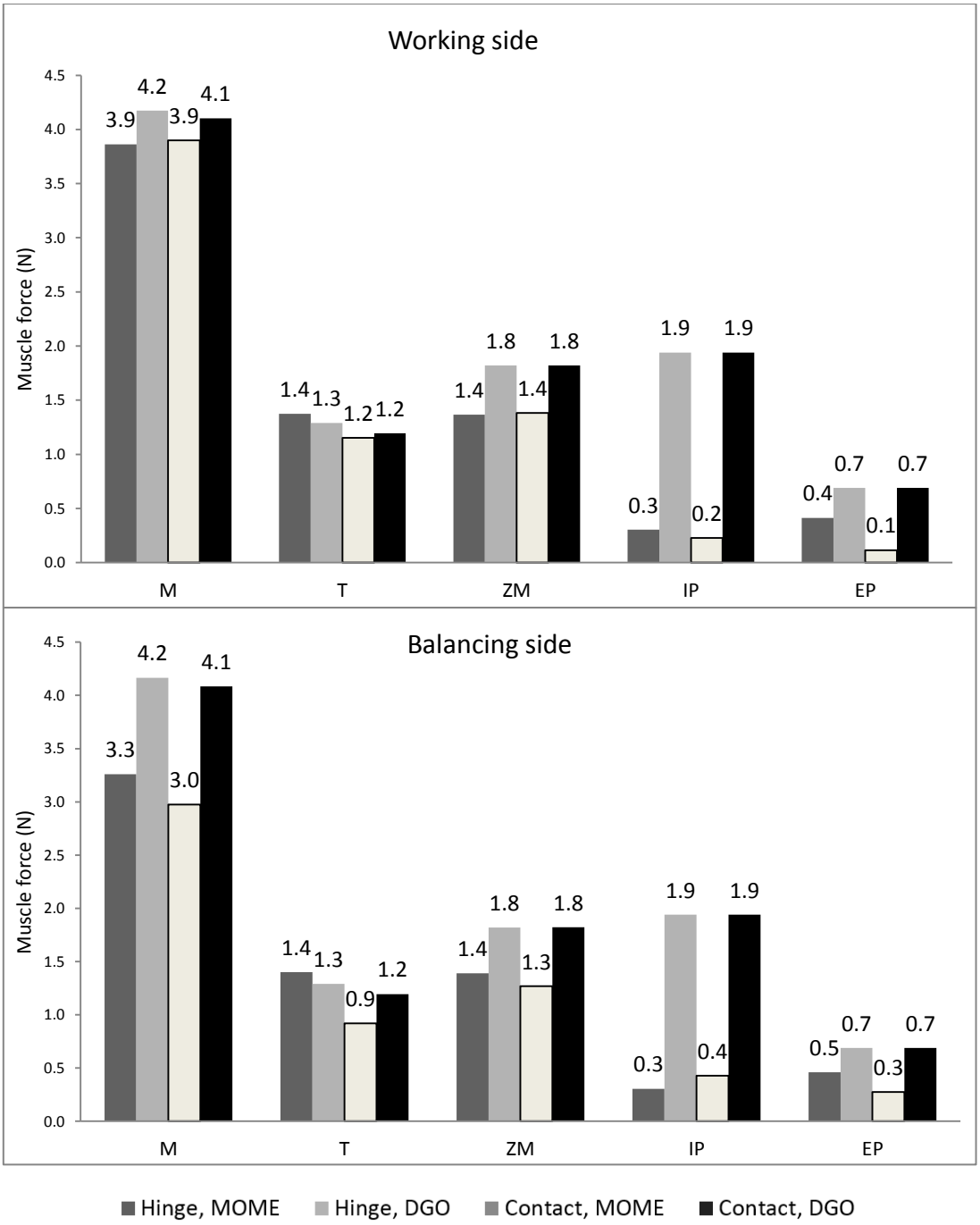

Figure 3.5 Absolute ensemble muscles force in A) working side and B) balancing side predicted from the modelling. Abbreviations: M: masseter; T: temporalis; ZM: zygomaticomandibularis; IP: internal pterygoid; EP: external pterygoid.

Regarding muscle functional sub-sections, MOME and DGO predict variable activations. MOME predicted higher activation for superficial masseter than DGO. In contrast, the deep masseter's activation was predicted lower by MOME than DGO. Likewise, anterior temporalis was predicted to activate to a higher level in MOME than DGO, in contrast to posterior temporalis which was activated to a

lower level in MOME than DGO. Also according to DGO, the suprazygomatic temporalis was inactive in both hinge and contact-constrained model, but had some activity in MOME.

While the only muscle that was activated maximally in all four models was infra-orbital zygomaticomandibularis, posterior and anterior divisions of zygomaticomandibularis were predicted to activate to a lower extent according to MOME compared to DGO.

The highest difference of relative and absolute activation level between DGO and MOME was for the internal pterygoid muscle which was predicted to activate up to 88% or 1.7 N higher in DGO than MOME in the contact constrained-model.

In regard to jaw closer ensemble muscles, DGO appeared to predict higher activation for all muscles in both hinge and contact-constrained models compared to MOME. The only exception was the temporalis muscle in the hinge-constrained model (Figure 3.5). However different functional divisions of masseter and temporalis muscles were estimated to act independently. The activation of superficial masseter was predicted lower in DGO whereas deep masseter was predicted to activate to a higher extent. Likewise DGO resulted in higher activity of anterior temporalis and lower activity of posterior temporalis.

The muscle activation in working and balancing side predicted from DGO was more or less analogous, and the minor difference was a result of asymmetry of the cranium and the mandible.

Muscle activation patterns predicted from MOME, however, were more varied. In the more constrained model (hinge joint) the deep masseter of the working side was 11% more activated than the balancing side, in contrast to the activation of external pterygoid, which was 7% higher in balancing side than working side.

The muscle activation pattern predicted from MOME in contact-constrained model was even more miscellaneous and their difference was more obvious. The activity of deep masseter in working side was 18% higher than the balancing side. Anterior and posterior temporalis and posterior zygomaticomandibularis were predicted to

show higher degree of activation (12%, 6% and 42% higher respectively) in working side compared to balancing side in the contact-constrained model, whereas these muscles had relatively analogous activation in the model with a hinge joint. On the other hand, Supra-zygomatic temporalis, anterior zygomaticomandibularis, internal and external pterygoid were estimated to have higher activation at the balancing side compared to working side in the contact model (18%, 11%, 12% and 23% respectively). The highest absolute difference between working and balancing side was in masseter and mostly deep masseter, which was equal to 0.9N higher activity in working side.

Table 3.7 Joint reaction forces and sum of muscle energy in hinge and contact-constrained models, predicted from MOME and DGO

	Hinge, MOME		Hinge, DGO		Contact, MOME		Contact, DGO	
	L (B S)	R (W S)	L (B S)	R (W S)	L (B S)	R (W S)	L (B S)	R (W S)
Joint reaction force	2.9	2.8	4.9	2.3	0	0	2.11	0.9
overall muscle energy	2.2		2.8		2.1		2.7	

Table 3.8 Three components of the joint reaction forces and associated bushing forces in the MOME and DGO model. X is at the antero-posterior direction, Y is dorso-ventral direction and Z represents the mediolateral direction (consult Figure 3.6). R: right side (working side); L: left side or balancing side

	MOME				**DGO**			
Force and Torque	X	Y	Z	Mag	X	Y	Z	Mag
Bushing force -R	-2.5	-0.1	0.4	2.5	-2.2	-0.9	0.1	2.4
Bushing force - L	-1.6	-0.1	-0.0	1.6	-1.9	-1.6	0.1	2.5
Reaction force - R	0	0	0	0	-0.5	1.6	-1.3	2.1
Reaction force - L	0	0	0	0	-0.2	0.6	0.6	0.9
Bushing Torque-R	-8.1	0	0	8.1	-10.7	0	0	-10.7
Bushing Torque-L	-8.1	0	0	8.1	-10.7	0	0	-10.7

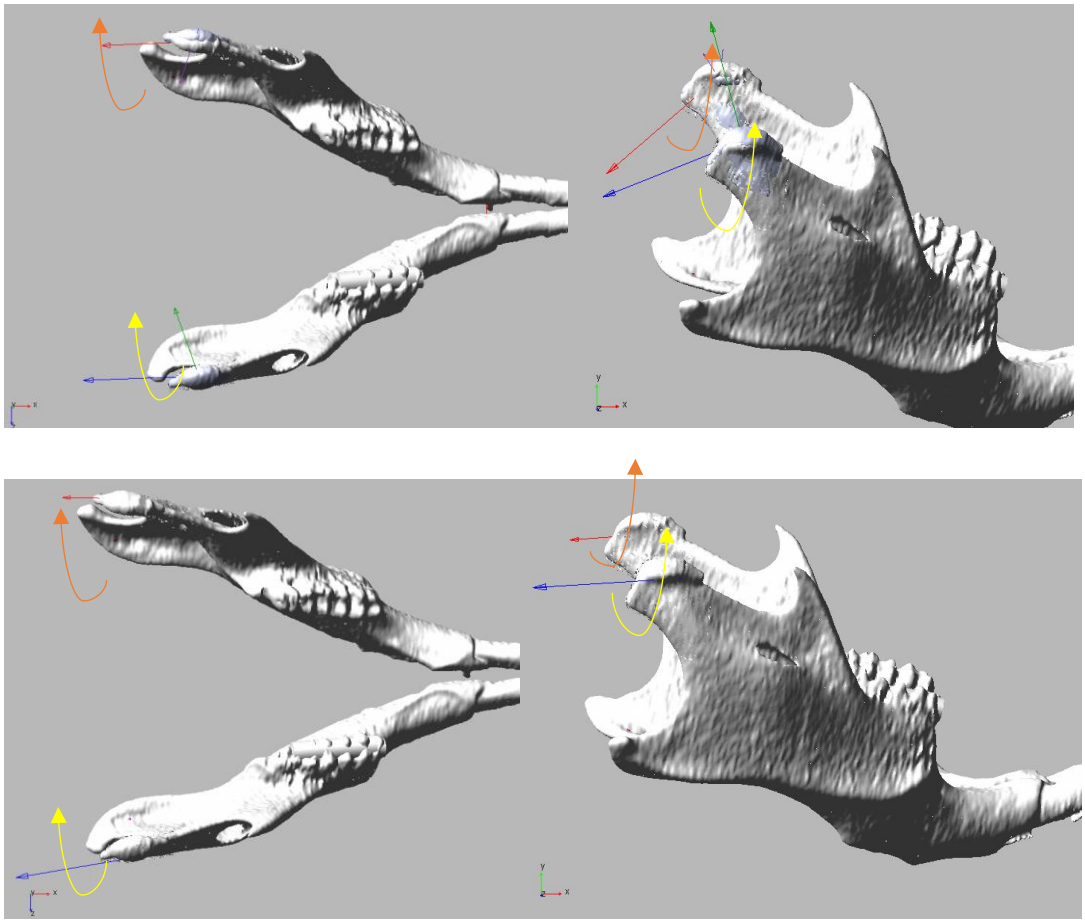

Figure 3.6 Top and side views of the mandible with contact and bushing forces represented as vectors resulted from DGO (top) and the MOME (bottom). Red: left bushing force; blue: right bushing force; violet: left contact force; green: right contact force. The violet and green are not present in MOME model as the contact force was found to be zero. The yellow and orange arrows are showing the torque resulted from bushing in working and balancing side respectively.

Joint reaction forces and sum of muscle energy in each of models are presented in Table 3.7. As expected the sum of muscle energy in models optimised using MOME was lower than DGO. Joint reaction forces were predicted to be zero in both working and balancing side of the models optimised with MOME, suggesting that TMJs were unloaded. Moreover, in the hinge joint model, the joint reaction forces were also predicted to be almost equal. DGO, on the other hand, predicted uneven joint reaction forces in working and balancing side. Furthermore, in the contact-constrained model both working and balancing side were predicted to bear lower load than the hinge-constrained model. The ratio of the working to balancing side in the model with a hinge joint was 0.47 and in the contact-constrained model was

0.43. These joint reaction forces and the associated bushing forces in the contact constrained models are resolved to their three Cartesian components and are presented in Table 3.8. The bushing force in X direction is substantial in both working and balancing side. Moreover, there is a high torque resulted from bushing stiffness in mediolateral direction towards the working side in both working and balancing sides (8.01 N.mm in both working and balancing side). The combination of the bushing force, the torques and muscle activations maintain the stability of the model.

3.4. Discussion

In this model, the molar bite force of 8.97N was modelled, whereas the *in vivo* bite force was measured at the position of incisors, because obtaining *in vivo* molar bite force was not feasible. Although the incisor biting could have been modelled, theoretically the muscles reach their 100% activation in order to produce the maximum bite force. Hence all muscles in both optimisation approaches would be fully active and the results were not revealing any information about the comparability of these two optimisation approaches. As there is a trade-off between leverage of the biting position and the maximum bite force (Gröning et al., 2013b), it was expected that the maximum bite force produced in molars to be higher than incisors, hence bite force of 8.97N was feasible and sub-maximal in position of M1. This theory was tested by simulating M1 biting and maximum bite force was investigated, which is presented in Chapter4, and it was observed that bite force of 8.97N is submaximal in M1 position.

Thus to generate the *in vivo* bite force of 8.97N, muscle were not maximally activated and there were indefinite muscle activation pattern that could result in required bite force. Therefore optimisation methods could be investigated and compared. Moreover as the *in vivo* bite force measurements were carried out at a bite gape of 25 ± 5^{o} the results too were compared at the same gape angle to assure the muscle orientations *in vivo* and modelling were comparable.

Accurate muscle attributes are crucial in developing MDA. Relative jaw closer's muscle volumes/mass was reported previously by Baverstock et al. (2013). The agreement of measured relative muscles volume to what has been reported previously demonstrates the accuracy of dissections and partly PCSA values (Figure 3.6).

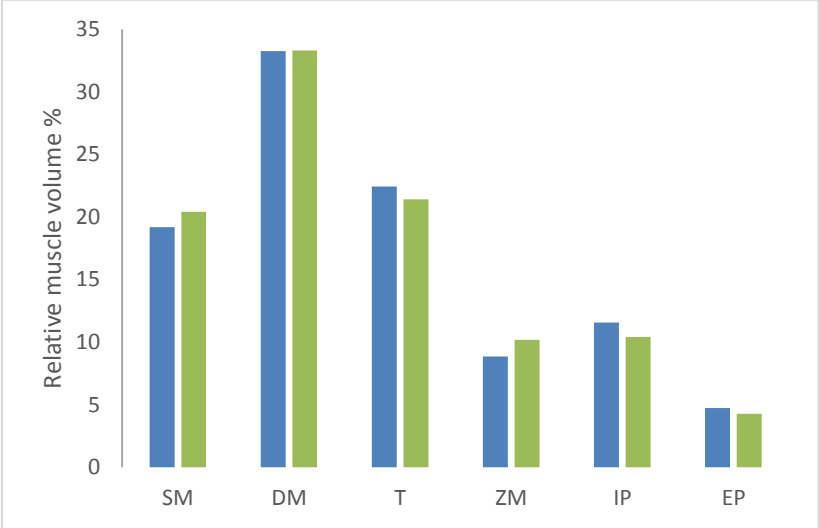

Figure 3.7 Relative muscle volume; blue: from measurement of mass; green: reported by Baverstock et al. (2013).

3.4.1 Type of constraint

Models were developed using both hinge joint and contact constraint at TMJs. It was observed that when the model was less constrained, as when using the contact constraints in the TMJs, the muscles were generally predicted to have lower activity compared to hinge-constrained model. DGO predicted slightly higher activity of masseter and temporalis in model with hinge joint compared to contact constraint model (0.1 N difference each).

Likewise, MOME predicted equal and higher activity for muscles in model with hinge joint than the model with contact constraints, and the difference was more considerable than DGO. The only exception was the internal pterygoid. Furthermore, MOME predicted variable muscle activations for working and balancing side. In working side the activity of masseter and zygomaticomandibularis was not affected by the type of the constraint. The activity of temporalis, internal and external pterygoid, however, was predicted to be higher at the working side of

the hinge-constrained model than the contact-constrained model. Nevertheless, the highest difference in working side, between the hinge and the contact constrained model, which belonged to external pterygoid, was less than 0.4N. On the other hand, in balancing side all muscles, except for internal pterygoid, were predicted to activate to a higher level in the hinge-constrained model. The highest difference, however, was as low as 0.5N. The higher activity of the internal pterygoid muscle in contact-constrained model could be linked to its controlling function to maintain the position of condyle and stability of the system in the less constrained joint.

The higher muscle activation in hinge constraint model was suggesting not only the overall muscle energy of the model with hinge joint would be higher, but also its reaction force were likely to be higher too. Indeed that was the case and over-constraining the joint not only resulted in over-estimation of the muscles activity and consequently overall muscle energy, but also joint reaction forces were higher too. However, the differences of neither individual muscle activity, nor the overall muscle energy were considerable, in contrast to the predicted joint reaction forces. On the other hand, substantial difference between working and balancing side muscle activity in the less constrained model was predicted in MOME, suggesting when joints had higher degree of freedom, activation of the muscles was more complex to provide balance and stability in the system.

Therefore if the general muscle activation pattern was of interest, the hinge joint could be a reasonable substitute, providing that joint reaction forces were not the matter of interest. However, if muscle activity between working and balancing sides were of importance, the hinge joint would not be a realistic constraint to use and the contact constraint would be more appropriate. Accordingly, in subsequent sections of this chapter MDA models of the mouse masticatory system with contact constraints were investigated and compared.

3.4.2 Optimisation method

Predictions of MOME and DGO in contact constrained model were compared at two levels: muscles ensemble and independent functional sub-sections of muscles. At the first level, it appeared that DGO was almost consistently predicting higher activity for all ensemble muscles; for some such as zygomaticomandibularis, internal and external pterygoid it predicted 100% of activation. More careful observation of different functional divisions of muscles, however, revealed that there was a more complex relationship between different parts of muscles. In masseter it was observed that superficial part was considerably more activated to achieve minimum muscle energy, whereas the activity of deep masseter was reduced compared to DGO. Likewise, according to MOME anterior temporalis was predicted to achieve lower level of activity at the balancing side and higher activation in working side compared to DGO, as opposed to posterior temporalis which was activated to a higher degree in both sides in MOME.

As it was pointed out by Shi et al. (2012), MOME predicted muscle activation by favouring anteriorly positioned muscles, hence muscles with high leverage activated to a high level. On the other hand, DGO predicted muscle activity based on vertical and horizontal components of the muscle orientation and of the required movement. Since in this model, the required movement was only vertical, DGO predicted muscle activation based on its vertical component. In other words, the muscles with higher vertical components were activated to a higher level.

Higher activity of superficial masseter in MOME can be explained by the mentioned principle; the more anterior the muscle was positioned, the higher level of activation it had. In contrast, the lower activity of posterior temporalis and posterior zygomaticomandibularis in MOME compared to DGO was due to their posterior position. On the other hand, the higher activation of the deep masseter and substantially higher activation of internal pterygoid in DGO can be explained by their high vertical component, the latter of which had considerably less activation in MOME due to its posterior position. Also DGO estimated the supra-zygomatic part of the temporalis to be completely inactive which can be explained by its relatively horizontal orientation. The only muscle which was activated maximally by both

DGO and MOME was infra-orbital zygomaticomandibularis which was positioned both anteriorly and vertically.

Moreover, DGO predicted analogous muscle activation patterns for working and balancing sides, this algorithm ignored the differences between the two sides. This was linked to the activation factor of the muscles in DGO which was a factor of the required movement and muscle orientation. The required movement was only considered in the sagittal plane and the movement in transverse direction was neglected; also muscle orientations were almost symmetric. Hence the muscle activation pattern was symmetric in DGO. Therefore, if investigation of working and balancing side is the objective of any study, MOME is more effective. Hence in next section, only results predicted by MOME were investigated to study working and balancing side differences.

Although overall muscle energy predicted by MOME was not greatly different from DGO, joint reaction forces were different. MOME predicted that both TMJs were evenly loaded in the hinge-constrained model and completely unloaded in the contact-constrained model. It could be that muscle activation was in a manner that put no loading on TMJs. This was in accordance to what Weijs and Dantuma (1975) have previously reported from their calculations in rat; during mastication TMJ of neither working side nor balancing side was loaded. However, in the model the bushings force is an important factor in stabilising the mandible too. Although the magnitude of the bushings force is less than 25% of the bite force, its torque in mediolateral direction is more substantial and prevents the mandible from rotating towards the balancing side (clockwise rotation).

Figure 3.8 is presenting the schematic of the mandible (in frontal view), which is modelled as one solid structure composing of two beams connecting in the symphysis region. The centre of mass of the whole mandible is assumed to be in the middle of the two centres of mass of the hemi-mandibles (which were extracted from ADAMS). All other dimensions are also extracted from the model in ADMAS/view. The muscle forces were assumed to be symmetrical in mediolateral direction, hence counterbalance each other (overall of almost zero in z-direction,

see Table IV.1). The vertical component of the sum of muscle forces (extracted from Table IV.1) at the working and balancing sides were applied at a point between TMJ and symphysis. The precise position of these two points is unknown. This is because the point of application of the overall force varies with the magnitude of overall force. The bushing forces and torques are applied to the system (Table 3.8). At the working side (right) the bushing force has both vertical and mediolateral components, whereas in the balancing side the bushing force only has a vertical component. From the sum of the forces in the vertical direction we have:

$$\Sigma F_Y = -BF+MF_R+MF_L-BU_YF_L- BU_YF_R$$
$$=-9+5.1+4.1-0.1-0.1= 0 \quad (3.1)$$

The torques resulted from bushing are equal at both working and balancing side's TMJ (8.1N). Taking the moment around the centre (O) (with convention of the clockwise moment being positive) we have:

$$\Sigma M_O=(-BF\times2.1)+(MF_R\times a)-(BU_ZF_R\times 0.8)-(BU_YF_R\times5.0)-(MF_L\times b)+(BU_YFL\times5.0)+(2\times Torque\ )$$

$$=-9\times2.1+5.1\times X-0.4\times0.8-0.1\times5.0-4.1\times Y+0.1\times5.0+2\times8.1=0 \quad (3.2)$$

$$5.1\times a- 4.1\times b=3.02$$

$$a-0.8b=0.59 \quad (3.3)$$

The equation (3.1) shows that the mandible can be stable in the frontal plane, even though the condyle and the glenoid fossa are not contacting. The sum of the forces in vertical direction is equal to zero which means that the mandible is in equilibrium. The mandible is in rotational equilibrium around the centre of the mandible (O) only if the equation (3.3) is true. So if the points of the application of the sum of muscle forces in the working side and balancing side have the relation as the equation (3.3), the mandible is in rotational equilibrium.

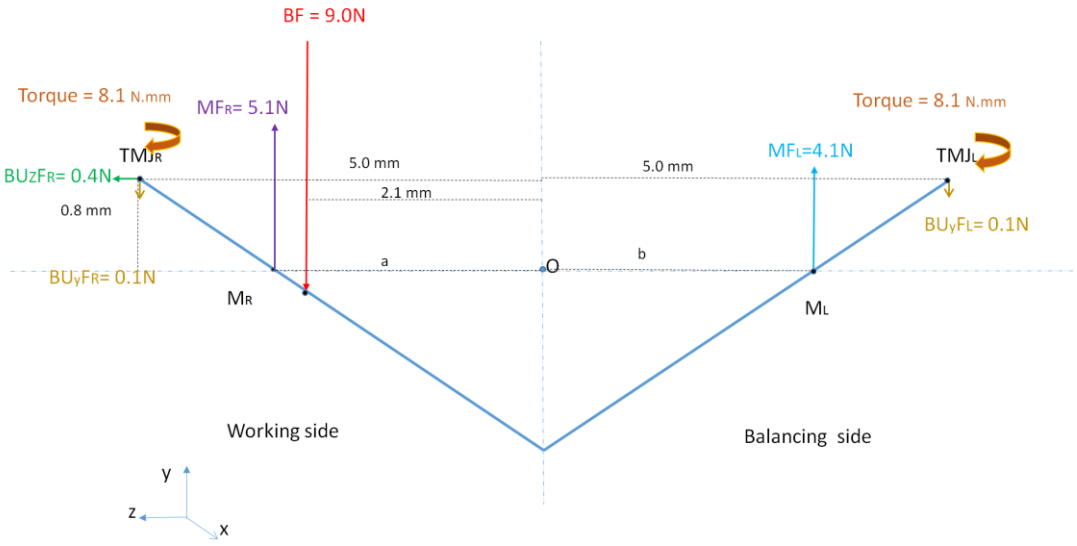

Figure 3.8 Free body diagram of the mandible in MOME in frontal view. O is assumed to be the centre of mass of the whole mandible at the mid-point between the centre of mass of the two hemi-mandibles; M_L and M_R : point of the application of the overall muscle force in the left and right side of the mandible; a and b: the distance between O and the M_R and M_L respectively. MF_L and MF_R: overall muscle forces in vertical direction in left and right respectively (consult Table IV.1); BU_yF_R and BU_yF_L are vertical component of the bushing force in the right and left side respectively; BU_ZF_R is the mediolateral component of the bushing force in right side (this force was zero in left side); BF: bite force which was applied at the position of the M1 in the right side of the mandible; Torque: is the torque resulted from bushing in both left and right sides

The rotational equilibrium of the mandible is highly dependent on the bushing torque. In the absence of bushing torques the forces intend to rotate the mandible towards the balancing side. The bushing torque prevents this rotation and stabilizes the mandible. This task is again carried out by the ligaments in the joint, however, the limit of the torque that the ligaments can withstand without being damaged is not known. Hence, the possibility of withstanding the torque of 8.1N.mm in TMJ in biological terms cannot be verified with our current knowledge.

Unlike MOME, DGO predicted higher reaction force in balancing side compared to working side (ratio of working to balancing side of 0.47 in hinge-joint and 0.42 in contact-constrained model). Considering activation of muscles predicted by DGO were analogous in working and balancing side, uneven joint reaction forces was expected for unilateral biting. Moreover, higher reaction force in balancing side was

reported in MDA model of macaque and pig too (Shi et al., 2012, Langenbach et al., 2002). Furthermore, similar to the model with DGO the bushing torque was also present in both working and balancing sides in MOME to prevent the rotation of the mandible towards the balancing side.

3.4.3 Working and balancing side

Differences between working and balancing side muscle activation for unilateral biting was predicted in MOME, whereas DGO predicted symmetrical muscle activations. Simulating unilateral biting at molars imposes high load on one side of the masticatory system and TMJ. Either the joints should be able to bear and accommodate the load, or the muscles ought to activate in a way that counteract the load and prevent joint distortion. To counteract the unbalanced load and prevent joint distortion, asymmetric pattern of muscle activation might occur. If this was the case, different activation of working and balancing side was expected, as it was predicted by MOME. Interestingly, MOME resulted in even joint reaction forces at the working and the balancing side and in the case of contact-constrained model, it was predicted that neither the working side nor the balancing side TMJs were loaded. In contrast, DGO predicted almost analogous muscle activity for working and balancing side, hence the unilateral biting resulted in difference of TMJ reaction forces at the working and the balancing sides.

The results derived from MOME included some variations between activation of muscles at the working and the balancing sides. In the hinge-constrained model only the activity of deep masseter at the working side was considerably higher (11% higher which resulted in 0.9N) whereas the activity of external pterygoid was higher at the balancing side (7% which resulted in only 0.1N).

Table 3.9 Working and balancing side activation and ratios in contact constrained model predicted by MOME

MUSCLES	WS%	B S%	WS/BS
SM	46	43.3	1.1
DM	42.4	26.3	1.6
AT	42.2	30	1.4
PT	23.2	17.3	1.3
SZT	17.7	35.8	0.5
AZM	75.6	86.1	0.9
IOZM	100	100	1.0
PZM	50	8	6.3
IP	11.7	22.1	0.5
EP	16.7	39.7	0.4

It appeared that difference in muscle activation between working and balancing side was to a higher extent in the less constrained model (contact). Both parts of masseter, anterior and posterior temporalis and posterior zygomaticomandibularis were more activated at the working side, whereas suprazygomatic temporalis, anterior zygomaticomandibularis, internal and external pterygoid were more activated at the balancing side (Table 3.9). It appeared that the muscles with substantial vertical component, i.e. both parts of masseter and of temporalis, which are known to have key role in elevation of the mandible against food resistance (Hiiemae, 1971a), were activated to a higher degree at the working side. The role of internal and external pterygoid and supra-zygomatic temporalis muscles in controlling the position of the condyle and maintaining the stability of the joint is known and their higher activity at the balancing side, which was more prone to joint distortion, is in agreement with MOME predictions of their function (Hiiemae, 1971a).

3.4.4 Selection of the optimisation criteria

Although both optimisation criteria have been validated previously in separate occasions and in different species, in the mouse they diverge to some extent. Activation factors predicted by DGO and MOME were more comparable in some muscles, including masseter, zygomaticomandibularis and tempo all ensemble, than the others, including internal and external pterygoid. Moreover, although the activation of masseter temporalis and zygomaticomandibularis ensemble were comparable to some extent, the two optimisation criteria predicted different

activation for sub-sections of these muscles. When there is a divergence between predictions of optimisation criteria, validity of the optimisation criteria can be tested through comparison of predictions to EMG data (Iwasaki et al., 2003a, Schindler et al., 2007, Rasmussen et al., 2001). However, detailed EMG data is neither available in this study nor in literature. Hence selection of the optimisation criteria, in this study, was based on the availability of the required data and practicality of modelling methods. Unlike MOME which required thousands of trials, DGO performed simulation of one trial. However, DGO required kinematics which was fortunately available in the literature. Moreover, selection of optimal combination of muscle activation in MOME was heavily based on optimisation software, whereas DGO was more convenient to understand. Most importantly, the DGO simulates one full cycle of chewing, as opposed to MOME which models one instant of power stroke. Therefore, DGO was chosen as the optimisation criteria for the remaining chapters of this thesis.

3.5. Conclusion

This chapter investigated two commonly used optimisation methods: dynamic geometric optimisation (DGO) and minimisation of overall muscle energy (MOME), both of which have been previously used and validated in the medical engineering group of University of Hull. Optimisation principles and associated methods were presented and two models were developed: initial over-simplified hinge-constrained model and more sophisticated contact-constrained model. Individual-specific muscle attributes were used to develop and simulate the model. The muscle activation factors were predicted using DGO and MOME in both simplified and realistic models. The results from simplistic model showed over-constraining the joint might result in prediction of higher reaction forces, as well as simplified muscle interactions and co-activations. Principle of muscle activation in DGO and MOME were different; DGO tended to activate more vertically aligned muscles for the required vertical movement in this model, whereas MOME tended to activate anteriorly positioned muscles to a higher level. Furthermore, DGO predicted symmetrical muscle activation in the model, whereas MOME predicted complex

non-symmetric muscle activations. The validity of optimisation method cannot be tested due to lack of EMG data, however, based on what data was required, the simulation process and the possibility of simulation of the full cycle of biting DGO was selected as the optimisation criteria in the remaining chapters of this thesis.

Chapter 4. MDA modelling of the adult mouse masticatory system: a case study of incisor and molar biting

4.1. Introduction

The feeding system of mammals is a highly complex integrated system which includes masticatory muscles that can be activated with different synergies and co-activation patterns to fulfil a wide range of functions. The mouse has been the animal of choice in craniofacial studies for many years, and the morphology of the skull, its development and variation have been investigated (Klingenberg, 2002, Leamy, 1993). Surprisingly however, despite the importance of the mouse as a craniofacial model, mastication, a key function of the craniofacial system, has been little studied in this species compared to other rodents. The forces that masticatory muscles can apply, muscle activation patterns and the resulted reaction forces on the temporomandibular joints are among the subjects that have not been well studied in the mouse.

The dental arch of the mouse has a peculiar setting, consisting of incisors and molars separated by a large gap, known as a diastema. This unusual arrangement of the teeth in the mouse, like other rodents, allows for two very distinct types of biting: incisal and molar biting. As the diastema in the lower tooth row is shorter than the upper one in the mouse, when shifting from molar to incisal biting, a considerable anterior displacement of the mandible is required in order to position the incisors in occlusion. Likewise a posterior translation is necessary to occlude the molars for molar biting. This peculiar masticatory setting is unique to rodents and is very different from the feeding system of other mammals. Hence studying these two distinct types of biting in the mouse is an important initial step to understand the function of the masticatory system of rodents in general. Therefore, this chapter aims to investigate the differences of muscle activations and joint reaction forces between the two types of biting in the mouse. The model of the full cycle of biting in the adult mouse, i.e. optimised using DGO, in the previous chapter

(chapter 3) was used as a reference to investigate the masticatory function of the mouse in molar and incisor biting.

Measuring the molar bite force *in vivo* in the mouse is difficult, in large part due to the small size of its skull. There are no studies, to the best knowledge of the author, reporting on the maximal bite force of the mouse at the molar region, nor at incisal region. In the previous chapters, however, we presented *in vivo* measured maximal bite force at incisor biting in the adult mouse. Nevertheless, despite our attempt to measure the bite force at molar region from the same specimens, this task was proven to be difficult as specimens were not willing to bite on the force plates. Hence, the initial measure of differences between the two types of biting is to estimate the maximal bite force at molar region, using the MDA model of the incisal biting as a reference.

The existence of the large diastema between molars and incisors in the mouse causes a significant difference in the lever arm of the incisal and molar biting point, hence a substantial difference between maximum bite force for incisor and molar biting is expected. In addition, the position of the mandible changes during molar and incisal biting, with a considerable translation of the mandible occurring between molar and incisal biting to bring teeth into occlusion. This translation results in changes of muscle positions and orientations in molar and incisal biting. Thus the maximum bite forces for the two situations cannot be predicted by a simple equilibrium calculation of the lever arms. Instead, account must be taken of variations in both muscle orientations and consequent muscle activations. Manual calculation of the shift in the orientations of all the muscles would be a very laborious procedure, whereas ignoring the variations would result in a simplified and inaccurate model.

Due to the large diastema, the out-lever arm of the incisal biting is considerably larger than the out-lever arm length during molar biting, therefore a given bite force at the incisors will impose a higher load on the temporomandibular joints (TMJs) than the same bite at the molars. In consequence, the muscles are expected to activate to a higher extent in incisal biting in order to regulate the resultant load

on the TMJs and to prevent their possible distraction. Accordingly the maximum bite force at the incisors is expected to be lower than the molar biting, and indeed such trade-offs between the lever arm of the bite point and the maximum bite force have been reported previously (Gröning et al., 2013b, Weijs et al., 1987).

In the mouse, measuring masticatory muscle forces and their activation pattern is difficult because of the size and complexity of the muscles involved. Nevertheless, EMG data have been reported for the masticatory system of the mouse (Utsumi et al., 2010, Sanefuji et al., 2008, Yamada et al., 2006, Okayasu et al., 2003, Kobayashi et al., 2002c), however, there are some limitations in the reported data; only one study reported EMG data for masseter and temporalis (Utsumi et al., 2010), with the rest of the studies reporting only activity of digastric and masseter muscles, and no studies reporting EMG activity of the remaining masticatory muscles. In addition, even though EMG data for masseter, temporalis and digastric muscles are available, each was considered as a single contractile unit, whereas in fact they can function in a modular manner with different regions of each muscle being activated independently. The difficulty in obtaining detailed EMG data from such a small, complex system with various layers of muscle is understandable and the limitations of what has been collected are not surprising. Multibody dynamic modelling is an alternative, virtual method to predict muscle activation patterns and provides the opportunity to investigate potential muscle activity at a much finer level of detail.

Multibody dynamics modelling (MDA) is a relatively new approach to study complex biological systems and their function. It is a 3D computer modelling technique, developed for engineering applications, that has previously been used to model masticatory system of different species including humans (Watson et al., 2014, Gröning et al., 2013b, Shi et al., 2012, Jones et al., 2012, Curtis et al., 2010b, Moazen et al., 2008b, Curtis et al., 2008, de Zee et al., 2007, Iwasaki et al., 2003b, Koolstra and van Eijden, 1992). It can be used to experiment with varying muscle forces or mandibular kinematics to predict bite forces, muscle activation patterns and joint reaction forces. This approach overcomes the difficulties of conventional modelling and experimental methods, such as difficulties of measuring the molar bite force in the mouse, and is ideally suited to understanding such complex

systems, yet no MDA study has been undertaken so far to investigate the biomechanics of the mouse masticatory system.

In addition to the investigation of the function of the masticatory system, MDA provides a means to develop more precise finite element analysis (FEA) of the cranium and mandible which has been commonly used to estimate the strain and stress on skull in recent years (Cox et al., 2012, Curtis et al., 2008, Moazen et al., 2008b, Moreno et al., 2008, Grosse et al., 2007, Kupczik et al., 2007, McHenry et al., 2007, Wroe et al., 2007, Rayfield et al., 2001). In order to obtain a more reliable prediction of the strains and stresses in the skull, the best approach is firstly to understand fully the function of the muscles, to predict their activity and to apply the predicted muscle forces and their activation patterns to the FEA models (Curtis et al., 2013, 2011, Gröning et al., 2013a, 2011b, 2011a).

Hence in this research, an MDA of the mouse masticatory was created for such applications. The model was developed in two stages. The first simplified model was constructed so that the mandible only had rotary (hinged) movement at the TMJs, but all muscles were applied correctly. The second, more complex model, had an unconstrained joint, imitating the natural joint, and permitting true propalinal motion of the mandible. The maximum bite force at the first molar and during incisor biting were predicted, with the incisor values compared to *in vivo* data. Greater maximum bite force was expected for molar biting than incisal biting, however, the ratio of maximum bite forces was not expected to be correlated with the ratio of lever arms. Molar and incisal biting were also modelled to generate maximal and sub-maximal equal bite forces and muscle activation patterns and joint reaction forces were calculated and compared. Different muscle activation patterns were expected for the two cases, with higher joint reaction forces expected for incisal biting compared to molar biting. Moreover, MDA model of the incisal biting was used to investigate sensitivity of bite force prediction to muscle attributes, such as muscle strand distribution and muscle intrinsic stress value.

4.2. Materials and methods

4.2.1. Collection of the experimental data

All experimental data were collected by one of the authors (A. Herrel) at the Muséum National d'Histoire Naturelle (MNHN), Paris. In the study, 10 C57 wild-type adult mice were used, obtained from Charles River Laboratories (Chatillon-sur-Chalaronne, France), with all subsequent experiments approved by the Animal Care and Use Committee at the MNHN. Incisor bite force measurements were collected from all mice using a piezoelectric isometric force transducer (Kistler type 9203, +/-500 N) connected to a bite plate and a Kistler charge amplifier (type 5995A, Kistler Inc., Winterthur, Switzerland). Measurements were taken with an incisal gape angle of 25±5° during voluntary biting, with 10 repeats for each mouse. The average of the maximum bite forces from the 10 mice was used for the MDA, and is referred to as the *in vivo* maximum bite force. All 10 mice were sacrificed by injecting pentobarbital, fixed overnight in a 15% formaldehyde solution, rinsed and transferred to a 70% ethanol solution. The masticatory muscles of one side of the head were dissected in five of the mice, each muscle was removed complete and transferred to labelled vials containing 70% ethanol aqueous solution and the attachment areas of each muscle was observed. The muscles were blotted and masses recorded to the nearest 0.01 mg using a microbalance (Mettler AE100), and averaged across the five dissected individuals. These average values were used in the physical cross sectional area (PCSA) calculations for each muscle type. Subsequently, each muscle was transferred to an individual vial of 30% aqueous nitric acid solution and left for 20–24 hours after which the solution was replaced by a 50% aqueous glycerin solution. Individual fibres were then teased apart using blunt tipped glass needles and 10 fibres were selected randomly from each muscle and drawn using a binocular microscope with an attached camera lucida (MT5 Wild). Drawings were scanned and fibre lengths determined using ImageJ V1.31 software. Fibre length was measured for all five individuals, leading to 50 length measurements for *each* muscle across the sample. The mean fibre length of each muscle was used to calculate the respective PCSA and maximum muscle force.

4.2.2. Calculation of PCSA and maximum muscle forces

Details regarding calculation of PCSA and maximum muscle forces are presented in section 2.2.3. It was not possible to measure the intrinsic stress of masticatory muscles in this study, however, previous studies reported on this value varying between 25 N/cm^2 and 87.1 N/cm^2 for different species, ages and muscle types (fast versus slow twitching muscles) (Gonzalez et al., 2000, Vanspronsen et al., 1989, Weijs and Hillen, 1985, Hatze, 1981), with predicted bite force in an MDA model linearly related to specific muscle force (Gröning et al., 2013b). Hence an initial value of 39.7 N/cm^2 was used; which is the value reported for the young adult mouse *soleus* muscle (Gonzalez et al., 2000). Due to exclusion of the pinnation angle in PCSA calculations and averaging the PCSA across the five specimens, the PCSA values were underestimated; subsequently the predicted bite force was underestimated too. To compensate for this underestimation of PCSA values, the intrinsic stress was increased to 50N/cm^2, which resulted in bite force prediction that matched *in vivo* bite forces (see section 2.2.3 for further details).

4.2.3. Model development

The skull and mandible geometries were reconstructed as 3D shells from high resolution micro-computed-tomography (µCT) scans of the full head of one of the five remaining undissected adult mice. The scans were performed on X-Tek HMX160 (X-Tek Systems Ltd, Tring, UK) in the School of Engineering, University of Hull. The voxel size was 0.0183 mm in all three directions. The µCT scans were segmented using AVIZO v6.3 image processing software (Visualization Science Group (VSG)), and 3D surfaces of the cranium and mandible were exported to MSC ADAMS/view 2013 multibody dynamics (MSC Software Corp, USA).

In this study the mouse masticatory system consisted of three rigid bodies: the cranium and the two hemi-mandibles. The cranium was fixed in space while the hemi-mandibles could move independently and were connected together at the symphysis and to the cranium at the temporomandibular joints (TMJs). In reality, the symphysis of the mouse is unfused and the hemi-mandibles are able to rotate about their long axes, with the range of movement controlled by both inter-

crossing and horizontal ligaments located between the two. In this study, the symphysis was modelled using a spherical joint, with a flexible 'ligament' element placed anterior to the symphysis to provide damping in the system and avoid instability during model solution.

The TMJs are also relatively unconstrained, but again regulated by both ligaments and surrounding muscles. Two different types of constraints were considered in the MDA model: initially gross over-simplified hinge joints (with only rotary movement) and more complex contact constrained joints (with six degrees of freedom) in which the movement of the mandible at the TMJs was controlled mainly by geometries of contact surfaces, i.e. the condyle and glenoid fossa. In order to define these surfaces, 3D geometries of the condyle and glenoid fossa were carefully reconstructed as solid parts in AVIZO v.6.3 and exported to ADAMS where they were locked to the shell surface of the mandible and cranium. The contact areas of TMJ were defined based on our observations of the attachment of the joint capsule around the condyle (unpublished observation). In addition, the role of ligaments *in vivo* in constraining the movement of the condyle was imitated in MDA models by using bushing (Watson et al., 2014, Gröning et al., 2013b, Shi et al., 2012).

Published data of cyclical jaw movement (Utsumi et al. (2010) were used to define the instantaneous position of the mandible during the simulation. The mandible was opened to a maximum gape of 1.187 mm (maximum gape of molar biting on the hard food reported by Utsumi et al. (2010) and presented in Table 1.2) and then closed to the gape specified from the *in vivo* bite force measurement (25°) by placing an object representing food between the upper and lower teeth in the MDA model. At this point, bite force, muscle forces and joint reaction forces were extracted from the MDA model.

The prediction of muscle activation is not a straightforward task, since there is significant redundancy in the masticatory system and the muscles can be recruited in very many ways to produce the desired movement or bite force. Hence some criteria must be defined to optimize the solution and identify the optimal pattern of muscle recruitment. In this study dynamic geometric optimization (DGO) was used

to estimate the most suitable muscle activation pattern (Curtis et al., 2010b). DGO is an optimization algorithm based on this assumptions that muscles function optimally along their line of action. DGO operates such that those muscles more aligned to the direction of required motion are activated preferentially to those that are more inclined to that motion direction. In this approach, kinematic data is used to define the movement of the mandible and the muscles are modelled to activate in a fashion that will produce the necessary force to maintain the desired movement. More details of this optimization algorithm is discussed in chapter 3.

The same model and gape angle was used to simulate the incisal and molar biting, except for the initial position of the mandible and the position of the food item. In the incisor biting model, the mandible was positioned slightly more anteriorly (0.4 mm) to place the incisors in the correct position to bite the food item, whereas the mandible was more posterior in the molar bite, with the food placed between the maxillary and mandibular first molars (Figure 4.1).

In order to study the maximum bite force, a very stiff food item (composed of two horizontal plates connected with a stiff spring of stiffness of 200 N/mm) was modelled between the incisors or first molars. The muscles then attempted to generate sufficient force to continue to move the mandible according to the predefined movement, until the muscle limits and/or maximum bite force was reached.

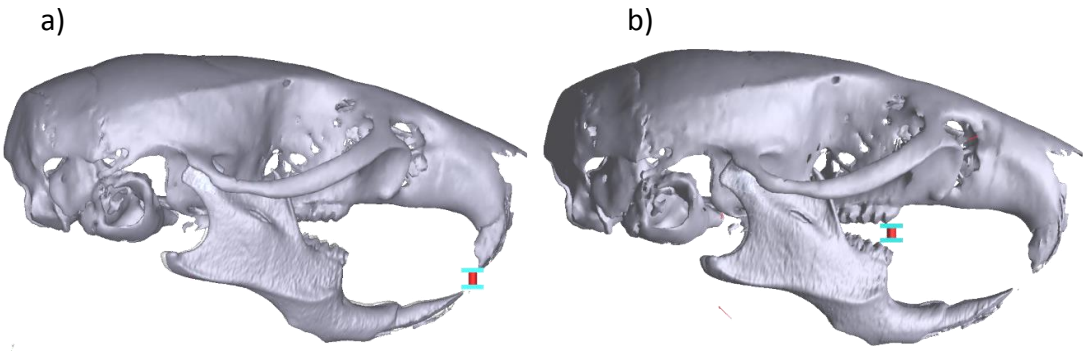

Figure 4.1 The position of the mandible and food item, a) in incisor biting with a more anterior position of the mandible; b) molar biting.

Muscle Attachments

The undissected side of the head in the same five mice was stained in phosphomolybdic acid 5% for four days and four of adult mice were scanned in one batch in MNHN (AST-RX platform) with voxel size of 0.046 mm in all three directions (v|tome|x L 240, GE Sensing & Inspection Technologies Phoenix). The different functional parts of the muscles were segmented out using AVIZO. The attachment area of each muscle on the cranium and mandible were studied and compared against earlier dissection observation and published data (Baverstock et al., 2013). The observed morphology of the majority of the masticatory muscles was consistent with Baverstock et al. (2013), except three parts of the temporalis muscle (anterior temporalis, posterior temporalis and suprazygomatic temporalis) were identified in the dissections and segmentations in the present study (Figure 4.2), whereas Baverstock et al. only described two, which they named as lateral and medial.

The separation of the anterior and posterior parts of the temporalis was difficult to see in AVIZO, however, together with dissection observations, the distinction could be found. It was observed that the anterior temporalis is attached superiorly to the anterior part of the temporal fossa, while inferiorly the muscle has two regions of attachment. The more anterior region wraps around the temporal fossa of the cranium dorsally and inserts on the medial part of mandible, just below the coronoid process. To model this part of the temporalis, each muscle strand was defined by two parts to allow similar wrapping in the MDA model, to ensure correct

muscle orientation (Figure 4.3). The more posterior region of the anterior temporalis inserts on the lateral part of tip of coronoid process, which was modelled as two single part strands. Moreover it was observed that supra-zygomatic temporalis was wrapped around zygomatic process of zygomatic process of squamosal bone, and accordingly the same wrapping was included in the MDA model (Figure 4.3). The infra-orbital zygomaticomandibularis is similarly not orientated in a simple straight line, thus it too was modelled in two segments to replicate the muscle orientation *in vivo*.

Number of muscle strand of jaw closers in MDA (superficial and deep masseter, anterior, posterior and supra-zygomatic temporalis, infra-orbital, anterior and posterior zygomaticomandibularis and internal and external pterygoid) is shown in Table 4.1 and their orientations are presented in Figure 4.3.

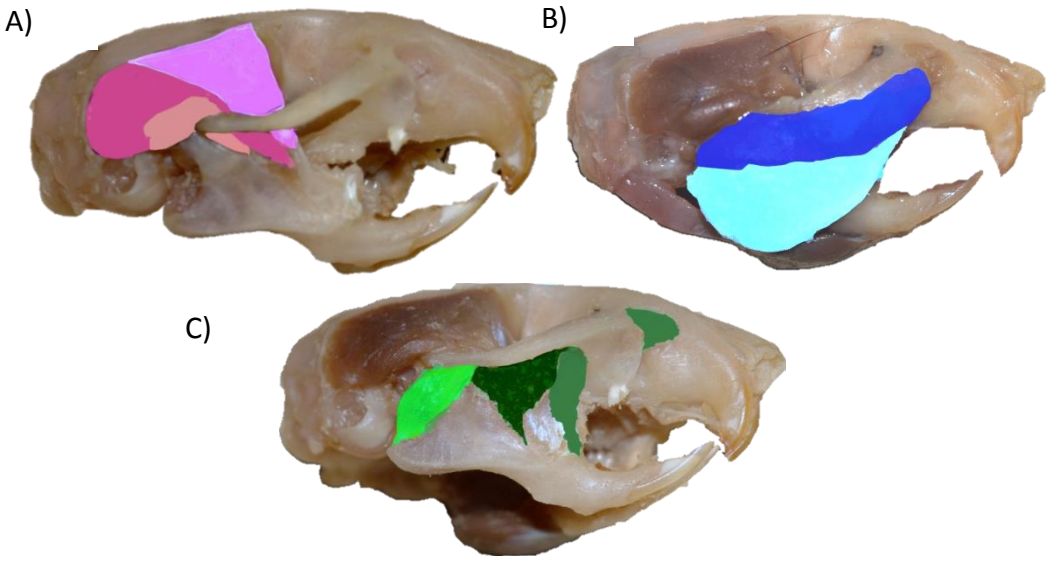

Figure 4.2 A) anterior (presented in pink), posterior (presented in fuchsia), and suprazygomatic temporalis (presented in peach) muscles; B) superficial masseter (presented in light blue) and showing part of deep masseter (presented in dark blue); C) infra-orbital zygomaticomandibularis (presented at the most right), anterior zygomaticomandibularis (the middle) and posterior zygomaticomandibularis (the left muscle).

Table 4.1 Number of muscle strands in the MDA

Muscles	Superficial masseter	Deep masseter	Anterior temporalis	Posterior temporalis	Supra zygomatic temporalis	Anterior zygomaticomandibularis	Infra orbital zygomaticomandibularis	Posterior zygomaticomandibularis	Internal pterygoid	External pterygoid	Digastric
Number of strands	4	6	5	2	1	4	2	2	4	4	2

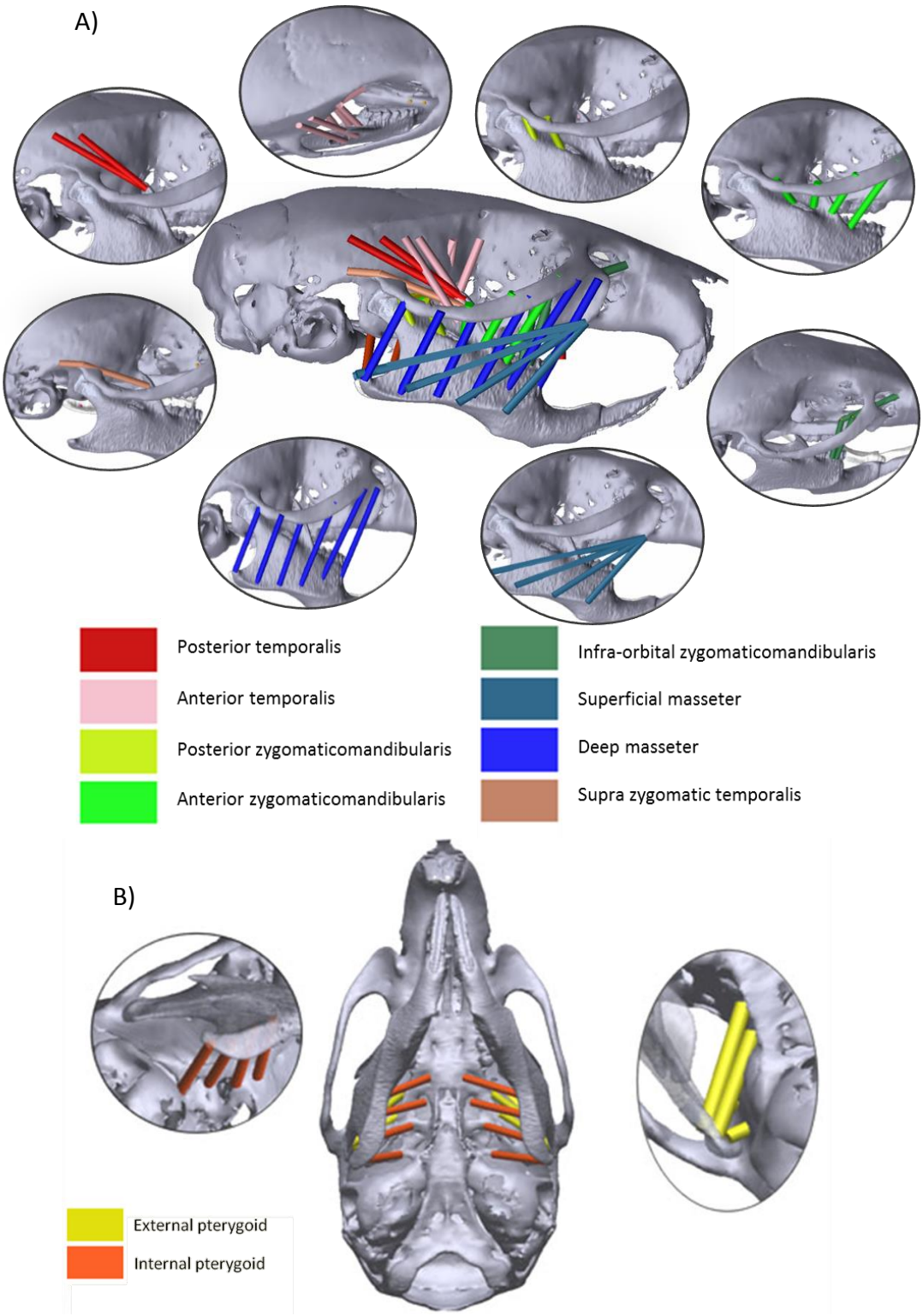

Figure 4.3 A) lateral view of muscle attachments in the MDA model with magnified pictures of individual abductor muscles; B) inferior view of the MDA model with only internal and external pterygoid muscles attached

In addition, segmented muscles were used to study the shape of their cross sectional area for sensitivity studies. The line of action of muscles were defined,

then muscle's cross sectional area which was perpendicular to, and in the mid-point of, the line of action was observed. The shape of the cross sectional area was determinant of the muscle distribution in the model. If the shape was close to rectangle, uniform distribution of the muscle strands was used in the model. In contrast, if the shape of the cross sectional area was close to triangle, then additional muscle strands were added to the thicker part of the cross sectional area.

4.2.4. Kinematic data of mouse incisal and molar biting

There is some inconsistency in kinematic studies of the molar chewing cycles in the mouse regarding the contribution of mediolateral movements. Relatively minor mediolateral movements were reported by Utsumi et al. (2010), but other studies described considerable lateral movements (Yamada et al., 2006, Okayasu et al., 2003). This inconsistency might arise due to the variable biting cycles between different specimens, different food properties or even inconsistent biting cycles of the same individual (Kobayashi et al., 2002). Minor horizontal movements have also been reported during incisal biting in the mouse (Kobayashi et al., 2002c). Because of this uncertainty and also for the sake of simplicity, only 2D movements of the mandible were studied here with transverse movement of the mandible neglected. Yet this method can readily be extended to include 3D motions (*e.g.* Watson et al. (2014)).

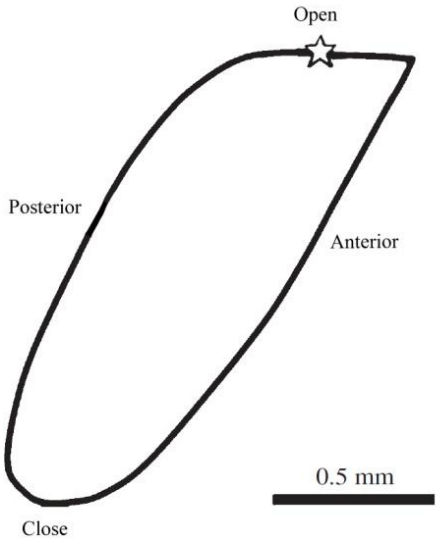

Figure 4.4 2D trajectories of the movement of mandible in the sagittal plane in the molar biting of the mouse. The star represents the fully-closed positioned, adapted from Utsumi et al. (2010)

The trajectory of the 2D movement of the mandible during molar biting in the sagittal plane is shown in Figure 4.4. It consists of an anterior movement at the start of the cycle, posterior and downward movement while opening until maximum gape, then simultaneous anterior and upward movement while closing. Because antereoposterior motion was obviously not possible with the hinged joint, this full trajectory was only modelled with the unconstrained joint. In the former, only rotary movement was considered. Furthermore for incisal biting, only a simple open-close motion was modelled for both cases, because only inconsistent minor horizontal movement has been reported previously (Kobayashi et al., 2002c).

4.3. Results

4.3.1. Estimation of maximum muscles force

PCSA and maximum muscle force values are presented in section 3.3.2 (Table 3.2). There are two sets of maximum forces presented, $Force_1$ which was calculated using muscle intrinsic stress value of 39.7 N/cm^2 and $Force_2$ which were calculated using muscle intrinsic stress value of 50 N/cm^2. Although the

range of intrinsic stress value has been reported in literature, this value has also been reported to vary for different ages, species and muscle types (Hatze, 1981, Vanspronsen et al., 1989, Weijs and Hillen, 1985, Gonzalez et al., 2000). Since this value for masticatory muscles in the mouse was not available in the literature and neither it was possible to measure this value, an initial intrinsic stress value, which was reported in the literature for *soleus* muscle in the mouse (Gonzalez et al. (2000)), was used. This value was later incaresed to 50 N/cm^2 to compensate for underestimation of the PCSA. Nevertheless both of these values were within the reported range of literature.

Using set of $Force_1$ (which were calculated using intrinsic stress value of 39.7 N/cm^2) resulted in an incisor bite force of 7.51N for the hinge- constrained model. On the other hand, when set of $Force_2$ were used as muscle forces, the maximal incisor bite force that was generated in hinge-constrained joint was 9.49N.

However, *in vivo* maximum bite force was found to be 8.97 N (see Table 3.1), showing that the MDA model is underestimating the bite force. As the PCSA values were averaged and pinnation angle was disregarded in the PCSA calculations, the possibility of the underestimation of the bite force could be likely. To calibrate the model and rectify this underestimation, the muscle intrinsic stree value was increased and the second sets of muscle forces ($Force_2$) were used, which generated maximum incisor bite force of 9.49 N. This bite force was more comparable to *in vivo* bite force measurements, hence maximum muscle forces calculated from intrinsic stress value of 50 N/cm^2 was used for the experiments comparing incisor and molar biting.

4.3.2. Muscle cross sectional areas and muscle distribution

To include the thickness of the muscle in MDA models, the shape of the cross sectional area of the muscle was studied and used as a determinant of muscle definition in MDA (see section 2.2.3). It was observed that all muscles, except for posterior zygomaticomandibularis, external pterygoid and anterior temporalis, had more or less rectangular shape of cross sectional area, hence the muscle

strands were equally spaced for these muscles. However, the cross sectional area of the posterior zygomaticomandibularis, external pterygoid and anterior temporalis was similar to triangle in shape. Thus to reflect varying thickness of these muscles in the model, additional muscle strand was defined at the thicker end of the muscle.

Using set of $Force_1$ for muscle forces, the incisal biting was modelled and the maximal incisal bite force was predicted. The result was 7.57N which was almost analogous to the incisal bite force predicted from model with uniform muscle distributions (7.51N) (less than 1% difference).

4.3.3. Predicted maximum incisor and molar bite forces

All muscles were activated at 100% to predict the maximum bite force from the contact and hinge constrained models for both incisor and molar biting. The bite forces from the hinge constraint model were 9.49 N and 15.85 N for incisal and molar bites, while the contact constrained model predicted values of 9.01 N and 15.52 N, respectively. Clearly, the maximum incisor bite force values are very close to the *in vivo* bite force value of 8.97 N, with the over-constrained model over-estimating the value by just 6%.

4.3.4. Muscle activation patterns

The degree of muscle activation of the jaw closing muscles for incisal and molar biting, with a gape of 25° and a predefined bite force of 8.97 N in both the hinge and contact-constrained models, are presented in Table 4.2. As expected from the previous analysis of maximum bite force, all muscles were fully activated in the contact constrained model in order to produce an incisor bite force which matches the average *in vivo* value of 8.97 N. The same was observed with the hinge constrained model, except the superficial masseter was not activated fully. The activation of muscles for generating molar bite force of 8.97 is lower, especially in larger masticatory muscles, i.e. masseter and temporalis.

Table 4.2 Comparison between muscle activation with incisor and molar bites in the hinge and contact constrained models, with the same gape and predefined force (of 8.97 N)

	Muscle activation					
	Contact constrained			Hinge constrained		
	Incisor bite %	Molar bite %	incisor : molar	Incisor bite %	Molar bite %	incisor : molar
Superficial masseter	100	25.09	3.99	77.67	25.03	3.10
Deep masseter	100	61.31	1.63	100	62.04	1.61
Anterior temporalis	100	35.42	2.82	100	40.04	2.50
Posterior temporalis	100	45.29	2.21	100	45.65	2.19
Supra zygomatic temporalis	100	0.00	-	100	0.00	-
Anterior zygomaticomandibularis	100	100	1.00	100	100	1.00
Infra-orbital zygomaticomandibularis	100	100	1.00	100	100	1.00
Posterior zygomaticmandibularis	100	100	1.00	100	100	1.00
Internal pterygoid	100	100	1.00	100	100	1.00
External pterygoid	100	100	1.00	100	100	1.00

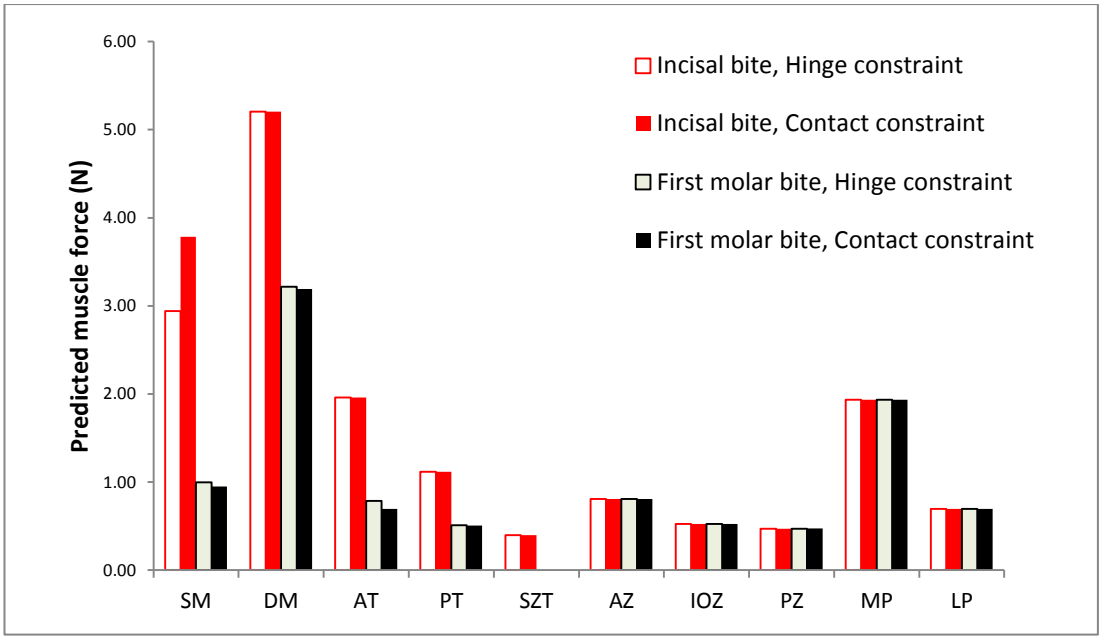

Figure 4.5 Muscle activation forces predicted with hinge and contact constrained models for incisor and molar biting. (SM: superficial masseter, DM; deep masseter, AT: anterior temporalis, PT: posterior temporalis, SZT: supra-zygomatic temporalis, AZ: anterior zygomaticomandibularis, IOZ: infra-orbital zygomaticomandibularis, PZ: posterior zygomaticomandibularis, MP: medial pterygoid, LP: lateral pterygoid).

The absolute predicted muscle force values during in incisal and molar biting in both hinge and contact constrained models are presented in Figure 4.5. The greatest difference between the two load cases was observed with the masseter muscle, in particular the superficial masseter, with values of 2.84N for the contact constrained model and 1.9N with the hinge constrained model. Deep masseter was activated fully during incisor biting for both models, but its activity was reduced to 60% during molar biting. The temporalis muscle was the only other muscle that was predicted to activate differently between incisor and molar biting. Activation in the anterior and posterior parts dropped to less than half in molar biting compared to incisor biting (35% and 40% for the anterior part of the hinge and contact constrained models respectively, and 45% for the posterior part in both models). The supra-zygomatic part of the temporalis was predicted to be completely inactive during molar biting.

Interestingly all the muscles were predicted to activate to a similar extent during the two loading scenarios, regardless of the joint condition, with the exception of the superficial masseter which was activated 22.3% more in the model with the less constrained TMJ.

Table 4.3 The TMJs reaction force predicted with hinge and contact constrained models for incisor and molar biting.

Model	Location of food	Right side TMJ reaction force (N) (Working side in first molar bite)	Left side TMJ reaction force (N) (Balancing side in first molar bite)
Hinge constrained model	Incisor	8.18	7.39
	First molar	1.82	4.91
Contact constrained model	Incisor	6.83	5.64
	First molar	0	2.66

Table 4.4 Three components of the joint reaction forces and associated bushing forces in the M1 and incisor biting model. X is at the antero-posterior direction, Y is dorso-ventral direction and Z represents the mediolateral direction. R: right side (working side); L: left side or balancing side

	First Molar				**Incisor**			
Force and Torque	X	Y	Z	Mag	X	Y	Z	Mag
Bushing force -R	-0.9	-0.5	-0.2	1.1	-3.6	-1.2	0.6	3.8
Bushing force - L	-1.5	-1.7	-0.2	2.3	-5.3	-1.8	0.6	5.6
Reaction force - R	0.0	0.0	0.0	0.0	0.2	-6.2	-2.8	6.8
Reaction force - L	0.1	-2.4	0.7	2.7	2.0	-5.0	1.8	5.6
Bushing Torque-R	-0.9	0.0	0.0	0.9	-0.5	0	0	0.5
Bushing Torque-L	-0.9	0.0	0.0	0.9	-0.5	0	0	0.5

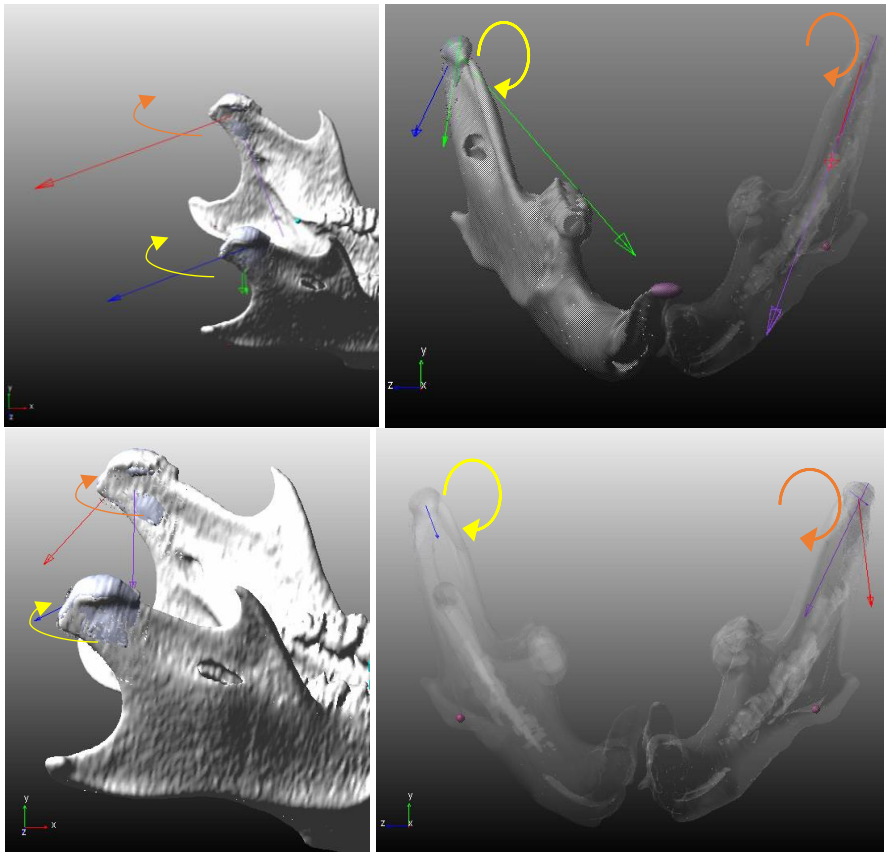

Figure 4.6 Side and frontal views of the mandible with contact and bushing forces represented as vectors resulted in incisor biting (top) and first molar biting (bottom). Red: left bushing force; blue: right bushing force; violet: left contact force; green: right contact force. The green is not present in molar bite model as the contact force was found to be zero. The yellow and orange arrows are showing the torque resulted from bushing in working and balancing side respectively.

The TMJ reaction forces are presented in Table 4.3. The three resolved components of the joint reaction force as well as the bushing force and the bushing torque in the contact constrained model is presented in Table 4.4. The working and balancing sides are presented separately because unilateral molar biting was modelled. Hence the system was asymmetric and despite muscle activation predictions of DGO being similar in the working and balancing side, the forces that were imposed in the TMJ were not similar and generally balancing side had higher joint reaction force. Moreover, joint reaction force at the working side in molar biting was predicted to be zero in less constrained model, which is suggesting that the joint of the working side was unloaded. The bushing force in X and Y direction is substantial in both working and balancing side of the molar bite. Equal clockwise torques around X-axis

(in mediolateral direction) resulted from bushing is present in both left and right TMJ. The combination of the bushing force, the torques and muscle activations maintain the stability of the mode in molar biting, despite the zero reaction force in the working side (see Figure 4.9).

Furthermore, it is worth noting that asymmetric joint reaction forces were observed during incisor biting, although they were expected to be equal.

As incisor bite force of 8.97N was very close to the maximal bite force predicted by the model, all muscles were maximally activated (especially in the contact model which had more realistic constraint). This made the comparison of muscle activation pattern between the molar and incisor difficult. Hence, contact constrained model was used to experiment with both incisor and molar biting generating 4.5, and 2.25N bite forces. The ratio of muscle activation in incisor and molar are presented in Figure 4.7 (see Appendix II for detailed activation pattern of each bite force).

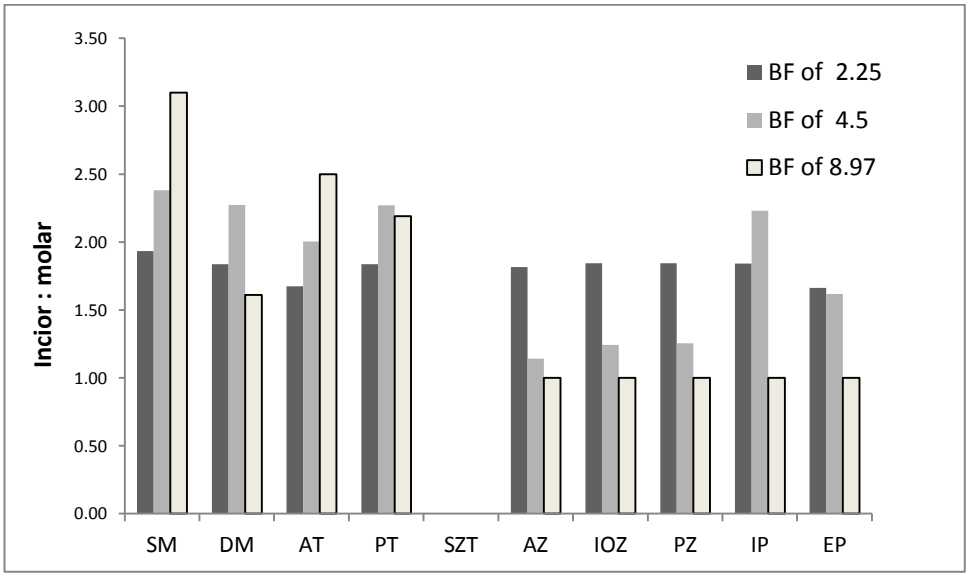

Figure 4.7 Ratio of muscle activation of incisor to molar biting for bite force of 2.25N, 4.5N and 8.97N.

The ratio of muscle activity in incisor to molar biting is more consistent in lower bite force of 2.25N than the other two. As the bite force increases, the difference of muscle activity between incisor and molar increases too. As it was expected, even

in lowest bite force, there was some fluctuation observed in ratio of muscle activity between molar and incisor biting. This was a result of the initial position of the mandible, which was more anteriorly in the incisor biting compared to molar biting.

The ratio of incisor to molar muscle activity was examined for producing sub-maximal biting force of 2.25N and 4.5N and compared against bite force of 8.97N. Although the chosen bite forces of 2.25N and 4.5N were within the range of the adult mouse bite force (0 to 8.97 N), it was not chosen based on a biological ground. Instead, they were chosen as a ratio of the maximal bite force (almost half and a quarter of the maximal bite force).

it was observed that for lower bite force (2.25N) the ratio of muscle activity was more consistent, although there was still some fluctuation which was expected as the mandible is positioned more anteriorly in incisor biting (about 0.4mm). Although not great, this translation of the mandible results in change of muscle orientation of the muscles, consequently their activity changes. For greater bite force, this ratio can be misleading, as some muscle reach their maximal activation and the ratio is not consistent anymore.

4.4. Discussion

The first MDA of the masticatory system of the mouse has been developed, using individual-specific data, where possible. Great care has been taken to create a mouse-specific model, so that the muscle sizes, forces and geometry of the cranium and the mandible are proportioned correctly. Although the MDA presented here is not constructed based on only one individual, muscle data of 5 specimens and bite force of 10 specimens were averaged to construct an accurate and representative model of the adult mouse. Tests on 10 specimens of the same type (C57) with similar skull length (23.90 ± 0.25 mm) resulted in a maximum incisor bite force of 8.97N. Two joint conditions were examined, to determine the sensitivity of the bite force result to how the mandible is constrained. These results showed that the estimated incisor bite force was comparable to *in vivo* measured incisal bite force, with values of 9.01N and 9.49N predicted for contact and hinge-constrained

models. Similar to findings of chapter 3, the accordance in the results suggest that although over-constraining the model, by using hinge joint in TMJs, resulted in overestimation of both joint reaction forces and muscle activations, their patterns were still in agreement with the realistic contact constrained model. Moreover, the correspondence in the results to *in vivo* bite force measurements suggests the definition of the muscles, their orientation and the model as a whole is valid.

Moreover, the sensitivity of the model to some muscle attributes were tested to determine robustness of the results. The sensitivity of MDA model to muscle intrinsic stress value was previously tested and linear correlation between this value and maximal bite force in MDA has previously been reported (Gröning et al., 2013b). Muscle intrinsic stress value was reported to vary with age, species and muscle types (fast versus slow twitching muscles) between 25 N/cm^2 and 87.1 N/cm^2 (Hatze, 1981, Vanspronsen et al., 1989, Weijs and Hillen, 1985), however, no published data was available for masticatory muscle of the mouse. Hence, as the initial step, muscle intrinsic stress value of 39.7 N/cm^2 which was reported for soleus muscle in the mouse was used which underestimated the incisal bite force (7.51N). When the intrinsic stress value of the 50 N/cm^2 was used, comparable incisor bite force to *in vivo* measurements was predicted from MDA (see section 2.2.3 for more details). Hence, as expected, current MDA model is highly correlated to the muscle intrinsic stress value too. However, MDA models presented here are predominantly intended to be used for comparison of muscle activation patterns for different functions rather than absolute values. Since varying muscle stress value affects model's attributes linearly, the effect of this value is minimised.

Additionally, the effect of muscle thickness was tested on incisal maximum bite force. Interestingly, including variability of the muscle thickness across its cross sectional area did not affect the maximum bite force predictions significantly, hence were excluded from remaining MDA models.

Furthermore, as expected the maximum bite force from incisal biting was less than the molar biting, due to its longer moment arm from the TMJ. Unfortunately, it was not possible to measure molar bite force *in vivo* and compare it to the value

predicted by the modelling. Nonetheless it can be estimated based on the geometry of the mandible and cranium by a simple ratio of the lever arms, assuming the position of the mandible remains constant in both molar and incisor biting and the muscle orientations do not alter (Figure 4.8). Thus,

$$\text{molar bite force} = 8.97 \times 14.2/7.5 = 16.98 \text{ N}$$

However, in reality the posterior shifting of the mandible to occlude the molars would vary the moment arm and orientation of the muscles. Hence the direction of the muscle forces in molar and incisor biting would vary and consequently the resultant bite force can be expected to be different from that calculated by simple lever arm relationships. The bite force at the position of incisors that was predicted from the models was 15.85N and 15.52N for the hinge and contact constrained model respectively, *i.e.* a maximum difference of 9.4%.

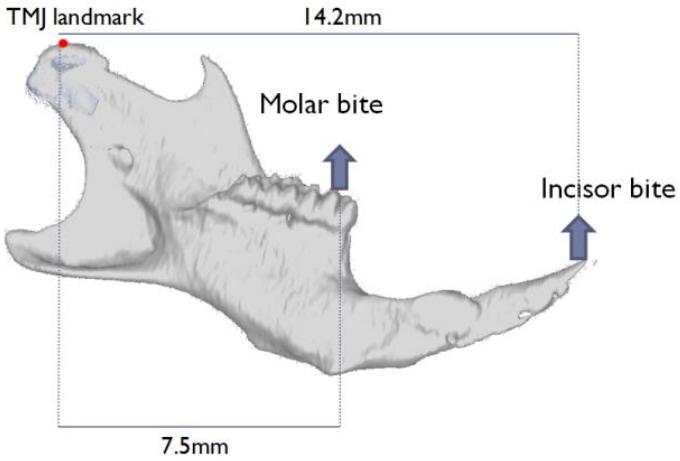

Figure 4.8 The mandible in the sagittal plane, showing the distance between the TMJ and first molar and incisors.

For an equal bite force of 8.97N, generally lower muscle activation was predicated in molar biting than incisal biting. The ratio of incisor/molar activity was not constant for the different muscles, and varied between 1 and 4 times. The most significant difference in muscle activation between molar and incisor biting was observed with the masseter muscle, followed by the temporalis. Considering that these two muscles accounted for 73.5% of the total mass of the jaw closing muscles, their activation was more effective. In contrast, all three parts of

zygomaticomandibularis and medial and lateral pterygoid were fully activated for both incisor and molar biting in both contact and hinged constrained models (Table 4.2). For sub-maximal bite force simulations, however, relative muscle activations in molar and incisors were more comparable, in particular, incisor/molar muscle activation ratios in bite force simulation of 2.25N was nearly constant because none of the muscles reached their maximal activity.

The difference in muscle activity of the hinge-constrained and contact-constrained models was largely limited to the activation of the superficial masseter muscle in incisor biting, during which it activated considerably more in the contact-constrained model. Presumably this arises because of the additional requirement for the muscles to actively maintain the position of the TMJ, while the fully constrained hinge joint guarantees no displacement from the required neutral position. For example in incisor biting, the temporalis muscle, which was aligned posteriorly, would tend to pull the condyle posteriorly along the glenoid fossa. Hence the superficial masseter would need to compensate with increased contraction to pull the mandible forward again.

Due to the greater moment arm of the incisors compared to the molars, for an equal bite force, higher reaction forces would be expected on the TMJs during incisor biting, as found in Table 4.3. The reaction forces during incisor biting are more similar than molar biting in right and left sides of both contact and hinge models. This was predictable as incisor biting is a near symmetric activity. The difference in the two sides could be the result of slight asymmetry of the skull and consequently asymmetry in the muscle orientations. As it was expected indeed, the TMJ reaction force for the incisor biting was considerably more than molar biting. The bigger lever arm of bite position in incisor biting imposed higher load force on the TMJ. Although the muscles were predicted to activate to a higher extent in order to minimise this TMJ reaction forces, still greater force was imposed to the TMJ in result of the equal incisor biting force.

The joint reaction forces during first molar biting were significantly different on the working and balancing sides. Interestingly, unilateral molar biting of the contact

constrained model led to a zero TMJ reaction force on the working side. The mechanical free body diagram of the mandible is presented in Figure 4.9.

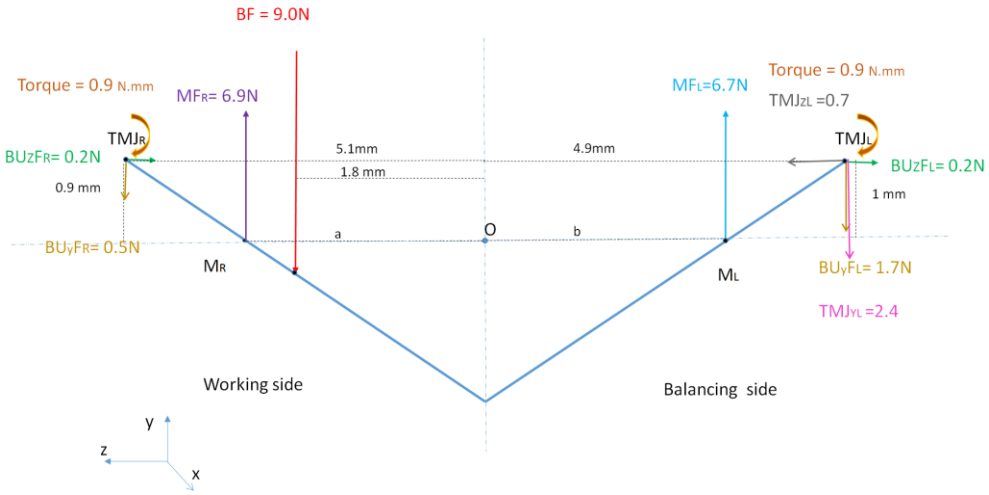

Figure 4.9 Free body diagram of the mandible at molar bite and DGO in frontal view. O is assumed to be the centre of mass of the whole mandible at the mid-point between the centre of mass of the two hemi-mandibles; M_L and M_R : point of the application of the overall muscle force in the left and right side of the mandible; a and b: the distance between O and the M_R and M_L respectively; MF_L and MF_R: overall muscle forces in vertical direction in left and right respectively (consult Table IV.2); BU_YF_R and BU_YF_L are vertical component of the bushing force in the right and left side respectively and BU_ZF_R and BU_ZF_L is the mediolateral component of the bushing force in right side and left sides; BF: bite force which was applied at the position of the M1 in the right side of the mandible; TMJ_{ZL} and TMJ_{YL} are joint reaction force at left side in mediolaterla and vertical directions respectively. Torque: is the torque resulted from bushing in both left and right sides

From the sum of forces in vertical direction (Y) we have:

$$\Sigma F_y = -BF+MF_R+MF_L-BU_YF_L-TMJ_{YL}- BU_YF_R \quad (4.1)$$

$$\Sigma F_y=-9+6.9+6.7-0.5-1.7-2.4=0$$

$$\Sigma M_O=(-BF\times1.8)+(MF_R\times a)+(BU_ZF_R\times0.9)-(BU_YF_R\times5.1)-(MF_L\times b)+(BU_YFL\times4.9)+ \quad (4.2)$$

$$(TMJ_{YL}\times4.9)-(TMJ_{ZL}\times1)+(BU_zFL\times1)+(2\times Torque)$$

$$\Sigma M_O=(-9\times1.8)+(6.9\times a)+(0.2\times0.9)-(0.5\times5.1)-(6.7\times b)+(1.7\times4.9)+$$

$$(2.4\times4.9)-(0.7\times1)+(0.2\times1)+(2\times0.9)=0$$

$$a-0.97b=0.41 \quad (4.3)$$

The sum of forces in vertical direction is equal to zero, which shows that the mandible is in equilibrium in vertical direction. The right and left muscle forces provide enough force to counteract the bite force. However, the bite force on the working side causes torque on the mandible and rotates the mandible towards the balancing side very minimally (0.08mm). This torque causes the surfaces of the condyle and glenoid fossa to contact and generates contact forces in the frontal plane (x component of the joint reaction force is minimal, hence not considerable rotation in antero-poterior direction). The tendency of rotation of the condyle of the working side triggers the bushing torque and the rotational stiffness of the joint controls the position of the condyle. Surprisingly, the vertical bushing force of the working side has a ventral direction, whereas it was expected that it counteracts the anticlockwise rotation of the mandible, hence would face upward. Although it seems unlikely, the unexpected appearance of this ventral bushing force in working side could be resulted from the impact of the contact force in the balancing side. The bushing force of the balancing side is more likely to be resulted from the impact force though. Moreover, the torque in the working and balancing side is counteracting the rotational tendency of the mandible towards the balancing side.

From the rotational equilibrium equation (4.2), the system is in rotational equilibrium only if the equation 4.3 is true. So if the position of overall sum of the force in the working and balancing side would follow the relation in equation of 4.3, the system will be stable. The validity of the latter, however, was not studied in the model.

Unfortunately, EMG data for the masticatory muscles of the mouse is unavailable, therefore it is difficult to validate the muscle activation patterns against *in vivo* EMG data. However there are other studies that report comparable findings to those reported here. A study conducted by Sellers and Crompton (2004) compared unilateral incisal and first molar biting in human. They reported higher TMJ reaction force for incisor biting compared to first molar biting, as observed in the current study. Moreover, they predicted that in first molar biting, the working side TMJ reaction force was half of the balancing side. Their results were in agreement to findings of Sellers and Crompton (2004) and Langenbach et al. (2002), which is in

close agreement with the predictions of current study in the hinge-constrained model (0.4 in our model vs. 0.5 predicted by them). Interestingly, the same ratio of 0.4 for joint reaction forces between working and balancing side was reported by Shi et al. (2012). These findings confirms the validity of the model to some extent, as well as prediction of comparable incisal bite force to *in vivo* measurements.

One limitation of the current model is prediction of symmetrical activation pattern for both incisal and molar biting. In the case of incisal biting, as the food is positioned centrally, symmetrical muscle activation of the muscles is likely and indeed is addressed in the rat (Weijs and Dantuma, 1975). In contrast, unilateral molar biting is likely to occur as a result of asymmetrical muscle activation. Because DGO algorithm predicts muscle activation as a factor of orientation and required movement, as the system is almost symmetrical and the mediolateral movement is excluded too, the muscles activate similarly in both sides. Inclusion of mediolateral movement will most probably result in variable activity in working and balancing side (Watson et al., 2014).

4.5. Conclusion

The first MDA model of the mouse masticatory system was developed and sensitivity of the model to constraint type, muscle intrinsic stress value and muscle thickness was tested. It was found that bite force prediction was highly correlated to muscle intrinsic stress value, in contrast to constraint type and muscle thickness which had little effect on incisal bite force production. Moreover, maximal incisal and molar bite force was predicted and the former was in agreement with *in vivo* measurements from the same specimens. Moreover, molar and incisal biting were modelled and muscle activation patterns were compared for both maximal-and sub-maximal bite force. The ratio of muscle activation in incisor to molar was more consistent for the lower bite forces. In addition, joint reaction forces were different for both incisal and molar biting, for the former difference was due to minor asymmetry of the skull, whereas the latter was expected to have different working and balancing side joint reaction forces. Furthermore, as expected, for equal bite force joint reaction force in incisor biting was higher than molar biting. In contact

constrained molar biting model, the joint reaction force of the working side was predicted to be zero, suggesting the joint was unloaded and muscles produce sufficient force to regulate the mandible. Although EMG data was unavailable, the validity of the model was verified against *in vivo* bite force measurements and findings of literature.

Chapter 5. Study of function and development of the mouse masticatory system using MDA

5.1. Introduction

Morphology and function have a reciprocal relationship during ontogeny. While masticatory function depends on its structure, it also has profound influence on further musculoskeletal growth (Herring, 1985). There are a number of simultaneous changes associated with craniofacial growth which all can influence its function, namely modelling and remodelling of the cranium and mandible (Hall, 1982, Atchley et al., 1985a, Byron et al., 2004, Willmore et al., 2006, Odman et al., 2008, Tanner et al., 2010, Anderson et al., 2014), enlargement of masticatory muscles (Rayne and Crawford, 1972, Houston, 1974, Nakata, 1981, Langenbach and Weijs, 1990), change of occlusal bite force (Dechow and Carlson, 1990), change of diet, and finally change of contact surfaces of the teeth. The latest, which occurs as a result of erosion, is a complex subject with many associated factors and is out of the scope of this study.

Function plays an important role in modulating the development and form of craniofacial development, an understanding of which requires in depth investigation of the different anatomical regions and tissue types (Dechow and Carlson, 1990). In particular, a dramatic change in masticatory function, during the transition from sucking behaviour to mastication after weaning, results in significant developmental changes during ontogeny. Weaning in the mouse occurs at day 21 (Willmore et al., 2006). In craniofacial studies, the role of altered function on features such as muscle attachment area, overall skeletal size and bone structure has been investigated (e.g. Avis (1961), Bouvier and Hylander (1981), (1982), Hendricksen et al. (1982), Herring and Lakars (1982), Yamada et al. (2006), Nakamura et al. (2013)) and the biomechanical changes during craniofacial growth were suggested to result in discrete morphological changes. Most of these studies involve the use of food with different properties, addressed as hard versus soft, or pellet versus paste food.

Developmental changes of the cranium, the mandible and masticatory muscles are not a simple scaling of their size. Different parts of the mandible and the cranium as well as individual masticatory muscles develop with variable rates and undergo various changes during different stages of their development. Moreover, understanding the adaptations of tissues during growth cannot be achieved without considering their concurrent functional changes, because the bone actively responds to its functional environment, for example to muscle activity, through modelling and remodelling (Tanaka et al., 2007). Bone modelling is the initial growth of the bone to its adult morphology, whereas bone remodelling is alterations of the bone morphology after adulthood. In the case of the mouse starts of adulthood coincides to the end of weaning (Zelditch et al., 2003). Hence not only do changes in masticatory muscle function during development influence the morphology of the cranium and the mandible, but also changes in diet result in change of stress and strain patterns experienced by the bone and which affects its morphology.

Cranial and mandibular ontogeny is influenced by a combination of developmental and functional factors. Developmental factors are related to tissue origin, whereas functional factors are linked to different regions of the cranium and mandible, each of which has specific functional demands (Willmore et al., 2006). The cranium can be divided into two developmental regions and four functional regions, which are presented in the mouse skull in Figure 5.1.

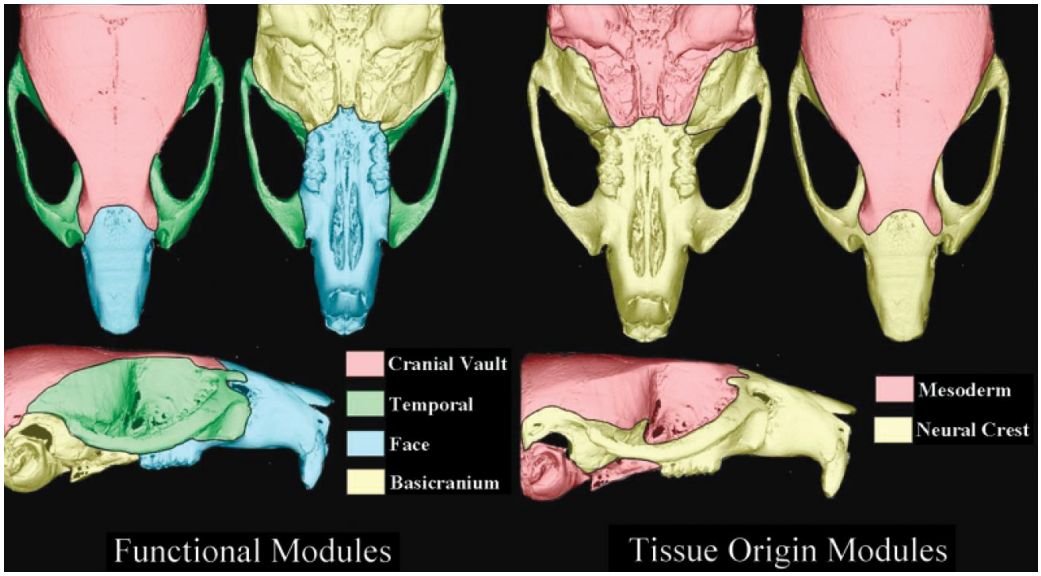

Figure 5.1 Functional and developmental regions of the mouse skull (Willmore et al., 2006).

Cranial development seems to follow a general pattern across mammals; the neurocranium develops first, whereas facial expansion occurs at later stages of ontogeny. Hence young mammals are relatively short faced (Langenbach and van Eijden, 2001). This pattern was indeed found in the mouse too; cranial morphology was found to be different in the young (35-day-old) mouse in comparison to adult (90-day-old and 150-day-old) mice (Willmore et al., 2006). The young mouse was found to have shortened face, more globular cranium vault and larger temporal bone compared to adult mouse. It was found that during the ontogeny of the mouse the face elongates, the cranium flattens and temporal region reduces in size (Willmore et al., 2006). The facial changes are due to differential growth (different rate of growth compared to other parts of cranium), but this allometric shape change continues for as long as the growth occurs. Moreover, the differential growth of the face was found to cause changes in masticatory muscle orientations in a number of mammals, which may cause further shape change in this cranial region (Langenbach and van Eijden, 2001). Moreover, as the masticatory function transits post-weaning, the facial and the temporal region of the cranium experience high stress and strain and undergo significant growth after postnatal day 21 (Willmore et al., 2006). An additional factor that influences cranial morphology is the diet. It was found that when mice were fed on a soft diet, as opposed to a solid

diet, they had significantly shorter and narrower nasal bone, compared to the group that were fed on a solid diet (Tokimasa et al., 2000). However, the diet did not seem to effect the growth of the glenoid fossa (Kuroe and Ito, 1990).

Although mandibular length has been found to be related to the cube root of body weight (Dechow and Carlson, 1990), as with the cranium, mandible growth is not isometric and experiences variable adaptations across its different regions. This differential growth is due to the different developmental and functional regions (Atchley and Hall, 1991). The latter is explained due to the different parts of functional apparatus, including the jaw closer muscles, TMJs and incisor and molar teeth, acting on different regions of the mandibular bone (Figure 5.2).

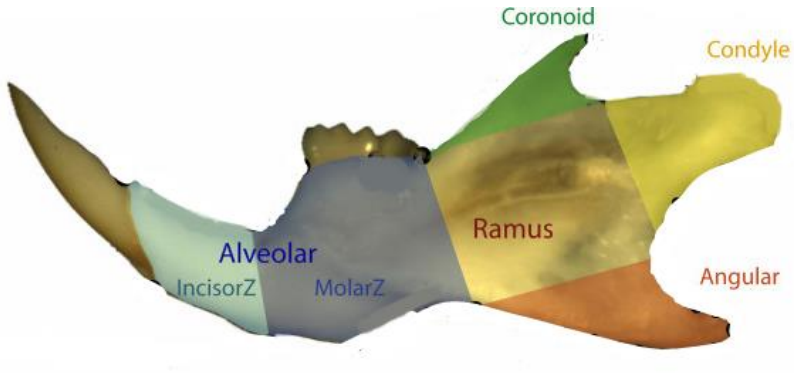

Figure 5.2 Developmental and functional regions in the mouse mandible (Anderson et al., 2014).

The developmental trajectories of mandible growth are complex and vary in different stages of growth. The mandibular growth in the first postnatal week involves deepening of the horizontal ramus and elongation of the condylar process, whereas in the second week changes involve the increasing relative height of the coronoid process along with increasing depth of the angular process and thickness of condylar process. In the third week of postnatal growth, the emphasis is on curvature of angular and coronoid processes. Hence the direction of mandibular development shifts during growth and this directional shift occurs twice during the ontogeny (Swiderski and Zelditch, 2013). This leads to a complex growth pattern which does not occur sequentially, i.e. first anterior regions, then posterior etc.

Interestingly, there is a correspondence between mandibular growth and teeth development (Swiderski and Zelditch, 2013). Initially, the anterior and ventral parts of the horizontal ramus as well as the condyle elongate to accommodate addition of the teeth and their crowns. With further development of the teeth, which transits from developing their crowns to increasing in height and developing their roots, the mandible also starts to deepen in the ramus area. Eruption of the molars starts at postnatal day 10 (Swiderski and Zelditch, 2013) and is near completion post-weaning (around postnatal day 21; (Willmore et al., 2006)), when the mastication starts. From this point the developmental changes in the mandible shifts from ramus shape into the coronoid and angular processes to match the more rapid rate of masticatory muscle growth. Moreover, the development of the condyle shifts from elongation into deepening, hence it does not add to the length of the ramus but adds more robustness to the mandible which is required to withstand higher loads from solid food mastication (Swiderski and Zelditch, 2013). It has been stated that this deepening is the bone's response to the mechanical stimuli from chewing (Rayne and Crawford, 1972).

Diet also influences the developmental changes within the mandible. The shape of the condyle head is affected by the diet and remained underdeveloped as a result of soft diet. The shape of the condyle goes through the following developmental changes: initially it is shaped as a bar, then transforms into a tear drop, ellipse and finally long ellipse. These transformational stages, however, do not occur completely in mice fed on soft diets which stop at the tear drop stage (Yamada et al., 2006, Kuroe and Ito, 1990). Moreover, it was found that mandible of the mouse fed on hard diet had more mechanical advantage, both in the masseter and temporalis muscles, and was more suited to process hard food (Anderson et al., 2014).

Masticatory muscle development affects biomechanical analysis of the masticatory system in two ways: through a change of mechanical advantage and a change of PCSA value. The mechanical advantage is a factor of muscle and biting point lever arm, and PCSA value is a factor of muscle mass. Hence both change of muscle attachment area and muscle mass affects their performance. Dechow and Carlson

(1990) found that muscle orientations remained more or less the same during growth in *rhesus monkeys*. Moreover, they found the lever arm of the temporalis and masseter muscles increase with age, however, the mechanical advantage of the masseter and temporalis remained the same for incisal biting during growth. Likewise, the mechanical advantage of the temporalis muscle in molar biting did not change significantly during growth, in contrast to the mechanical advantage of the masseter muscle which increased significantly. In addition, the growth of muscles in rabbits showed differential growth rates, with jaw openers developed with negative allometry (i.e. mass increased at a lower rate than body size) and their contribution to overall mass decreased with age. Temporalis muscle showed negative allometric growth, but its contribution to overall masticatory function remained the same. In contrast, the masseter and medial pterygoid muscles grew with positive allometry and their share of overall muscle mass increased during growth. More interestingly, physiological cross section area (PCSA) of the jaw closers grew with positive allometry, whereas jaw openers grew with negative allometry. The lateral pterygoid muscle changed from negative to positive allometric growth after weaning. Hence, both individual muscle performance and overall muscles function are age-dependant (Langenbach and Weijs, 1990). For the mouse, however, data on muscle growth, their mechanical advantage and their capability in force generation is not available in the literature to the best of the knowledge of the author. Although Anderson et al. (2014) report on the change in the mechanical advantage of the masseter and temporalis muscles due to diet, they do not report on changes in these values through ontogeny. During growth, not only muscle length and thickness increases, but also their compositions (related to muscle fibre types) change too (Nakata, 1981). Although these changes can influence muscle function, they are out of the scope of current study.

Thus, in summary, many simultaneous changes occur during development of the mouse masticatory system. These changes are not solely the scaling of the size of muscles and bones, but different muscles and different parts of the cranium and the mandible transform independently. Moreover the transformation of the bone during development is affected by the strain resulted from muscle activation.

Therefore, on one hand transformation of the bone influences the muscle attachment area and consequently the muscle development, and on the other hand the muscle activation and its resultant strains affects the bone modelling and remodelling. Studying the masticatory function of the juvenile mouse and its comparison to the adult mouse is very informative to understand the intertwined relationship between function and morphology.

As weaning in the mouse occurs at around 21 days old (Willmore et al., 2006), and sucking behaviour changes to mastication, significant developmental change of masticatory are expected after this point. Hence this age is suitable for comparison with the adult mouse. Moreover, there were only few significant differences found between 90 and 150-day old mice in the literature (Willmore et al., 2006), hence a 90-day old specimen is representative of the masticatory system of the adult mouse. This decision is also supported by findings of Nakata (1981), who reported that the growth of the mandible was complete after day 85. Hence in this study, the masticatory function of a 21-day old and 90-day old mice were investigated using MDA, for which individual-specific data were used.

Compared to an adult mouse, a young mouse has a shortened face which is suggesting that the lever arm of the biting points, especially the incisors, and the more anterior muscles, such as superficial masseter, might be shorter than the adult mouse. Considering that the mandible and consequently, the leverage of the bite point grows through ontogeny too, it is unclear how the mechanical advantage changes. Thus, studying the TMJ reaction force of the masticatory system of the juvenile mouse is one objective of this chapter, together with comparing the muscle activation patterns of the juvenile and adult mice. Moreover, the temporal bone in the young mouse is relatively wider compared to the adult mouse (Willmore et al., 2006). Having a wider temporal bone could be an indication of larger temporal muscle and higher temporal relative mass too. This question is studied in this chapter, using relative mass and PCSA value of the juvenile and adult specimens. Moreover, there is no published data on how the maximal bite force changes with age in the mouse, especially from weaning until adulthood. In this chapter, the

maximal incisal bite force between at 3-weeks (just after weaning) to 12-week is presented.

5.2. Methods

5.2.1 Experimental methods

All experimental data were collected at the Muséum National d'Histoire Naturelle Paris, France. For measuring the maximum bite force, five C57 wild-type mice at age 3, 6, 9 and 12 weeks were used, obtained from Charles River Laboratories (Chatillon-sur-Chalaronne, France). All experiments were approved by the animal care and use committee at the Muséum National d'Histoire Naturelle, Paris, France. Incisor bite force measurements at a gape angle of 25±5 degrees were collected from all specimens using equipment described in Chapter 2. The bite force measurements were repeated 10 times and the maximum measurement was used to compare against the MDA results. Next, all individuals were recorded during feeding using cineradiography techniques (note that these videos were not available at the time of developing of the MDA adult model). All the videos were reviewed and one video of a 3 week old individual, with good visibility and sufficient chewing cycles was selected. The rest of the videos and specimens were not included in this thesis, expect for the age-dependant maximum bite force study.

The same individual was then sacrificed, dissected on one side of the head, and PCSA data were collected as described in Section 2.2.2 and 2.2.3, using a muscle intrinsic stress of 39.7 N/cm^2. The remaining intact side of the head was stained and scanned the School of Engineering, University of Hull (X-Tek HMX160; X-Tek Systems Ltd, Tring, UK) with a voxel size of 0.014 mm in all three directions as described on Section 2.2.3.

The kinematics of the juvenile mouse were obtained through landmarking of cineradiography data. Three incision cycles were used to obtain the average maximum gape angle from which the maximum bite gape dimension was calculated, calibrated to the cranial length, where the length of the cranium was measured from a 3D reconstruction in AVIZO. Only incisal biting of the juvenile

mouse was modelled, hence to maintain comparability of the model to the adult incisal biting, only the rotary movement of the mandible was included in the MDA model.

5.2.2 Model construction

The details of the model construction of the adult mouse are explained in Section 2.3, and geometries of the skull and the mandible were obtained from scans of the stained mouse head mentioned in Section 5.2.1. The masticatory muscle geometries were segmented using AVIZO and muscle definitions were carried out using landmarking of the muscles as explained in Section 2.3.2. The number of muscle strands was identical to the model of adult mouse (Section 2.3.3). Hinge joint at the TMJs and a spherical joint at the symphysis were used to constrain the mandible to the cranium. As only a hinge joint (with simple rotary movement) was used at the TMJs, the stability of the system, caused by open contact surfaces, was not an issue. Hence no bushing elements were defined in the model.

The food item was defined as two plates connected by a spring which was moved in between the incisors. Incisal biting with bite gape of 0.8 mm was modelled, which was the same gape used previously for the MDA of the adult mouse. According to the cineradiography of the individual, the maximum gape size in this individual was 3.4 mm. However, the bite gape, in which the power stroke occurred could not be determined. Moreover, with respect to the aim of this chapter, which was to study the differences in masticatory function resulted from differences in the morphologies, all factors except for the latter should remain unchanged. Hence the bite gape of 0.8 mm, which was below the maximal gape of the juvenile and comfortably achievable, is justified considering the comparative nature of this study. To simulate the model, the DGO algorithm was used and one full biting cycle was modelled.

Initially, a very stiff food item (stiffness of 200 N/mm^2) was used to activate all the muscle maximally and predict the maximum incisors bite force by MDA model. Next, the model was used to simulate an incisal bite force of 4.5 N and muscle

activation and joint reaction force were studied, and compared to the adult mouse under identical conditions.

5.3. Results

5.3.1 Age-dependant bite force measurements

The *in vivo* measurements of maximal incisal bite force for different ages is presented in Figure 5.3. The bite force for the 3 week-old mice varies between 4.7 and 5.7 N.

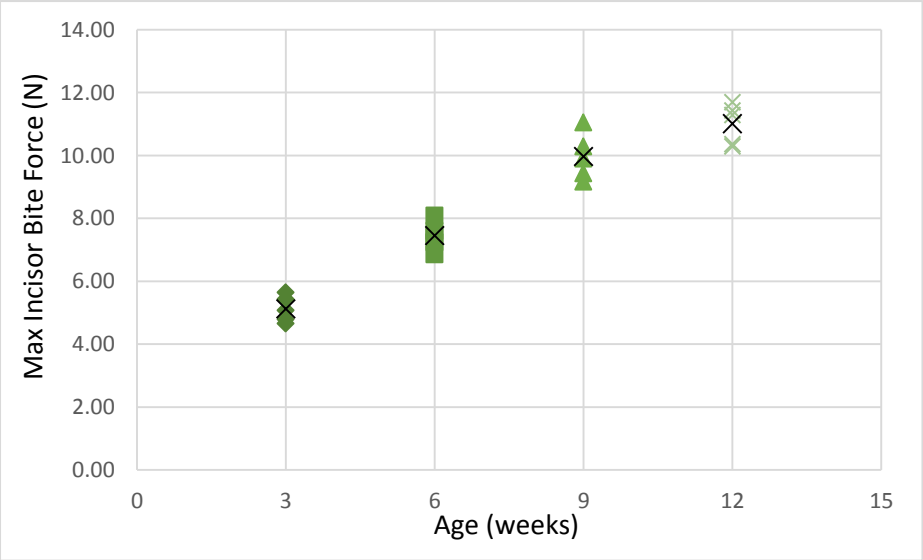

Figure 5.3 Maximum in vivo incisal bite force measurements

The specimen chosen for the MDA modelling had a maximum bite force of 5.08 N, with a range of bite forces between 3.67 N and 5.08N. Moreover, it was in the acceptable range compared to all other same age individuals (Figure 5.4).

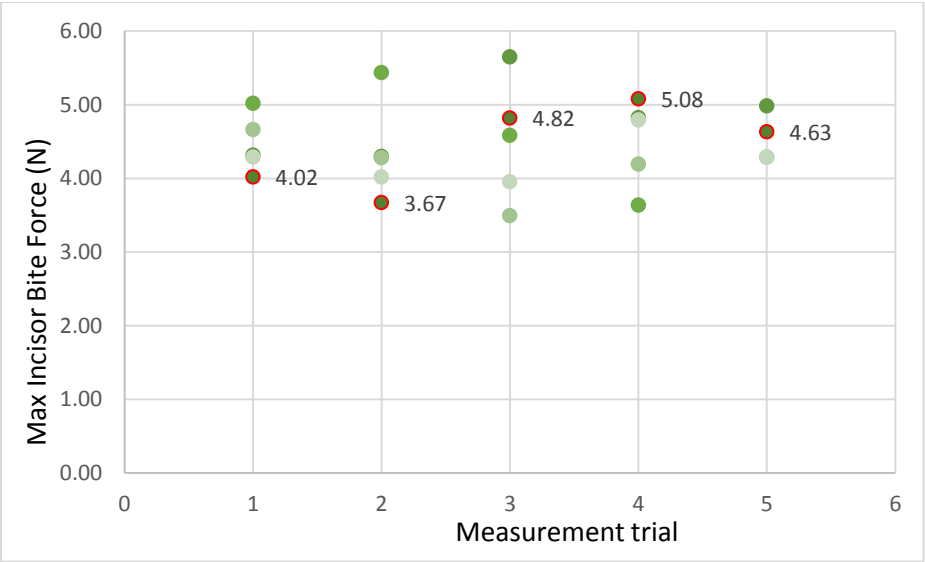

Figure 5.4 Bite force measurements were repeated 5 times for every three week old specimen. The specimen which its bite force is presented in red was used in MDA models.

5.3.2 PCSA calculations

PCSA values and relative muscle forces are presented in Table 5.1, with the deep masseter being the most prominent, followed by the superficial masseter.

Table 5.1 PCSA values and relative muscle forces in the 3-week-old mouse

Muscles	Mass (g)	Muscle fibre length (cm)	PCSA(cm^2)	Force (N)
SM	0.0142	0.29	0.05	2.07
DM	0.0216	0.30	0.08	3.05
AT	0.0063	0.24	0.03	1.09
PT	0.0072	0.23	0.03	1.32
SZT	0.0018	0.25	0.01	0.31
AZM	0.0029	0.22	0.01	0.55
IOZM	0.0042	0.26	0.02	0.69
PZM	0.0011	0.16	0.01	0.28
EP	0.0030	0.32	0.01	0.40
IP	0.0083	0.25	0.04	1.39
DG	0.0062	0.29	0.02	0.89

The pie chart in Figure 5.5 presents the relative masses of each of the jaw closer muscles, while the pie chart in Figure 5.6 shows the relative muscle force capability of each of the muscles. The deep masseter and superficial masseter are the most prominent muscles in terms of mass and force production. The next largest muscles are the internal pterygoid, posterior temporalis and anterior temporalis respectively. There are small differences between relative muscle force and muscle mass, in particular in the masseter and temporalis muscles. The share of both the deep and superficial master in the overall jaw closing muscle force is lower than their share in overall jaw closing muscle mass. In contrast, all three parts of the temporalis have a higher proportion of overall muscle force than the overall muscle mass, although only by a maximum of 4%.

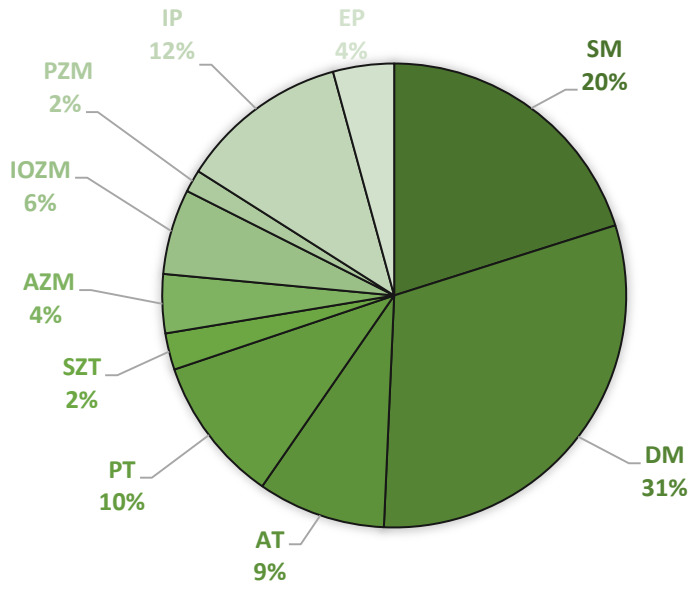

Figure 5.5 Relative mass of jaw closer muscles in juvenile mouse, which is calculated as the ratio of mass of each jaw closer to the overall mass of jaw closer muscles. For abbreviations see Table 3.2.

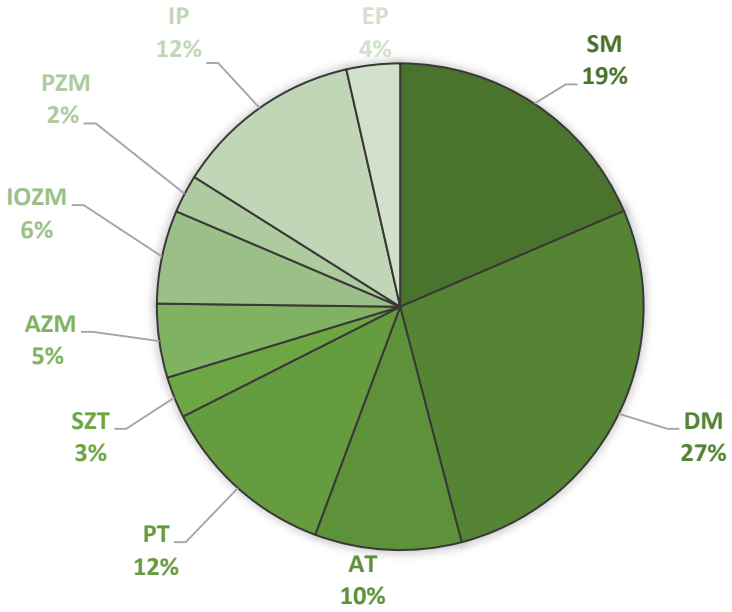

Figure 5.6 Relative force of jaw closer muscles in juvenile mouse. For abbreviations see Table 3.2.

5.3.3 Modelling results

In the first part of the MDA study, all the muscles were activated maximally to investigate the maximum bite force of the juvenile mouse. The value predicted by the MDA was 5.94N, which was above, but comparable to the *in vivo* maximum bite force of 5.08N.

The muscle activation patterns predicted for incisal biting with a bite force of 4.5N and gape size of 0.8mm are presented in Table 5.2 and compared with similar adult results in Figure 5.7. The highest level of activation was in the infra-orbital and anterior zygomaticomandibularis (both 100%), deep masseter (93%) and external pterygoid (88%). The highest absolute activation force was predicted for deep masseter (2.85N), internal pterygoid (1.12N) and superficial masseter (0.94N, table 5.2)

Table 5.2 Absolute and relative muscle forces predicted by the juvenile MDA model

	max force (N)	activated (N)	% activation
SM	2.07	0.94	45.4
DM	3.05	2.85	93.4
AT	1.09	0.65	60.0
PT	1.32	0.55	41.3
SZT	0.31	0.22	70.3
AZM	0.55	0.55	100
IOZM	0.69	0.69	100
PZM	0.28	0.20	69.9
EP	0.40	0.35	88.8
IP	1.39	1.12	80.1

The difference between the muscle activation level in the adult and juvenile MDA models, was mainly in the superficial and deep masseter and all three parts of the pterygoid muscles (Figure 5.7). The juvenile generally had higher activation level compared to adults, except for the anterior temporalis, posterior zygomaticomandibularis and internal pterygoid.

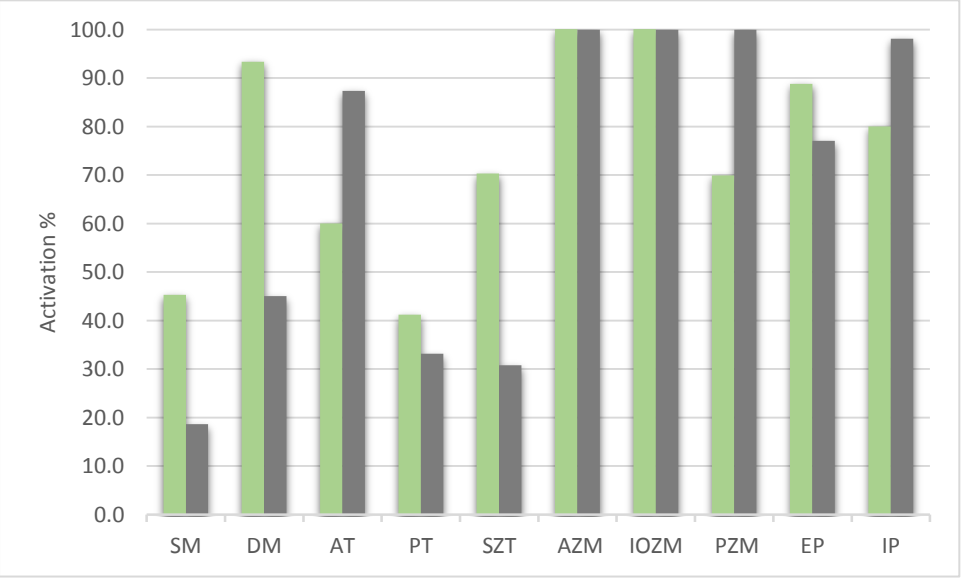

Figure 5.7 Muscle activation levels predicted from MDA models of juvenile (green) and adult (grey) mouse

Table 5.3 Joint reaction force and total muscle force of both sides of the head predicted in MDA model of juvenile and adult mouse and 2D measurement of the cranium and out lever of the cranial and mandibular incisor bite in the juvenile and adult from segmentations

	Juvenile		Adult		Juvenile: Adult
Joint reaction force (N)	Left	Right	Left	Right	--
	4.8	4.7	4.8	5.2	
Total muscle force(N)	8.10		9.49		--
Average TMJ reaction force (N)	4.75		5.00		0.95
Cranium length	19.18		21.02		0.91
Lower incisor lever arm	11.88		12.13		0.98
Upper incisor lever arm	12.27		12.92		0.95

The joint reaction forces predicted for the adult and juvenile mice were similar, and while the right and left sides of the juvenile model had very similar magnitudes, the adult mouse had different joint reaction forces on each side. Also the total muscle force in the juvenile mouse was smaller than the adult, as expected (Table 5.3).

The 2D lever arms of the cranial and mandibular incisors are also presented in Table 5.3, together with cranial length. The ratio of the cranial lengths and higher incisor lever arms show greater differences than the mandibular lever arm.

5.4. Discussion

To study the developmental function of the mouse masticatory system, a 21-day-old mouse was chosen to compare with the adult mouse. This age was selected because weaning occurs around this age in the mouse and the 90-day old mouse was considered to have reached adulthood.

The difference between muscle mass and muscle force proportion was observed in both parts of the masseter and all three parts of the temporalis, however these differences were not substantial. In the masseter, they occur as a result of the longer fibre length in the deep and superficial masseter, compared to their muscle mass. This pattern was not observed on the adult mouse, suggesting that muscle structure changes during ontogeny. However, only one individual was studied here

and further investigation with a larger number of specimens is required before that can be confirmed.

Previous developmental studies of the mouse had reported on a wider temporal fossa in the cranium of the juvenile mouse, however, as observed in Figure 5.5 and Figure 5.6, the temporalis muscle was neither more prominent in relative mass or relative force compared to adult mouse. However, again this observation is based only on one individual.

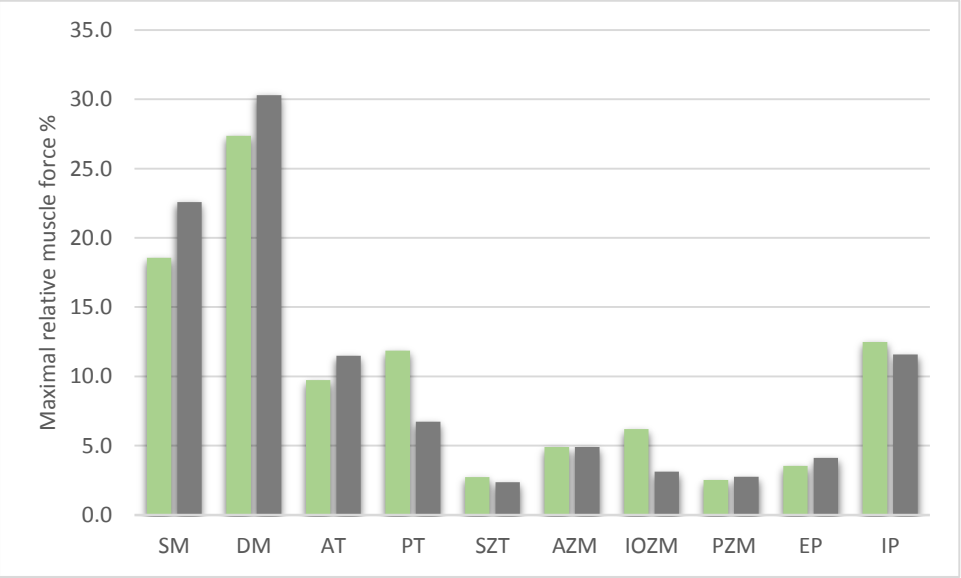

Figure 5.8 Percentage of the relative maximal muscle force in juvenile (green) and adult (grey) mouse

As with the adult MDA model, the intrinsic muscle stress value used in the PCSA calculations was 39.7N/cm^2 (reported for mouse soleus muscle, Gonzalez et al. (2000)). However, the maximal bite force predicted from the MDA model of the adult mouse was below the *in vivo* maximum measured bite force, indicating the model was underestimating the forces. It was only after increasing the intrinsic stress value to 50 N/cm^2 that the adult model prediction matched the *in vivo* measurement. The bite force predicted by the MDA model of the juvenile mouse, however, predicted a comparable bite force value to the *in vivo* measurements (5.94 N *vs.* 5.08N) using with an intrinsic stress value of 39.7N/cm^2. This could be as a result of the fact that the adult model PCSA values were averaged across 5 individuals, as well as the maximal *in vivo* bite force measurements. It also may be

that the muscle properties of the adult and juvenile are different. This difference has indeed been reported by Gonzalez et al. (2000), who found different intrinsic muscle stress values for different ages (in the soleus muscle of the mouse). It has also been found that intrinsic muscle stress is different for different muscle types (*i.e.* fast versus slow twitch muscles, Weijs and Hillen (1985)). There is no study comparing masticatory muscles with *soleus* muscle to determine how these muscles compare. Hence, it is difficult to define precisely what a realistic intrinsic stress value is for either the adult or juvenile. However, the activation pattern results are compared in the form of ratios of activity to maximal force, hence the effect of the intrinsic value is minimised.

The highest level of activation was predicted for the deep masseter, anterior and infra-orbital zygomaticomandibularis which all have substantial dorso-ventral components. As discussed in previous chapters, the DGO algorithm predicts muscle activations according to their orientation and required movement. In this model, the required movement of the mandible was only in the vertical direction (open-close), hence high activation of muscles which were aligned more vertically was expected.

The adult mouse was capable of producing much higher incisal bite forces than the juvenile (9N versus 4.5N, see chapter 4). Hence to produce bite force of 4.5N, generally lower activation of the muscles was expected for the adult. Although this was true in the majority of the muscles, there were some exceptions. The anterior temporalis, posterior zygomaticomandibularis and internal pterygoid had higher level of activation in the adult than the juvenile. This difference is the result of muscle definition in the model, showing these muscles were less vertically aligned. In anterior temporalis and posterior zygomaticomandibularis of the juvenile, either the cranial attachment area is more posterior or the mandibular attachment area was more anterior than the adult mouse, resulting in a lower vertical component of the muscle strands (Figure 5.9). In the case of the external pterygoid muscle, the orientation of muscle strands was different due to the difference in muscle attachment areas (Figure 5.10).

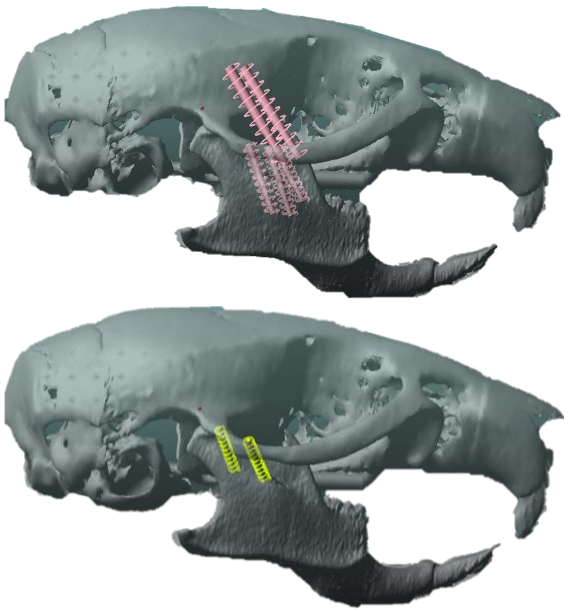

Figure 5.9 Anterior temporalis (left) and posterior zygomaticomandibularis (right) muscle definition in MDA model of the adult

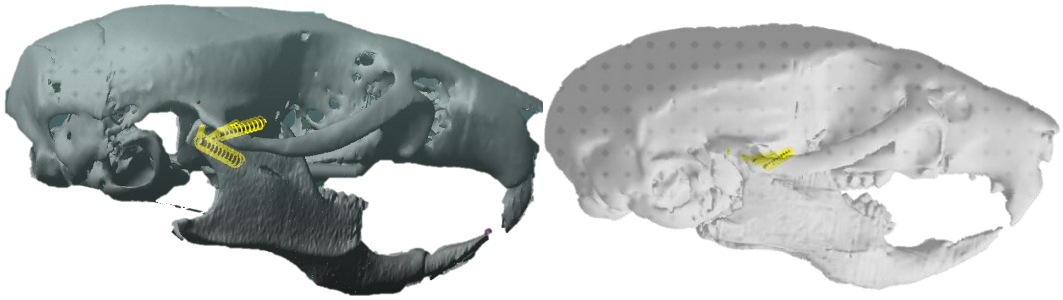

Figure 5.10 Posterior Zygomaticomandibularis in adult (left) and juvenile (right). These images are not to scale.

Interestingly, the juvenile and adult MDA models predicted comparable joint reaction forces at the TMJs. Incisal biting was modelled, in which the food item was positioned central, and equal joint reaction forces were expected for both sides. The minor difference between the two sides, in particular in the adult model, arises from difference of muscle strand definitions due to asymmetry of two sides. The ratio of the joint reaction force to the total muscle force in the juvenile was 0.58 (average TMJ reaction force/ total muscle force) whereas the ratio of the adult was 0.52. This shows that although total muscle force of the juvenile mouse is smaller, the relative TMJ reaction force is higher than the adult mouse, due to smaller leverage of the bite.

The difference in ratio of cranial length and mandibular lever arm between the juvenile and adult specimens (0.91 versus 0.98) suggests that the juvenile cranium was indeed relatively shorter than the mandible. The lever arm of the higher incisors suggests that part of the cranial difference is accommodated between the incisors and the condyle, in other words the juvenile was short-faced. Moreover, the ratio of the TMJ reaction forces corresponded well with the cranial incisor lever arm. However, the difference between cranial length and mandibular lever arm was also small, but further studies are required to conclude any correspondence between any of these ratios.

Thorough understanding of the intertwined relationship of the form and function in the masticatory system of the mouse during ontogeny requires many more experiments. The model presented here is a simplistic initial step of a series of more sophisticated MDA models, which ought to be developed at different ages, for both incisal and molar biting, with experiments at different gapes and bite forces. Only then, meaningful conclusions can be made from MDA predictions.

5.5. Conclusions

In summary, the maximal *in vivo* bite force measurements were presented for the age group ranging from 3 to 12 weeks, which has never been reported before. Moreover, it was hypothesized that the temporalis muscle might be relatively larger in the juvenile than adult as the temporal bone was reported to be relatively wider than the adult. The result showed that unlike our prediction, the relative mass of the temporalis muscle was not different from the adult specimen. The leverage of the mandibular incisors also remained almost the same, whereas leverage of the cranial incisors varied, with that variation corresponding well with the ratio of joint reaction forces. However, this study was limited, and more sophisticated models are required to study different gapes, bite force and bite positions to thoroughly understand the functional changes of the masticatory system of the mouse through ontogeny.

Chapter 6. General discussion and conclusions

In this thesis, the first multibody dynamic model of the masticatory system of the mouse has been developed. To ensure correct proportions between muscle sizes, forces, the cranium and the mandible µCT scans of a specimen was used; this specimen was one out of the 10 specimens that were used for *in vivo* bite force measurements. To develop a representative model of the masticatory system of the adult mouse, muscle data of 5 and bite force of 10 specimens were averaged, in order to include the divergence of the age group in the model. Experimental tests on 10 specimens of the same type (C57) with similar skull length (23.90 ± 0.25 mm) and same age (90 days) resulted in an average maximum incisor bite force of 8.97N, which was used to validate the MDA model of the adult mouse. The maximal incisal bite force was predicted from the MDA model and compared against *in vivo* average bite force. Subsequently, maximal molar bite force, which was unfortunately infeasible to measure *in vivo*, was predicted from MDA. MDA of the adult mouse was then used to study a number of sensitivity factors and functional circumstances, namely optimisation algorithms, constraint types, muscle attributes, as well as comparative studies of incisal and molar biting with maximal and sub-maximal bite force conditions.

In addition to MDA of the adult mouse, functional changes resulting from development of the masticatory system were of interest in this thesis. Hence, an individual-specific MDA of one juvenile specimen (age 3 weeks) was developed, in which, unlike the adult model, all muscle data, bite force measurements and kinematic data as well as the mandible and cranium geometries were obtained from the exact same specimen. Time constraints did not allow for comprehensive experiments of the juvenile model, however, maximal incisal bite force production and muscle activation pattern in sub-maximal biting was studied in a simplistic hinge-constrained model and the latter was compared against the equivalent adult model.

6.1. Anatomy of the masticatory system in the mouse

The anatomy of the masticatory system of the mouse was studied through virtual segmentation and dissection to obtain the required input data for the modelling. Although description of the anatomy and morphology of the masticatory system in the mouse was not the main aim of this study, some of our observations were found to be somewhat different from previously reported data.

The orientation of the posterior zygomaticomandibularis (PZM) in our dissected specimen, as well as the virtually segmented specimens, was found to have a posterior component, in contrast to Baverstock et al. (2013) who found the muscle to run anterocentrally. This discrepency might arise from using different strains of the mouse (BALB/c background strain in Baverstock vs. C57 used in this study). Moreover, the vertical component of the PZM seems to be larger in our specimen than the BALB/c. Baverstock also reported that PZM accounted for only 13% of the ZM muscle, whilst in our specimens this ratio is close to 20%. So it seems that the PZM is larger and has a different orientation in C57 than BALB/c strain. However, it only accounts for 3% of the overall jaw closing force. In addition, its leverage is small, making this muscle inefficient in producing vertical bite force. The function of this muscle in C57 is potentially controlling the antero-posterior position of the condyle and counterbalancing the anterior component of the powerful superficial masseter. Furthermore, we observed three sections of the temporalis muscle in our dissections which could also be distinguished in the segmentations. The third component, suprazygomatic temporalis (SZT), was not reported as a separate section previously (Baverstock et al. , 2013).

In addition to the masticatory system of the adult mouse, the morphology of the masticatory system of a juvenile mouse was studied too. Although only one juvenile specimen was used in dissection and virtual segmentation, some divergence was observed between the juvenile and the adult specimens. To validate these discrepancies however, a larger group of samples is required. In the juvenile mouse, not only is the relative percentage of masticatory muscle mass different to

the adult, but so are the muscle orientations. This suggests that the rate of growth varies between the muscles during their development. In particular, the superficial and the deep masseter as well as the anterior temporalis could generate relatively smaller forces than in the adult, which is compatible with the masticatory requirements of the juvenile mouse before weaning.

Another interesting point observed in the growth series was the variation of the measured *in vivo* bite forces between the 12-week old specimens of this series and that of the first batch. Even though both groups of specimens were from the same strain, and were at the same age, average measured maximal bite force was significantly different. This indicates the high range of variation within specimens and highlights the necessity of individually specific model development for understanding the intricate masticatory system.

6.2. MDA modelling, advantages and disadvantages

MDA provides a dynamic, sophisticated technique to study any complex system, including the masticatory system. Manual estimation of the forces, torques, displacements, velocities and accelerations of each component of the dynamic system at every time instant would be a very laborious procedure. MDA, unquestionably, facilitates this procedure and provides the means to calculate and solve multiple equations. ADAMS/view also has an interface, in which the behaviour of the dynamic system is animated at every time step. The animation interface is a great illustration to evaluate the model configurations and behaviour. These are all valuable outputs that could hardly be achieved without MDA. In the case of the MDA of the masticatory system, the ability to predict activation of each muscle, and even each muscle sub-section, independently is an important feature.

Nevertheless, MDA is associated with some inaccuracies and assumptions. Predictions are affected by the model inputs and configurations. Simplifications are essential in every modelling technique to make the system solvable; however, they introduce error to the system. In MDA of the masticatory system, the accuracy of muscle orientation and maximal muscle force estimation, constraints of the model

and the gape angle are among the factors that influence the predictions of muscle activation, joint reaction force and/or the bite force. Moreover, to tackle the indeterminacy of the system, which is an inherit characteristic of the MDA in complex systems, additional optimisation criteria ought to be added to the system. As the optimisation criteria that the central nervous system employs to coordinate the muscle recruitment in the masticatory system is not fully understood, the model optimisation criteria should be chosen based on physiologically reasonable neuromuscular strategies. In this thesis, two of the several previously proposed strategies are studied. However, the actual strategy that is used in muscle recruitment might not be any of the previously studied strategies, or could be a combination of few of them. This again introduces inaccuracy into model predictions.

6.2.1 Assumptions

Maximum muscle force calculation

A requirement for an accurate MDA model of the masticatory system is accurate calculation of maximum muscle forces. This is dependent on two other factors: accurate PCSA data calculations and precise intrinsic muscle stress value.

In this study, the effect of pinnation angle on the PCSA value of the muscle was excluded and all muscles were assumed to be uni-pinnate and parallel fibered. This exclusion has two contradicting effects on maximum muscle force predictions. On one hand, assuming all muscles are parallel fibred results in underestimation of the number of fibres in pinnate muscles , which consequently leads to underestimation of the PCSA value. On the other hand, only one component of the pinnate muscle is effective in the muscle's line of action ; hence exclusion of the pinnation angle overestimates the effective muscle force. Disregarding the pinnation angle in our MDA therefore inevitably introduces error to the model. However, due to the contradicting effects of this assumption, it is difficult to determine the precise effect on the model's output without knowing the exact pinnation angle and muscle structure. Nevertheless, as the

purpose of this thesis is to provide a comparative study, the effect of this error is consistent across all models and can be neglected.

Another source of error in the calculation of PCSA values in the adult model was due to averaging PCSA across five specimens. The average PCSA values were used in order to include the natural divergence of 12-week-old house mice with comparable skull lengths (23.90 ± 0.25 mm) in the model. However, as it was later observed, average PCSA values were consistently lower than the PCSA values of the chosen specimen (between 6% and 43%), from which the muscle attachment data and the geometries of the cranium and mandible were obtained. The importance of individual-specific data in MDA modelling has also been reported by Gröning et al., (2013b). Thus using the average PCSA data can potentially lead to underestimation of the predicted bite force.

As previously discussed, the intrinsic muscle stress value, which varies over a relatively wide range for different species, ages and muscles (Vanspronsen et al., 1989, Weijs and Hillen, 1985, Hatze, 1981), is essential for accurate estimation of maximum muscle force. It was observed in this thesis, and had already been reported in the literature (Gröning et al., 2013b), that the maximal bite force production in MDA was highly sensitive to the muscle intrinsic stress value. Unfortunately, an accurate intrinsic stress value for the masticatory muscles of the mouse was not available. The most comparable available value was intrinsic stress for the *soleus* muscle of a 90-day old mouse (39.7 N/cm^2, Gonzalez et al., 2000). However, the bite force predicted from a model with intrinstic muscle stress of 39.7 N/cm^2 did not match the *in vivo* bite force.

Taking into account all former assumptions and their resultant errors, it is difficult to conclude whether the underestimation of the maximal bite force is mostly caused by one of the factors or if they all are involved to some extent. However, interestingly the MDA model of the juvenile mouse, which was developed using individual-specific PCSA data, as opposed to the average PCSA in the adult model, predicted comparable maximal bite force to the *in vivo* measurement. This might suggest that averaging PCSA data is, in large part,

responsible for the underestimation of the bite force in the adult model. Nevertheless, the effect of other factors cannot be ignored either.

Regardless of the reason, to compensate for underestimation of the PCSA and to address the uncertainty of the intrinsic stress value, a correction factor of 25% was added to intrinsic stress in the adult model. This resulted in a value of 50 N/cm^2, which was well within the reported range of 25 to 87 N/cm^2 (Vanspronsen et al., 1989, Weijs and Hillen, 1985, Hatze, 1981) and increased the predicted maximum incisal bite force to 9.49N in the in hinge-constrained model.

Force/length relationship of the muscle

Another simplification which again causes inaccuracy in the model is exclusion of the muscle's force/length relationship. The force production of the muscle is a factor of its length; it is maximal at the optimal length and decays below and above that length. Hence, through one chewing cycle, as the muscle is stretched or contracted, its capability for force production changes. To include this force/length relationship, an additional coefficient is often added to the force production formula which varies between zero and one; zero when inactive and one for fully active at the optimal length. In this thesis however, it was assumed that all muscles are functioning in their optimal length, hence are capable of producing 100% of their maximal force at every instance of the modelling and the coefficient is equal to one. This leads to overestimation of muscle activation at lengths other than the optimal length. Nevertheless, determination of each muscle's optimal length was out of the scope of this study.

Maximal bite force measurements

The MDA model prediction was compared against the *in vivo* measurements which were obtained at 25^o bite gape. Although the measurements were repeated 5 times in each of the 10 specimens, it is difficult to conclude that the absolute maximum bite force was measured because the measurements were carried out only for one gape angle. As it was discussed earlier, both the orientation and the force/length relationship of the muscle changes with the bite

gape. Therefore, although we cannot claim that the measured bite force was the absolute maximum bite force that any of the specimens could produce, we can claim that it was the highest bite force that could be produced at bite gape of 25^{o}. Thus the MDA model was simulated for biting gape of 25^{o} to ensure that the muscles are capable of producing the measured bite force and the bite force of 8.97N is realistic.

Constraint type

There are a number of constraint types that could be used to model the TMJ in the MDA, among which the joint with one degree of freedom (hinge) and the constraint with 6 degrees of freedom (contact) were studied. Although the constraint type was not found to affect the muscle activation patterns considerably, it did significantly affect the joint reaction forces. The hinge joint predicts higher reaction forces than the contact constraint.

To control the excessive movement of the TMJ and maintain stability in the system in the contact constrained model, the bushing can be added. The bushing imitates the function of temporomandibular ligaments in the actual masticatory system, and is defined by three rotational and three translational stiffnesses. Defining the suitable bushing stiffness, which allows the required movements in the system whilst maintaining its stability, varies depending on the system. Moreover, in order to determine the validity of bushing stiffness's value, more data about the temporomandibular ligaments and capsule is required. The maximal tension they can withstand as well as their detailed orientation are of key importance. The bushing configurations also affect the predicted joint reaction forces. An example of this is the unexpected zero reaction force for the simulation of the molar biting of the contact-constrained model at both the working and balancing side in the MOME and at the working side in the DGO models. The zero reaction force at the joint indicates that the glenoid fossa and the condyle head are not in contact. The bushing forces and toques were keeping the joint mechanically stable, which is equivalent to the TMJ ligaments being subject to tension in the biological sense. However, verification of biological possibility of this loading condition requires

further knowledge of the characteristics of TMJ ligaments and capsule and the maximal tension they can withstand.

Therefore, on one hand the simple hinge joint results in overestimation of the joint reaction forces. On the other hand, the joint reaction force of the contact constrained-model is sensitive to the bushing stiffness, the validity of which cannot be determined without further morphological details of the actual ligaments. If comparative muscle activation patterns and joint reaction forces are of interest, both hinge joint and contact-constrained TMJs are reasonable choices. However, to report the actual magnitude of the joint reaction forces, the contact-constrained model should be validated against the threshold of the ligament's tensile tolerance.

6.2.2 Optimisation algorithms

The effect of optimisation algorithm on muscle activation patterns in the adult model was studied using DGO and MOME. DGO algorithm was associated with simulation of one full biting cycle as opposed to MOME which required thousands of simulations with random muscle activation combinations. Due to the large number of simulations and time and computer memory requirements, simulation of the full cycle of biting was not feasible in MOME and only one instant of biting (the power stroke) was modelled. The feasibility of simulation of a full biting cycle in DGO was its main advantage over MOME.

The result of comparison between the two revealed that muscle activation pattern was highly sensitive to the optimisation algorithm, as expected. As it was pointed out by Shi et al. (2012), MOME predicted muscle activation by favouring anteriorly positioned muscles, hence muscles with large leverage activated to a high level. In contrast, DGO predicted muscle activity based on vertical and horizontal components of the muscle orientation and of the required kinematics (Curtis et al., 2010a). Accordingly, muscles with large vertical component such as the deep masseter and the internal pterygoid were highly activated in DGO, in contrast to the inactivity of supra-zygomatic part of the temporalis due to its small vertical component. MOME however, predicted high activity of the superficial masseter due

to its larger leverage and low activity of posterior temporalis and posterior zygomaticomandibularis due to their shorter leverage.

In an efficient biomechanical system, with tendency to minimise energy consumption, the leverage of the muscle is obviously taken into account. Because a small activation, hence small energy consumption, of a muscle with large in-lever would result in considerable movement of the mandible. Although the current DGO algorithm used in this thesis does not include the muscle leverage in the prediction of its activation, it could be added to the algorithm in future studies.

Moreover, DGO with 2D kinematics tends to predict analogous muscle activation pattern for the working and balancing sides and disregards the activation divergence between the two sides. This is linked to the activation factor of a muscle in DGO which is a factor of the 2D required movement and muscle orientation (in sagittal plane). Prediction of MOME however, showed complex co-activation patterns between working and balancing side muscles. Therefore, DGO's modelling technique with 2D movements, which is presented here, is more suited for symmetrical systems, such as the incisal biting of the mouse. For unilateral biting where investigation of muscle activation in the working and the balancing sides is of interest, current DGO is not sufficient. Furthermore, the usage of DGO with 2D kinematics tends to underestimate the activity of the muscles with high mediolateral component, such as the internal and external pterygoids. It is worth noting that adding the third component of the movement, i.e. mediolateral movement, can result in asymmetric muscle activation patterns in DGO (Watson et al., 2014). Hence, to achieve more realistic and detailed muscle activation in asymmetrical systems, such as the unilateral molar biting, the third component of the movement should be added to the algorithm.

Although both optimisation criteria were validated in separate occasions and in different species, they have never been compared. The initial rationale for this comparison was to assess the vicinity and divergence of the resulted predictions. In DGO, the assumption is based on this principle that the muscles aligned in the direction of the required movement would be more effective in force production.

The principle of MOME is based on minimisation of the overall muscle energy, which in a way, is similar to using muscles that are more effective, so that the overall muscle energy would be minimised. Hence our hypothesis was that the DGO's predictions could be comparable to MOME's. However, we found that in the MDA of the mouse they diverge to some extent. There was unfortunately no biologically relevant data such as EMG or evidence of the optimisation criterion in the actual masticatory system. We suggest however, to develop the DGO algorithm to include both the leverage and the mediolateral component of the movement in future studies. This can provide a more biologically relevant optimisation algorithm which takes the leverage and the third component of the movement into account while maintains its capability of the dynamic modelling of one full biting cycle.

6.2.3 Predictions

MDA of the adult mouse was developed to predict the maximal bite force at the incisor and M1 positions and to compare the muscle activation patterns for an equal bite force at the two biting positions.

It was not possible to measure molar bite force *in vivo* and compare it to the value predicted by the modelling. Nonetheless the maximal molar biting can be estimated based on the geometry of the mandible and the cranium and the value of incisor bite force by a simple ratio of the lever arms, assuming the position of the mandible remains constant in both molar and incisor biting and the muscle orientations do not alter. This resulted in a bite force that was 9.4% higher than the model predictions (see section 4.4). The difference in estimation is indeed expected due to the posterior shifting of the mandible in reality, to occlude the molars which resulted in the change of muscle orientations and the bite force.

As maximal molar bite force was significantly higher than that of the incisors, simulation of equal bite force was expected to associate with lower muscle activation in the molar biting than the incisors biting. The ratio of incisor/molar muscle activation was not constant in simulations of the high bite force. Simulations of submaximal biting conditions, especially in the case of bite force equal to 25% of the maximum bite force (2.25N), however, revealed nearly constant muscle

activation ratio. This highlights the valuable application of the MDA modelling in the craniofacial studies; even though the maximal bite force at different biting positons could be estimated to 90% accuracy with a simple leverage calculation, the muscle activation patterns cannot be estimated in the same manner. In particular, for the higher bite force some muscles reach their 100% activation whilst others are far from being fully activated. This underlines the importance of MDA in muscle activation patterns.

6.3. MDA of juvenile mouse

With the aim of investigation of functional development in the mouse, an individually specific MDA of the juvenile mouse in 21-day of age was developed, which was the age that weaning occurred. The model, unlike the adult MDA, predicted the maximal bite force that matched the *in vivo* measurement from the same individual. The difference of the bite force production between the adult and the juvenile is due to either the underestimation of the maximal bite force in the adult model caused by averaging PCSA values, or the difference of the muscle properties between the adult and juvenile.

The adult mouse was capable of producing much higher incisal bite forces than the juvenile (almost double). Hence to produce an equal bite force, lower activation of the muscles was expected for the adult. However, relatively shorter face of the juvenile mouse resulted in some variability in muscle orientations and some muscles were predicted to have higher relative activation in juvenile. Moreover, for an equal bite force the juvenile and adult MDA models interestingly predicted comparable joint reaction forces at the TMJs.

Although MDA is valuable for simultaneous functional and developmental studies, the developmental study of this thesis was rather limited. In order to thoroughly understand the functional changes of the masticatory system of the mouse through ontogeny larger sample size is required to study the developmental changes whilst more sophisticated models are required to study different gapes, bite force and

bite positions This chapter serves as an initial step towards the better understating of the functional changes through the development.

6.4. Conclusion

The first MDA model of the mouse masticatory system was developed and two optimisation algorithms, *i.e.* DGO and MOME, were used to study the vicinity and divergence of the predictions. Some divergence were observed in the muscle activation patterns. Nevertheless, DGO was chosen as the optimisation algorithm mainly because it allowed for dynamic simulation of one full biting cycle. However, it was suggested that inclusion of the third component of the movement and the leverage in the DGO algorithm would result in a more biologically relevant algorithm with ability of dynamic modelling of the one full biting cycle.

Sensitivity of the model to constraint type, muscle intrinsic stress value and muscle thickness was tested. It was found that bite force prediction was highly correlated to muscle intrinsic stress value, in contrast to constraint type and muscle thickness which had little effect on incisal bite force production. Moreover, maximal incisal bite force was predicted in the adult model and was found to be lower than the *in vivo* measurements from the same group of specimens. It was suggested that averaging PCSA values for the adult mouse is likely to be the main reason of the underestimation. To compensate the effects, the muscle intrinsic stress was increased by 25%. Furthermore, maximal-and sub-maximal molar and incisal biting were modelled and muscle activation patterns were compared. Although the maximal bite force could be estimated from a simple lever arm ratio based on the incisor biting and the mandible morphology with 90% of accuracy, the muscle activation patterns, especially in higher bite forces, could not be estimated without the MDA's aid. Furthermore, as expected, for simulation of an equal bite force, joint reaction force in incisor biting was higher than molar biting. In contact-constrained models, the joint reaction forces were highly sensitive to the bushing stiffness. An example was the prediction of zero reaction force at the working side, suggesting the joint was unloaded and muscles produce sufficient force to counteract the bite force and stable the mandible with assistance from the bushing. Although the possibility of the latter loading condition is verified in mechanical sense, it cannot

be verified biologically without further knowledge of the TMJ's ligaments and capsule.

In addition, the maximal *in vivo* bite force measurements were presented for the age group ranging from 3 to 12 weeks, which has never been reported before. The leverage of the mandibular incisors also remained almost the same, whereas leverage of the cranial incisors varied, variation of which corresponded well with the ratio of joint reaction forces. However, this study was limited, and more sophisticated models are required to study different gapes, bite force and bite positions to thoroughly understand the functional changes of the masticatory system of the mouse through ontogeny.

6.5. Future work

As mediolateral movement of the mandible was neglected in this study, DGO predicted similar working and balancing side muscle activation in the adult and juvenile model. In future, the third component of the movement should be included in the model, to mimic the kinematics of the system more accurately. Moreover the DGO algorithm which was used in this study did not take leverage of the muscles into consideration for prediction of muscle activation. In future the leverage of the muscle should also be added to DGO algorithm.

As the joint reaction forces were found to be affected by the bushing stiffness, thorough investigation of biologically reasonable bushing stiffness and its effects on the joint reaction force is very important to generate an accurate and meaningful joint reaction forces and should be covered in the future.

Furthermore, time constraints of this project did not allow for comprehensive studies of the functional development of the juvenile mouse. Simulations of incisal and molar biting with different gapes and bite forces is essential to understand the differences between the function of the adult and juvenile mouse masticatory system. In addition, this thesis only presented simplistic hinge-constrained model of the TMJ, whereas realistic contact constraint of TMJ is important, in particular for

prediction of joint reaction forces. And last but not the least, MDA model of mouse in different stages of their ontogeny is invaluable to understand the complex relationship between function and development and should be developed.

References

ALAQEEL, S. M., HINTON, R. J. & OPPERMAN, L. A. 2006. Cellular response to force application at craniofacial sutures. *Orthodontics & Craniofacial Research,* 9**,** 111-122.

ALEXANDER,R. McN. & VERNON, A. 1975. The dimensions of knee and ankle muscles and the forces they exert. *Journal of Human Movement Studies,* 1, 115-123.

ALEXANDER & VERNON, A. 1975. The dimensions of knee and ankle muscles and the forces they exert. *Journal of Human Movement Studies,* 1**,** 115-123.

ANAPOL, F. & BARRY, K. 1996. Fiber architecture of the extensors of the hindlimb in semiterrestrial and arboreal guenons. *American Journal of Physical Anthropology,* 99**,** 429-47.

ANDERSON, P. S., RENAUD, S. & RAYFIELD, E. J. 2014. Adaptive plasticity in the mouse mandible. *BMC Evolutionary Biology,* 14**,** 85.

ATCHLEY, W. R. & HALL, B.(Mcn and Vernon, 1975) K. 1991. A model for development and evolution of complex morphological structures. *Biological reviews of the Cambridge Philosophical Society,* 66**,** 101-57.

ATCHLEY, W. R., PLUMMER, A. A. & RISKA, B. 1985a. Genetic-Analysis of Size-Scaling Patterns in the Mouse Mandible. *Genetics,* 111**,** 579-595.

ATCHLEY, W. R., PLUMMER, A. A. & RISKA, B. 1985b. Genetics of mandible form in the mouse. *Genetics,* 111**,** 555-77.

AVIS, V. 1961. The significance of the angle of the mandible: an experimental and comparative study. *American Journal of Physical Anthropology,* 19**,** 55-61.

BAB, I., HAJBI-YONISSI, C., GABET, Y. & MÜLLER, R. 2007. Hyoid, Mandible, and Temporo-Mandibular Joint, Micro-Tomographic Atlas of the Mouse Skeleton. Springer US.

BARTON, N. H. & KEIGHTLEY, P. D. 2002. Understanding quantitative genetic variation. *Nature Reviews Genetics,* 3**,** 11-21.

BATES, K. T. & FALKINGHAM, P. L. 2012. Estimating maximum bite performance in Tyrannosaurus rex using multi-body dynamics. *Biology Letters,* 8**,** 660-664.

BAVERSTOCK, H., JEFFERY, N. S. & COBB, S. N. 2013. The morphology of the mouse masticatory musculature. *Journal of Anatomy,* 223**,** 46-60.

BERNICK, S. & PATEK, P. Q. 1969. Postnatal development of the rat mandible. *Journal of Dental Research,* 48**,** 1258-63.

BERTRAM, J. E. & SWARTZ, S. M. 1991. The 'law of bone transformation': a case of crying Wolff? *Biological reviews of the Cambridge Philosophical Society,* 66**,** 245-73.

BJERTNESS, E. 1991. [Alzheimer's disease--a challenge for dental personnel]. *Nor Tannlaegeforen Tid,* 101**,** 404-7.

BOUVIER, M. & HYLANDER, W. L. 1981. Effect of bone strain on cortical bone structure in macaques (*Macaca mulatta*). *Journal of Morphology,* 167**,** 1-12.

BOUVIER, M. & HYLANDER, W. L. 1982. The effect of dietary consistency on morphology of the mandibular condylar cartilage in young macaques (Macaca mulatta). *Progress in Clinical & Biological Research,* 101**,** 569-79.

BYRD, K. E. 1981. Mandibular Movement and Muscle-Activity during Mastication in the Guinea-Pig (*Cavia-Porcellus*). *Journal of Morphology,* 170**,** 147-169.

BYRON, C. D., BORKE, J., YU, J., PASHLEY, D., WINGARD, C. J. & HAMRICK, M. 2004. Effects of increased muscle mass on mouse sagittal suture morphology and mechanics. *The anatomical record. Part A, Discoveries in molecular, cellular, and evolutionary biology,* 279**,** 676-84.

COBOS, A. R., SEGADE, L. A. & FUENTES, I. 2001. Muscle fibre types in the suprahyoid muscles of the rat. *Journal of Anatomy,* 198**,** 283-94.

COX, P. G. & JEFFERY, N. 2011. Reviewing the Morphology of the Jaw-Closing Musculature in Squirrels, Rats, and Guinea Pigs with Contrast-Enhanced MicroCT. *Anatomical Record-Advances in Integrative Anatomy and Evolutionary Biology,* 294**,** 915-928.

COX, P. G., RAYFIELD, E. J., FAGAN, M. J., HERREL, A., PATAKY, T. C. & JEFFERY, N. 2012. Functional Evolution of the Feeding System in Rodents. *Plos One,* 7.

CUCCIA, A. M., CARADONNA, C. & CARADONNA, D. 2011. Manual therapy of the mandibular accessory ligaments for the management of temporomandibular joint disorders. *The Journal of the American Osteopathic Association,* 111**,** 102-12.

CURTIS, N. 2011. Craniofacial biomechanics: an overview of recent multibody modelling studies. *Journal of Anatomy,* 218**,** 16-25.

CURTIS, N., JONES, M. E., EVANS, S. E., O'HIGGINS, P. & FAGAN, M. J. 2013. Cranial sutures work collectively to distribute strain throughout the reptile skull. *Journal of the Royal Society Interface,* 10**,** 20130442.

CURTIS, N., JONES, M. E., EVANS, S. E., SHI, J., O'HIGGINS, P. & FAGAN, M. J. 2010. Predicting muscle activation patterns from motion and anatomy: modelling the skull of Sphenodon (*Diapsida: Rhynchocephalia*). *Journal of the Royal Society Interface,* 7**,** 153-60.

CURTIS, N., JONES, M. E., SHI, J., O'HIGGINS, P., EVANS, S. E. & FAGAN, M. J. 2011a. Functional relationship between skull form and feeding mechanics in Sphenodon, and implications for diapsid skull development. *PLoS One,* 6**,** e29804.

CURTIS, N., JONES, M. E. H., LAPPIN, A. K., O'HIGGINS, P., EVANS, S. E. & FAGAN, M. J. 2010c. Comparison between in vivo and theoretical bite performance: Using multi-body modelling to predict muscle and bite forces in a reptile skull. *Journal of Biomechanics,* 43**,** 2804-2809.

CURTIS, N., KUPCZIK, K., O'HIGGINS, P., MOAZEN, M. & FAGAN, M. 2008. Predicting skull loading: Applying multibody dynamics analysis to a macaque skull. *Anatomical Record-Advances in Integrative Anatomy and Evolutionary Biology,* 291**,** 491-501.

CURTIS, N., WITZEL, U., FITTON, L., O'HIGGINS, P. & FAGAN, M. 2011c. The mechanical significance of the temporal fasciae in Macaca fascicularis: an investigation using finite element analysis. *Anat Rec (Hoboken),* 294**,** 1178-90.

DE BEER, G. 1937. *The development of the vertebrate skull.,* Oxford, The Clarendon press.

DE GUELDRE, G. & DE VREE, F. 1988. Quantitative electromyography of the masticatory muscles of Pteropus giganteus (Megachiroptera). *Journal of Morphology,* 196**,** 73-106.

DE ZEE, M., DALSTRA, M., CATTANEO, P. M., RASMUSSEN, J., SVENSSON, P. & MELSEN, B. 2007. Validation of a musculo-skeletal model of the mandible and its application to mandibular distraction osteogenesis. *Journal of Biomechanics,* 40**,** 1192-1201.

DECHOW, P. C. & CARLSON, D. S. 1990. Occlusal force and craniofacial biomechanics during growth in rhesus monkeys. *American Journal of Physical Anthropology,* 83**,** 219-37.

DRUZINSKY, R. E. 1995. Incisal biting in the mountain beaver (Aplodontia rufa) and woodchuck (Marmota monax). *Journal of Morphology,* 226**,** 79-101.

DRUZINSKY, R. E. 2010a. Functional anatomy of incisal biting in *Aplodontia rufa* and *sciuromorph* rodents - part 1: masticatory muscles, skull shape and digging. *Cells Tissues Organs,* 191**,** 510-22.

DRUZINSKY, R. E. 2010b. Functional anatomy of incisal biting in *Aplodontia rufa* and *sciuromorph* rodents - part 2: *sciuromorphy* is efficacious for production of force at the incisors. *Cells Tissues Organs,* 192**,** 50-63.

DRUZINSKY, R. E., DOHERTY, A. H. & DE VREE, F. L. 2011. Mammalian Masticatory Muscles: Homology, Nomenclature, and Diversification. *Integrative and Comparative Biology,* 51**,** 224-234.

GLITSCH, U. & BAUMANN, W. 1997. The three-dimensional determination of internal loads in the lower extremity. *Journal of Biomechanics,* 30**,** 1123-1131.

GONZALEZ, E., MESSI, M. L. & DELBONO, O. 2000. The specific force of single intact extensor digitorum longus and soleus mouse muscle fibers declines with aging. *Journal of Membrane Biology,* 178**,** 175-183.

GORNIAK, G. C. 1977. Feeding in golden hamsters, Mesocricetus auratus. *Journal of Morphology,* 154**,** 427-58.

GRÖNING, F., FAGAN, M. & O'HIGGINS, P. 2013a. Comparing the distribution of strains with the distribution of bone tissue in a human mandible: a finite element study. *The Anatomical Record (Hoboken),* 296**,** 9-18.

GRÖNING, F., FAGAN, M. J. & O'HIGGINS, P. 2011a. The effects of the periodontal ligament on mandibular stiffness: a study combining finite element analysis and geometric morphometrics. *Journal of Biomechanics,* 44**,** 1304-12.

GRÖNING, F., JONES, M. E. H., CURTIS, N., HERREL, A., O'HIGGINS, P., EVANS, S. E. & FAGAN, M. J. 2013b. The importance of accurate muscle modelling for biomechanical analyses: a case study with a lizard skull. *Journal of the Royal Society Interface,* 10.

GRÖNING, F., LIU, J., FAGAN, M. J. & O'HIGGINS, P. 2011b. Why do humans have chins? Testing the mechanical significance of modern human symphyseal morphology with finite element analysis. *American Journal of Physical Anthropology,* 144**,** 593-606.

GROSSE, I. R., DUMONT, E. R., COLETTA, C. & TOLLESON, A. 2007. Techniques for modeling muscle-induced forces in finite element models of skeletal structures. *Anatomical Record-Advances in Integrative Anatomy and Evolutionary Biology,* 290**,** 1069-1088.

HALL, B. K. 1982. Mandibular Morphogenesis and Craniofacial Malformations. *Journal of Craniofacial Genetics and Developmental Biology,* 2**,** 309-322.

HANNAM, A. G., STAVNESS, I., LLOYD, J. E. & FELS, S. 2008. A dynamic model of jaw and hyoid biomechanics during chewing. *Journal of Biomechanics,* 41**,** 1069-1076.

HATZE, H. 1981. Estimation of myodynamic parameter values from observations on isometrically contracting muscle groups. *European Journal of Applied Physiology and Occupational Physiology,* 46**,** 325-38.

HAUTIER, L. & SAKSIRI, S. 2009. Masticatory muscle architecture in the Laotian rock rat Laonastes aenigmamus (Mammalia, Rodentia): new insights into the evolution of hystricognathy. *Journal of Anatomy,* 215**,** 401-410.

HEINTZ, S. & GUTIERREZ-FAREWIK, E. M. 2007. Static optimization of muscle forces during gait in comparison to EMG-to-force processing approach. *Gait & Posture,* 26**,** 279-288.

HENDRICKSEN, R. P., MCNAMARA, J. A., JR., CARLSON, D. S. & YELLICH, G. M. 1982. Changes in the gonial region induced by alterations of muscle length. *Journal of Oral and Maxillofacial Surgery,* 40**,** 570-7.

HERRING, S. W. 1985. The Ontogeny of Mammalian Mastication. *Integrative and Comparative Biology,* 25**,** 339-350.

HERRING, S. W. 2007. Masticatory muscles and the skull: a comparative perspective. *Archives of Oral Biology,* 52**,** 296-9.

HERRING, S. W. & LAKARS, T. C. 1982. Craniofacial development in the absence of muscle contraction. *Journal of craniofacial genetics and developmental biology,* 1**,** 341-57.

HERZOG, W. 1994. *BIOMECHANICS of the muscle-skeletal system*

HIIEMAE, K. 1971a. Structure and Function of Jaw Muscles in Rat (*Rattus Norvegicus L*) .3. Mechanics of Muscles. *Zoological Journal of the Linnean Society,* 50**,** 111-&.

HIIEMAE, K. 1971b. Structure and Function of Jaw Muscles in Rat (*Rattus Norvegicus L*).1. Their Anatomy and Internal Architecture. *Zoological Journal of the Linnean Society,* 50**,** 75-&.

HIIEMAE, K. & HOUSTON, W. J. B. 1971. The structure and function of the jaw muscles in the rat (Rattus norvegicus L.). *Zoological Journal of the Linnean Society,* 50**,** 75-99.

HIIEMAE, K. M. 1967. Masticatory function in the mammals. *Journal of Dental Research,* 46**,** 883-93.

HIIEMAE, K. M. 1967. Masticatory Function in the Mammals. *Journal of Dental Research Supplement,* 46**,** 883-893.

HIIEMAE, K. M. & ARDRAN, G. M. 1968. A cinefluorographic study of mandibular movement during feeding in the rat (*rattus norvegicus*). *Journal of Zoology. ,Lond.,* 154**,** 139-154.

HOUSTON, W. J. 1974. Growth of the muscles of mastication in the rat. *European Orthodontic Society***,** 85-90.

IWASAKI, L. R., PETSCHE, P. E., MCCALL, W. D., JR., MARX, D. & NICKEL, J. C. 2003a. Neuromuscular objectives of the human masticatory apparatus during static biting. *Archives of Oral Biology,* 48**,** 767-77.

IWASAKI, L. R., PETSCHE, P. E., MCCALL, W. D., MARX, D. & NICKEL, J. C. 2003b. Neuromuscular objectives of the human masticatory apparatus during static biting. *Archives of Oral Biology,* 48**,** 767-777.

JONES, J. A., LAVALLEE, N., ALMAN, J., SINCLAIR, C. & GARCIA, R. I. 1993. Caries incidence in patients with dementia. *Gerodontology,* 10**,** 76-82.

JONES, M. E., O'HIGGINS, P., FAGAN, M. J., EVANS, S. E. & CURTIS, N. 2012. Shearing mechanics and the influence of a flexible symphysis during oral food processing in Sphenodon (Lepidosauria: Rhynchocephalia). *The Anatomical Record (Hoboken),* 295**,** 1075-91.

JONES, M. E. H., CURTIS, N., FAGAN, M. J., O'HIGGINS, P. & EVANS, S. E. 2011. Hard tissue anatomy of the cranial joints in Sphenodon (Rhynchocephalia): sutures, kinesis, and skull mechanics. *Palaeontologia Electronica,* 14.

KAWAKAMI, M. & YAMAMURA, K. I. 2008. Cranial bone morphometric study among mouse strains. *BMC Evolutionary Biology,,* 8.

KAWATA, T., NIIDA, S., KAWASOKO, S., KAKU, M., FUJITA, T., SUGIYAMA, H. & TANNE, K. 1997. Morphology of the mandibular condyle in "toothless" osteopetrotic (op/op) mice. *Journal of Craniofacial Genetics and Developmental Biology,* 17**,** 198-203.

KIST, R., WATSON, M., WANG, X., CAIRNS, P., MILES, C., REID, D. J. & PETERS, H. 2005. Reduction of Pax9 gene dosage in an allelic series of mouse mutants causes hypodontia and oligodontia. *Human Molecular Genetics,* 14**,** 3605-17.

KLINGENBERG, C. P. 2002. Morphometrics and the role of the phenotype in studies of the evolution of developmental mechanisms. *Genetica,* 287**,** 3-10.

KLINGENBERG, C. P., MEBUS, K. & AUFFRAY, J. C. 2003. Developmental integration in a complex morphological structure: how distinct are the modules in the mouse mandible? *Evolution & Development,* 5**,** 522-31.

KOBAYASHI, M., MASUDA, Y., FUJIMOTO, Y., MATSUYA, T., YAMAMURA, K., YAMADA, Y., MAEDA, N. & MORIMOTO, T. 2002a. Electrophysiological analysis of rhythmic jaw movements in the freely moving mouse. *Physiology & Behavior,* 75**,** 377-385.

KOBAYASHI, M., MASUDA, Y., FUJIMOTO, Y., MATSUYA, T., YAMAMURA, K., YAMADA, Y., MAEDA, N. & MORIMOTO, T. 2002b. Electrophysiological analysis of rhythmic jaw movements in the freely moving mouse. *Physiology & Behavior,* 75**,** 377-85.

KOBAYASHI, M., MASUDA, Y., KISHINO, M., ISHIDA, T., MAEDA, N. & MORIMOTO, T. 2002c. Characteristics of mastication in the anodontic mouse. *Journal of Dental Research,* 81**,** 594-597.

KOGA, Y., YOSHIDA, N., KOBAYASHI, K., ICHIRO, O. & YAMADA, Y. 2001. Development of a three-dimensional jaw-tracking system implanted in the freely moving mouse. *Medical Engineering & Physics,* 23**,** 201-6.

KOOLSTRA, J. H. & VAN EIJDEN, T. M. 1992. Application and validation of a three-dimensional mathematical model of the human masticatory system in vivo. *Journal of Biomechanics,* 25**,** 175-87.

KOOLSTRA, J. H., VAN EIJDEN, T. M., WEIJS, W. A. & NAEIJE, M. 1988. *A three-dimensional mathematical model of the human masticatory system predicting maximum possible bite forces*.

KOOLSTRA, J. H. & VAN EIJDEN, T. M. G. J. 2001. A method to predict muscle control in the kinematically and mechanically indeterminate human masticatory system. *Journal of Biomechanics,* 34**,** 1179-1188.

KUPCZIK, K., DOBSON, C. A., FAGAN, M. J., CROMPTON, R. H., OXNARD, C. E. & O'HIGGINS, P. 2007. Assessing mechanical function of the zygomatic region in macaques: validation and sensitivity testing of finite element models. *Journal of Anatomy,* 210**,** 41-53.

KUROE, K. & ITO, G. 1990. Age changes of mandibular condyles and glenoid fossae in mice fed a liquid diet. *The Japanese dental science review (Tokyo),* 27**,** 91-6.

LANGENBACH, G. E. & WEIJS, W. A. 1990. Growth patterns of the rabbit masticatory muscles. *Journal of Dental Research,* 69**,** 20-5.

LANGENBACH, G. E. J. & VAN EIJDEN, T. M. G. J. 2001. Mammalian Feeding Motor Patterns. *American Zoologist,* 41**,** 1338-1351.

LANGENBACH, G. E. J., ZHANG, F., HERRING, S. W. & HANNAM, A. G. 2002. Modelling the masticatory biomechanics of a pig. *Journal of Anatomy,* 201**,** 383-393.

LEAMY, L. 1993. Morphological Integration of Fluctuating Asymmetry in the Mouse Mandible. *Genetica,* 89**,** 139-153.

LI, G. A., PIERCE, J. E. & HERNDON, J. H. 2006. A global optimization method for prediction of muscle forces of human musculoskeletal system. *Journal of Biomechanics,* 39**,** 522-529.

LIEBER, R. L. & WARD, S. R. 2011. Skeletal muscle design to meet functional demands. *Philosophical transactions of the Royal Society of London. Series B, Biological sciences,* 366**,** 1466-76.

LIEBERMAN, D. E. & CROMPTON, A. W. 2000. Why fuse the mandibular symphysis? A comparative analysis. *American Journal of Physical Anthropology,* 112**,** 517-40.

LLEWELLYN, M. E., BARRETTO, R. P. J., DELP, S. L. & SCHNITZER, M. J. 2008. Minimally invasive high-speed imaging of sarcomere contractile dynamics in mice and humans. *Nature,* 454**,** 784-788.

LYNGSTADAAS, S. P., MOINICHEN, C. B. & RISNES, S. 1998. Crown morphology, enamel distribution, and enamel structure in mouse molars. *Anatomical Record,* 250**,** 268-280.

MAO, J. J. 2002. Mechanobiology of craniofacial sutures. *Journal of Dental Research,* 81**,** 810-6.

MCHENRY, C. R., WROE, S., CLAUSEN, P. D., MORENO, K. & CUNNINGHAM, E. 2007. Supermodeled sabercat, predatory behavior in Smilodon fatalis revealed by high-resolution 3D computer simulation. *Proceedings of the National Academy of Sciences of the United States of America,* 104**,** 16010-5.

MCN, R. & VERNON, A. 1975. The dimensions of knee and ankle muscles and the forces they exert*. Journal of Human Movement Studies,* 1:115–123.

MOAZEN, M., CURTIS, N., EVANS, S. E., O'HIGGINS, P. & FAGAN, M. J. 2008a. Combined finite element and multibody dynamics analysis of biting in a Uromastyx hardwickii lizard skull. *Journal of Anatomy,* 213**,** 499-508.

MOAZEN, M., CURTIS, N., EVANS, S. E., O'HIGGINS, P. & FAGAN, M. J. 2008b. Rigid-body analysis of a lizard skull: Modelling the skull of Uromastyx hardwickii. *Journal of Biomechanics,* 41**,** 1274-1280.

MOINICHEN, C. B., LYNGSTADAAS, S. P. & RISNES, S. 1996. Morphological characteristics of mouse incisor enamel. *Journal of Anatomy,* 189**,** 325-333.

MORENO, K., WROE, S., CLAUSEN, P., MCHENRY, C., D'AMORE, D. C., RAYFIELD, E. J. & CUNNINGHAM, E. 2008. Cranial performance in the Komodo dragon (Varanus komodoensis) as revealed by high-resolution 3-D finite element analysis. *Journal of Anatomy,* 212**,** 736-746.

MURPHY, R. A. & BEARDSLEY, A. C. 1974. Mechanical properties of the cat soleus muscle in situ. *American Journal of Physiology,* 227**,** 1008-13.

NAKAMURA, A., ZEREDO, J. L., UTSUMI, D., FUJISHITA, A., KOGA, Y. & YOSHIDA, N. 2013. Influence of malocclusion on the development of masticatory function and mandibular growth. *Angle Orthodontist,* 83**,** 749-57.

NAKATA, S. 1981. Relationship Between the Development and Growth of Cranial Bones and Masticatory Muscles in Postnatal Mice. *Journal of Dental Research,* 60**,** 1440-1450.

ODMAN, A., MAVROPOULOS, A. & KILIARIDIS, S. 2008. Do masticatory functional changes influence the mandibular morphology in adult rats. *Archives of Oral Biology,* 53**,** 1149-54.

OKAYASU, I., YAMADA, Y., KOHNO, S. & YOSHIDA, N. 2003. New animal model for studying mastication in oral motor disorders. *Journal of Dental Research,* 82**,** 318-321.

ONOZUKA, M., WATANABE, K., MIRBOD, S. M., OZONO, S., NISHIYAMA, K., KARASAWA, N. & NAGATSU, L. 1999. Reduced mastication stimulates impairment of spatial memory and degeneration of hippocampal neurons in aged SAMP8 mice. *Brain Research,* 826**,** 148-153.

OPPERMAN, L. A. 2000. Cranial sutures as intramembranous bone growth sites. *Developmental Dynamics,* 219**,** 472-85.

OSBORN, J. W. & BARAGAR, F. A. 1985. Predicted Pattern of Human-Muscle Activity during Clenching Derived from a Computer-Assisted Model - Symmetric Vertical Bite Forces. *Journal of Biomechanics,* 18**,** 599-612.

OTTEN, E. 2003. Inverse and forward dynamics: models of multi-body systems. *Philosophical transactions of the Royal Society of London. Series B, Biological sciences,* 358**,** 1493-500.

PATEL, N. G. 1978. Functional morphology of the masticatory muscles ofMus musculus L. *Proceedings of the Indian Academy of Sciences - Section B, Animal Sciences,* 87**,** 51-57.

PEARSON, O. M. & LIEBERMAN, D. E. 2004. The aging of Wolff's "law": ontogeny and responses to mechanical loading in cortical bone. *American Journal of Physical Anthropology,* Suppl 39**,** 63-99.

POPWICS, T. E. & HERRING, S. W. 2006. Teeth,Jaws and Muscles in Mamalian Mastication. *In:* BELS, V. L. (ed.) *Feeding in domestic vertebrates : from structure to behaviour.* Wallingford, UK ; Cambridge, MA: CABI Pub.

PORTO, G. G., VASCONCELOS, B. C. D., ANDRADE, E. S. D. & SILVA, V. A. 2010. Comparison between human and rat TMJ: anatomic and histopathologic features. *Acta Cirurgica Brasileira,* 25**,** 290-293.

PURCELL, P., JHEON, A., VIVERO, M. P., RAHIMI, H., JOO, A. & KLEIN, O. D. 2012. Spry1 and Spry2 Are Essential for Development of the Temporomandibular Joint. *Journal of Dental Research,* 91**,** 387-393.

RANA, N. & JOAG, P. 1991. *Classical Mechanics,* New Delhi, Tata McGraw Hill.

RASMUSSEN, J., DAMSGAARD, M. & VOIGT, M. 2001. Muscle recruitment by the min/max criterion - a comparative numerical study. *Journal of Biomechanics,* 34**,** 409-415.

RAYFIELD, E. J., NORMAN, D. B., HORNER, C. C., HORNER, J. R., SMITH, P. M., THOMASON, J. J. & UPCHURCH, P. 2001. Cranial design and function in a large theropod dinosaur. *Nature,* 409**,** 1033-1037.

RAYNE, J. & CRAWFORD, G. N. 1972. The growth of the muscles of mastication in the rat. *Journal of Anatomy,* 113**,** 391-408.

RUES, S., LENZ, J., TUERP, J. C., SCHWEIZERHOF, K. & SCHINDLER, H. J. 2008. Forces and motor control mechanisms during biting in a realistically balanced experimental occlusion. *Archives of Oral Biology,* 53**,** 1119-1128.

RUFF, C., HOLT, B. & TRINKAUS, E. 2006. Who's afraid of the big bad Wolff?: "Wolff's law" and bone functional adaptation. *American Journal of Physical Anthropology,* 129**,** 484-98.

SANEFUJI, K., ZEREDO, J. L., KUROSE, M., TANAKA, M., KOGA, Y., YAMADA, Y. & YOSHIDA, N. 2008. Possible effects of periodontal inputs on the masticatory function. *The Journal of Japanese Society of Stomatognathic Function,* 14**,** 89-95.

SATOH, K. 1997. Comparative functional morphology of mandibular forward movement during mastication of two murid rodents, Apodemus speciosus (Murinae) and Clethrionomys rufocanus (Arvicolinae). *Journal of Morphology,* 231**,** 131-41.

SATOH, K. 1998. Balancing function of the masticatory muscles during incisal biting in two murid rodents, Apodemus speciosus and Clethrionomys rufocanus. *Journal of Morphology,* 236**,** 49-56.

SATOH, K. 1999. Mechanical advantage of area of origin for the external pterygoid muscle in two murid rodents, Apodemus speciosus and Clethrionomys rufocanus. *Journal of Morphology,* 240**,** 1-14.

SCHINDLER, H. J., RUES, S., TURP, J. C., SCHWEIZERHOF, K. & LENZ, J. 2007. Jaw clenching: Muscle and joint forces, optimization strategies. *Journal of Dental Research,* 86**,** 843-847.

SELLERS, W. I. & CROMPTON, R. H. 2004. Using sensitivity analysis to validate the predictions of a biomechanical model of bite forces. *Annals of Anatomy-Anatomischer Anzeiger,* 186**,** 89-95.

SHABANA, A. A. 2005. *Dynamics of multibody systems,* Cambridge ; New York, Cambridge University Press.

SHI, J. F., CURTIS, N., FITTON, L. C., O'HIGGINS, P. & FAGAN, M. J. 2012. Developing a musculoskeletal model of the primate skull: Predicting muscle activations, bite force, and joint reaction forces using multibody dynamics analysis and advanced optimisation methods. *Journal of Theoretical Biology,* 310**,** 21-30.

SPENCER, M. A. 1998. Force production in the primate masticatory system: electromyographic tests of biomechanical hypotheses. *Journal of Human Evolution,* 34**,** 25-54.

SWIDERSKI, D. L. & ZELDITCH, M. L. 2013. The complex ontogenetic trajectory of mandibular shape in a laboratory mouse. *Journal of Anatomy,* 223**,** 568-80.

TANAKA, E., SANO, R., KAWAI, N., LANGENBACH, G. E., BRUGMAN, P., TANNE, K. & VAN EIJDEN, T. M. 2007. Effect of food consistency on the degree of mineralization in the rat mandible. *Annual Review Of Biomedical Engineering,* 35**,** 1617-21.

TANNER, J. B., ZELDITCH, M. L., LUNDRIGAN, B. L. & HOLEKAMP, K. E. 2010. Ontogenetic change in skull morphology and mechanical advantage in the spotted hyena (Crocuta crocuta). *Journal of Morphology,* 271**,** 353-65.

TOKIMASA, C., KAWATA, T., FUJITA, T., KAKU, M., KAWASOKO, S., KOHNO, S. & TANNE, K. 2000. Effects of insulin-like growth factor-I on nasopremaxillary growth under different masticatory loadings in growing mice. *Archives of Oral Biology,* 45**,** 871-8.

TURNBULL, W. 1970a. Mammalian masticatory apparatus. *Fieldiana (Geol)***,** 147–356.

TURNBULL, W. D. 1970b. *Mammalian masticatory apparatus*.

UTSUMI, D., NAKAMURA, A., MATSUO, K., ZEREDO, J. L., KOGA, Y. & YOSHIDA, N. 2010. Motor coordination of masseter and temporalis muscle during mastication in mice. *International Journal of Stomatology & Occlusion Medicine,* 3**,** 187-194.

VAN RUIJVEN, L. J. & WEIJS, W. A. 1990. A new model for calculating muscle forces from electromyograms. *European Journal of Applied Physiology and Occupational Physiology,* 61**,** 479-85.

VANSPRONSEN, P. H., WEIJS, W. A., VALK, J., PRAHLANDERSEN, B. & VANGINKEL, F. C. 1989. Comparison of Jaw-Muscle Bite-Force Cross-Sections Obtained by Means of Magnetic-Resonance Imaging and High-Resolution Ct Scanning. *Journal of Dental Research,* 68**,** 1765-1770.

VINYARD, C. J. & PAYSEUR, B. A. 2008. Of "mice" and mammals: utilizing classical inbred mice to study the genetic architecture of function and performance in mammals. *Integrative and Comparative Biology,* 48**,** 324-37.

WANG, W. J., CROMPTON, R. H., CAREY, T. S., GUNTHER, M. M., LI, Y., SAVAGE, R. & SELLERS, W. I. 2004. Comparison of inverse-dynamics musculo-skeletal models of *AL 288-1 Australopithecus afarensis* and *KNM-WT 15000 Homo ergaster* to modern humans, with implications for the evolution of bipedalism. *Journal of Human Evolution,* 47**,** 453-478.

WANG, Y., LIU, C., ROHR, J., LIU, H. B., HE, F. L., YU, J., SUN, C., LI, L., GU, S. P. & CHEN, Y. P. 2011. Tissue Interaction Is Required for Glenoid Fossa Development During Temporomandibular Joint Formation. *Developmental Dynamics,* 240**,** 2466-2473.

WATSON, P. J., GRÖNING, F., CURTIS, N., FITTON, L. C., HERREL, A., MCCORMACK, S. W. & FAGAN, M. J. 2014. Masticatory biomechanics in the rabbit: a multi-body dynamics analysis. *Journal of the Royal Society Interface,* 11.

WEIJS, W. A. 1973. MORPHOLOGY OF MUSCLES OF MASTICATION IN ALBINO-RAT, RATTUS-NORVEGICUS (BERKENHOUT, 1769). *Acta Morphologica Neerlando-Scandinavica,* 11**,** 321-340.

WEIJS, W. A. 1975. Mandibular Movements of Albino-Rat during Feeding. *Journal of Morphology,* 145**,** 107-124.

WEIJS, W. A., BRUGMAN, P. & KLOK, E. M. 1987. The Growth of the Skull and Jaw Muscles and Its Functional Consequences in the New-Zealand Rabbit (Oryctolagus-Cuniculus). *Journal of Morphology,* 194**,** 143-161.

WEIJS, W. A. & DANTUMA, R. 1975. Electromyography and Mechanics of Mastication in Albino-Rat. *Journal of Morphology,* 146**,** 1-&.

WEIJS, W. A. & HILLEN, B. 1985. Cross-Sectional Areas and Estimated Intrinsic Strength of the Human Jaw Muscles. *Acta Morphologica Neerlando-Scandinavica,* 23**,** 267-274.

WILLIAMS, S. H., PEIFFER, E. & FORD, S. 2009. Gape and bite force in the rodents Onychomys leucogaster and Peromyscus maniculatus: does jaw-muscle anatomy predict performance? *Journal of Morphology,* 270**,** 1338-47.

WILLMORE, K. E., LEAMY, L. & HALLGRIMSSON, B. 2006. Effects of developmental and functional interactions on mouse cranial variability through late ontogeny. *Evolution & Development,* 8**,** 550-67.

WILSON, A. & LICHTWARK, G. 2011. The anatomical arrangement of muscle and tendon enhances limb versatility and locomotor performance. *Philosophical transactions of the Royal Society of London. Series B, Biological sciences,* 366**,** 1540-53.

WOOD, A. E. 1965. Grades and Clades Among Rodents. *Evolution,* 19**,** 115-130.

WOODS, C. 1972. Comparative myology of jaw, hyoid, and pectoral appendicular regions of New and Old World hystricomorph rodents. *Bulletin of the American Museum of Natural History,* 147**,** 115–198.

WOODS, C. A. & HOWLAND, E. B. 1979. Adaptive Radiation of Capromyid Rodents: Anatomy of the Masticatory Apparatus. *Journal of Mammalogy,* 60**,** 95-116.

WROE, S., CLAUSEN, P., MCHENRY, C., MORENO, K. & CUNNINGHAM, E. 2007. Computer simulation of feeding behaviour in the thylacine and dingo as a novel test for convergence and niche overlap. *Proceedings of the Royal Society B: Biological Sciences Publications,* 274**,** 2819-28.

YAMADA, M., KOGA, Y., OKAYASU, I., SANEFUJI, K., YAMADA, Y., OI, K. & YOSHIDA, N. 2006. Influence of soft diet feeding on development of masticatory function. *The Journal of Japanese Society of Stomatognathic Function,* 12**,** 118-125.

ZATSIORSKY, V. M. & PRILUTSKY, B. I. 2012. *Biomechanics of skeletal muscles,* Champaign, IL, Human Kinetics.

ZELDITCH, M. L., LUNDRIGAN, B. L., SHEETS, H. D. & GARLAND, T., JR. 2003. Do precocial mammals develop at a faster rate? A comparison of rates of skull development in Sigmodon fulviventer and Mus musculus domesticus. *Journal of Evolutionary Biology,* 16**,** 708-20.

Appendix I. Muscle fibre measurements

Muscle		mouse 10	mouse 7	mouse 6	mouse 2	overall mean
SM	Muscle Fibre 1	0.197	0.232	0.24	0.292	
	Muscle Fibre 2	0.265	0.262	0.243	0.263	
	Muscle Fibre 3	0.257	0.277	0.264	0.222	
	Muscle Fibre 4	0.214	0.278	0.22	0.242	
	Muscle Fibre 5	0.233	0.23	0.256	0.265	
	Muscle Fibre 6	0.22	0.242	0.248	0.23	
	Muscle Fibre 7	0.259	0.239	0.309	0.264	
	Muscle Fibre 8	0.233	0.207	0.291	0.255	
	Muscle Fibre 9	0.26	0.244	0.269	0.248	
	Muscle Fibre 10	0.223	0.233	0.287	0.231	
Mean (cm)		**0.2361**	**0.2444**	**0.2627**	**0.2512**	**0.2486**
ADM*	Muscle Fibre 1	0.341	0.28	0.228	0.273	
	Muscle Fibre 2	0.31	0.239	0.278	0.291	
	Muscle Fibre 3	0.328	0.227	0.322	0.263	
	Muscle Fibre 4	0.329	0.268	0.303	0.274	
	Muscle Fibre 5	0.307	0.205	0.201	0.297	
	Muscle Fibre 6	0.345	0.192	0.243	0.236	
	Muscle Fibre 7	0.269	0.224	0.256	0.239	
	Muscle Fibre 8	0.298	0.174	0.273	0.271	
	Muscle Fibre 9	0.276	0.179	0.26	0.282	
	Muscle Fibre 10	0.268	0.205	0.25	0.27	
Mean (cm)		**0.3071**	**0.2193**	**0.2614**	**0.2696**	**0.2644**
PDM*	Muscle Fibre 1	0.297	0.281	0.312	0.365	
	Muscle Fibre 2	0.287	0.327	0.304	0.329	
	Muscle Fibre 3	0.264	0.335	0.368	0.331	
	Muscle Fibre 4	0.272	0.286	0.404	0.342	
	Muscle Fibre 5	0.25	0.376	0.283	0.318	
	Muscle Fibre 6	0.269	0.422	0.39	0.371	
	Muscle Fibre 7	0.29	0.346	0.393	0.34	
	Muscle Fibre 8	0.288	0.359	0.388	0.368	
	Muscle Fibre 9	0.328	0.286	0.379	0.359	
	Muscle Fibre 10	0.305	0.321	0.422	0.379	
Mean (cm)		**0.285**	**0.3339**	**0.3643**	**0.3502**	**0.3334**

*ADM (anterior deep masseter) and PDM (posterior deep masseter) were dissected individually and their mass and fibres were weighed individually, but their average was used for DM (deep master) in modelling.

Muscle		mouse 10	mouse 7	mouse 6	mouse 2	overall mean
AT	Muscle Fibre 1	0.175	0.31	0.272	0.285	
	Muscle Fibre 2	0.241	0.305	0.264	0.325	
	Muscle Fibre 3	0.222	0.305	0.236	0.295	
	Muscle Fibre 4	0.167	0.294	0.277	0.267	
	Muscle Fibre 5	0.19	0.309	0.302	0.285	
	Muscle Fibre 6	0.221	0.287	0.264	0.322	
	Muscle Fibre 7	0.232	0.276	0.259	0.268	
	Muscle Fibre 8	0.257	0.244	0.296	0.216	
	Muscle Fibre 9	0.213	0.245	0.312	0.214	
	Muscle Fibre 10	0.174	0.205	0.271	0.212	
Mean (cm)		**0.2092**	**0.278**	**0.2753**	**0.2689**	**0.2579**
PT	Muscle Fibre 1	0.26	0.356	0.348	0.341	
	Muscle Fibre 2	0.272	0.302	0.409	0.373	
	Muscle Fibre 3	0.314	0.32	0.361	0.321	
	Muscle Fibre 4	0.279	0.322	0.367	0.27	
	Muscle Fibre 5	0.328	0.378	0.414	0.337	
	Muscle Fibre 6	0.314	0.341	0.417	0.349	
	Muscle Fibre 7	0.328	0.339	0.374	0.317	
	Muscle Fibre 8	0.317	0.362	0.342	0.331	
	Muscle Fibre 9	0.339	0.366	0.363	0.34	
	Muscle Fibre 10	0.332	0.333	0.421	0.367	
Mean (cm)		**0.3083**	**0.3419**	**0.3816**	**0.3346**	**0.3416**
SZT	Muscle Fibre 1	0.372	0.176	0.201	0.224	
	Muscle Fibre 2	0.359	0.166	0.316	0.328	
	Muscle Fibre 3	0.363	0.191	0.259	0.368	
	Muscle Fibre 4	0.238	0.206	0.352	0.293	
	Muscle Fibre 5	0.267	0.223	0.192	0.372	
	Muscle Fibre 6	0.263	0.17	0.183	0.275	
	Muscle Fibre 7	0.284	0.208	0.188	0.288	
	Muscle Fibre 8	0.309	0.235	0.274	0.281	
	Muscle Fibre 9	0.306	0.227	0.312	0.288	
	Muscle Fibre 10	0.286	0.175	0.216	0.287	
Mean (cm)		**0.3047**	**0.1977**	**0.2493**	**0.3004**	**0.2630**
AZM	Muscle Fibre 1	0.2	0.296	0.274	0.273	
	Muscle Fibre 2	0.151	0.251	0.271	0.263	
	Muscle Fibre 3	0.238	0.28	0.259	0.301	
	Muscle Fibre 4	0.226	0.16	0.304	0.266	
	Muscle Fibre 5	0.158	0.197	0.315	0.271	
	Muscle Fibre 6	0.189	0.261	0.299	0.227	
	Muscle Fibre 7	0.197	0.284	0.23	0.263	
	Muscle Fibre 8	0.22	0.255	0.306	0.282	
	Muscle Fibre 9	0.152	0.236	0.265	0.266	
	Muscle Fibre 10	0.216	0.257	0.267	0.193	
Mean (cm)		**0.1947**	**0.2477**	**0.279**	**0.2605**	**0.2455**

Muscle		mouse 10	mouse 7	mouse 6	mouse 2	overall mean
IOZM	Muscle Fibre 1	0.301	0.325	0.251	0.269	
	Muscle Fibre 2	0.353	0.289	0.246	0.261	
	Muscle Fibre 3	0.301	0.311	0.322	0.223	
	Muscle Fibre 4	0.272	0.27	0.256	0.239	
	Muscle Fibre 5	0.286	0.24	0.273	0.272	
	Muscle Fibre 6	0.377	0.284	0.243	0.265	
	Muscle Fibre 7	0.327	0.291	0.236	0.264	
	Muscle Fibre 8	0.367	0.268	0.216	0.261	
	Muscle Fibre 9	0.294	0.241	0.243	0.277	
	Muscle Fibre 10	0.282	0.288	0.245	0.314	
Mean(cm)		**0.316**	**0.2807**	**0.2531**	**0.2645**	**0.2786**
PZM	Muscle Fibre 1	0.235	0.275	0.238	0.224	
	Muscle Fibre 2	0.234	0.231	0.288	0.214	
	Muscle Fibre 3	0.21	0.278	0.263	0.198	
	Muscle Fibre 4	0.208	0.231	0.266	0.226	
	Muscle Fibre 5	0.198	0.233	0.3	0.193	
	Muscle Fibre 6	0.258	0.218	0.207	0.22	
	Muscle Fibre 7	0.255	0.245	0.231	0.218	
	Muscle Fibre 8	0.231	0.283	0.23	0.226	
	Muscle Fibre 9	0.232	0.27	0.22	0.212	
	Muscle Fibre 10	0.256	0.274	0.272	0.235	
Mean(cm)		**0.2317**	**0.2538**	**0.2515**	**0.2166**	**0.2384**
IP	Muscle Fibre 1	0.221	0.26	0.287	0.217	
	Muscle Fibre 2	0.281	0.271	0.242	0.247	
	Muscle Fibre 3	0.265	0.26	0.252	0.237	
	Muscle Fibre 4	0.248	0.237	0.209	0.209	
	Muscle Fibre 5	0.219	0.242	0.2	0.229	
	Muscle Fibre 6	0.208	0.237	0.231	0.261	
	Muscle Fibre 7	0.207	0.277	0.2	0.234	
	Muscle Fibre 8	0.199	0.218	0.26	0.315	
	Muscle Fibre 9	0.239	0.227	0.247	0.228	
	Muscle Fibre 10	0.231	0.227	0.29	0.238	
Mean(cm)		**0.2318**	**0.2456**	**0.2418**	**0.2415**	**0.2402**
EP	Muscle Fibre 1	0.296	0.279	0.285	0.219	
	Muscle Fibre 2	0.327	0.294	0.299	0.205	
	Muscle Fibre 3	0.303	0.24	0.264	0.211	
	Muscle Fibre 4	0.404	0.268	0.322	0.237	
	Muscle Fibre 5	0.403	0.245	0.26	0.221	
	Muscle Fibre 6	0.397	0.225	0.298	0.24	
	Muscle Fibre 7	0.323	0.201	0.296	0.247	
	Muscle Fibre 8	0.276	0.207	0.329	0.3	
	Muscle Fibre 9	0.35	only 8	0.29	0.259	
	Muscle Fibre 10	0.301		0.294	0.261	
Mean(cm)		**0.338**	**0.2449**	**0.2937**	**0.24**	**0.2791**

Muscle		mouse 10	mouse 7	mouse 6	mouse 2	overall mean
DG	Muscle Fibre 1	0.354	0.383	0.324	0.372	
	Muscle Fibre 2	0.33	0.39	0.32	0.331	
	Muscle Fibre 3	0.334	0.365	0.319	0.38	
	Muscle Fibre 4	0.31	0.324	0.354	0.328	
	Muscle Fibre 5	0.317	0.322	0.3	0.353	
	Muscle Fibre 6	0.345	0.321	0.418	0.321	
	Muscle Fibre 7	0.288	0.287	0.337	0.385	
	Muscle Fibre 8	0.307	0.292	0.288	0.321	
	Muscle Fibre 9	0.266	0.328	0.353	0.335	
	Muscle Fibre 10	0.332	0.326	0.388	0.322	
Mean(cm)		**0.3183**	**0.3338**	**0.3401**	**0.3448**	**0.3343**

Appendix II. Relative muscle activation in sub-maximal molar and incisor biting

	Molar bite of 2.25		Incisor bite of 2.25		Molar bite of 4.5		Incisor bite of 4.5	
Activation	(N)	%	(N)	%	(N)	%	(N)	%
SM	0.17	4.6	0.33	8.8	0.34	8.9	0.80	21.2
DM	0.54	10.4	1.00	19.2	1.07	20.47	2.42	46.5
AT	0.46	23.7	0.78	39.7	0.91	46.57	1.83	93.3
PT	0.10	8.9	0.18	16.3	0.19	17.36	0.44	39.4
SZT	0.03	8.4	0.00	0.0	0.07	16.4	0.00	0.0
AZ	0.37	46.1	0.68	83.7	0.71	87.66	0.81	100
IOZ	0.21	40.9	0.40	75.5	0.42	80.49	0.53	100
PZ	0.19	40.6	0.35	74.8	0.38	79.85	0.47	100
IP	0.42	21.9	0.78	40.3	0.83	43.02	1.86	96.0
EP	0.23	33.7	0.39	56.0	0.41	58.4	0.66	94.5

Appendix III. Results of time dependant muscle activation of individual muscle fibres in working (right) and left (balancing) side of the molar biting of 8.97N

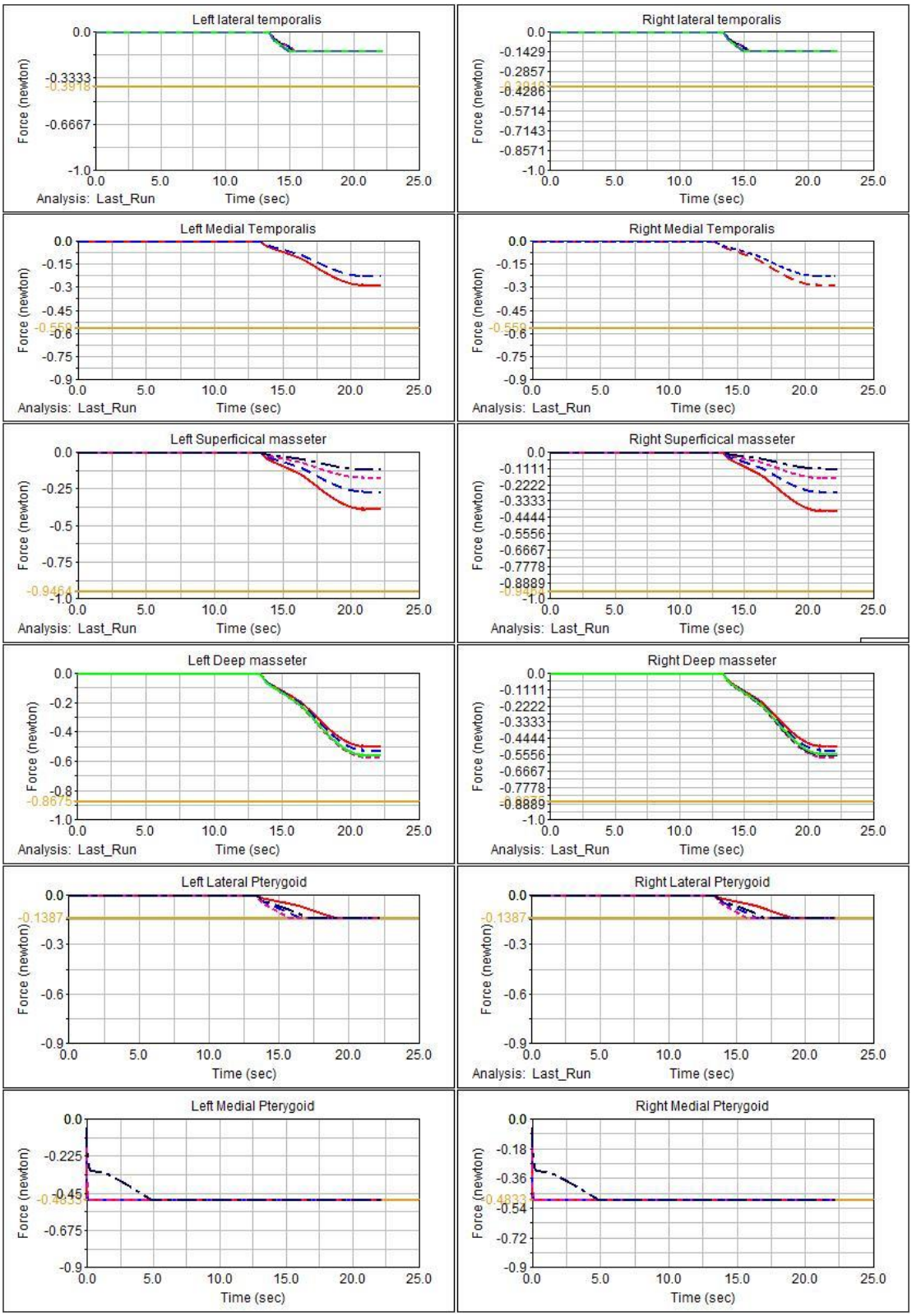

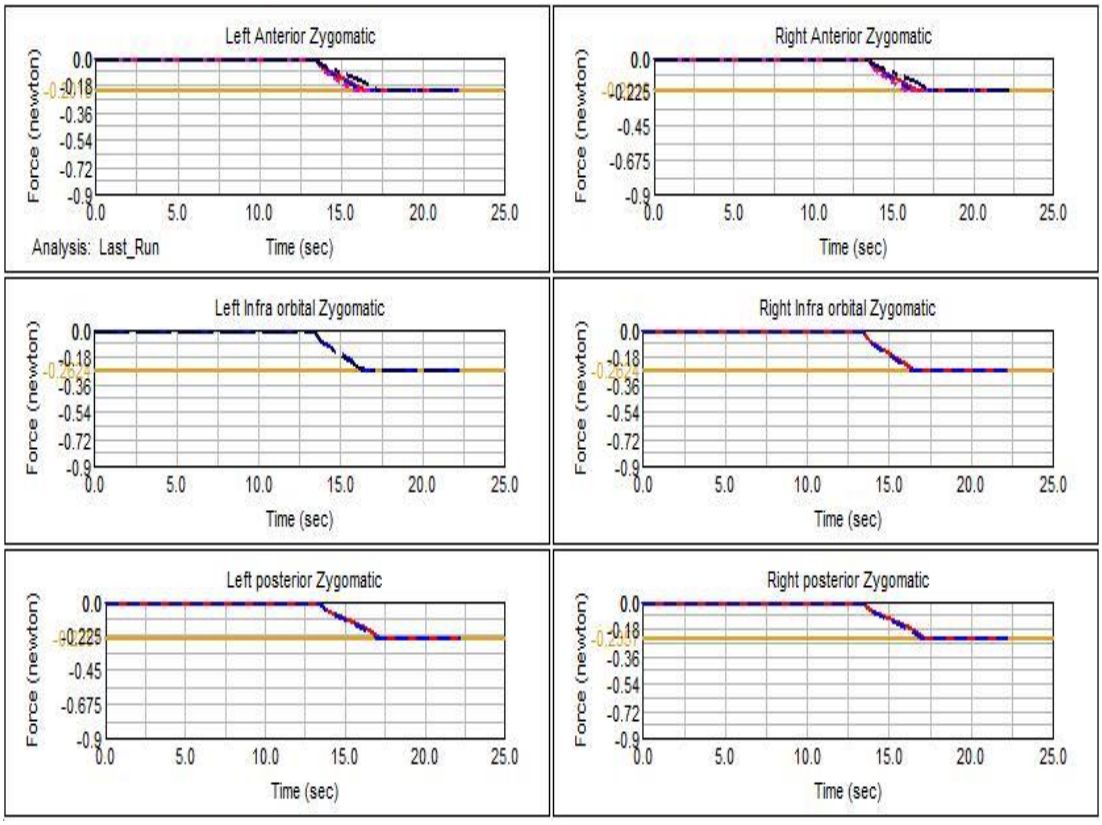

The chewing cycle was decelerated 100 times.

Appendix IV. Individual muscle fibers and their activation in MOME

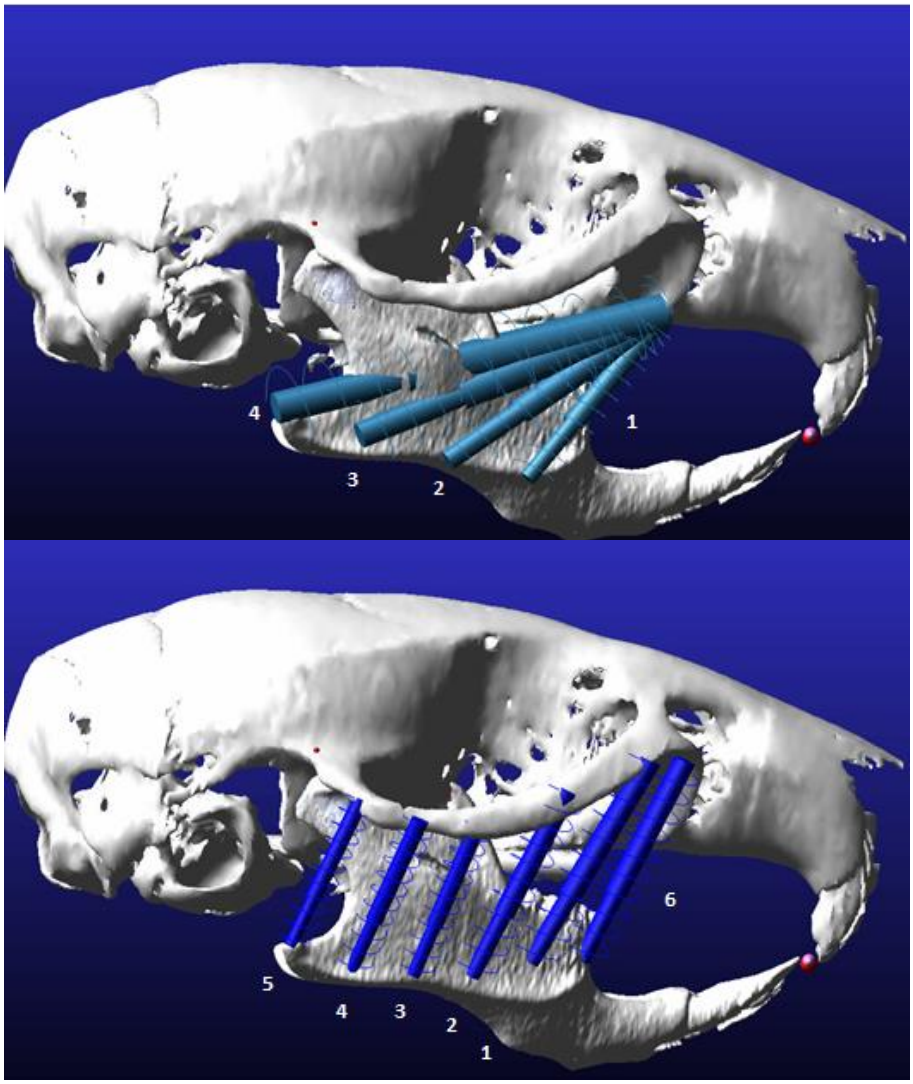

Figure IV.1 Superficial (top) and deep (bottom) masseter muscles. The number of each muscle strand used in Table IV.1 is presented.

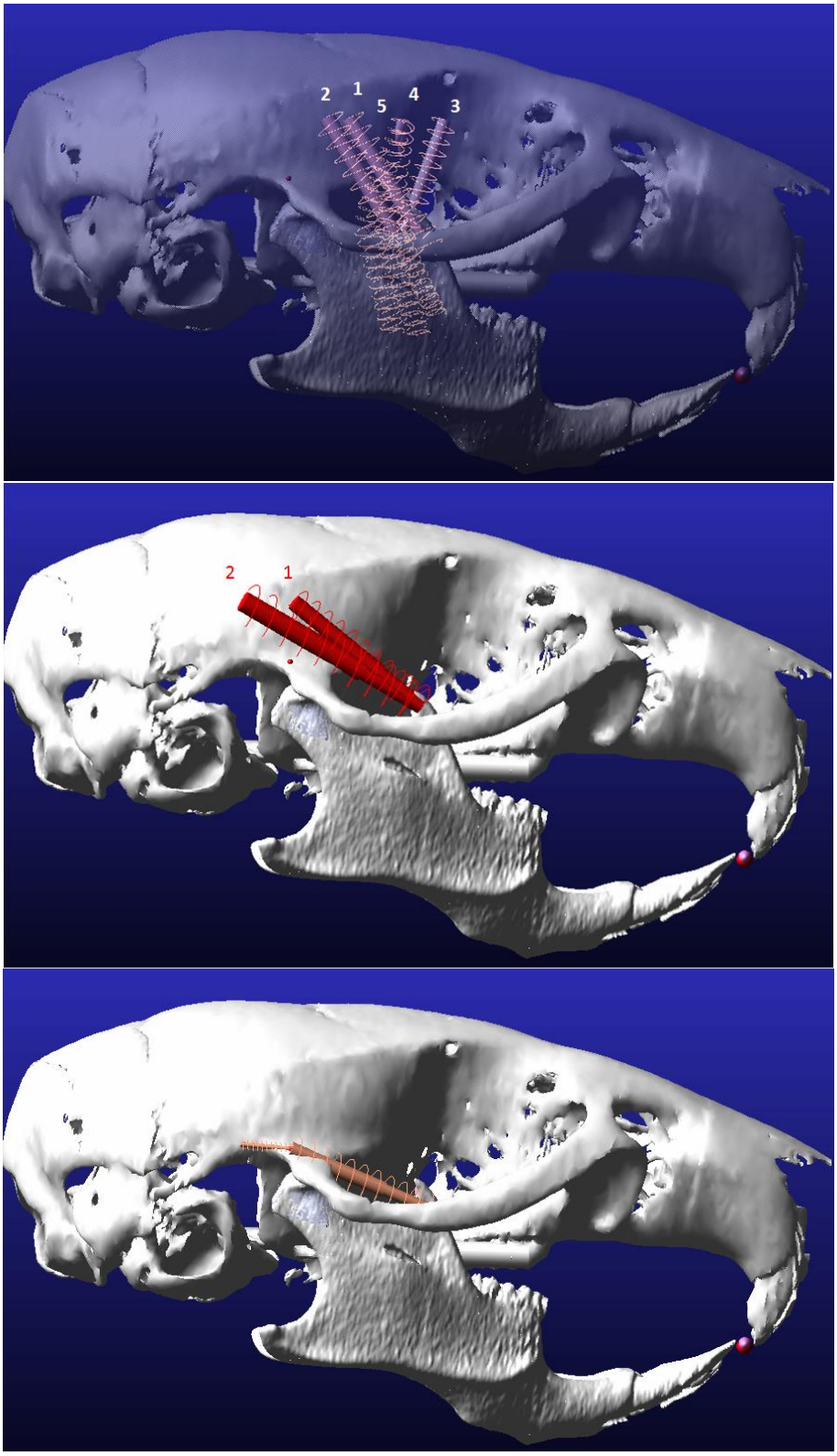

Figure IV.2 Anterior (top), posterior (middle) and suprazygomatic (bottom) temporalis muscles.

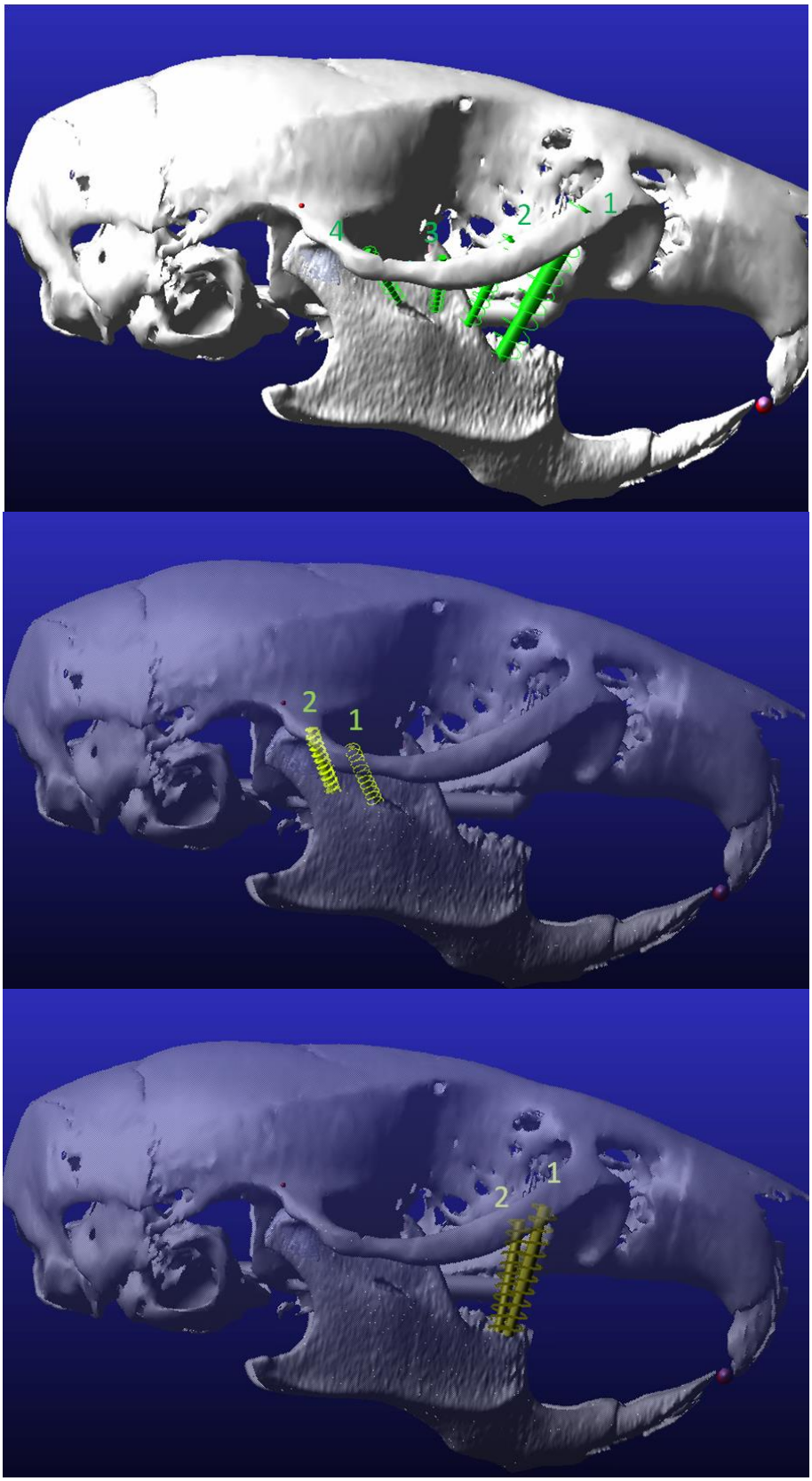

Figure IV.3 Anterior (top), posterior (middle) and infraorbital (bottom) zygomaticomandibularis muscles.

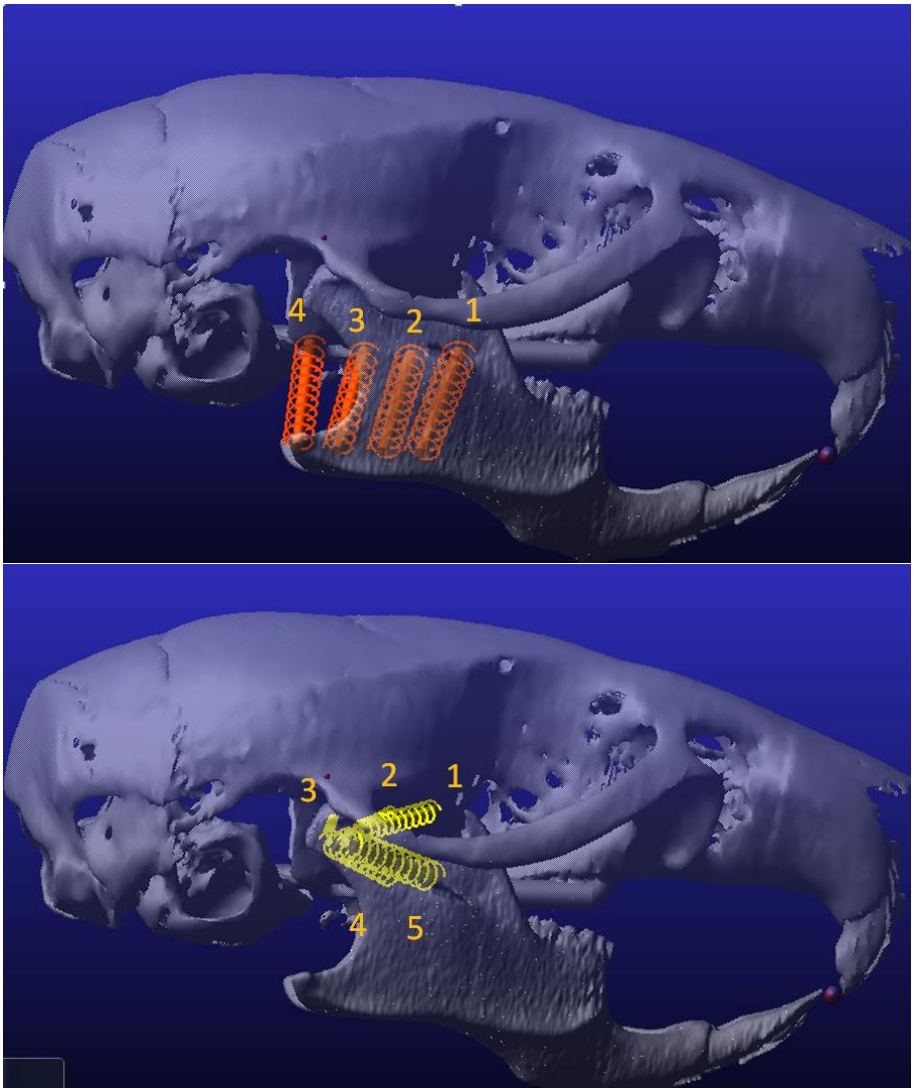

Figure IV.4 The internal (top) and external (bottom) Pterygoid muscles.

Table IV.1 Individual muscle strand activations resulted from molar bite in MOME

Muscles	Strands	Left (balancing side)(N)				Right (working side)(N)			
		x	y	z	mag	x	y	z	mag
SM	1	-0.43	-0.49	-0.08	0.66	-0.39	-0.48	0.10	0.63
	2	-0.38	-0.25	-0.07	0.47	-0.39	-0.27	0.11	0.49
	3	-0.30	-0.12	-0.07	0.33	-0.32	-0.13	0.09	0.35
	4	-0.18	-0.04	-0.04	0.18	-0.25	-0.06	0.06	0.27
DM	1	-0.30	-0.51	0.07	0.60	-0.34	-0.57	-0.10	0.67
	2	-0.21	-0.40	0.12	0.47	-0.20	-0.39	-0.10	0.45
	3	-0.08	-0.19	0.08	0.22	-0.12	-0.28	-0.09	0.32
	4	-0.03	-0.07	0.03	0.08	-0.07	-0.14	-0.06	0.17
	5	0.00	0.00	0.00	0.00	0.00	0.00	0.00	0.00
	6	0.00	0.00	0.00	0.00	-0.27	-0.53	-0.09	0.60
AT	1	0.06	-0.09	0.00	0.11	0.15	-0.24	0.01	0.29
	2	0.04	-0.06	0.00	0.07	0.05	-0.08	0.00	0.10
	3	0.09	-0.19	-0.09	0.23	0.06	-0.11	0.05	0.14
	4	0.05	-0.14	-0.04	0.15	0.07	-0.20	0.05	0.21
	5	0.01	-0.02	0.00	0.02	0.03	-0.08	0.01	0.09
PT	1	0.13	-0.10	0.01	0.16	0.10	-0.08	-0.02	0.12
	2	0.03	-0.02	0.00	0.03	0.11	-0.07	-0.03	0.13
SZT	1	0.13	-0.05	0.04	0.14	0.06	-0.03	-0.01	0.07
AZM	1	-0.09	-0.17	0.05	0.20	-0.10	-0.17	-0.05	0.20
	2	-0.09	-0.16	0.09	0.20	-0.08	-0.17	-0.08	0.20
	3	-0.02	-0.14	0.15	0.20	-0.02	-0.16	-0.12	0.20
	4	0.03	-0.05	0.06	0.09	0.00	0.00	0.00	0.01
IOZM	1	-0.07	-0.24	0.06	0.26	-0.07	-0.25	-0.01	0.26
	2	-0.06	-0.26	0.03	0.26	-0.05	-0.26	0.02	0.26
PZM	1	0.00	0.00	0.00	0.00	0.08	-0.17	-0.14	0.24
	2	0.01	-0.03	0.02	0.04	0.00	0.00	0.00	0.00
IP	1	-0.08	-0.19	-0.19	0.28	-0.03	-0.07	0.08	0.11
	2	-0.03	-0.09	-0.11	0.15	-0.02	-0.07	0.09	0.12
	3	0.00	0.00	0.00	0.00	0.00	0.00	0.00	0.00
	4	0.00	0.00	0.00	0.00	0.00	0.00	0.00	0.00
EP	1	0.00	0.00	0.00	0.00	-0.03	-0.01	0.03	0.04
	2	-0.08	-0.04	-0.10	0.14	0.00	0.00	0.01	0.01
	3	-0.01	-0.02	-0.05	0.05	0.00	0.00	0.00	0.00
	4	-0.04	0.02	-0.07	0.08	-0.02	0.01	0.03	0.04
	5	0.00	0.00	0.00	0.00	-0.02	0.01	0.02	0.03
Total		**-1.91**	**-4.13**	**-0.10**	**4.55**	**-2.07**	**-5.07**	**-0.15**	**5.48**

Table IV.2 Individual muscle strand activations resulted from molar bite of 8.97N in DGO

Muscles	Strands	Left (balancing side)(N)				Right (working side)(N)			
		x	y	z	mag	x	y	z	mag
SM	1	-0.25	-0.27	-0.04	0.37	-0.25	-0.29	0.06	0.38
	2	-0.21	-0.14	-0.04	0.26	-0.21	-0.14	0.05	0.26
	3	-0.15	-0.06	-0.03	0.16	-0.15	-0.06	0.04	0.17
	4	-0.10	-0.02	-0.02	0.11	-0.10	-0.02	0.02	0.11
DM	1	-0.25	-0.40	0.05	0.48	-0.25	-0.40	-0.07	0.47
	2	-0.25	-0.42	0.12	0.50	-0.24	-0.43	-0.11	0.50
	3	-0.24	-0.45	0.19	0.54	-0.24	-0.46	-0.16	0.54
	4	-0.24	-0.43	0.21	0.53	-0.24	-0.43	-0.19	0.53
	5	-0.26	-0.45	0.12	0.53	-0.26	-0.44	-0.11	0.53
	6	-0.24	-0.44	0.06	0.50	-0.24	-0.44	-0.07	0.50
AT	1	0.07	-0.12	0.00	0.14	0.07	-0.12	0.00	0.14
	2	0.07	-0.12	0.00	0.14	0.07	-0.12	0.00	0.14
	3	0.04	-0.12	-0.05	0.14	0.05	-0.12	0.05	0.14
	4	0.03	-0.13	-0.04	0.14	0.03	-0.13	0.03	0.14
	5	0.04	-0.13	-0.01	0.14	0.04	-0.13	0.02	0.14
PT	1	0.21	-0.17	0.02	0.27	0.20	-0.18	-0.04	0.27
	2	0.18	-0.11	0.02	0.22	0.18	-0.11	-0.04	0.22
SZT	1	0.00	0.00	0.00	0.00	0.00	0.00	0.00	0.00
AZM	1	-0.10	-0.17	0.04	0.20	-0.10	-0.17	-0.04	0.20
	2	-0.09	-0.16	0.08	0.20	-0.09	-0.17	-0.07	0.20
	3	-0.03	-0.14	0.14	0.20	-0.03	-0.16	-0.11	0.20
	4	0.07	-0.13	0.14	0.20	0.07	-0.14	-0.12	0.20
IOZM	1	-0.08	-0.24	0.06	0.26	-0.08	-0.25	-0.01	0.26
	2	-0.07	-0.25	0.02	0.26	-0.06	-0.25	0.02	0.26
PZM	1	0.06	-0.17	0.15	0.24	-0.18	-0.14	0.24	-0.24
	2	0.07	-0.20	0.11	0.24	-0.20	-0.10	0.24	-0.24
IP	1	-0.17	-0.32	-0.32	0.48	-0.15	-0.30	0.35	0.48
	2	-0.13	-0.29	-0.36	0.48	-0.13	-0.30	0.36	0.48
	3	-0.15	-0.33	-0.32	0.48	-0.14	-0.33	0.32	0.48
	4	-0.10	-0.35	-0.32	0.48	-0.09	-0.33	0.34	0.48
EP	1	-0.09	-0.02	-0.10	0.14	-0.10	-0.03	0.10	0.14
	2	-0.08	-0.04	-0.11	0.14	-0.09	-0.05	0.10	0.14
	3	-0.02	-0.02	-0.13	0.14	-0.02	-0.04	0.13	0.14
	4	-0.07	0.04	-0.11	0.14	-0.07	0.04	0.11	0.14
	5	-0.08	0.04	-0.10	0.14	-0.08	0.03	0.11	0.14
Total		**-2.61**	**-6.74**	**-0.59**	**7.25**	**-2.57**	**-6.85**	**0.80**	**7.36**